Modification of Phenolic Oximes for Copper Extraction

Ross Stewart Forgan

Doctor of Philosophy

University of Edinburgh

May 2008

Preface and Declaration

Since graduating from the University of Edinburgh in 2004 with a MChem. (Hons) degree in Chemistry, the author has been engaged in a programme of full time research under the supervision of Professor P. A. Tasker at the University of Edinburgh.

No part of the work referred to in this thesis has been submitted previously in whole or in part for another degree or qualification from this or any other university or institute of learning. In accordance with the regulations this thesis does not exceed 70,000 words in length.

Ross Stewart Forgan

May 2008

Abstract

The thesis deals with the modification of salicylaldoxime-based reagents used in hydrometallurgical extraction, addressing rational ligand design to tune copper(II) extractant strengths and also the development of reagents which are capable of transporting transition metal *salts*.

Chapter 1 reviews current solvent extractant technology for metal recovery, including the limited knowledge of the effect of substituents on extractive efficacy. Advances in leaching technology have led to systems wherein increases in process efficiency could be obtained using reagents which can transport both a transition metal cation and its attendant anion(s), and the potential advantages of metal *salt* extractants are discussed. The problems encountered when trying to extract hydrophilic anions selectively into organic media are also considered.

Chapter 2 discusses techniques used in industry to tune reagent properties, many of which depend on the importance of H-bonding in non-polar solvents. Synthesis of a series of 5-alkyl-3-X-2-hydroxybenzaldehyde oximes (X = a range of substituents) is described and copper extraction experiments are reported. 3-Substitution is found to alter reagent strength by two orders of magnitude, with 3-bromo-5-*tert*-butyl-2-hydroxybenzaldehyde oxime the strongest extractant. An analysis of X-ray structures of several ligands and copper(II) complexes is given in an attempt to establish whether trends in the solid state structures can account for variations in extractant strength. A more detailed analysis of the hydrogen bonding in salicylaldoximato copper(II) complexes and ligand dimers is carried out in Chapter 3, with the aim of defining how substituent effects could be used to design reagents with appropriate extractive behaviour. 3-X-2-Hydroxybenzaldehyde oximes with no 5-alkyl substituent are synthesised and subjected to a detailed study by X-ray crystallography and computational techniques, which, alongside evidence provided by CID-MS experiments, suggest that the dominant substituent effect in determining extractant strength is the ability to "buttress" the *pseudo*macrocyclic hydrogen bonding motif involving the oximic hydrogen and phenolic oxygen. Ligands with 3-

substituents capable of accepting H-bonds were found to be stronger extractants than those which could not, and the steric hindrance afforded by bulky substituents made 3,5-di-tert-*butyl*-2-hydroxybenzaldehyde oxime the weakest extractant. Ligand acidity is also noted to have a significant effect on reagent strength, with electron-withdrawing substituents lowering the pK_a of the phenolic proton and increasing extractive efficacy.

Chapter 4 focuses on metal *salt* extraction, and the development of selective, robust and hydrolytically stable reagents. Six novel extractants, based on a salicylaldoxime scaffold with a pendant dialkylaminomethyl arm, are described. Only 5-*tert*-butyl-3-dihexylaminomethyl-2-hydroxybenzaldehyde oxime and 3-*tert*-butyl-5-dihexylaminomethyl-2-hydroxybenzaldehyde oxime have sufficient solubility to be effective reagents. The former extracts $CuCl_2$ and $ZnCl_2$ in a highly efficient manner, with one mole of metal salt extracted per mole of ligand, twice the expected capacity. X-ray structure determination of complexes of the related ligand 5-*tert*-butyl-2-hydroxy-3-piperidin-1-ylmethylbenzaldehyde oxime defines the binding mode, with the chloride anions bound to the inner sphere of the metal cations. Loading and stripping experiments show it to be an extractant with potential commercial application. Cation and anion selectivity of the two extractants defined above is the focus of Chapter 5, which begins with an overview of techniques and attempts to attenuate the Hofmeister bias, the main factor in the selective extraction of hydrophilic anions into organic media. pH loading profiles show the 3-dihexylaminomethyl isomer to be an effective $CuCl_2$ and $CuSO_4$ extractant, but the cation extractive efficacy of the 5-isomer is hampered by the 3-*tert*-butyl group. Both ligands are found to be selective for $Cl^- > SO_4^{2-}$, following the Hofmeister bias. Further information on anion binding is provided by solid state structures of copper salt complexes, showing that in all cases the copper(II) cation interacts in some way with the anion. Cation extraction is affected significantly by the anion present, with Fe^{III} selectively extracted against Cu^{II} in the presence of SO_4^{2-} which is consistent with cation-anion interactions having great influence on the overall stability of the ligand-metal salt assembly.

Acknowledgements

A lot of people have helped me in my time at Edinburgh, and I really feel lucky to have had the opportunity to study here. Firstly my supervisor Prof. Peter Tasker, who has been a real inspiration and assisted me greatly – all your time, patience and support are much appreciated, and the opportunities you have helped me grasp have been amazing. The fountain of knowledge that is Dr Dave Henderson has been invaluable, and thanks for the proof reading! I have to show gratitude for Fiona McAllister's diligence, as her undergraduate research project initiated the work that makes up half my thesis. Also, the guidance and input of Ron Swart and John Campbell from Cytec Industries has been gratefully received.

Prof. Simon Parsons and his crystallography service have been fantastic, particularly Fraser White and Pete Wood. If it wasn't for you guys my thesis would be a bit thin! Thanks also to Dr Bridgette Duncombe, Andy Stopford, Chris Brooks and Alan Taylor for various mass spectrometry work, John Millar for NMR assistance, Lorna Eades for ICP-OES and Dr Andy Turner at the EaStChem RCF for help with computational work.

Everyone who has been part of the Tasker group has helped make it a fun and friendly place to work, but thanks in particular to Dot, Dave and Ross G for the chat (and the moaning!). While I've been here I've made too many friends to list but thanks to everyone who has propped up KB bar with me on Fridays, everyone who has booted away their frustrations on the astroturf, the boys that take the 9am train to Queen St and who went to Bari, everyone who helped me "run" ChemSoc for a year, and finally cheers to Andy for the billiard breaks and for helping paying my mortgage - now that this is done I want my Wii back!

So many thanks are due to my family for supporting me every step of the way - I couldn't have done it without you guys, and I mean that. Finally, thanks to Claire, for putting up with Ryanair and with me for so long and for coming away with me on our wee adventure. I've loved every minute, and here's to our future.

Contents

Ligands

Ligand	X	Name
L1	H	5-*t*-Butyl-2-hydroxybenzaldehyde oxime
L2	Me	5-*t*-Butyl-2-hydroxy-3-methylbenzaldehyde oxime
L3	*t*-Bu	3,5-di-*t*-Butyl-2-hydroxybenzaldehyde oxime
L4	NO$_2$	5-*t*-Butyl-2-hydroxy-3-nitrobenzaldehyde oxime
L5	Cl	5-*t*-Butyl-3-chloro-2-hydroxybenzaldehyde oxime
L6	Br	3-Bromo-5-*t*-butyl-2-hydroxybenzaldehyde oxime
L7	OMe	5-*t*-Butyl-2-hydroxy-3-methoxybenzaldehyde oxime
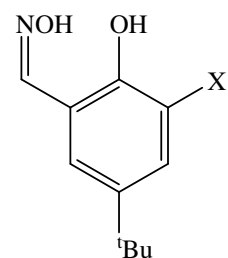
Ligand	X	Name
L8	H	2-Hydroxy-5-*t*-octylbenzaldehyde oxime
L9	NO$_2$	2-Hydroxy-3-nitro-5-*t*-octylbenzaldehyde oxime
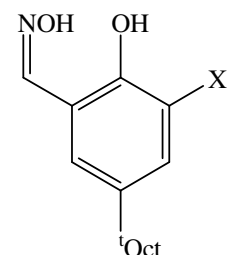
Ligand	X	Name
L10	H	2-Hydroxybenzaldehyde oxime
L11	Me	2-Hydroxy-3-methylbenzaldehyde oxime
L12	*t*-Bu	3-*t*-Butyl-2-hydroxybenzaldehyde oxime
L13	Cl	3-Chloro-2-hydroxybenzaldehyde oxime
L14	Br	3-Bromo-2-hydroxybenzaldehyde oxime
L15	OMe	2-Hydroxy-3-methoxybenzaldehyde oxime
L16	NO$_2$	2-Hydroxy-3-nitrobenzaldehyde oxime
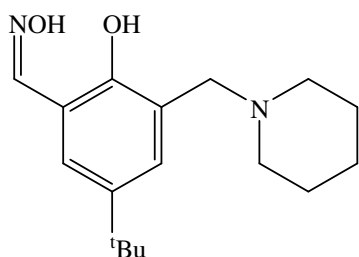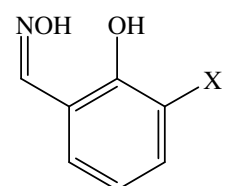
L17: 5-*t*-Butyl-2-hydroxy-3-piperidin-1-ylmethyl benzaldehyde oxime
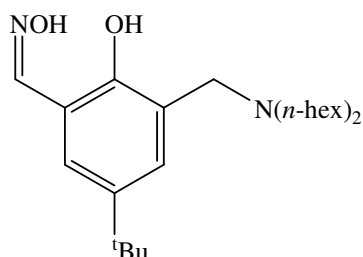
L18: 5-*t*-Butyl-3-dihexylaminomethyl-2-hydroxybenzaldehyde oxime
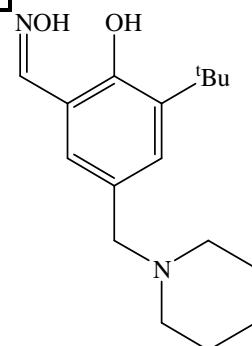
L19: 3-*t*-Butyl-2-hydroxy-5-piperidin-1-ylmethyl benzaldehyde oxime
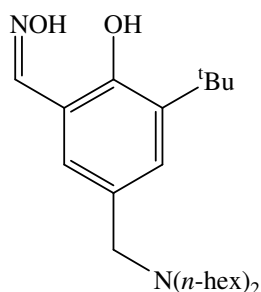
L20: 3-*t*-Butyl-5-dihexylaminomethyl-2-hydroxybenzaldehyde oxime
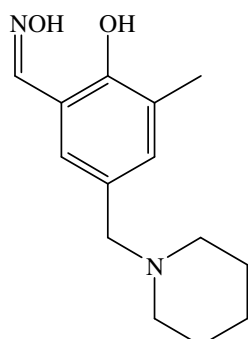
L21: 2-Hydroxy-3-methyl-5-piperidin-1-ylmethyl benzaldehyde oxime
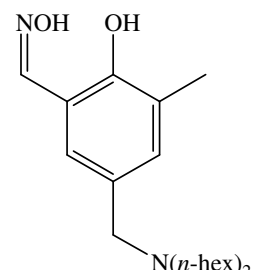
L22: 5-Dihexylaminomethyl-2-hydroxy-3-methyl benzaldehyde oxime

Abbreviations

Δ	change in
δ	chemical shift
°	Degrees
°C	degree centigrade
$	Dollars
<	less than
≤	less than or equal to
>	greater than
≥	greater than or equal to
%	percent
±	plus or minus
~	approximately
√	square route
ν	wavenumber (IR)
λ	wavelength
μ_B	Bohr magneton
1D	one-dimensional
2D	two-dimensional
Å	Angstrom
A	hyperfine coupling constant (EPR)
AD	*Anno Domini*
aq	aqueous phase
anal.	analysis
Ar	aromatic; aryl
B	base
B_0	applied magnetic field
BC	Before Christ
bn	billion
b.p.	boiling point
br	broad (spectroscopy)

BuOH	butan-1-ol
C_6H_5	phenyl
C_9H_{19}	nonyl
calc.	calculated
CID	Collision Induced Dissociation (MS)
cis	cisoid
cm^{-1}	wavenumber (IR)
CSD	Cambridge Structural Database
d	doublet (NMR)
D	distribution coefficient
D2EHPAH	di(2-ethyl hexyl)phosphoric acid
DCE	1,2-dichloroethane
DCM	dichloromethane
DFT	Density Functional Theory
DMSO	dimethylsulfoxide
ΔE	difference in energy
ed.	editor(s)
e.g.	for example
ENDOR	Electron Nuclear Double Resonance
EPR	Electron Paramagnetic Resonance
ESI	electrospray (MS)
et al	*et alli* (and others)
EtO	ethoxy
EtOH	ethanol
EW	electrowinning
FAB	fast atom bombardment (MS)
FTIR	Fourier Transform Infrared
g	gram; gaseous; g-factor, or spectroscopic splitting factor (EPR)
$g\ L^{-1}$	grams per litre
GPa	gigapascal
ΔH	difference in enthalpy
HF	Hartree-Fock

HMT	hexamethylenetetramine
hr	hour
I	nuclear spin quantum number
ICP-OES	inductively coupled plasma optical emission spectroscopy
i.e.	that is
in situ	in the natural place
in vacuo	under vacuum
IR	infrared
K	degree Kelvin
K_a	association constant
$kJ\ mol^{-1}$	kilojoules per mole
l	liquid
m	multiplet (NMR), metre
m	*meta*
M	molar
Me	methyl
MeO	methoxy
MeOH	methanol
MH^+	positively charged parent molecular ion (MS)
MHz	frequency (NMR)
μL	microlitre
mg	milligram
ml	millilitre
mm	millimetre
mm Hg	pressure
mmol	millimole
mol	mole
$mol\ dm^{-3}$	mole per litre
MP2	truncated second order Moller Plesset
MS	mass spectrometry
M_s	molecular spin number
m/z	mass to charge ratio

n	normal
NOBA	3-nitrobenzylalcohol
nm	nanometres (10^{-9} m)
NMR	nuclear magnetic resonance
o	*ortho*
obs.	observed
org	organic phase
p	*para*
P50	5-nonyl-2-hydroxybenzaldehyde oxime
PGMs	platinum group metals
pH	$-\log_{10}[H^+]$
$pH_{0.5}$	pH when D = 0
pK_a	$-\log_{10}K_a$
pls	pregnant leach solution
pp.	inclusive pages
ppm	parts per million
py	pyridine
q	quartet (NMR)
s	singlet (NMR); strong (IR); second; solid
salen	*N,N'*-ethylenebis(salicylideneaminato)
SX	solvent extraction
t	triplet (NMR)
t	tertiary
T	temperature
^{t}Bu	tertiary butyl
TBP	tri-*n*-butylphosphate
tert	tertiary
TFA	trifluoroacetic acid
TFA^-	trifluoroacetate anion
THF	tetrahydrofuran
^{t}Oct	tertiary octyl
TPSSTPSS	DFT exchange function of Tao, Perdew, Staroverov and Scuseria

trans	transoid
TXIB	2,2,4-trimethyl-1,3-pentanediol diisobutyrate
UV-Vis	ultraviolet-visible
via	by way of
Vol.	volume
vs.	versus
XRD	X-Ray Diffraction

CHAPTER 1

INTRODUCTION

Contents

1.1 Thesis Aims

The underlying principle of the thesis is the modification of simple phenolic oximes to affect their functionality, in order to widen their applicability in the field of metal extraction. Two main themes are investigated: the tuning of copper extraction strength of phenolic oximes by introduction of substituents in the 3-position, and the inclusion of an anion binding site to yield polytopic ligands capable of extracting and transporting both a metal cation and its attendant anion(s) across a hydrometallurgical circuit. This chapter gives an introduction to the chemistry and uses of copper, the current methods of recovering copper from its constituent ores, details the various reagents involved in its recovery and the principles behind metal salt extraction.

1.2 Copper

Copper is the 29th element of the periodic table, is a metal and is often found in its native form. Copper has a relative abundance of 68 ppm in the Earth's crust, and approximately 50% of copper is found as the ore chalcopyrite, $CuFeS_2$. A ductile, malleable and corrosion resistant metal, copper has many properties which make it attractive to human usage, *e.g.* it has an electrical conductivity second only to that of silver.[1] Copper also forms many useful alloys with other metals, for example bronze (with tin) and brass (with zinc) which are harder and more durable materials than the pure metal.[2]

Artefacts dating from over 10,000 years ago are known, with early copper use based around ritual and decorative items and also currency.[1, 3] The discovery of pyrometallurgical processes to liberate copper from its ores approximately 6000 years ago is accompanied by an increase in the copper concentrations of ice cores from Greenland, and these values can be used to estimate global copper production until the present.[4] A steady increase in production through the Bronze Age (3000-500 BC) is noted, with subsequent peaks corresponding to the Roman Empire (250-

350 AD) and the Sung Dynasty of China (960-1127 AD). A massive increase occurs with the advent of the industrial revolution, which is sustained until the present day (Figure 1.1).[5]
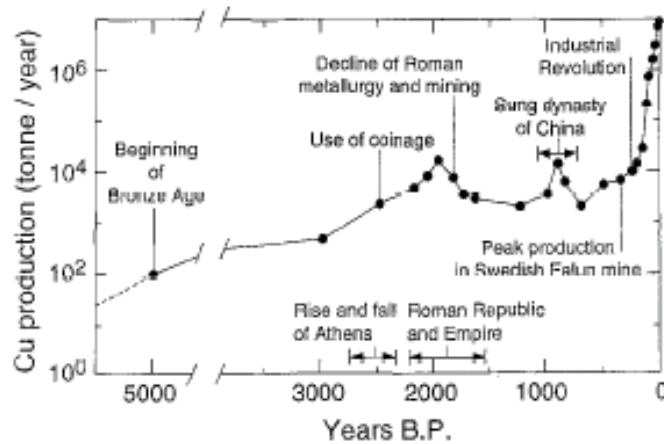
Figure 1.1: Copper production from 5500 years ago until the present day.[5]

In the modern age, copper is used extensively in its pure form in electrical applications, due to its high electrical conductivity. As a major component of alloys, it is a vital part of modern day infrastructure, and is used in piping, major industrial installations, transport and as coinage. Compounds of copper also find application as catalysts and fungicides.[2, 6]

In the 21st Century the demand for copper has experienced an extraordinary resurgence, and prices reached record highs in 2007. The rapid increase in value of copper and other metals has resulted in a burgeoning criminal trade in the material, with thefts of large quantities of copper, lead, aluminium and steel becoming common. Thieves have even attempted to steal live electrical cables, but were fortunate enough to be unsuccessful.[7] 15 million tonnes of copper were produced in 2006, falling short of the global consumption of 17 million tonnes, with demand fuelled by the growing industrialisation of China and India.[2, 8] This demand has led to the commencement of many new projects around the world, and global copper supply is expected to meet demand within the decade and so stabilise the price of copper.[8]

Clearly, copper is of great importance to the continuing development of the human race, and the economies of scale dictate that any improvements in the efficiency of copper processing may result in considerable increases in profits.

1.3   Extractive Metallurgy

In their natural state, metals are found as low concentration, mixed metal ores. Early Earth's atmospheric conditions involved an abundance of SO_2 and CO_2, and consequently metal ores formed as sulfidic ores. The advent of plant life and photosynthesis 2.5 bn years ago lead to oxygen becoming a major component of the atmosphere. Exposed metal sulfides were therefore oxidised to metal oxides, leaving metal deposits with three layers: a superficial oxidic layer, a mixed oxide/sulfide middle layer (transition ore) and an inner sulfidic layer.[4, 9]

In order to purify the metals of value, four steps must be taken:

- *concentration* of the metals of value,
- *separation* from the unwanted metals of the ore,
- *reduction* of the oxidised metals of value, and
- *refinement* to a purity suitable for commercial use.

These four steps comprise extractive metallurgy,[10] a technique which, in the case of copper, is known to have existed over 6000 years ago.[4, 9]

1.4   Pyrometallurgy

Pyrometallurgy is defined as the technique of separating metals from their ores by oxidative and reductive processes under the application of heat.[11] Dating back to 4000 BC,[4, 9] the technique originally involved heating ore to a high temperature in the presence of a reducing agent, often carbon, to generate the pure metal. Formation

of a thermodynamically stable by-product during the reduction, *e.g.* CO or CO_2, is the driving force behind the reaction. When processing sulfidic ores, in some cases roasting the metal sulfides in air produces metal oxides and SO_2, driving forward the reaction due to the enthalpic favourability of its formation:

Equation 1.1 $\qquad\qquad MS + 3/2\ O_2 \longrightarrow MO + SO_2$

Equation 1.2 $\qquad\qquad MO + C \longrightarrow M^0 + CO$

The oxides are then smelted in the presence of carbon to give the metal.[9] In some cases, heat alone is enough to liberate the metal.

Modern pyrometallurgical applications are massive scale, profitable operations which have benefited from years of technological refinement and subsequent reductions in operation costs.[12] The recovery of copper from sulfidic ores (*e.g.* chalcopyrite) is an example of this (Figure 1.2).
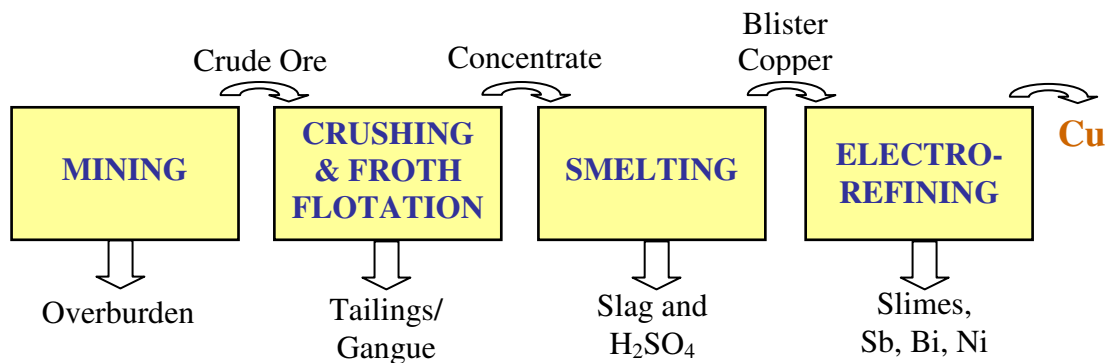
Figure 1.2: Flowsheet for the extraction of copper from sulfidic ores by pyrometallurgy.

Firstly, the ore is mined and crushed, then milled with water to produce ore particles approximately 0.25 mm in diameter.[3] These particles are subjected to a concentration process known as froth flotation, which separates the sulfide mineral particles from the silicate waste minerals, or gangue. Froth flotation involves the use of collectors or flotation agents, which attach themselves to the desired hydrophilic ore particles and turn them into hydrophobic solids. Rapid agitation of the mixture produces an oily froth containing these metal-bearing particles, which is removed

from the separator, and the wetted gangue materials are drawn off from the bottom of the tank.[10]

This copper concentrate is removed and subjected to a two stage smelting process at 1300 °C. A copper "matte" is generated in the first step, by heating the concentrate with sand (flux) and air in a blast furnace to yield Cu_2S, a dense solid which is drawn off from the base of the furnace. Addition of flux removes iron as a silicaceous slag, which floats to the surface of the mixture, and sulfur dioxide is vented at the top of the smelter:[13]

Equation 1.3 $\quad\quad 2CuFeS_2 + 2O_2 \longrightarrow Cu_2S + 2FeO + 2SO_2$

Equation 1.4 $\quad\quad 2FeO + SiO_2 \longrightarrow 2Fe_2SiO_4$
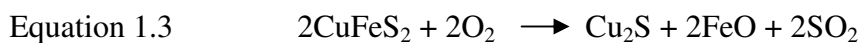
The second step involves further heating, converting the copper matte by controlled oxidation with air, producing further sulfur dioxide.[3]

Equation 1.5 $\quad\quad Cu_2S + O_2 \longrightarrow 2Cu^0 + SO_2$
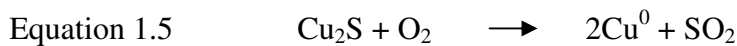
The product is known as "blister copper", which is 98% pure, contains impurities such as silver and gold and must be further refined by electrochemical methods. "Blister anodes" are cast and purified in an electrolytic cell with an acidic copper sulfate electrolyte and a stainless steel cathode. On application of current copper is oxidised and dissolved at the anode, reduced at the cathode, where it is deposited, and the cathodes can be sold directly. The redox equations for the process show its simplicity:

Equation 1.6 $\quad\quad Cu^0 \longrightarrow Cu^{2+} + 2e^- \quad$ (anode)

Equation 1.7 $\quad\quad Cu^{2+} + 2e^- \longrightarrow Cu^0 \quad\quad$ (cathode)
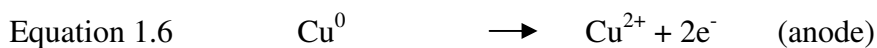
Any impurities present in the blister copper fall to the bottom of the cell beneath the anode, and are known as anode slimes. These slimes contain economically important metals (Ag, Au) which can be recovered and processed separately.[3]

While pyrometallurgy is an important and relevant technique for the processing of copper ores, there are reasons to pursue alternative methods, including:

- The capital cost of smelting is very high, at $3000-5000 per annual ton of copper smelted.
- Smelters are poor in treating concentrates containing deleterious impurities.
- Precious metal by-products are often floated with copper, and their separation by pyrometallurgy is often slow and costly.[14]

Hydrometallurgy is a modern alternative to pyrometallurgy which may overcome many of these issues, and is discussed in detail in the next section.

1.5   Hydrometallurgy

Hydrometallurgy can be defined as "the use of wet (aqueous) chemistry for the recovery of metals".[15]   The process involves leaching metal ions from the ore into solution, followed by separation and purification by precipitation, cementation, electrowinning, reverse osmosis, ion exchange methods or solvent extraction.[16]

In contrast to pyrometallurgy the technique is relatively modern, with its first major industrial application the purification of gold by the cyanidation process dating from 1887.[15, 17]   The dissolution of gold depends on its oxidation, which is favourable when it is complexed with the cyanide ligand, CN^-:

Equation 1.8 $2Au_{(s)} + O_2 + 4CN^- + 2H_2O \longrightarrow 2[Au(CN)_2]^- + H_2O_2 + 2OH^-$
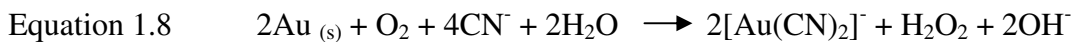
As the undesired silicate materials in the surrounding material do not dissolve, filtration and separation yields a solution of the pure gold complex, and the gold can be precipitated with another reactive metal, for example zinc,[9] or purified by electrolysis (electrowon).[18]

Further advances in the field include the Bayer process for recovering alumina (Al_2O_3) by pressure leaching of bauxite with sodium hydroxide followed by crystallisation of $Al(OH)_3$ and calcining to alumina (1892), and also the introduction of leach/electrowinning processes for the recovery of copper in Chile in 1912. This involved the leaching of copper from weathered pyrite ore and its subsequent purification by electrolysis, an important precursor to the current hydrometallurgical extractive processes for copper.[15]

The development of solvent extraction techniques prompted a massive increase in industrial hydrometallurgical applications. Solvent extraction is based on a two phase, liquid-liquid equilibrium and is used to separate and concentrate species from mixtures.[10] Since its introduction in the 1940's for uranium extraction[19] it has proved to be a robust yet flexible technique for recovery of metals from aqueous acidic leach solutions, including thorium, uranium,[19] platinum group metals (PGMs),[20] zinc,[21, 22] nickel and cobalt,[23] but particularly copper.[16] A typical flowsheet for a hydrometallurgical process is detailed in Figure 1.3.
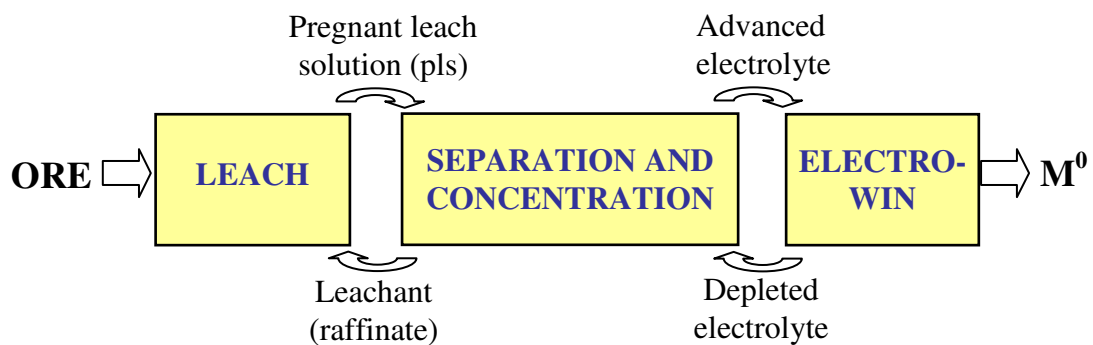
Figure 1.3: A typical flowsheet for the hydrometallurgical recovery of metals.

The metals of value are released from the ore into an aqueous media by the leaching process, which generates a mixed metal aqueous solution known as the pregnant leach solution (pls). Selective binding agents in organic media are introduced to the pls, with the target species binding to the extractant, moving into the organic phase and regenerating the leachant, also known as the raffinate. On separation of the phases, the target species is then stripped from the extractant into a concentrated,

separate aqueous phase, the advanced electrolyte, and the extractant solution is subsequently reused. Electrolysis produces pure metal cathodes and the depleted electrolyte is reused to strip further cycles of loaded extractant.[10] The extractants used in the separation and concentration step have varying structures and functions but can be sub-divided into three distinct groups: solvating reagents, anion exchange reagents and cation exchange reagents.[10, 15]

Solvating reagents are neutral species which impart stability and organic phase solubility to metal salts *via* the displacement of water molecules in the coordination sphere.[10] An example with major commercial relevance is the extraction of uranyl nitrate by tri-*n*-butylphosphate (TBP), which occurs by the equilibrium:

Equation 1.9 $UO_2(NO_3)_2 + 2\textbf{TBP}_{(org)} \rightleftharpoons [UO_2(NO_3)_2(\textbf{TBP})_2]_{(org)}$

Both the TBP extractant and the nitrate anion address the inner coordination sphere of the U^{IV} cation, and the extraction equilibrium can be manipulated by careful control of the aqueous phase nitrate concentration.[10, 19]

Anion exchange extractants are capable of binding to a metal anion, *e.g.* a chlorometallate, and extracting it into organic media.[11] Tetraalkylammonium salts can extract metal anions by an ion pair mechanism, *e.g.* $FeCl_4^-$:

Equation 1.10 $FeCl_4^- + \textbf{R}_4\textbf{NCl}_{(org)} \rightleftharpoons [\textbf{R}_4\textbf{NFeCl}_4]_{(org)} + Cl^-$

Trialkylamine reagents are used industrially in the recovery of platinum group metals (PGMs) as their chlorometallate anions from acidic media, which occurs *via* a pH-dependent extraction equilibrium:

Equation 1.11 $\quad PtCl_6{}^{2-} + 2R_3N_{(org)} + 2HCl \rightleftharpoons [(R_3NH)_2PtCl_6]_{(org)} + 2Cl^-$

The kinetic inertness of PGMs ensures chloride ligand substitution does not occur, however, the dearth of information on actual industrial processes means design of selective extractants to be utilised in this area is challenging.[20]

Cation exchange extractants address the inner coordination sphere of the metal to generate neutral complexes which are soluble in water-immiscible media. Acidic ligands are normally employed which generate conjugate bases capable of binding to metal cations:

Equation 1.12 $\qquad nLH_{(org)} + M^{n+} \rightleftharpoons [ML_n]_{(org)} + nH^+$
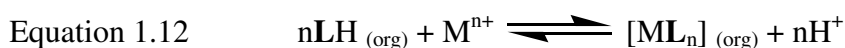
As protons are released in the binding of the metal cation, the extraction equilibrium can be controlled by pH. Phenolic oxime cation exchange reagents are used extensively in the recovery of copper from oxidic ores,[16] and shall be detailed in the next section.

1.6 Copper(II) Recovery by Phenolic Oxime Extractants

1.6.1 Copper(II) Extraction from Oxidic Ores

Between 20%[8] and 30%[24] of the world's copper is recovered using hydrometallurgical methods involving phenolic oxime extractants. A simplified flowsheet detailing the hydrometallurgical production of copper from oxidic ores is shown overleaf in Figure 1.4. The leach step involves the dissolution of copper with sulfuric acid, achieved by passing the acid through a "heap pad" of oxidic ore. This transfers most of the metals in the ore into the aqueous pls in which Cu^{II} is present at concentrations of usually 3-10 gL^{-1}, along with high concentrations of Fe^{II} and Fe^{III}.[10]

- Leach: $CuO_{(s)} + H_2SO_4 \longrightarrow CuSO_4 + H_2O$
- Extract: $CuSO_4 + 2LH_{(org)} \longrightarrow CuL_{2\,(org)} + H_2SO_4$
- Strip: $CuL_{2\,(org)} + H_2SO_4 \longrightarrow CuSO_4 + 2LH_{(org)}$
- Electrowin: $CuSO_4 + H_2O \longrightarrow Cu_{(s)} + \tfrac{1}{2}O_{2\,(g)} + H_2SO_4$

- Overall: $\mathbf{CuO_{(s)}} \longrightarrow \mathbf{Cu_{(s)} + \tfrac{1}{2}O_{2\,(g)}}$
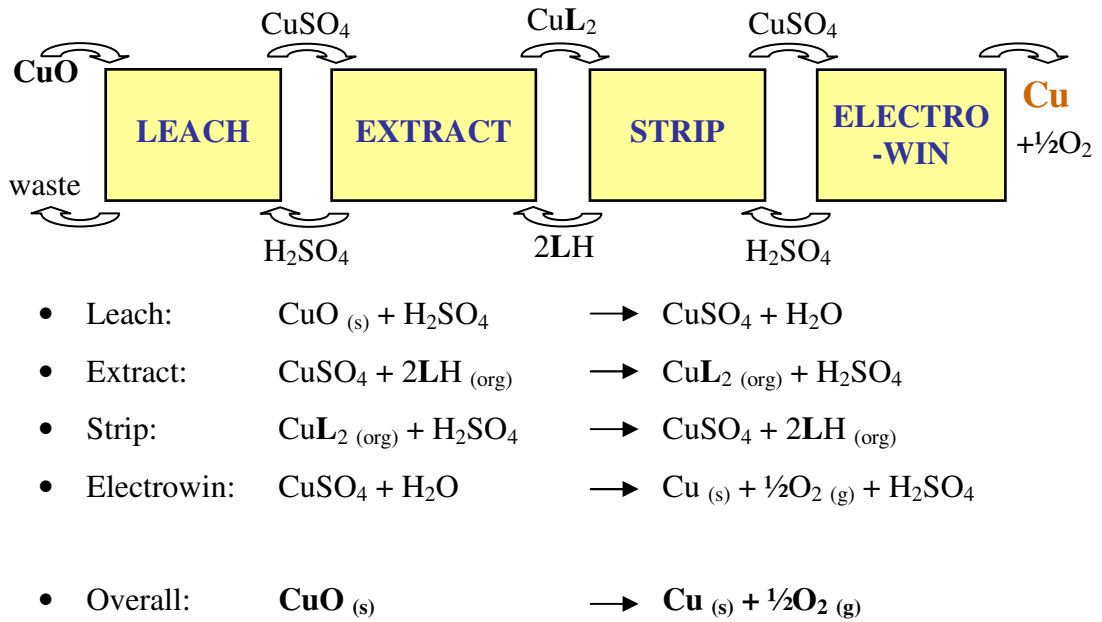
Figure 1.4: Recovery of copper from oxidic ores by hydrometallurgy.

A cation exchange reagent is utilised in the extraction step, which imparts stability and solubility of the Cu^{II} ion in the organic phase, normally kerosene,[15] by forming a neutral metal-ligand complex:

Equation 1.13 $\qquad Cu^{2+} + 2LH_{(org)} \rightleftharpoons [CuL_2]_{(org)} + 2H^+$

As the equilibrium is pH-dependent, with the acidic extractant **LH** loaded at higher pH and stripped at lower pH values, it is termed a "pH-swing" process. By contacting the organic phase with a low pH aqueous sulfate solution, the Cu^{II} ions are stripped into the aqueous phase as a pure copper sulfate electrolyte, and the extractant is regenerated in the organic phase for continuous load/strip cycles. Subsequent electrowinning generates conductivity grade copper cathode products and sulfuric acid to be reused in the stripping stage.[16]

The equations in Figure 1.4 illustrate the excellent materials balance of the process. This balance ensures both its commercial and environmental success as a method for recovering copper.[24]

1.6.2   Phenolic Oxime Extractants

The extractants used in the process described in Section 1.6.1 are based on phenolic oximes, the commercial variants of which are detailed in Figure 1.5.

R	R'	R''	Commercial Name
C_9H_{19}	H	H	P50
C_9H_{19}	$C_6H_5CH_2$	H	P17
C_9H_{19}	CH_3	H	LIX84
$C_{12}H_{25}$	C_6H_5	H	LIX64
C_9H_{19}	C_6H_5	H	HS-LIX 65N
C_9H_{19}	C_6H_5	Cl	LIX70
$C_{12}H_{25}$	H	H	LIX860
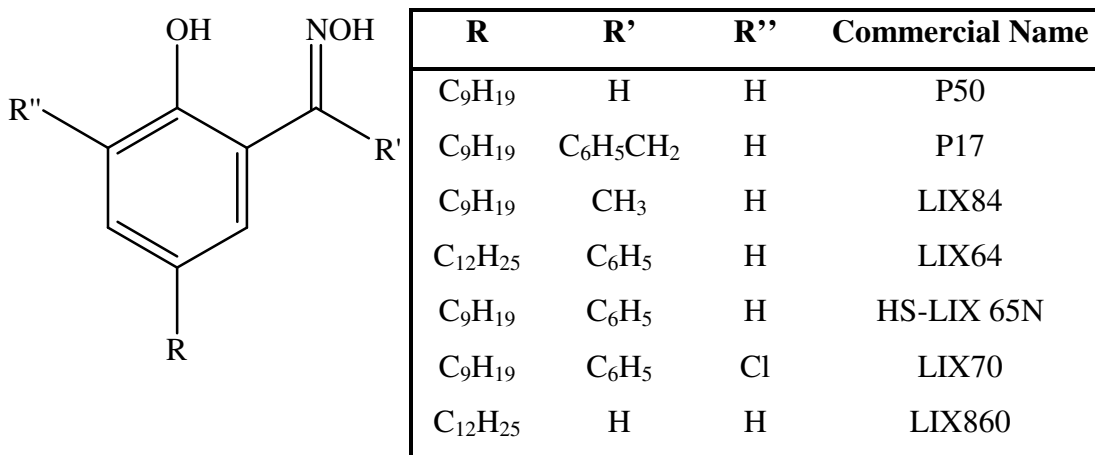
Figure 1.5: Structures of some phenolic oximes used commercially.

The highly branched alkyl groups located in the R-position impart solubility in the hydrocarbon diluents preferred in industry, whilst the groups in the R' position can tune the strength of the reagent; ketoximes are slightly weaker extractants than aldoximes and so operate at higher temperatures and pH values.[24] The group in the R" position can also have an effect on extraction strength,[25] and this will be discussed in detail in Section 1.7. Deprotonation of the phenolic group allows metal complexation *via* the "pH swing" controlled extraction equilibrium shown in Equation 1.13.

The strength and selectivity of Cu^{II} extraction by phenolic oximes arises from features seen in the structures of the neutral 2:1 complexes formed. Cu^{II} complexes of phenolic oximes show a square planar coordination environment containing a 14-membered *pseudo*macrocyclic hydrogen bonded array (Figure 1.6), with the H-bonds between the oximic H and phenolate O atoms thought to impart additional stability to the complex.[26] Some phenolic oximes display this H-bonding array in solution when no copper is present, demonstrating their preorganisation for binding (Figure 1.6).[27]

13
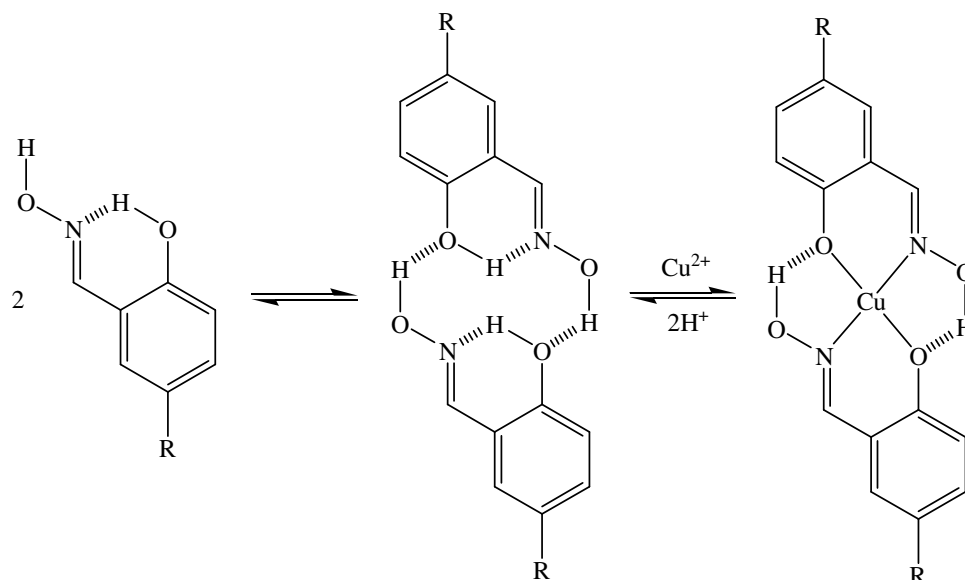
Figure 1.6: Preorganisation of phenolic oximes for *pseudo*macrocyclic Cu[II] complex formation. The smaller inner ring defined by H-bonding in the free ligand dimer is defined[28, 29] by the graph set descriptor $R_4^4(10)$.

Their selectivity for Cu[II] is thought to arise from the goodness-of-fit of the cavity size (the mean distance of the donor atoms to the metal centre) for the Cu[II] ion. Determination of the strength and selectivity of extractants is achieved by measurement of the $pH_{0.5}$ – the pH at which half the ligand in the organic phase is loaded with the appropriate metal ion during extraction.[16] Plotting pH against the percentage of copper in the organic phase gives a characteristic graph, known as an S-curve due to its shape, and will yield the $pH_{0.5}$ value. Typically, Cu[II] extractants have $pH_{0.5}$ values of 0-2[30] which are ideal for optimum extraction from oxidic ores, where heap leaching generates aqueous solutions which usually have pH 1.5-2.3.[16] Figure 1.7 illustrates the selectivity of the industrial extractant P50 (2-hydroxy-5-nonylbenzaldehyde oxime) with the higher $pH_{0.5}$ values for other metals enhancing Cu[II] selectivity.[16]
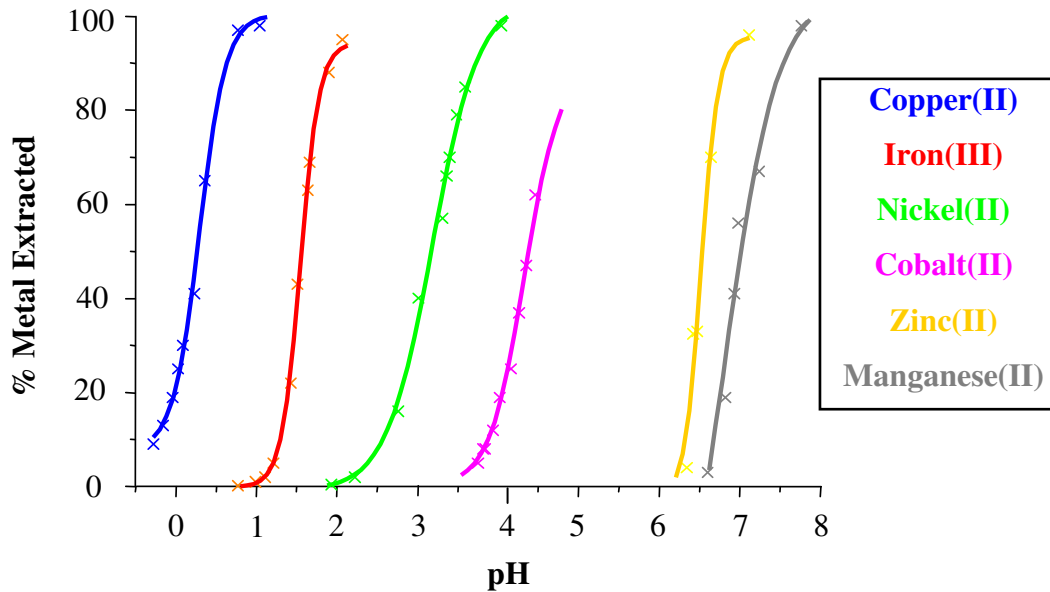
Figure 1.7: pH loading profiles for a range of metals using P50 in kerosene.[16]

The properties of phenolic oximes discussed in this section ensure that they are very successful and are almost ideal technocommercially for the processing of oxidic copper ores.

1.6.3 The Benefits of Hydrometallurgy in the Processing of Copper

The massive increases in copper production in the 20th century (Section 1.2) have led to the necessity of processing lower grade ores, *i.e.* those with less copper content, in order to satisfy demand. In the Middle Ages, the copper content of exploited ores averaged 8%, whereas by the mid 1990s this value had decreased to an average of 0.9% copper content.[16] Hydrometallurgy is well suited to processing lower grade ores, depending on the leach technique, and so it is preferable to pyrometallurgy which requires large amounts of energy to melt and remove the gangue minerals.[13, 31]

A recent article on metal stocks and the sustainability of metal production by Graedel *et al*[6] highlights the importance of recycling metals to ensure future supplies meet demand, with an estimated 34% of the copper mined in the 20th Century now in landfill. Pyrometallurgical treatment of complex metal sources, such as alloys and

other recycled materials, is not suitable or economically viable and so hydrometallurgy is becoming increasingly important in the production of copper from such sources. Graedel also estimates that ~18% of the copper mined in the 20th century was lost as tailings and other wastes during milling and smelting,[6] indicating not only the inefficiency of some pyrometallurgical installations but the potential sources of copper for hydrometallurgical plants, which are suited to the processing of wastes such as slags,[32] tailings,[33] post-flotation waste and mine waters.[16]

Further advantages originate in the versatility and intelligent flowsheet design of hydrometallurgical plants.[13, 31] The materials balance attained when processing oxidic ores (Section 1.6.1) dramatically reduces the consumption of raw materials such as SiO_2 (flux) associated with smelting, whilst also ensuring that the generation of wastes such as slag, toxic heavy metals and SO_2 is kept to a minimum. However, sulfur dioxide can be fixed as sulfuric acid and new technology is leading to a large decrease in emissions, with ~20% of the sulfur consumed globally originating as sulfuric acid from base metal smelters.[8] Hydrometallurgy is also much less energy intensive, lowering both costs and the emission of greenhouse gases.[15] Hydrometallurgical installations are also much smaller, allowing *in situ* processing of the metals in close proximity to the mine site, reducing transport costs and emissions.[10, 15]

Both the increased energy efficiency and reduced levels of waste make hydrometallurgy a much more attractive proposition than traditional pyrometallurgical methods. In a world increasingly concerned with "green" technologies and environmental safety, the development of newer, cleaner processes is paramount for both ecological and economical reasons. Economic factors also ensure that hydrometallurgy, with its versatility in processing both low grade copper ores and recycled materials, has long-term commercial viability.[24]

1.7 Substitution Effects on Copper(II) Binding Strength

Currently, the tuning of the extraction strength of a phenolic oxime formulation is achieved by reagent blending and "modification",[16] which will be discussed in Chapter 2. There have been few systematic studies on the effects of benzene-ring substitution on strength and selectivity. The work presented in Chapters 2 and 3 deals with 3-substitution (X in Figure 1.8).
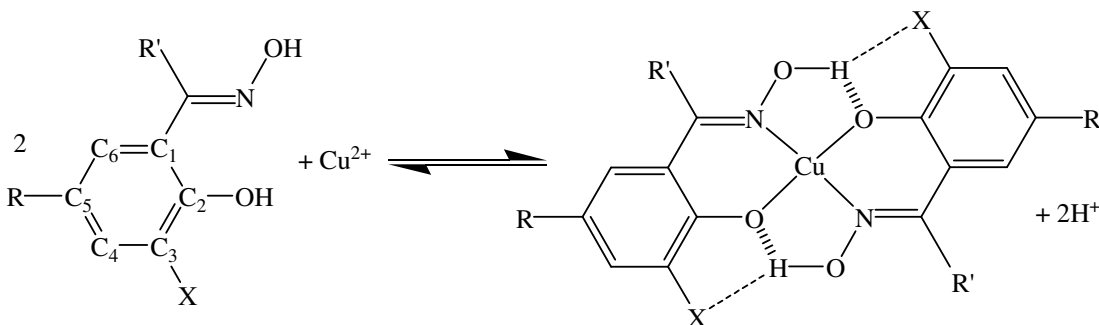
Figure 1.8: 5-Alkylsubstituted salicylaldoximes derivatives used in copper recovery, showing potential interaction with a 3-substituent (X).

Burger *et al*[34] showed in a spectrophotomeric study of 5-substituted salicylaldoximes that a nucleophilic (*i.e.* potentially electron-donating) substituent increases both the pK_a of the phenol group and overall complex formation constant, thought to be due to the effect of the substituent on the ligands' σ-donating abilities. This electronic effect is expected to persist when similar substituents are located in the 3-position. It is also possible to vary extractive efficacy by substitution in the 3-position; 3-nitro-2-hydroxy-5-nonylbenzophenone oxime ($R = C_9H_{19}$, $R' = C_6H_5$, $X = NO_2$ in Figure 1.8) operates in a lower pH range than its unsubstituted analogue. In this study, Parrish *et al*[35] concluded that substituents affect ligand properties in many ways, which makes prediction of extractant strength difficult.

In 1971, General Mills introduced the LIX70™ extractant, with the active component being 3-chloro-2-hydroxy-5-nonylbenzophenone oxime ($R = C_9H_{19}$, $R' = C_6H_5$, $X = Cl$ in Figure 1.8). The 3-chloro group resulted in high extractant strength,

providing a reagent for copper recovery from highly acidic and chloridic media.[36] In practise, the reagent has only been used as a component of extractant blends.[37-40]

To date, an empirical approach has been used within the industry to study the effect of substitution on extractant strength, giving the overall view that increasing phenol acidity of phenolic oxime ligands enhance their extractive efficiency.[25] These conclusions have been made without a systematic study and without consideration of other substituent effects.

In addition to influencing the electronic properties of the donor atoms which bond to the copper atom, substituents in the 3-position could also have a significant effect on the interligand hydrogen bonding (Figure 1.8) which is thought to contribute to the stability of resulting *pseudo*macrocyclic complexes.[41] X-groups with H-bond accepting properties could promote formation of bifurcated H-bonds which are expected to stabilise the complex,[42] but bulky groups could also weaken the oximic H to phenolate H-bond by steric interference. Chapters 2 and 3 consider each effect and attempt to elucidate their significance in copper extraction.

1.8 Extraction of Metal Salts

1.8.1 Extraction of Copper from Sulfidic Ores

An area where pyrometallurgy still holds key advantages over hydrometallurgy is the processing of sulfidic copper ores. Pyrometallurgical processing of these ores can still be more economical and carried out in larger scale than hydrometallurgical methods,[16] and the materials balances obtained in hydrometallurgical circuits are not as advantageous as in the processing of oxidic ores. Conventional sulfuric acid leaching does not effectively leach sulfidic copper and so an oxidative leaching process is used to generate a copper sulfate pls. When this solution is extracted with a cation exchange reagent, such as a phenolic oxime, one mole of sulfuric acid is

generated per mole of copper extracted and is not consumed in the leach stage (Figure 1.9).
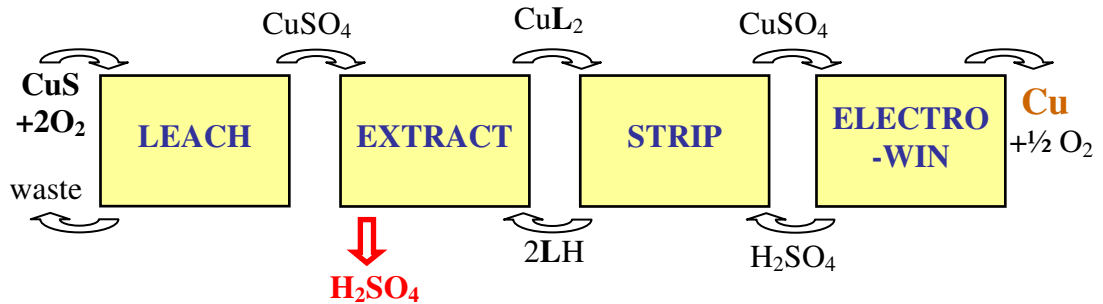
- Leach: $CuS_{(s)} + 2O_{2\ (g)} \longrightarrow CuSO_4$
- Extract: $CuSO_4 + 2LH_{(org)} \longrightarrow CuL_{2\ (org)} + \mathbf{H_2SO_4}$
- Strip: $CuL_{2\ (org)} + H_2SO_4 \longrightarrow CuSO_4 + 2LH_{(org)}$
- Electrowin: $CuSO_4 + H_2O \longrightarrow Cu_{(s)} + ½O_{2\ (g)} + H_2SO_4$

- **Overall:** $\mathbf{CuS_{(s)} + 3/2\,O_{2\ (g)} + H_2O} \longrightarrow \mathbf{Cu_{(s)} + H_2SO_4}$

Figure 1.9: Sulfuric acid build up in the front end of the circuit during hydrometallurgical processing of sulfidic copper ores.

This acid build up in the front end of the circuit means either an expensive acid recovery process, or neutralisation, which generates a salt waste that must be removed, is required. These are undesirable and expensive, and the detrimental effect on the materials balance makes the process uneconomical.[43]

To overcome this problem, the sulfuric acid could be transported across the circuit in the form of sulfate. Polytopic ligands containing separate cation and anion binding sites can extract both a metal cation and its attendant anion(s), *i.e.* a metal *salt*, into a water-immiscible solvent. Combining a deprotonatable cation binding site with a protonatable anion binding site gives a polytopic ligand capable of binding a metal salt in a zwitterionic form, allowing both cation and anion binding to be controlled by pH (Figure 1.10).[44]
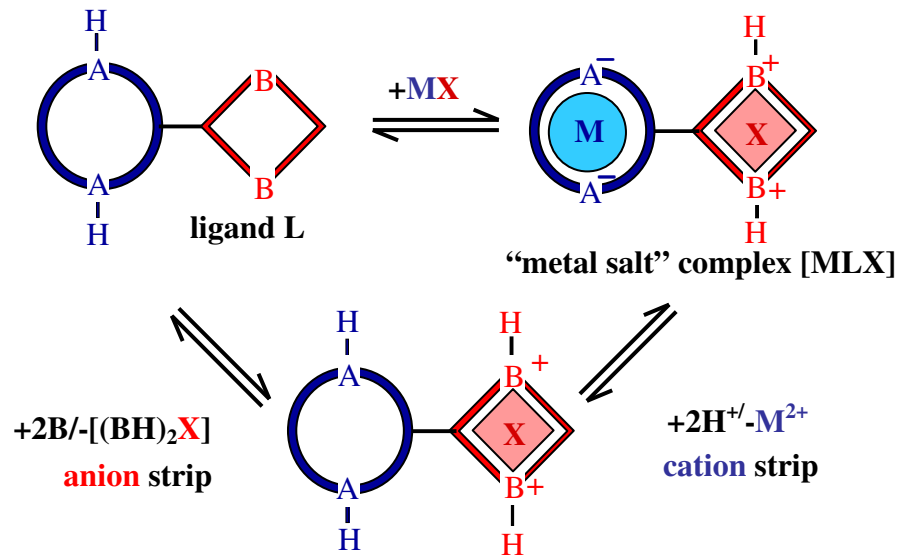
Figure 1.10: Schematic diagram showing metal salt extraction and sequential stripping of a ditopic ligand.

As with the conventional "pH-swing" reagents, sulfuric acid could be used to strip the cation, producing an aqueous solution of pure metal sulfate (Scheme 1.1). Anion-stripping would utilise an aqueous base (B), generating a salt [BH]₂SO₄ which, with appropriate systems-engineering, could be removed as a saleable by-product. Finally, electrowinning would produce electrical grade copper and sulfuric acid, to be reused in the stripping stage.

Leach:	$MS_{(s)} + 2O_{2\ (g)}$	$\longrightarrow$	MSO_4
Extract:	$MSO_4 + \mathbf{L}_{(org)}$	$\longrightarrow$	$[\mathbf{ML}SO_4]_{(org)}$
Cation Strip:	$[\mathbf{ML}SO_4]_{(org)} + H_2SO_4$	$\longrightarrow$	$MSO_4 + [\mathbf{L}H_2]SO_{4\ (org)}$
Anion Strip:	$[\mathbf{L}H_2]SO_{4\ (org)} + 2B$	$\longrightarrow$	$\mathbf{L}_{(org)} + [BH]_2SO_4$
Electrowin:	$MSO_4\ + H_2O$	$\longrightarrow$	$M_{(s)} + \tfrac{1}{2}O_{2\ (g)} + H_2SO_4$

Overall: $\quad \mathbf{MS_{(s)} + 3/2O_{2\ (g)} + H_2O + 2B} \longrightarrow \mathbf{M_{(s)} + [BH]_2SO_4}$
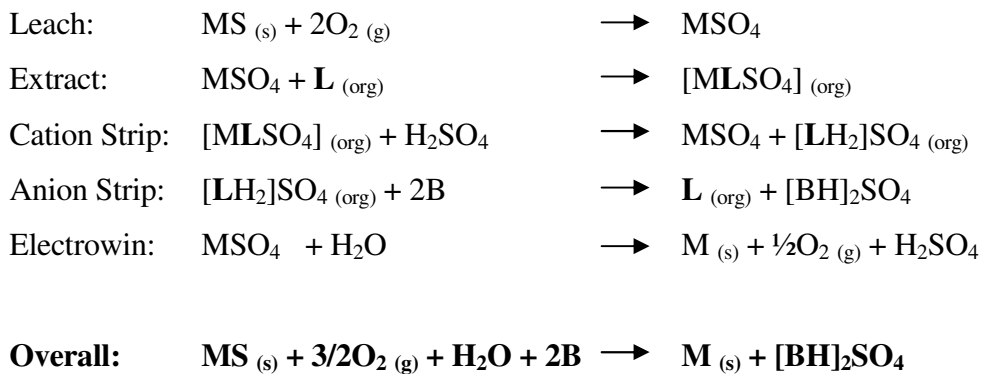
Scheme 1.1: Materials balance for copper recovery with a metal salt extractant

The overall materials balance for this flowsheet is much enhanced, and solves the problem of sulfuric acid build-up in the front end of the circuit, provided a commercially available sulfate salt is generated.[45]   Some examples of metal salt extractants are detailed in Chapter 4.

1.8.2   Leaching Sulfidic Ores

Improvement of leaching techniques for sulfidic copper ores such as chalcopyrite has received much attention in recent years, with a number of new leaching processes currently in commercial operation or in the final stages of development,[46] and such processes generate feeds which are suited to processing by metal salt extractants.

The Total Pressure Oxidation[47] process is currently in operation at the Bagdad plant in Arizona and involves high temperature and pressure oxidation conditions, which oxidise all sulfides to sulfates and sulfuric acid:

Equation 1.14 $\qquad CuFeS_2 + O_2 + 2H_2SO_4 \longrightarrow CuSO_4 + FeSO_4 + 2H_2O + 2S$
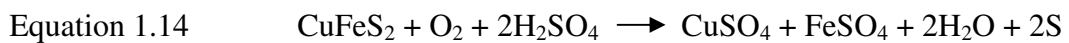
Around 16,000 tonnes of copper per annum are leached in this way at the installation, which also generates sulfuric acid to be used in alternative leach processes:

Equation 1.15 $\qquad S + H_2O + 3/2O_2 \longrightarrow H_2SO_4$
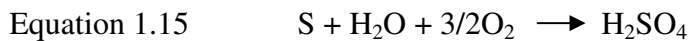
Bioleaching is finding a niche in the leaching of copper-gold concentrates which have high arsenic levels and no nearby heap leach sites available for excess acid consumption.[46]   The BioCOP™ process developed by BHP Billiton uses thermophilic bacteria to oxidise sulfidic minerals to metal sulfates at temperatures of 65-80 °C.[48]

The redox chemistry is similar to that of ferric ion oxidation in acidic solutions:

Equation 1.16 $\qquad CuFeS_2 + 4Fe^{3+} \longrightarrow 5Fe^{2+} + Cu^{2+} + 2S$
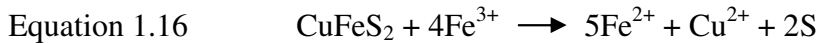
The microbes catalytically oxidise the ferrous ion back to the ferric ion, regenerating the oxidant whilst oxidising sulfur to sulfate:

Equation 1.17 $\qquad 2Fe^{2+} + 2H^+ + \frac{1}{2}O_2 \longrightarrow 2Fe^{3+} + H_2O$

Equation 1.18 $\qquad 2S + 3O_2 + 2H_2O \longrightarrow 2H_2SO_4$
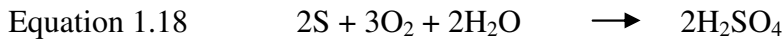
Commercial application of this process at the Chiquicamata mine in Chile produces 20,000 tonnes of copper per annum, from a leach solution containing 25 gL^{-1} copper. An excess of sulfuric acid is again produced, but less is available for secondary use due to necessary neutralisation during the process.[49]

The ferric/ferrous ion redox couple is also utilised in the oxidative ferric leach stage of the CUPREX process,[50] which will be discussed in detail in Chapter 4. Elemental sulfur is precipitated and removed in the leach stage, which generates an aqueous copper chloride leach liquor:

Equation 1.19 $\qquad 4FeCl_3 + 2Cu_2S_{(s)} \longrightarrow 2CuCl_2 + 4FeCl_2 + S_{(s)}$
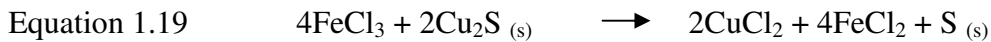
These novel leach processes tend to generate[51] high tenor (high $[Cu^{2+}]$) leach solutions, with copper concentrations ranging from 30-90 gL^{-1}. Metal salt extractants are much better suited than conventional cation exchange reagents to process these high tenor feeds, as protons are not released during the extraction step (Scheme 1.1). Metal extraction by cation exchange reagents is limited by the release of protons during extraction (Figure 1.9) and the subsequent acidification of the raffinate to pH values below the operating range of the extractant before significant copper loading can occur. As metal salt extractants can remove this acid in the form of bound anion(s), loading is potentially only hindered by the solubility of the metal salt complex in the diluent. The prevalence of these new leaching techniques makes the

development of metal salt extractants, to transport copper and either sulfate or chloride, imperative.[52]

1.8.3   Anion Binding

The coordination chemistry of anions is a fast growing area of supramolecular chemistry. Cations have traditionally dominated the field of coordination chemistry, but the importance of anions in modern day applications such as biology, medicine, catalysis and the environment has ensured its rapid development.[53] Designing anion receptors is much more challenging than designing cation receptors, for a number of reasons. Table 1.1 illustrates the differences in ionic radii of isoelectronic anions and cations, with the greater size of anions meaning they have a much lower charge to radius ratio and thus are less efficiently bound by electrostatic interactions.[54]

Cation	Radius / Å	Anion	Radius / Å
Na^+	1.16	F^-	1.19
K^+	1.52	Cl^-	1.67
Rb^+	1.66	Br^-	1.82
Cs^+	1.81	I^-	2.06

Table 1.1: Ionic radii of selected isoelectronic anions and cations.[54]

Further difficulties are encountered when considering the protonation of anions, which results in a decrease in charge as the pH is decreased. Receptors must be designed to operate at a specific pH range to maximise the potential interaction with the anion.

The solvation of anions is very important, especially when extracting anions into non-polar solvents. In 1888, Franz Hofmeister ranked the ability of a series of anions to precipitate a mixture of hen egg white proteins, concluding the ordering

stemmed from their "water attracting capacities", listed below from strongly hydrated anions on the left to weakly hydrated anions on the right:[55]

$$Citrate^{3-} > SO_4^{2-} = tartrate^{2-} > HPO_4^{2-} > CrO_4^- > OAc^- > HCO_3^- > Cl^- > NO_3^- > ClO_4^-$$

This ranking has huge implications in the field of anion extraction and can generally predict why anions such as ClO_4^- are extracted from aqueous solutions into non-polar solvents with much greater ease than anions such as SO_4^{2-}. Sulfate is much more hydrated than perchlorate, so has a greater hydrophilicity, and is therefore harder to extract from an aqueous medium. This results in the more facile extraction of larger, more charge-diffuse anions, and it is often possible to predict distribution coefficients from the Gibbs free energies of solvation.[53, 56] Moyer *et al*[57] proposed that the term Hofmeister bias be used to describe the effects of anion solvation on extraction, to avoid confusion with the original series. In the liquid/liquid extraction of anions, the following series is usually observed, with the best extracted anions on the left and the poorly extracted anions on the right:[53]

$$ClO_4^- > I^- > SCN^- > NO_3^- > Br^- > Cl^- \gg SO_4^{2-} > CO_3^{2-} > PO_4^{3-}$$
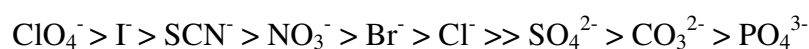
A further factor which introduces complexity into the design of anion receptors is their varying geometries, some examples of which are displayed in Table 1.2. This design complexity is, however, a double edged sword, as the variations in anion geometry allow some selectivity to be inbuilt into receptors.[58]

Each geometry illustrated in Table 1.2 has examples of anions which are of interest to extractive metallurgists, underlining the need for the principles of supramolecular chemistry to be uppermost in the mind of metallurgists during the rational design of new reagents. However, the metal salt extractants synthesised in this project contain very simple, protonatable tertiary amine anion binding sites, as the aim was to establish proof-of-concept of anion binding. Previous work within the group indicates that the main factor in influencing anion selectivity in two phase solvent extraction experiments is the relative solvation of the anions, rather than complex

receptor design.[43]   For this reason, anion coordination is not investigated in further detail, although the interested reader is directed to an excellent recent review by Beer and Gale.[58]

Anion Structure	Geometry	Examples
	Spherical	F^-, Cl^-, Br^-, I^-
	Linear	N_3^-, SCN^-, OH^-
	Trigonal Planar	CO_3^{2-}, NO_3^-
	Tetrahedral	PO_4^{3-}, SO_4^{3-}, $CoCl_4^-$
	Octahedral	$PdCl_6^{2-}$, $PtCl_6^{2-}$

Table 1.2: Typical anion geometries and examples of each relevant to hydrometallurgy.[58]

1.9   Thesis Outline

Chapter 2 discusses the synthesis and characterisation of the 3-substituted phenolic oxime ligand series **L1**-**L9** alongside their copper(II) complexes, with the aim of studying the effect of the 3-substituent on the extractive efficacy of the ligands. A review of substituent effects on copper extraction by phenolic oximes and methods to tune extraction strength precedes the synthesis and characterisation of nearly all ligands and complexes by X-ray diffraction. The effects of 3-substitution on solid state architectures are discussed, and the relative copper(II) binding strengths measured by solvent extraction, with striking differences observed.

Chapter 3 aims to rationalise these differences in extractive efficacies by subjecting the ligands and complexes to various analytical techniques, including EPR, DFT calculations, solid state analysis and CID MS, which are discussed in the opening section. Further ligands are synthesised (**L10**-**L16**) to investigate the effect of the 3-substituent on cavity sizes in the solid state, and a tentative model for predicting the effect of substitution is formulated.

Chapter 4 establishes that simple modification of phenolic oximes gives ligands capable of bind a metal cation and its attendant anion, *i.e.* a metal *salt*. Ligands **L17**-**L22** are synthesised and proof-of-concept solvent extraction studies reveal unexpectedly efficient loading of $CuCl_2$ and $ZnCl_2$ by **L17** and **L18**, with the mode of binding revealed by X-ray crystallography. Experiments to determine the commercial viability of this ligand type are reported.

Chapter 5 scrutinises the anion selectivity of **L18** and **L20**, and shows **L18** has the potential for commercial development as a metal salt extractant, with crystallographic evidence of the binding motifs of various anions presented. Cation selectivity experiments show competition with Fe^{III} may be problematic, and potential ways to overcome this are discussed in the conclusions of Chapter 6.

1.10   References

[1]   N. N. Greenwood and A. Earnshaw, 'Chemistry of the Elements', Butterworth-Heinemann, 1997.

[2]   A. Cole, *Metal Bulletin Monthly supplement*, 2004, **copper**, 6.

[3]   Kirk-Othmer Encyclopaedia of Chemical Technology, ed. M. Grayson and D. Eckroth, New York, 1978.

[4]   S. Hong, J.-P. Candelone, C. C. Patterson, and C. F. Boutron, *Science*, 1996, **272**, 246.

[5]   S. Hong, J.-P. Candelone, M. Soutif, and C. F. Boutron, *Science of the Total Environment*, 1996, **188**, 183.

[6]   R. B. Gordon, M. Bertram, and T. E. Graedel, *Proceedings of the National Academy of Sciences of the United States of America*, 2006, **103**, 1209.

[7]   http://news.bbc.co.uk/1/hi/england/6937491.stm.

[8]   P. J. Mackey, *CIM Magazine*, 2007, **2**, 35.

[9]   P. W. Atkins and D. F. Shriver, 'Inorganic Chemistry', Oxford University Press, 1999.

[10]   P. A. Tasker, P. G. Plieger, and L. C. West, *Comprehensive Coordination Chemistry II*, 2004, **9**, 759.

[11]   M. J. Nicol, C. A. Fleming, and J. S. Preston, *Comprehensive Coordination Chemistry*, 1987, **6**, 779.

[12]   F. Habashi, 'Handbook of Extractive Metallurgy', Wiley-VCH Verlag GmbH, 1997.

[13]   T. W. Swaddle and Editor, 'Inorganic Chemistry: An Industrial and Environmental Perspective', 1996.

[14]   D. B. Dreisinger, P. Dempsey, J. D. T. Steyl, K. C. Sole, and J. Gnoinski, *Proceedings of Copper/Cobre Conference 2003*, 2003.

[15]   F. Habashi, 'A Textbook of Hydrometallurgy', 1994.

[16]   J. Szymanowski, 'Hydroxyoximes and Copper Hydrometallurgy', CRC Press, 1993.

[17]   F. Habashi, *Hydrometallurgy*, 2005, **79**, 15.

18   D. Pletcher and F. C. Walsh, 'Industrial Electrochemistry', Chapman & Hall, 1990.

19   H. Singh and C. K. Gupta, *Mineral Processing and Extractive Metallurgy Review*, 2000, **21**, 307.

20   F. L. Bernardis, R. A. Grant, and D. C. Sherrington, *Reactive & Functional Polymers*, 2005, **65**, 205.

21   P. M. Cole and K. C. Sole, *Mineral Processing and Extractive Metallurgy Review*, 2003, **24**, 91.

22   P. M. Cole, K. C. Sole, and A. M. Feather, *Tsinghua Science and Technology*, 2006, **11**, 153.

23   T. Zhu, *Mineral Processing and Extractive Metallurgy Review*, 2000, **21**, 1.

24   G. A. Kordosky, *International Solvent Extraction Conference, Cape Town, South Africa, Mar. 17-21*, 2002, 853.

25   J. Szymanowski and A. Borowiak-Resterna, *Critical Reviews in Analytical Chemistry*, 1991, **22**, 519.

26   A. G. Smith, P. A. Tasker, and D. J. White, *Coordination Chemistry Reviews*, 2003, **241**, 61.

27   J. Szymanowski, *Critical Reviews in Analytical Chemistry*, 1995, **25**, 143.

28   P. A. Wood, R. S. Forgan, D. Henderson, S. Parsons, E. Pidcock, P. A. Tasker, and J. E. Warren, *Acta Crystallographica, Section B*, 2006, **62**, 1099.

29   J. Bernstein, R. E. Davis, L. Shimoni, and N.-L. Chang, *Angewandte Chemie International Edition*, 1995, **34**, 1555.

30   G. A. Kordosky, *Jom*, 1992, **44**, 40.

31   F. Habashi, *Minerals Engineering*, 1994, **7**, Chapter 2.

32   A. N. Banza, E. Gock, and K. Kongolo, *Hydrometallurgy*, 2002, **67**, 63.

33   L. Li, H. Wang, and D. Liu, *GME '99, Global Metals Environment, Proceedings of Global Conference on Environmental Control in Mining and Metallurgy, Beijing, China, May 24-27, 1999*, 1999, 173.

34   K. Burger and I. Egyed, *Journal of Inorganic and Nuclear Chemistry*, 1965, **27**, 2361.

35   J. R. Parrish, *Journal of the South African Chemical Institute*, 1970, **23**, 129.

36   V. I. Lakshmanan and G. J. Lawson, *Journal of Inorganic and Nuclear Chemistry*, 1975, **37**, 207.

37   D. W. Agers and R. Dement, *Solvent Extr. Met. Processes, Proc. Int. Symp.*, 1972, 31.

38   D. W. Agers and R. Dement, *Ingenieursblad*, 1972, **41**, 433.

39   P. L. Mattison and R. R. Swanson, in 'Substituted 2-hydroxybenzophenoximes and the extraction of copper with them', USA Patent, 1976.

40   P. L. Mattison and R. R. Swanson, in 'Extracting copper with 2-hydroxybenzophenone oximes containing an electron-withdrawing substituent', USA Patent, 1972.

41   K. Burger and I. Egyed, *Magyar Kemiai Folyoirat*, 1965, **71**, 143.

42   K. Burger, F. Ruff, I. Ruff, and I. Egyed, *Magyar Kemiai Folyoirat*, 1965, **71**, 282.

43   S. G. Galbraith, 'PhD Thesis', Edinburgh University, 2005.

44   P. A. Tasker and D. J. White, in 'Extraction of metal salts from aqueous solutions', WO 2000-GB1251, 2000.

45   S. G. Galbraith and P. A. Tasker, *Supramolecular Chemistry*, 2005, **17**, 191.

46   D. Dreisinger, *Hydrometallurgy*, 2006, **83**, 10.

47   J. O. Marsden, R. E. Brewer, and N. Hazen, *Hydrometallurgy 2003, Proceedings of the International Symposium honoring Professor Ian M. Ritchie, 5th, Vancouver, BC, Canada, Aug. 24-27, 2003*, 2003, **2**, 1429.

48   J. D. Batty and G. V. Rorke, *Hydrometallurgy*, 2006, **83**, 83.

49   M. E. Clark, J. D. Batty, C. B. van Buuren, D. W. Dew, and M. A. Eamon, *Hydrometallurgy*, 2006, **83**, 3.

50   R. W. Gibson and N. M. Rice, *Hydrometallurgy and Refining of Nickel and Cobalt, Annual Hydrometallurgy Meeting of CIM, 27th, Sudbury, Canada, Aug. 17-20, 1997*, 1997, 247.

51   K. Sole, *Solvent Extraction and Ion Exchange*, 2002, **20**, 601.

52   D. C. R. Henry, 'PhD Thesis', University of Edinburgh, 2007.

53   A. Bianchi, K. Bowman-James, E. Garcia-Espana, and Editors, 'Supramolecular Chemistry of Anions', 1997.

54   R. D. Shannon, *Acta Crystallographica, Section A: Crystal Physics, Diffraction, Theoretical and General Crystallography*, 1976, **A32**, 751.

55   F. Hofmeister, *Arch. Exp. Pathol. Pharmakol.*, 1888, 247.

56   B. A. Moyer, P. V. Bonnesen, L. H. Delmau, T. J. Haverlock, K. Kavallieratos, and T. G. Levitskaia, *International Solvent Extraction Conference, Cape Town, South Africa, Mar. 17-21, 2002*, 2002, 299.

57   K. Kavallieratos and B. A. Moyer, *Chemical Communications*, 2001, 1620.

58   P. D. Beer and P. A. Gale, *Angewandte Chemie International Edition*, 2001, **40**, 486.

CHAPTER 2

SYNTHESIS OF 3-SUBSTITUTED SALICYLALDOXIMES

Contents

2.1   Introduction

2.1.1   Aims

As explained in the introduction, this chapter deals with the use of substituent effects in salicylaldoxime ligands to tune their strength and selectivities to meet requirements of new metallurgical flowsheets whilst functioning as *cation exchange* reagents:

Equation 2.1 $\qquad 2\mathbf{L}_{(org)} + M^{2+} \ \rightleftharpoons \ [M(\mathbf{L}\text{-H})_2]_{(org)} + 2H^+$
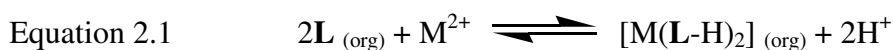
In this chapter and subsequently in Chapter 3, particular attention is paid to the consideration of interligand hydrogen bonding and its contribution to the extractive properties of ligands. The objective of the work in this chapter was to consider the effects of 3-substitution of salicylaldoximes on copper(II) extractive efficacy, and the chapter includes:

- the synthesis of a coherent series of 3-substituted salicylaldoxime ligands with the aim of tuning their copper(II) binding strengths,
- the characterisation of the ligands and their copper(II) complexes *via* X-ray crystallography,
- a discussion on the effects of 3-substitution on the supramolecular architectures formed in the solid state structures of bis-salicylaldoximato copper(II) complexes, and
- the study of the copper(II) binding affinity of the series *via* solvent extraction.

Discussion of structure activity relationships associated with incorporation of substituents in the 3-position is deferred to Chapter 3. A short review of the importance of supramolecular hydrogen bonding in extractive chemistry and methods to tune the extractant strength of phenolic oximes follows.

2.1.2 The Importance of Supramolecular H-Bonding in Extraction

Liquid-liquid extraction using phenolic oxime reagents (Figure 2.1) accounts for between 20%[1] and 30%[2] of the global production of copper metal. In the high boiling hydrocarbon solvents preferred by industry *inter*molecular forces between extractants, particularly hydrogen bonding, contribute very significantly to the stability of any complexes formed in the water-immiscible phase. Historically, both aromatic and aliphatic hydroxyoximes have been utilised as selective copper extractants,[3] but this chapter focuses solely on salicylaldoxime reagents (R = alkyl, R' = H in Figure 2.1). Their strength and selectivity of extraction, coupled with the excellent materials balances achieved in the processing of oxidic ores have led to their commercial success.[4] Each hydrometallurgical circuit has unique properties, particularly the composition and acidity of the pregnant leach solution, and requires an extractant formulation suited to its specific needs. Information on reagent properties is provided by suppliers, allowing metallurgists to design the circuit and choose an appropriate extractant blend.[5]
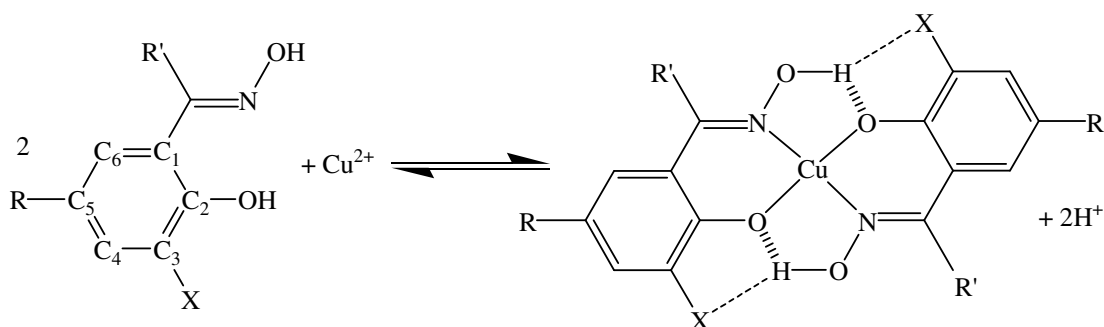
Figure 2.1: 5-Alkyl-substituted salicylaldoxime derivatives used in copper recovery, showing potential interaction of intracomplex H-bonding with a 3-substituent (X).

Solid state structures of copper(II) complexes of phenolic oximes show the formation of square planar coordination environments containing a 14-membered *pseudo*macrocyclic hydrogen bonded array (Figure 2.1) with the H-bonds between the oximic H and phenolate O atoms thought impart additional stability to the complex.[6]

Extraction by organophosphorus acids, *e.g.* by the commercial reagent di-(2-ethylhexyl)phosphoric acid (D2EHPAH), is often associated with retention of strong interligand H-bonding and the formation of 8-membered *pseudo*-chelate rings, as in Figure 2.2.[4, 7]
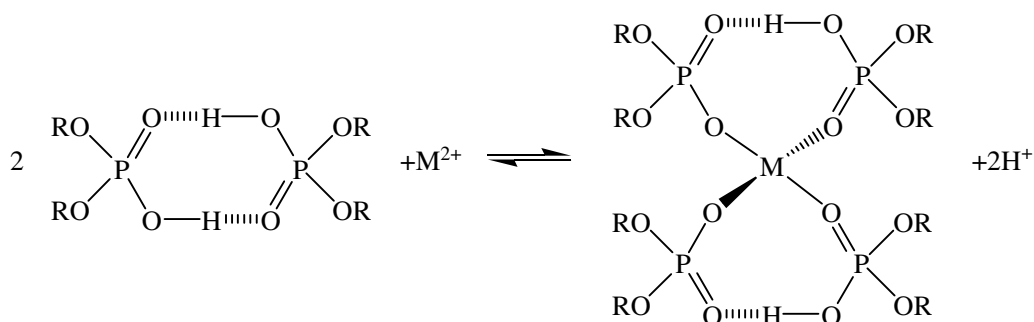
Figure 2.2: Formation of 8-membered *pseudo*-chelates by phosphoric acid diesters, **LH**, such as D2EHPAH in "pH-swing" extractions $2n\mathbf{LH}_{(org)} + M^{n+} \rightleftharpoons [ML_n(\mathbf{LH})_n]_{(org)} + nH^+$.

Consequently, unusual anti Irving-Williams[8] orders of stability of divalent 1st row transition metal complexes are observed,[7] and D2EHPAH shows selectivity for dications favouring tetrahedral geometry. Plants using D2EHPAH for the recovery of zinc have been opened recently, including Anglo American's massive Skorpion zinc installation in Namibia.[9] Processing 150,000 tonnes of zinc per annum by SX-EW, it is the world's 8th largest zinc mine and yields very high purity (>99.995%) zinc cathodes at very low costs.[10]

Figure 2.3: The Anglo American Skorpion Zinc installation in Namibia.[11]

2.1.3 Tuning Extractant Strength

There are different ways to tune the extractive ability of a reagent formulation. Many aldoxime extractants (R' = H in Figure 2.1) are "strong extractants", loading copper even at low pH, and require modification to facilitate stripping.[12] Modifiers are usually hydrogen bond donor/acceptor molecules which are thought to disrupt the stabilising intracomplex hydrogen bonds, allowing the copper to be removed more easily.[13]

By varying the amount of modifier relative to the oxime, it is possible to optimise the formulation strength to match circuit conditions/needs and maximise net copper transfer. A large number of compounds are used (Figure 2.4) and the choice and amount of modifier (or modifier blend) is critical to the metallurgical and physical properties (*e.g.* viscosity) of the reagent.
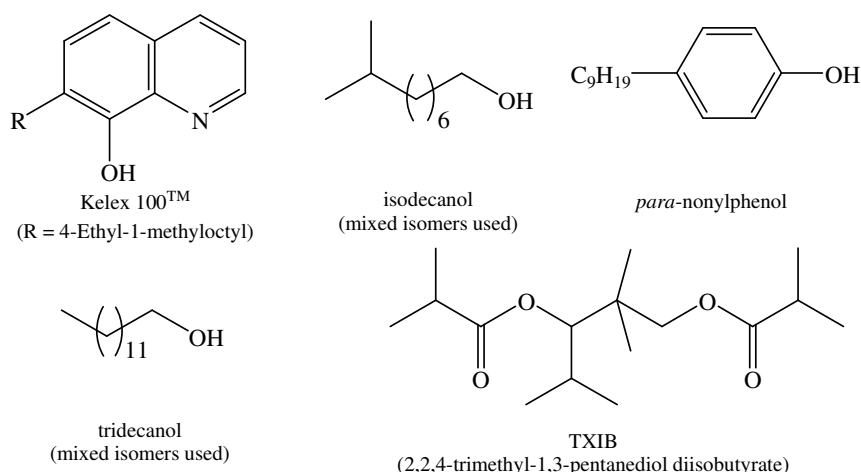
Figure 2.4: Structures of described reagents and modifiers.

The first use of modifier molecules involved the 8-hydroxyquinoline-based extractant Kelex 100™, which contained isodecanol. Although never used commercially for copper extraction, the concept of extractant modification was subsequently developed by many companies.[3] The Acorga P5000™ series of reagents contained 2-hydroxy-5-nonylbenzaldehyde oxime (R = C_9H_{19}, R' = H in Figure 2.1) as the active component, with varying quantities of *para*-nonylphenol to

tune extractant strength.[14, 15] Tridecanol was later introduced as a modifier, requiring only half the quantity compared with that of *para*-nonylphenol.[2] Further advances in modifier technology came with the introduction of Cytec Industries Inc.'s highly branched esters (*e.g.* Acorga M5640™) which can also increase Cu/Fe selectivity and oxime stability.[15-17] Esters, such as TXIB, have since become the SX industry's most commonly used modifier.[2]

Aldoxime reagents are stronger extractants than ketoximes (R' = alkyl, aromatic in Figure 2.1)[2] therefore blending ketoxime and aldoxime reagents allows the metallurgist to tailor further the properties of the extractant formulation.[4] This concept was introduced commercially by Henkel in 1982 with the LIX 860™ series, which combined the advantageous properties of each type of reagent, and now these blends are used in many modern applications.[2, 4]

Recent work by Cytec has shown that incorporation of selected modifiers into these blended reagents results in increased copper transfer. These new formulations also show a significant improvement in Cu/Fe selectivity, which can result in lower bleed and copper reprocessing costs.[18]

The mode of action of modifiers at the molecular level remains unclear, although it is known that extractants and modifiers interact *via* H-bonding in solution.[3, 12] The enhancement of copper stripping is not accompanied by a significant decrease in copper loading, which is counterintuitive and suggests that many equilibria are present in the organic phase.

The examples presented in Chapter 1 show that it is also possible to alter the strength of an extractant by introducing substituents in the 3-position, although the mode of action of the substituent is unclear and a rational study has not been carried out. Studying these effects requires a systematic series of ligands, and their design is described below.

2.1.4 Ligand Design

To ensure comparability of data, a coherent series of ligands was required with 3-substituents which affect the electronic, steric and hydrogen bonding properties of the extractant to varying degrees. Substituents were chosen with electron-donating properties (Me, OMe, ^{t}Bu) and electron-withdrawing properties (NO$_2$, Cl, Br). The steric interaction of X with the stabilising oximic H-bond donating group on the adjacent ligand was investigated using substituents with the potential to form attractive bifurcated hydrogen bonds (NO$_2$, Cl, Br, OMe) or repulsive interactions with bulky groups (^{t}Bu). The oximes **L1**-**L9** used in solvent extraction experiments are detailed in Figure 2.5.

	L1	**L2**	**L3**	**L4**	**L5**	**L6**	**L7**	**L8**	**L9**
X	H	Me	^{t}Bu	NO$_2$	Cl	Br	OMe	H	NO$_2$
R	^{t}Bu	^{t}Bu	^{t}Bu	^{t}Bu	^{t}Bu	^{t}Bu	^{t}Bu	^{t}Oct	^{t}Oct
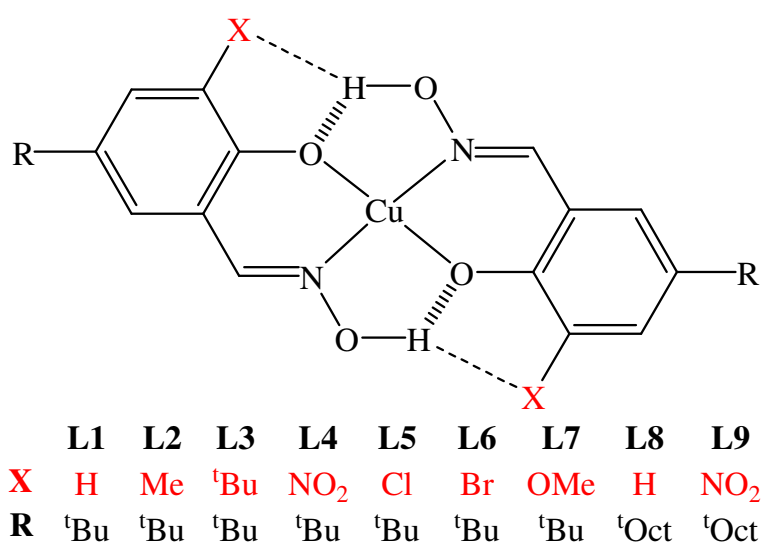
Figure 2.5: 3-Substituted salicylaldoximes studied in this chapter.

The ligands are based on a 5-*tert*-butyl-2-hydroxybenzaldehyde oxime scaffold, which aids purification and characterisation and was found to favour crystallisation of copper(II) complexes, allowing structures to be determined by single crystal X-ray diffraction. Whilst the 5-*t*-butyl groups ensure copper(II) complexes have good solubility in water-immiscible solvents, it was necessary to synthesise a "greasier" analogue of the NO$_2$-substituted ligand (**L4**) due to the limited solubility of its copper(II) complex. Changing the 5-alkyl group to *t*-octyl increased solubility whilst still allowing full characterisation of ligand **L9**. An unsubstituted *t*-octyl analogue

(**L8**) was synthesised as a control, to ensure that changing the nature of alkyl chain had no effect on extractant strength.

2.1.5   Measuring Copper(II) Binding Strengths

As discussed in Chapter 1, solvent extraction experiments can be used to determine the cation selectivity of an extractant.[3] The relative strengths of Cu^{II} extraction of **L1**-**L9** could be measured in a similar fashion, by determining the concentrations of Cu^{II} extracted by each ligand over a pH range, provided conditions are kept constant throughout all solvent extraction experiments.

To determine copper uptake into an organic phase, a robust, reliable detection method is required. There are many methods of analysis for metal ions, including UV/Vis and atomic absorption spectroscopies, but ICP-OES (Inductively Coupled Plasma Optical Emission Spectrometry) was chosen as it can accurately analyse metal ion content from both organic and aqueous solutions with low detection limits.[19] The sample is dissolved in solution and passed as an aerosol through a plasma at temperatures of over 6500 K. This high temperature will atomise, vaporise and excite the sample into high-energy states. The excited atoms and ions are virtually independent of one another, and emit energy as photons in the UV and visible range as they decay back to lower energy states. The intensity of analyte emission is proportional to analyte concentration, so initial calibration of the spectrometer with known standard samples allows accurate detection of concentrations of many elements, in this case copper, but also other transition metals and sulfur later in the thesis.[19]

2.2   Ligand Syntheses

The oxime ligands **L1**-**L9** were easily prepared from their salicylaldehyde precursors. In the cases of **L3**[20] and **L7**[21] these precursors were commercially

available, but all other ligands were prepared from the appropriate 4-alkylphenol by literature methods.[22-27] The synthetic strategy involved two steps, formylation and inclusion of the 3-substituent, with the method and order of these reactions dependent on the ligand (Scheme 2.1).
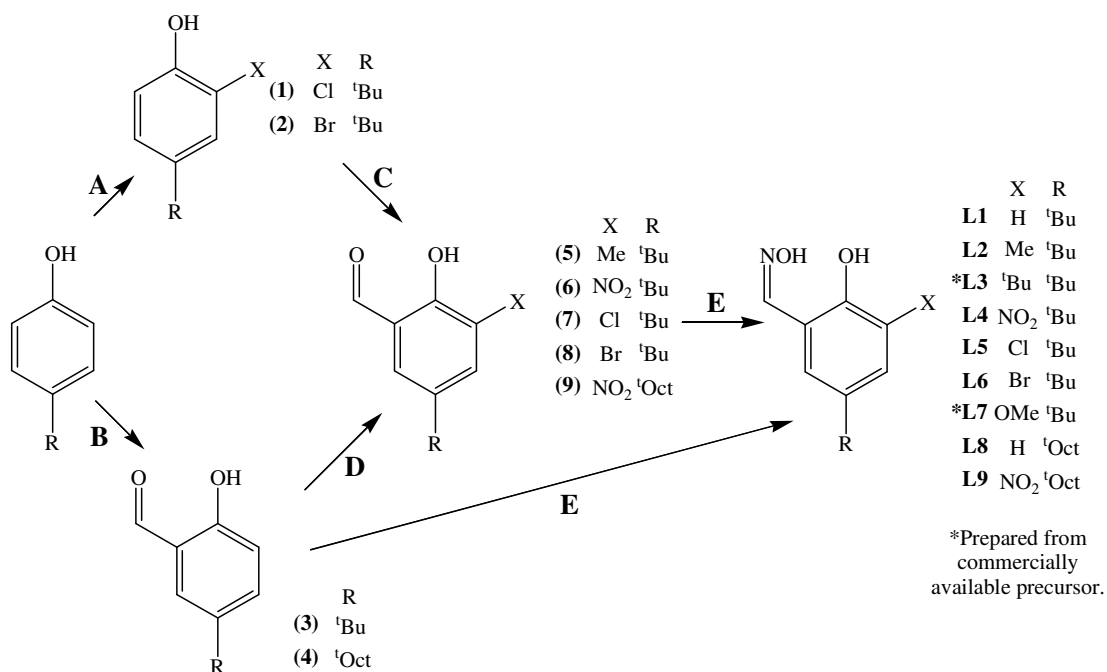
Scheme 2.1: Synthetic routes to all the salicylaldoxime ligands prepared in this chapter.

2.2.1   Incorporation of the 3-Substituent

The synthetic strategy depended on where in the sequence of reactions to incorporate the 3-substituent. If possible in a simple and efficient manner, this was carried out prior to formylation, to generate a 2-X-4-alkylphenol (route **A** in Scheme 2.1). This was the case for the 3-halogenated ligands, where preparation of the phenols **(1)** and **(2)** involved simply stirring 4-*tert*-butylphenol with the appropriate halogenating agent, sulfuryl chloride[24] or tetra-*n*-butylammonium tribromide.[25] Both phenols were isolated in high yields and purity but discoloured when exposed to sunlight over periods of days, indicating possible photodegradation.

The introduction of a nitro group *ortho* to a phenolic OH unit can be achieved using nitric acid and glacial acetic acid.[27] No simple, high yielding methods to synthesise 4-*tert*-butyl-2-nitrophenol were seen in the literature, and as it was already known that nitration of salicylaldehydes is facile and high yielding[28] incorporation of the nitro group was carried out *after* the formylation step, allowing a clean reaction with high yields (route **B** in Scheme 2.1).

2.2.2 The Levin Method of Formylation

Formylation could be achieved by one of two possible reactions. When selective monoformylation was required and more than one site for incorporation of the HCO group is possible, the Levin[22] method was chosen, which involved magnesium mediated *ortho*-formylation. Magnesium bis-phenoxides are formed on addition of magnesium methoxide to alkyl phenols in methanol, and react with paraformaldehyde in toluene by the mechanism proposed by Levin *et al* in Figure 2.6 to yield the product after an acidic work up.
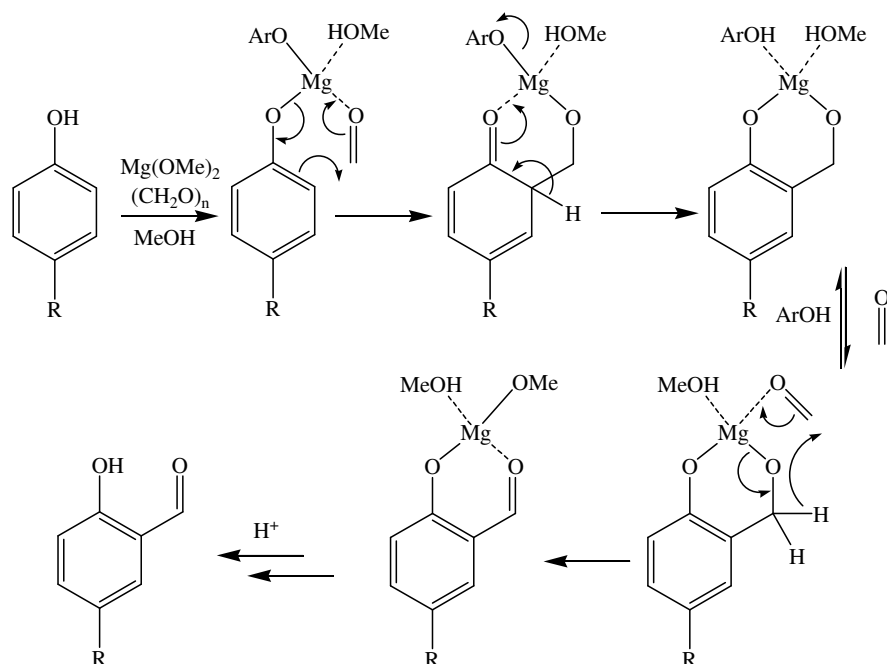
Figure 2.6: Proposed mechanism of the Levin synthesis.[22]

42

Control of methanol levels is required as high concentrations can result in competition with the phenoxides for magnesium coordination and hence it is an inhibitor. This is a controlled reaction which yields primarily a monoformylated product and was successful in producing large quantities of the salicylaldehydes **(3)** and **(4)**. These are the precursors for ligands **L1** and **L8**, but they can also be nitrated[27] using nitric acid and glacial acetic acid to give **(6)** and **(9)**, the precursors for **L4** and **L9**.

2.2.3   A Modified Duff Reaction for Formylation

Preparation of the precursor aldehydes **(5)**, **(7)** and **(8)** involved a modified Duff reaction, as described by Lindoy *et al.*[23]   In many cases this yields the salicylaldehyde without the need for further purification, and is a much simpler procedure than the Levin method. The main disadvantage of the Duff reaction is the lack of regioselectivity in the formylation process. Substitution can occur in both the *ortho* and *para* positions to the phenol, and diformylated products are common.[23] For this reason, the Duff reaction was used only when formylation could be restricted to the required *ortho* position, due to all other possible reaction sites being blocked.

The reaction was carried out using hexamethylenetetramine (HMT) as reagent, and anhydrous TFA as solvent. A large excess (4-5 equivalents) of HMT ensured complete reaction. Following overnight heating, the reaction mixture was poured into 2 M HCl and after stirring for ~6 hr, in most cases the pure product precipitates in about 75% yield. This did not occur for **(5)** and extraction into DCM was necessary, yielding a product which required purification by column chromatography before oximation.

2.2.4 Oximation

The simplest method of oxime formation involves the addition of hydroxylamine to aldehydes or ketones. The hydroxyimino-de-oxo-bisubstitution reaction proceeds by the mechanism shown in Figure 2.7.
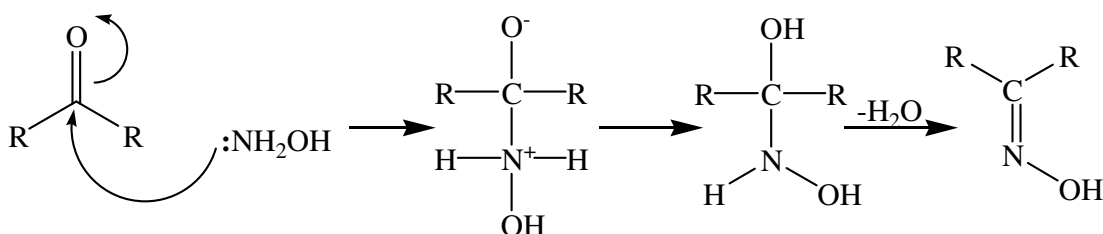
Figure 2.7: Mechanism of oximation by reaction with hydroxylamine.

The dehydration step is acid-catalysed and so the reaction rate is faster at lower pH, but this effect is countered as hydroxylamine molecules are converted to NH_3OH^+ ions in acidic conditions and so cannot react. A balance between these factors results in an optimum pH 4 for reaction rate, while NMR studies have proven the existence of the zwitterionic reaction intermediate.[29]

Hydroxylamine can decompose rapidly and dangerously in the presence of metal or metal ions, redox agents, at high temperatures or at high concentration.[30] For this reason hydroxylamine was generated immediately prior to oximation by mixing the stable salt hydroxylamine hydrochloride and potassium hydroxide in ethanol. This forms an insoluble precipitate of KCl which is removed by filtration to leave a solution of hydroxylamine in ethanol suitable for immediate use.

The oximation step was found to be facile and high yielding, with yields of ~90% achieved after overnight reflux, and so pH control was not required. A colour change is noted over the course of the reaction, from a yellowish aldehyde solution to a much paler oxime solution, although the 3-nitro ligands **L4** and **L9** remained bright yellow. This change can sometimes be seen almost immediately with no reflux, but overnight heating was employed to ensure full conversion.

2.3 Ligand Characterisation

2.3.1 NMR Spectroscopy

All ligands and precursors were fully characterised by both ^{1}H and ^{13}C NMR spectroscopy. During the oximation step, ^{1}H NMR spectroscopy proved a very effective tool for indicating purity and monitoring conversion to the oxime, with the aldehyde proton having a characteristic signal at δ ~10 and the oximino proton at δ ~8. The spectra of **L3** and its aldehyde precursor 3,5-di-*tert*-butyl-2-hydroxybenzaldehyde[20] are shown in Figure 2.8.
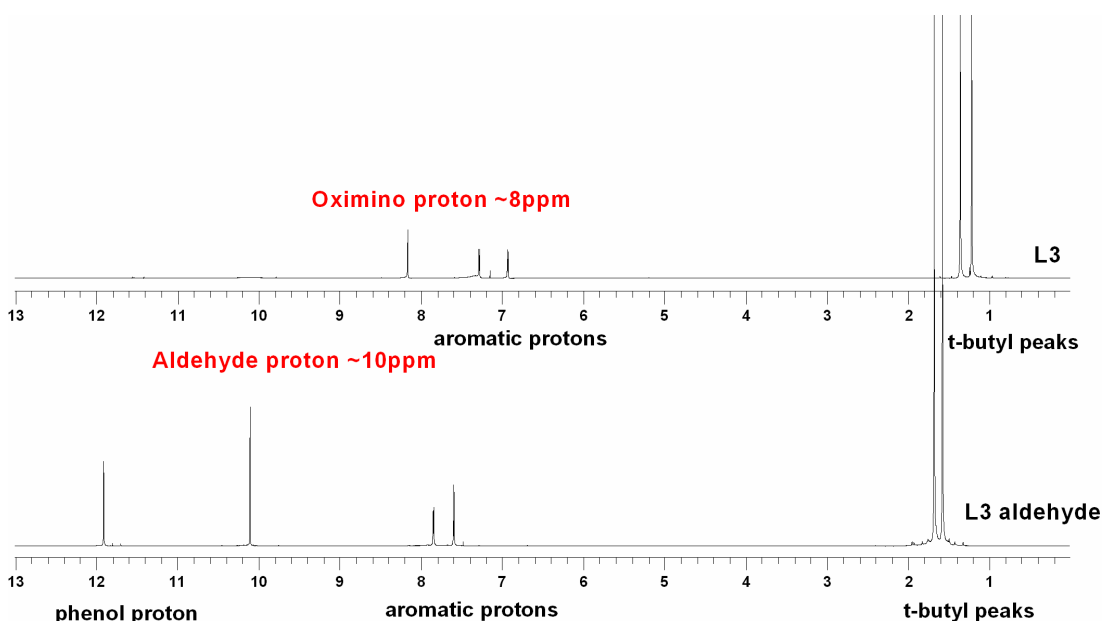
Figure 2.8: ^{1}H NMR spectra of **L3** and its aldehyde precursor, showing the distinctive oximino H and aldehyde H peaks. *NB* the phenol proton was often seen in aldehyde but not oxime spectra.

2.3.2 Mass Spectrometry

FAB MS was used to characterise all ligands and precursors. For the ligands, appropriate peaks were seen for each molecular ion (MH$^+$), indicating successful synthesis of each salicylaldoxime. Each ligand peak has an intensity of > 80 % apart from **L6** which has value of only 9 %, suggesting that it is less stable under the

ionisation conditions. Analysis of the breakdown peaks reveals a distinct pattern which is present throughout the oxime series (Table 2.1), indicating that the major breakdown mechanism(s) are independent of the 3-substituent.

	MH$^+$	[M-16]H$^+$	[M-32]H$^+$	[M-56]H$^+$
L1	194 (100%)	178 (93%)	162 (46%)	138 (21%)
L2	208 (88%)	192 (100%)	176 (50%)	152 (19%)
L3	250 (99%)	234 (93%)	218 (43%)	194 (22%)
L4	239 (81%)	223 (61%)	207 (30%)	183 (8%)
L5	228 (100%)	212 (83%)	196 (42%)	172 (22%)
L6	273 (9%)	257 (37%)	241 (100%)	217 (0%)
L7	224 (100%)	208 (99%)	192 (19%)	168 (15%)
L8	250 (82%)	234 (34%)	218 (5%)	194 (1%)
L9	295 (86%)	279 (45%)	263 (10)	239 (2%)

Table 2.1: The mass and relative intensities of the breakdown peaks seen in FAB mass spectra of **L1**-**L9**.

All ligands have significant breakdown peaks at [M-16]H$^+$, [M-32]H$^+$ and [M-56]H$^+$, although the last is not seen for the *t*-octyl substituted ligands **L8** and **L9**, indicating the mechanism involves the 5-*t*-butyl group present in **L1**-**L7**. Proposed breakdown products are displayed in Figure 2.9.
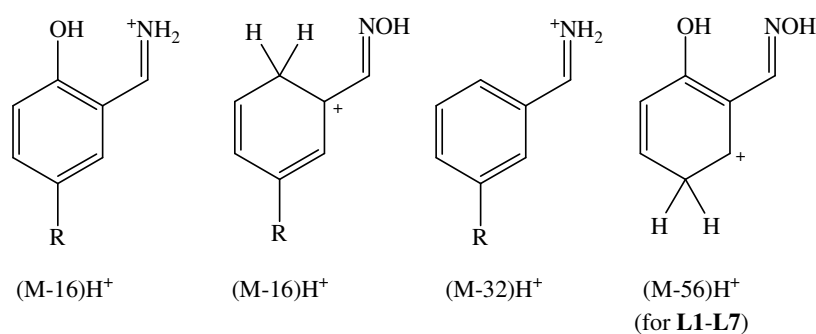
Figure 2.9: Proposed breakdown products formed during FABMS analysis of **L1**-**L9**.

Dealkylation is a known mechanism of breakdown in mass spec[31] and loss of the 5-*t*-butyl group would account for the peaks at [M-56]H$^+$. As this peak is not seen in the spectra of **L8** and **L9**, which contain a *t*-octyl group in the 5-position instead of a *t*-butyl group, it is highly likely this is the breakdown mechanism depends on the release of the stable *t*-butyl radical. Loss of the phenolic hydroxyl group or conversion of the oxime to an imine could account for the peak at [M-16]H$^+$, with the two alternative decomposition routes accounting for the high intensity of the peak with this *m/z* ratio. A *combination* of the two routes results in the peak at [M-32]H$^+$. Only **L4** showed a small peak corresponding to a dimer, and the absence of such peaks is to be expected, as FAB ionisation breaks weak interactions *e.g.* hydrogen bonds.[31]

2.3.3 X-Ray Crystallography

Characterisation of **L1**-**L9** by X-ray diffraction analysis was also successful. The solid state structures of the ligands can be divided into 3 distinct types:

- those which form 14-membered *pseudo*macrocyclic hydrogen bonded dimers (**L2**, **L3**, **L5** and **L6**),
- those which form infinite 1D hydrogen bonded ribbons (**L1**, **L7** and **L8**), and
- those which form 6-membered hydrogen bonded dimers at the oxime functionality (**L4** and **L9**).

Each type of structure is described below, with one sample illustration and a table of notable bond lengths for the remaining ligands.

2.3.3.1 14-Membered *Pseudo*macrocyclic Dimers

Salicylaldoximes can form 14-membered *pseudo*macrocyclic hydrogen bonded dimers *via* intermolecular H-bonds from oximic H atoms to adjacent phenolic O

atoms in the solid state (Figure 2.10).[6] The cavity size or "hole size" in these dimers, defined as the mean distance of the donor N and O atoms from the centroid, may give information on the effects of substitution, with more favourable dimerisation expected to result in smaller hole size.
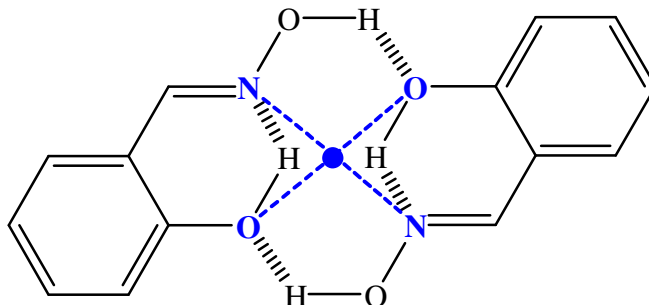
Figure 2.10: Schematic formation of *pseudo*macrocyclic dimers in the solid state structures of some phenolic oximes. Hole size of salicylaldoxime dimers is defined as the average distance from the donor atoms to the centroid, displayed in blue.[6]

A review of the literature in 2000 by Tasker *et al* suggested that this dimerisation occurs only when monoatomic substituents are present on the benzene ring.[6] The X-ray crystal structures of **L2**, **L3**, **L5** and **L6** challenge this theory, as all form centrosymmetric dimers. Figure 2.11 shows this dimerisation in the crystal structure of **L2**.

The data presented reveal some interesting trends. Cavity sizes seem to depend on the nature of the substituent, and their significance will be discussed in depth in Chapter 3. The length of the intramolecular H-bond from the phenolic proton to the imine nitrogen seems to depend on the size of the substituent. Larger 3-groups, in this case the ᵗBu and Br substituents, seem to exert a steric influence on the phenol group, pushing it slightly closer to the oxime moiety.
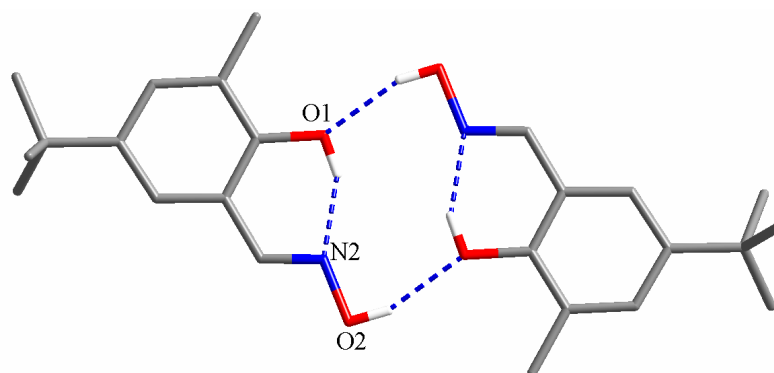
	Hole Size / Å	O1···N2 / Å
L2	2.003(2)	2.603(2)
L3	2.025(1)	2.578(1)
L5[a]	1.973(8)	2.611(8)
L6[a]	1.968(8)	2.599(7)

Figure 2.11: Crystal structure of **L2** showing the 14-membered *pseudo*macrocyclic H-bonded dimeric assembly, with relevant contact distances for the dimers of **L3**, **L5** and **L6** listed. Hydrogen atoms not involved in H-bonding omitted for clarity. [a]Average of 4 crystallographically independent dimers.

2.3.3.2 1D Hydrogen Bonded Ribbons

A second previously described packing arrangement of salicylaldoximes involves the formation of 1D hydrogen bonded ribbons.[6] An infinite 1D ribbon is formed by hydrogen bonds between the oxime proton of one molecule and the phenolic oxygen of the adjacent. The intramolecular hydrogen bond between the phenol proton and the oximino nitrogen remains (Figure 2.12).[6]
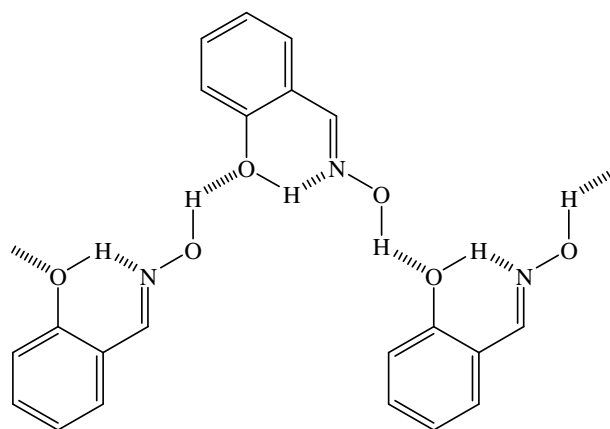
Figure 2.12: Schematic of the formation of 1D polymeric ribbons in the solid state of some phenolic oximes.[6]

L1, **L7** and **L8** form this structure in the solid state, with **L7** particularly interesting as the ribbon-forming H-bonds are bifurcated (Figure 2.13). The methoxy group provides an additional H-bond acceptor adjacent to phenol oxygen, prompting the formation of the bifurcated H-bonds (Figure 2.13).
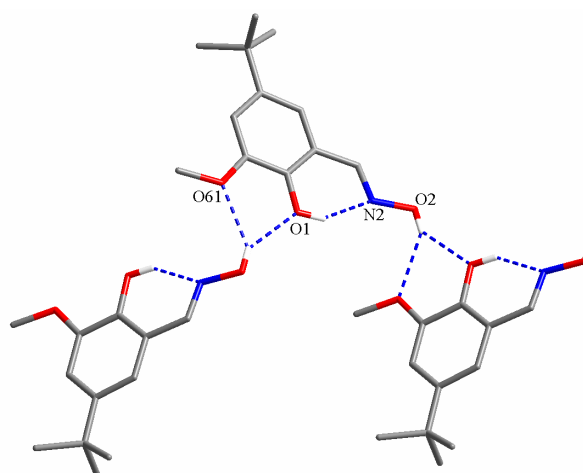
	O1···N2 / Å	O2···O1A / Å	O2···O61A / Å
L1	2.618(2)	2.762(2)	n/a
L7	2.630(2)	2.890(2)	2.950(2)
L8	2.607(1)	2.769(1)	n/a

Figure 2.13: Crystal structure of **L7** showing the 1D H-bonded ribbon array, with contact distances associated with H-bonds shown in **L7** and listed for the structures **L1** and **L8**. Hydrogen atoms not involved in H-bonding omitted for clarity.

Formation of bifurcated H-bonds in **L7** (Figure 2.13) means the ribbon-forming H-bonds are longer than in the structures of **L1** and **L8**, as the donor oxygen atom is positioned between the two acceptor atoms.

2.3.3.3 6-Membered Hydrogen Bonded Dimers

The 3-NO$_2$-substituted ligands **L4** and **L9** form a different type of solid state structure not seen previously in salicylaldoximes. Introduction of the nitro group provides a second hydrogen bond acceptor site for the phenolic hydrogen and, as the nitro oxygen atom is a better H-bond acceptor than the oximino nitrogen atom, the intramolecular H-bond forms between the NO$_2$ group and the phenolic proton. This is further demonstrated in the length of the O1···O62 contacts in **L4** and **L9**, which are shorter than the analogous intraligand O1···N2 contacts in the previous structures, indicating a stronger intramolecular H-bond in the 3-NO$_2$-substituted structures. The oxime group now has conformational freedom, and rotates 180° around the ArC-C bond to form a 6-membered hydrogen bonded dimer with an adjacent oxime moiety (Figure 2.14) while retaining the (*E*)-configuration seen in all previous structures of the series.

	O62···O1 / Å	O2···N22' / Å
L4	2.587(1)	2.817(1)
L9	2.579(2)	2.830(2)
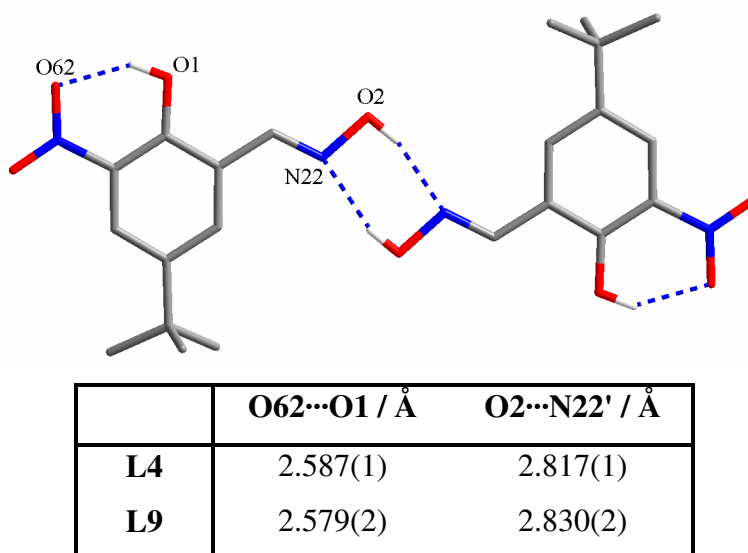
Figure 2.14: Crystal structure of **L4** showing the 6-membered H-bonded dimer, with relevant bond distances for the structures of **L4** and **L9** listed. Hydrogen atoms not involved in H-bonding omitted for clarity.

Interestingly, this 6-membered H-bonded dimer structure has recently been observed in the high pressure polymorph salicylaldoxime-II. Application of pressure to a single crystal of salicylaldoxime-I, a 14-membered *pseudo*macrocyclic dimer, results in a phase change at 5.93 GPa to this new type of structure.[32]

2.4 Copper(II) Complex Synthesis and Characterisation

Synthesis of the copper(II) complexes of **L1**-**L9** was simple and was achieved by mixing stoichiometric amounts of the ligand and copper(II) acetate in methanol. Precipitation occurred over a period of up to 24 hr, and the pure complexes were collected by filtration (yields could be improved by reducing the volume of the filtrates to induce further precipitation). All complexes were isolated successfully as brown solids, except [Cu(**L4**-H)$_2$] and [Cu(**L9**-H)$_2$] which were green in colour.

2.4.1 Mass Spectrometry

All copper(II) complexes were studied by FABMS and molecular ion peaks were seen in all cases, confirming their successful synthesis. The most commonly observed breakdown peak was that of the free ligand, with intensities of both listed overleaf in Table 2.2.

	$[Cu(L-H)_2]H^+$	LH^+
L1	447 (100%)	194 (93%)
L2	475 (36%)	208 (42%)
L3	559 (24%)	250 (54%)
L4	538 (16%)	239 (12%)
L5	516 (66%)	228 (21%)
L6	607 (7%)	273 (12%)
L7	507 (100%)	224 (6%)
L8	560 (42%)	250 (25%)
L9	649 (11%)	295 (2%)

Table 2.2: The mass and relative intensities of the molecular ion and ligand peaks seen in FAB mass spectra of the copper(II) complexes of **L1**-**L9**.

2.4.2 X-Ray Crystallography

Attempts were made to crystallise all complexes, for characterisation and in the hope that solid state structures would provide information on substituent effects. It was possible to obtain the structures of [Cu(**L1**-H)$_2$], [Cu(**L2**-H)$_2$], [Cu(**L3**-H)$_2$], [Cu(**L6**-H)$_2$] and [Cu(**L7**-H)$_2$], whilst [Cu(**L4**-H)$_2$] could only be crystallised as a bis-pyridine adduct. Crystals of [Cu(**L5**-H)$_2$] were isolated but were badly twinned and diffracted poorly, giving unsolvable data sets. The complexes of the 5-*t*-octyl substituted ligands **L8** and **L9** are waxy solids, and as single crystals of the complexes of their 5-*t*-butyl analogues **L1** and **L4** were successfully isolated, attempts to crystallise them were not pursued.

All structures contain the *pseudo*macrocyclic unit with interligand H-bonds typical of bis-salicylaldoximato copper(II) complexes.[6] The 3-substituents impart a range of interesting and different structural characteristics, and they are described below. The nature of interactions *between* [Cu(**L**-H)$_2$] units varies considerably and is dependent

on the nature of the 3-substituent. A comparison of relevant contacts and bond distances is presented at the end of this section in Table 2.4.

2.4.2.1 [Cu(L1-H)$_2$]

The solid state structure of [Cu(L1-H)$_2$] is dominated by axial contacts between Cu^{II} atoms and oxime O atoms of adjacent molecules (Figure 2.15), which results in three crystallographically independent half-molecules in the unit cell, each based around a centre of symmetry on the Cu^{II} atom.
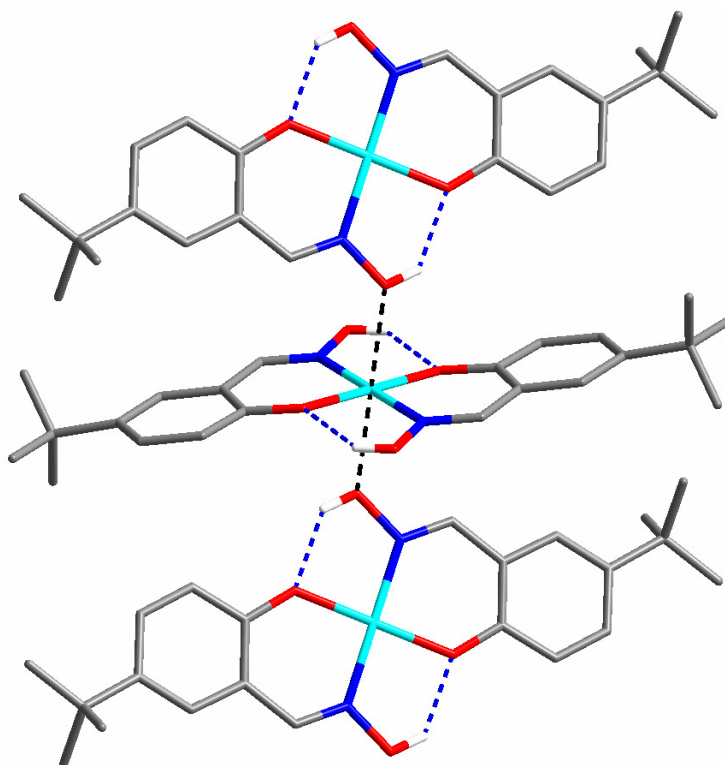
Figure 2.15: Axial Cu^{II} contacts in the solid state structure of [Cu(**L1-**H)$_2$]. Hydrogen atoms not involved in H-bonding omitted for clarity.

Each copper atom has oxime O atoms from adjacent molecules in both axial positions, giving it an overall Jahn-Teller distorted octahedral coordination sphere. These axial interactions involve every copper atom and every oximic O atom, leading to an infinite 2D network arrangement, with 2D sheets parallel to the *ab* plane. The network of copper, nitrogen and oxygen atoms can be seen clearly by

removing all C and H atoms in the structure and viewing down the *c* axis (Figure 2.16).
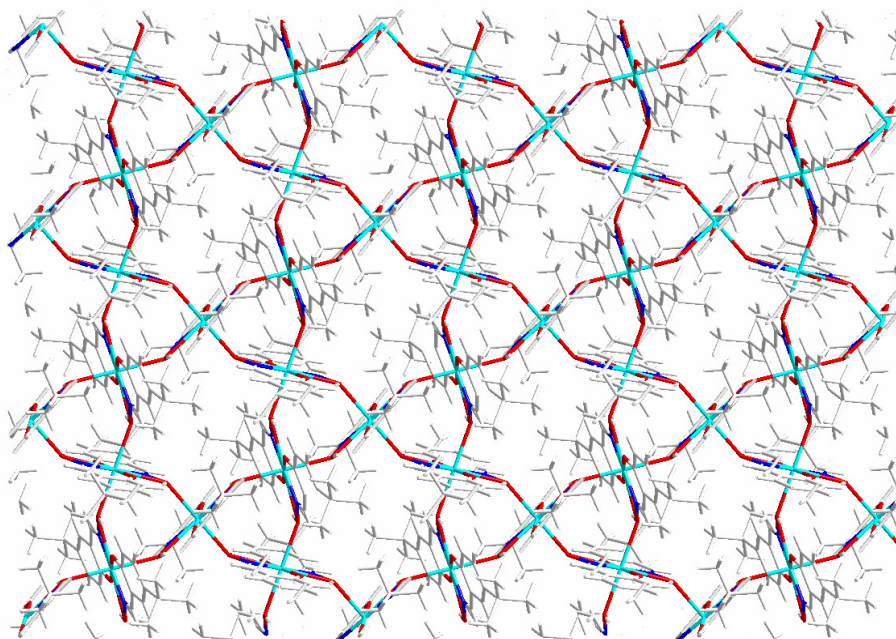
Figure 2.16: Infinite 2D network of Cu, N and O atoms in the solid state structure of [Cu(**L1-**H)$_2$] viewed down the *c* axis (C and H atoms removed for clarity).

This ordering of the atoms on the microscopic scale manifests itself in the macroscopic properties of the solid, and crystals of [Cu(**L1**-H)$_2$] grow as very thin, hexagonal plates.

2.4.2.2 [Cu(**L2**-H)$_2$]

The most interesting feature in the solid state structure of [Cu(**L2**-H)$_2$] is the way in which the [Cu(**L2**-H)$_2$] units pack. There are two independent molecules in the unit cell, which are positioned directly above each other at a rotation of 45°. A 4$_2$ axis runs through the copper atoms, parallel to the *c* axis, generating a helical structure and an inversion centre in the middle of the cell generates a symmetry related, opposite handed helix. The copper atoms within the helices (Figure 2.17) are separated by distances of 3.345(8) Å and 3.341(8) Å.
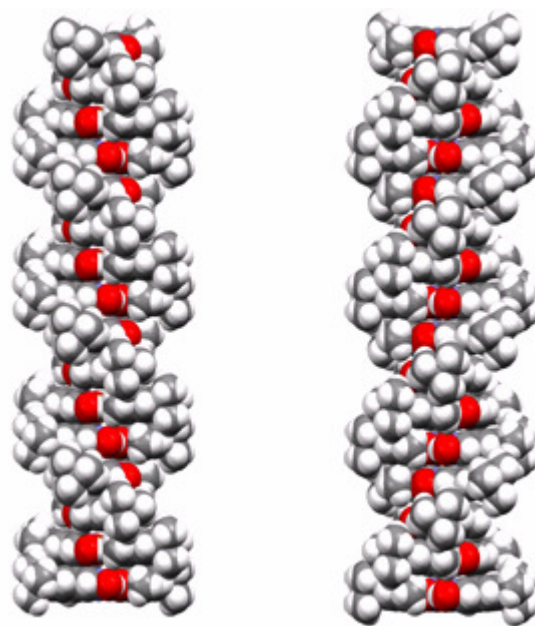
Figure 2.17: Space-filling representation of the left and right handed supramolecular helices of [Cu(**L2**-H)$_2$].

2.4.2.3 [Cu(**L3**-H)$_2$]

In comparison to the previously described complexes, the solid state structure of [Cu(**L3**-H)$_2$] is relatively simple: there are no significant supramolecular interactions between complex units. There are two independent molecules in the unit cell, one centrosymmetric and one not, and the former is displayed in Figure 2.18.
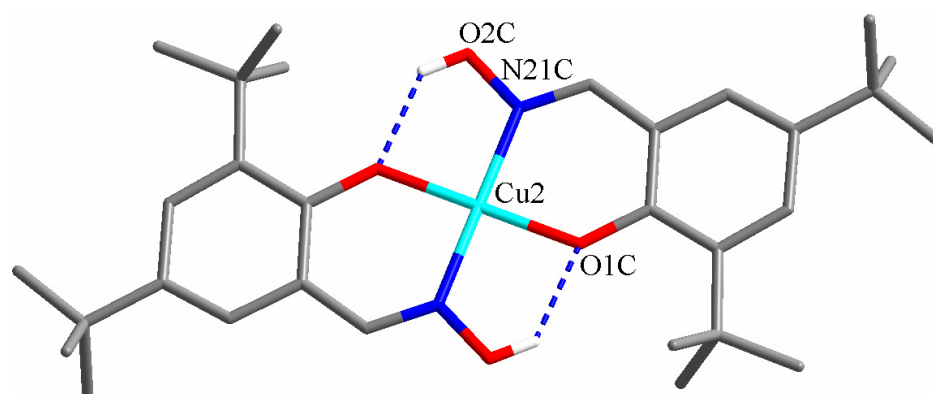
Figure 2.18: Solid state structure of the centrosymmetric molecule of [Cu(**L3**-H)$_2$] with selected atom labels. Hydrogen atoms not involved in H-bonding omitted for clarity.

The steric bulk of the 3-^{t}Bu group is evident, and its potential disrupting effect on the intracomplex H-bonding is discussed in Chapter 3. It was also thought to be responsible for suppressing intermolecular contacts between the coordination spheres of complex units.

2.4.2.4 [Cu(**L4**-H)$_2$(py)$_2$]

Coordination in the Cu^{II} axial sites is not limited to atoms from other complex molecules. [Cu(**L4**-H)$_2$] is only soluble in the highly donating solvents THF, DMSO and pyridine, indicating that solubility is imparted by axial coordination of the solvent. The crystal structure of [Cu(**L4**-H)$_2$(pyridine)$_2$] shows this axial coordination in the solid state (Figure 2.19).
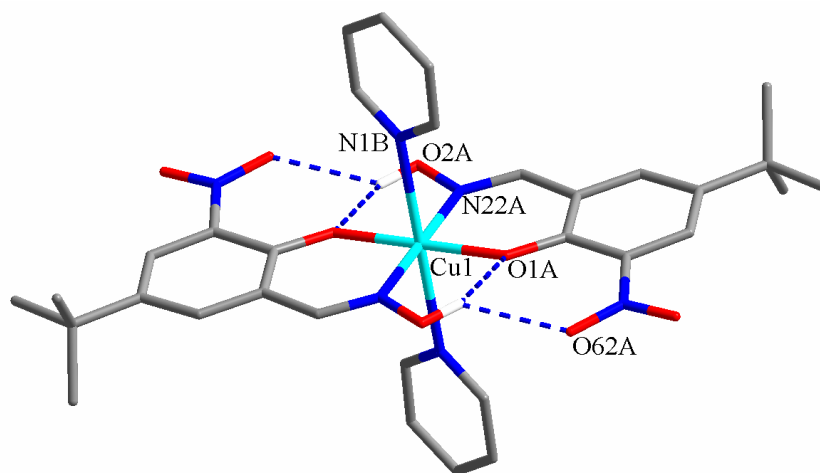
Figure 2.19: Solid state structure of one of the two crystallographically independent centrosymmetric complexes, [Cu(**L4**-H)$_2$(py)$_2$] (py = pyridine), with selected atom labels. Hydrogen atoms not involved in H-bonding omitted for clarity.

There are two crystallographically independent half-complexes in the asymmetric unit, with the extent of axial coordination slightly different in each case. One molecule has the pyridine nitrogen atom (N1) closer to the copper centre (Table 2.3) which causes the cavity size to be slightly larger, due to Jahn-Teller distortions.[33]

	Cu-N22 / Å	Cu-O1 / Å	Hole Size / Å	Cu-N1(py) / Å
Molecule 1	1.956(5)	1.926(4)	1.941(6)	2.483(5)
Molecule 2	1.957(5)	1.911(4)	1.934(6)	2.560(4)

Table 2.3: The effect of axial pyridine coordination on the hole sizes of the crystallographically independent molecules in the unit cell of [Cu(**L4**-H)$_2$(py)$_2$] (py = pyridine).

2.4.2.5 [Cu(**L6**-H)$_2$]

The solid state structure of [Cu(**L6**-H)$_2$] is similar to that of [Cu(**L3**-H)$_2$], in that there are no axial interactions with the centrosymmetric copper centre (Figure 2.20).
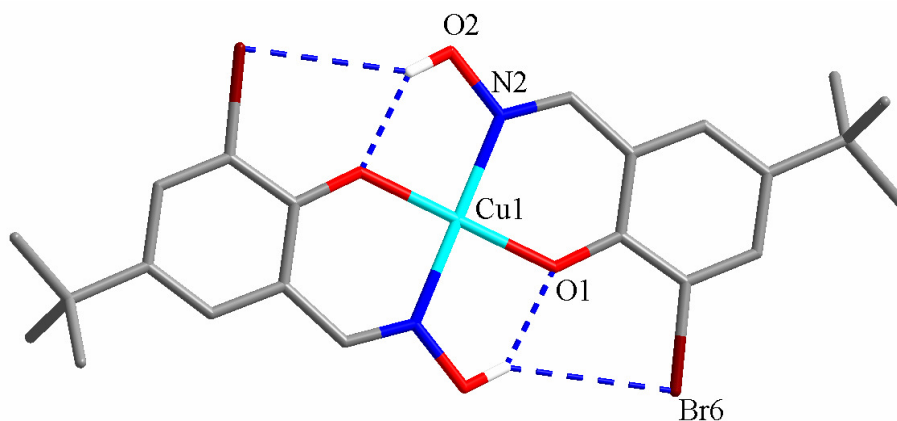
Figure 2.20: Solid state structure of [Cu(**L6**-H)$_2$] with selected atoms labels. Hydrogen atoms not involved in H-bonding omitted for clarity.

2.4.2.6 [Cu(**L7**-H)$_2$]

As with [Cu(**L3**-H)$_2$] and [Cu(**L6**-H)$_2$], the solid state structure of [Cu(**L7**-H)$_2$] contains no axial interactions. The structure differs from both in that there is no centre of symmetry on the Cu^{II} atom (Figure 2.21).
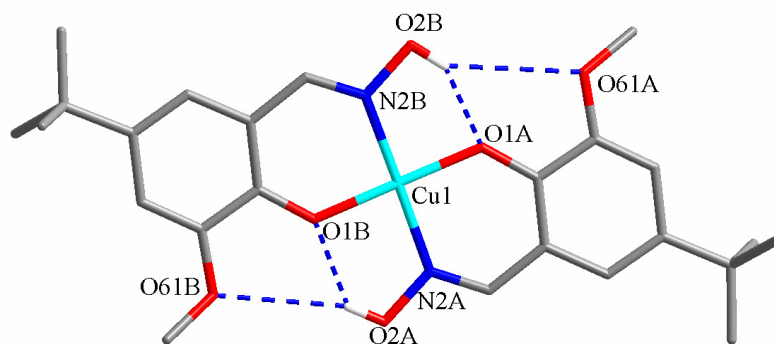
Figure 2.21: Solid state structure of [Cu(**L7**-H)$_2$] with selected atoms labels. Hydrogen atoms not involved in H-bonding omitted for clarity.

2.4.2.7 Comparisons

A comparison of some relevant bond and contact distances in the complexes may reveal some interesting solid state trends (Table 2.4).

Contact / Bond (Å)	[Cu(L1-H)$_2$]$^{[a]}$	[Cu(L2-H)$_2$]$^{[b]}$	[Cu(L3-H)$_2$]$^{[b]}$	[Cu(L4-H)$_2$]$^{[b,c]}$	[Cu(L6-H)$_2$]	[Cu(L7-H)$_2$]$^{[d]}$
Cu-N	1.943(3)	1.936(4)	1.923(8)	1.957(7)	1.954(3)	1.947(4)
Cu-O	1.904(3)	1.881(3)	1.920(8)	1.919(6)	1.885(2)	1.871(4)
Hole Size	1.924(4)	1.909(5)	1.922(11)	1.938(9)	1.920(4)	1.909(6)
NO···OPh	2.583(5)	2.616(6)	2.625(10)	2.655(9)	2.627(4)	2.609(6)
Cu-axial	2.579(4)	3.343(11)	n/a	2.522(6)	n/a	n/a
NO···X	n/a	n/a	n/a	2.933(9)	3.722(2)	3.666(6)
NOH···X	n/a	n/a	n/a	2.305(6)	3.00(4)$^{[e]}$	2.88(4)$^{[e]}$

[a]Values are average of 3 crystallographically independent half-molecules. [b]Values are average of 2 crystallographically independent half-molecules. [c]Bis-pyridine adduct. [d]Values are average of the two crystallographically halves of the molecule. [e]From calculated H-positions.

Table 2.4: Some relevant bond and contact distances in the crystal structures of copper(II) complexes solved in this chapter.

Before the structures were solved it was hoped that determination of the "hole sizes" produced by the $N_2O_2^{2-}$ donor sets would help define the effect of the 3-substituents. In practice, as the intermolecular interactions involving the copper coordination spheres varied significantly between the structures, this was unlikely to be the case. The observed cavity sizes are all relatively similar and do not show the variations seen in the hole sizes of the free ligand dimers (Section 2.3.3.1). However, the cavity sizes do reveal the effect of axial coordination, with Jahn Teller distortions ensuring the largest hole sizes belong to the two complexes with the greatest axial interactions, [Cu(**L1**-H)$_2$] and [Cu(**L4**-H)$_2$(py)$_2$].

2.5 Evaluation of Copper Binding Strength by Solvent Extraction

Experiments were carried out to assess the relative "strengths" as copper(II) extractants of the ligand series (Figure 2.22). Stoichiometric quantities of the ligand in chloroform and copper sulfate in water at different pH values were mixed overnight, separated, the copper content of the organic phase measured by ICP-OES (Section 2.1.4) and the pH of the aqueous phase measured (the equilibrium pH).
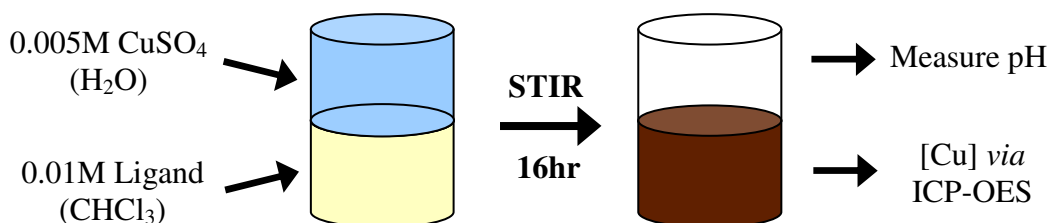
Figure 2.22: Solvent extraction protocols for the measurement of relative extractive efficacies of the extractant series.

Plotting percentage copper in the organic phase against equilibrium pH gives characteristic S-curves, which define loading behaviour as described in Chapter 1. The pH$_{0.5}$, the pH at which 50% loading of copper in the organic phase is achieved, was used as a measure of extractant strength. As protons are liberated in the binding of copper and its transfer from the aqueous phase, the ligand with the lowest pH$_{0.5}$

value is the strongest extractant. A successful extraction will show a range of copper loadings from 0-100 % over the appropriate pH range.

Figure 2.23: Photograph of the organic phases of the extraction of copper(II) by **L2**, showing an ideal range of copper loading from pH 0-3.5.

Figure 2.23 depicts the organic phases for the extraction of copper(II) by **L2**, with little colour on the left hand side showing very low copper loading, and the brown copper complex on the right hand side showing high loading.

The relative strengths of copper(II) extraction were determined using the procedure outlined in Section 2.7.5. It was not possible to determine the binding strength of **L4** due to the limited solubility of its copper(II) complex, but the effect of 3-nitro substitution was examined using **L9**, an analogue with a larger 5-*t*-octyl group to ensure solubility. To ensure that changing the nature of the alkyl chain in the 5-position had no effect on $pH_{0.5}$, the binding strength of the unsubstituted 5-*t*-octyl analogue **L8** was also investigated. The pH loading profiles for all ligands are shown overleaf in Figure 2.24.

Extraction strengths follow the order **L6 > L9 > L5 > L7 > L2 ≥ L1 ≥ L8 > L3**, or by substituent, $Br > NO_2 > Cl > OMe > Me ≥ H > {}^tBu$. The $pH_{0.5}$ values for **L1** and **L8** are very similar, showing that changing the length of the alkyl chain in the 5-position has little influence on extractive ability, in agreement with the literature.[34] 3-Substitution clearly has a major influence on extractant strength, with the substituents changing the distribution coefficients for copper by two orders of magnitude.

L	L1	L2	L3	L5	L6	L7	L8	L9
pH$_{0.5}$	1.68	1.67	2.64	0.91	0.42	1.09	1.73	0.70
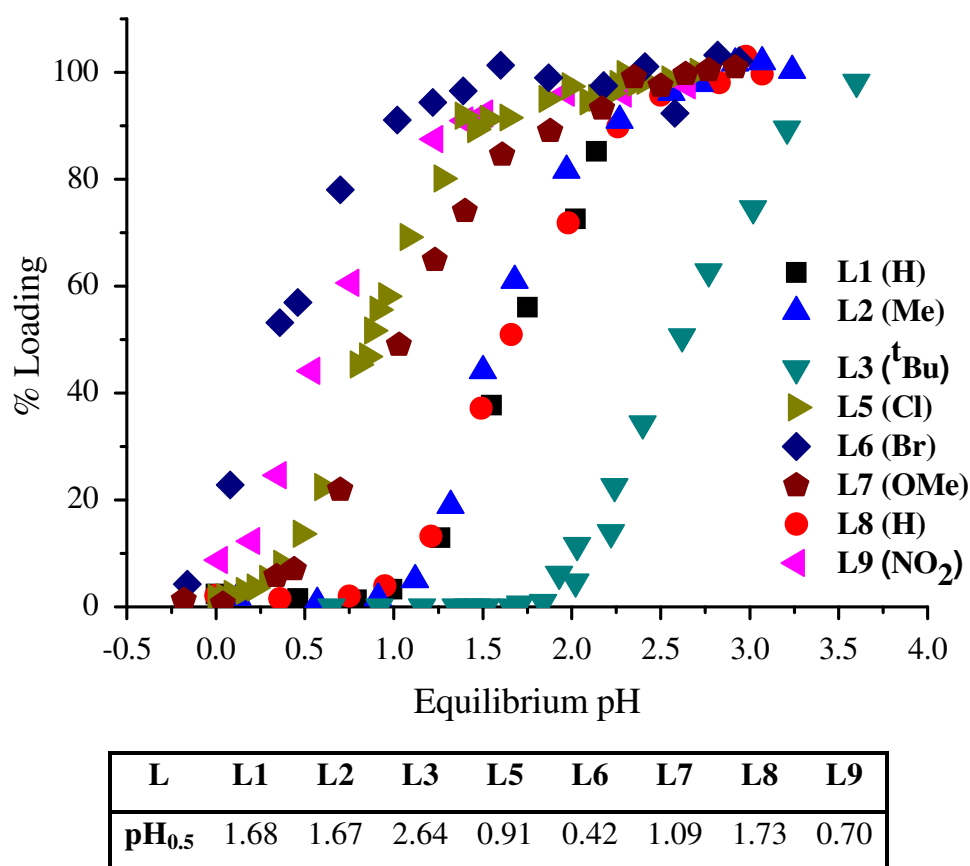
Figure 2.24: pH loading profiles and pH$_{0.5}$ values for loading of copper by 0.01 M chloroform solutions of **L1**-**L9** from equal volumes of 0.01 M aqueous solutions of copper sulfate. 100% copper loading based on a 1Cu:2**L** ratio..

A rough trend can be seen, with electron-withdrawing groups tending to increase extraction strength, whilst electron-donating groups seem to have the opposite effect. One obvious deviation from this observation is the fact that **L7** has an electron-donating group but has increased extraction strength.

Another trend is discernable. Substituents that can act as H-bond acceptors, *i.e.* those with the potential to form bifurcated hydrogen bonds (Figure 2.1) increase extraction strength, while **L3**, with a bulky *t*-butyl group in the 3-position, is the weakest extractant. Added to the fact that the 3-methyl group has very little effect on extractant strength, it would seem that the 3-substituent's ability to interact with the stabilising intracomplex hydrogen bonding motif, both in a positive and negative fashion, has a large influence on extractive efficacy.

2.6   Conclusions and Future Work

The syntheses of **L1**-**L9** have shown that 3-substituted salicylaldoximes can be prepared on the gram scale using facile, high yielding methods.   The synthetic strategies employed have demonstrated the feasibility of large scale syntheses in order to further analyse these ligands and their copper(II) complexes.

Characterisation of **L1**-**L9** by X-ray crystallography has shown the effects of 3-substitution on salicylaldoxime solid state assemblies, including the formation of a novel, 6-membered H-bonded dimer by the 3-NO$_2$ substituted ligands **L4** and **L9**. Crystallographic characterisation of copper(II) complexes of **L1**, **L2**, **L3**, **L4**, **L6** and **L7** has illustrated the wide variety of supramolecular architectures facilitated by axial interactions with the copper(II) centres, including infinite 2D networks and nano-helices.   Further analysis of the solid state structures, with particular focus on the effect of 3-substitution on the cavity size of 14-membered *pseudo*macrocyclic dimers, is detailed in Chapter 3.

Solvent extraction experiments have confirmed that **L1**-**L9** are effective copper(II) extractants.   The first systematic study on a coherent 3-substituted salicylaldoxime ligand series has demonstrated that simply by changing the nature of the 3-substituent, the extractive efficacies of the ligands can be tuned over a range of two pH units, or two orders of magnitude.   Strength is increased by substitution of groups with hydrogen bond acceptor properties and also electron-withdrawing groups, and *vice versa*.

Having shown the effect of 3-substitution on copper extractive efficacy, experiments were devised to explain this phenomenon.   These experiments, alongside attempts to identify the prominent substituent effect and so form a tentative model for prediction of effects on the extractive behaviour of ligands, are described in Chapter 3.

2.7 Experimental

2.7.1 Chemicals and Instrumentation

All solvents and reagents were used as received from Aldrich, Fisher, Fluorochem and Acros. ^{1}H and ^{13}C NMR were obtained using a Bruker AC250 spectrometer at ambient temperature. Chemical shifts (δ) are reported in parts per million (ppm) relative to internal standards. Fast atom bombardment mass spectrometry was carried out using a Kratos MS50TC spectrometer with a 3-nitrobenzyl alcohol (NOBA) or thioglycerol matrix. IR spectra were collected on a JASCO FT/IR 410 spectrometer in a glass cell. Analytical data was obtained on a CE-440 Elemental Analyser by the University of Edinburgh Microanalytical Service. ICP-OES analysis was carried out using a Perkin Elmer Optima 5300DV spectrometer. The measurement of pH was carried out using a Fisher Scientific AR50 pH meter. CHN analyses are not available for (**1**) and (**2**) due to their tendency to degrade.

2.7.2 Ligand Synthesis

4-*tert*-Butyl-2-chlorophenol (1). 4-*tert*-Butylphenol (5.00 g, 33.3 mmol) was dissolved in DCM (50 ml) and cooled to 0 °C in an ice bath. Sulfuryl chloride (5.00 g, 37.0 mmol) was added dropwise and stirred for 3 hr, after which MeOH (1.2 g, 37.5 mmol) was added dropwise and the solution stirred overnight. The solvent was removed *in vacuo* to give a cloudy oil, which was purified by silica-60 wet flash column chromatography (5% ethyl acetate in hexane eluent) to give a colourless oil (5.73 g, 93%). ^{1}H NMR (250 MHz, CDCl$_3$): δ_H (ppm) 1.15 (s, 9H, C(C*H*$_3$)$_3$), 6.85 (d, 1H, Ar*H*), 7.05 (d, 1H, Ar*H*), 7.18 (s, 1H, Ar*H*); ^{13}C NMR (63 MHz, CDCl$_3$): δ_C (ppm) 31.8 (3C, C(**C**H$_3$)$_3$), 34.6 (1C, **C**(CH$_3$)$_3$), 116.3 (1C, aromatic **C**H), 119.8 (1C, aromatic **C**), 125.7 (1C, aromatic **C**H), 126.4 (1C, aromatic **C**H), 145.0 (1C, aromatic **C**), 149.5 (1C, aromatic **C**); FABMS *m/z* 185 (MH$^+$).

2-Bromo-4-*tert*-butylphenol (2). 4-*tert*-Butylphenol (5.140 g, 34 mmol) and tetra-*n*-butylammonium tribromide (16.50 g, 34 mmol) were dissolved in dichloromethane (100 ml) and methanol (60 ml) and stirred for 30 min. The solvent was removed *in vacuo* and the resulting orange oil partitioned between diethyl ether (100 ml) and water (100 ml). The organic phase was separated, washed with saturated brine (2 x 50 ml) and water (50 ml), dried over MgSO$_4$ and the solvent removed to give a slightly pink oil which was purified by silica-60 wet flash column chromatography (2% ethyl acetate in hexane eluent) to give a colourless oil (5.82 g, 75%). ^{1}H NMR (250 MHz, CDCl$_3$): δ_H (ppm) 1.13 (s, 9H, C(CH_3)$_3$), 6.83 (d, 1H, ArH), 7.05 (dd, 1H, ArH), 7.32 (d, 1H, ArH); ^{13}C NMR (63 MHz, CDCl$_3$): δ_C (ppm) 31.9 (3C, C(**C**H$_3$)$_3$), 34.6 (1C, **C**(CH$_3$)$_3$), 110.4 (1C, aromatic **C**), 116.2 (1C, aromatic **C**H), 126.6 (1C, aromatic **C**H), 129.3 (1C, aromatic **C**H), 145.5 (1C, aromatic **C**), 150.4 (1C, aromatic **C**); FABMS *m/z* 230 (MH$^+$).

5-*tert*-Butyl-2-hydroxybenzaldehyde (3). Magnesium turnings (20 g, 800 mmol), methanol (373 ml), toluene (160 ml) and magnesium methoxide (a few drops of 8% w/w methanol solution) were refluxed until all magnesium was dissolved and H$_2$ evolution stopped. 4-*tert*-Butylphenol (200 g, 1.3 mol) was added and refluxed for 1 hr. Toluene (333 ml) was added and the mixture distilled under vacuum to remove the methanol/toluene azeotrope. A slurry of paraformaldehyde (120 g, 4 mol) in toluene (200 ml) was added slowly with continuous distillation, and heated for a further 2 hrs. After cooling to room temperature, H$_2$SO$_4$ (20%, 800 ml) was added slowly with stirring and heated to 50 °C to dissolve all solids. The product was extracted with toluene (2 x 400 ml), washed with H$_2$SO$_4$ (10%, 2 x 150 ml) and water (150 ml), dried over MgSO$_4$ and the solvent removed *in vacuo*. Purification by vacuum distillation (1 mm Hg, 120 °C) and silica-60 wet flash column chromatography (2% ethyl acetate in hexane eluent) yielded a bright yellow oil (144.2 g, 62.3%). (Anal. Calc. for C$_{11}$H$_{14}$O$_2$: C, 74.1; H, 7.9. Found: C, 73.4; H, 8.3%); ^{1}H NMR (250 MHz, CDCl$_3$): δ_H (ppm) 1.25 (s, 9H, C(CH_3)$_3$), 6.87 (d, 1H, ArH), 7.43 (d, 1H, ArH), 7.52 (dd, 1H, ArH), 9.81 (s, 1H, CHO), 10.80 (s, 1H, OH); ^{13}C NMR (63 MHz, CDCl$_3$): δ_C (ppm) 31.5 (3C, C(**C**H$_3$)$_3$), 34.0 (1C, **C**(CH$_3$)$_3$), 117.0 (1C, aromatic **C**H), 120.0 (1C, aromatic **C**), 129.5 (1C, aromatic **C**H), 134.5

(1C, aromatic **CH**), 142.5 (1C, aromatic **C**), 159.5 (1C, aromatic **C**), 197.0 (1C, Ar**C**HO); FABMS m/z 179 (MH)$^+$.

2-Hydroxy-5-*tert*-octylbenzaldehyde (4). Magnesium turnings (20 g, 800 mmol), methanol (373 ml), toluene (160 ml) and magnesium methoxide (a few drops of 8% w/w methanol solution) were refluxed until all magnesium was dissolved and H_2 evolution stopped. 4-*tert*-Octylphenol (268.2 g, 1.3 mol) was added and refluxed for 1 hr. Toluene (333 ml) was added and the mixture distilled under vacuum to remove the methanol/toluene azeotrope. A slurry of paraformaldehyde (120 g, 4 mol) in toluene (200 ml) was added slowly with continuous distillation, and heated for a further 2 hrs. After cooling to room temperature, H_2SO_4 (20%, 800 ml) was added slowly with stirring and heated to 50 °C to dissolve all solids. The product was extracted with toluene (2 x 400 ml), washed with H_2SO_4 (10%, 2 x 150 ml) and water (150 ml), dried over $MgSO_4$ and the solvent removed *in vacuo*. Purification by silica-60 wet flash column chromatography (2% ethyl acetate in hexane eluent) yielded an off white solid (196.2 g, 64.5%). (Anal. Calc. for $C_{15}H_{22}O_2$: C, 76.9; H, 9.5. Found: C, 77.2; H, 9.9%); ^{1}H NMR (250 MHz, CDCl$_3$): δ_H (ppm) 0.68 (s, 9H, C(CH_3)$_3$), 1.30 (s, 6H, C(CH_3)$_2$), 1.66 (s, 2H, CH_2), 6.85 (d, 1H, ArH), 7.42 (s, 1H, ArH), 7.48 (dd, 1H, ArH), 9.82 (s, 1H, ArCHO), 10.80 (s, 1H, ArOH); ^{13}C NMR (63 MHz, CDCl$_3$): δ_C (ppm) 30.4 (2C, C(**C**H$_3$)$_2$), 30.8 (3C, C(**C**H$_3$)$_3$), 31.3 (1C, **C**(CH$_3$)$_3$), 36.9 (1C, **C**(CH$_3$)$_2$), 55.6 (1C, **C**H$_2$) 116.0 (1C, aromatic **C**H), 119.0 (1C, aromatic **C**), 129.5 (1C, aromatic **C**H), 134.4 (1C, aromatic **C**H), 140.8 (1C, aromatic **C**), 158.4 (1C, aromatic **C**), 195.8 (1C, Ar**C**HO); FABMS m/z 235 (MH$^+$).

5-*tert*-Butyl-2-hydroxy-3-methylbenzaldehyde (5). A mixture of hexamethylenetetramine (20.0 g, 142 mmol) and 4-*tert*-butyl-2-methylphenol (4.93 g, 30 mmol) was heated in trifluoroacetic acid (60 ml) to 90˚C for 16 h under reflux. The mixture was poured still hot into 1 M HCl (200 ml), stirred for 6 h and extracted with DCM (3 x 150 ml). The combined organic phases were washed with water, dried over $MgSO_4$ and the solvent removed *in vacuo*. The sticky orange solid was purified by silica-60 wet flash column chromatography (5% ethyl acetate in hexane eluent) to yield a pale orange solid (4.24 g, 73%). (Anal. Calc. for $C_{12}H_{16}O_2$: C,

75.0; H, 8.4. Found: C, 74.3; H, 8.7%); ^{1}H NMR (250 MHz, CDCl$_3$): δ_H (ppm) 1.24 (s, 9H, C(C*H*$_3$)$_3$), 2.20 (s, 3H, C*H*$_3$), 7.28 (m, 1H, Ar*H*), 7.37 (m, 1H, Ar*H*), 9.79 (s, 1H, C*H*O), 11.02 (s, 1H, O*H*); ^{13}C NMR (63 MHz, CDCl$_3$): δ_C (ppm) 15.7 (1C, **CH**$_3$) 31.7 (3C, C(**CH**$_3$)$_3$), 34.4, (1C, **C**(CH$_3$)$_3$), 119.8 (1C, aromatic **C**), 126.6 (1C, aromatic **CH**), 127.7 (1C, aromatic **CH**), 136.2 (1C, aromatic **C**), 142.6 (1C, aromatic **C**), 158.3 (1C, aromatic **C**), 197.4 (1C, Ar**C**HO); FABMS *m/z* 192 (MH$^+$).

5-*tert*-Butyl-2-hydroxy-3-nitrobenzaldehyde (6). Nitric acid (70%, 7.0 ml, 160 mmol) was added dropwise to a solution of **(3)** (25.2 g, 140 mmol) in glacial acetic acid (25 ml) at 0 °C. The mixture was stirred at 55 °C for 16 h, cooled to room temperature and the thick mother liquors were decanted from the bright yellow solid, which was washed with 50:50 hexane: diethyl ether. Recrystallisation from hexane yielded a deep yellow product (10.4 g, 33%). (Anal. Calc. for C$_{11}$H$_{13}$NO$_4$: C, 59.2; H, 5.9; N, 6.3. Found: C, 58.7; H, 5.7; N, 6.4%); ^{1}H NMR (250 MHz, CDCl$_3$): δ_H (ppm) 1.33 (s, 9H, C(C*H*$_3$)$_3$), 8.12 (d, 1H, Ar*H*), 8.31 (d, 1H, Ar*H*), 10.38 (s, 1H, C*H*O), 11.22 (s, 1H, ArO*H*); ^{13}C NMR (63 MHz, CDCl$_3$): δ_C (ppm) 30.8 (3C, C(**CH**$_3$)$_3$), 34.4 (1C, **C**(CH$_3$)$_3$), 124.8 (1C, aromatic **C**), 127.8 (1C, aromatic **CH**), 134.2 (1C, aromatic **CH**), 134.6 (1C, aromatic **C**), 143.3 (1C, aromatic **C**), 154.4 (1C, aromatic **C**), 189.3 (1C, Ar**C**HO); FABMS *m/z* 223 (MH$^+$).

5-*tert*-Butyl-3-chloro-2-hydroxybenzaldehyde (7). A mixture of hexamethylenetetramine (14.0 g, 100 mmol) and **(1)** (4.00 g, 21.6 mmol) was heated in trifluoroacetic acid (60 ml) to 90°C for 72 h under reflux. The reaction mixture was poured still hot into 1 M HCl (200 ml) and stirred for 6 h. A yellow precipitate was filtered, washed with water (3 x 50 ml) and redissolved in DCM (200 ml). The organic phase was washed with water (3 x 100 ml), separated and dried over MgSO$_4$. The solvent was removed *in vacuo* to yield a yellow solid which was used without further purification (3.23 g, 70%). (Anal. Calc. for C$_{11}$H$_{13}$ClO$_2$: C, 62.1; H, 6.2. Found: C, 61.7 H, 6.2%); ^{1}H NMR (250 MHz, CDCl$_3$): δ_H (ppm) 1.24 (s, 9H, C(C*H*$_3$)$_3$), 7.40 (s, 1H, Ar*H*), 7.58 (s, 1H, Ar*H*), 9.82 (s, 1H, C*H*O), 11.23 (s, 1H, O*H*); ^{13}C NMR (63 MHz, CDCl$_3$): δ_C (ppm) 31.5 (3C, C(**CH**$_3$)$_3$), 34.7, (1C, **C**(CH$_3$)$_3$), 121.2 (1C, aromatic **C**), 122.0 (1C, aromatic **C**), 128.9 (1C, aromatic **CH**),

135.0 (1C, aromatic **CH**), 144.1 (1C, aromatic **C**), 155.3 (1C, aromatic **C**), 196.7 (1C, Ar**C**HO); FABMS *m/z* 213 (MH$^+$).

3-Bromo-5-*tert*-butyl-2-hydroxybenzaldehyde (8). A mixture of hexamethylenetetramine (9.1 g, 65 mmol) and **(2)** (3.00 g, 13.1 mmol) was heated in trifluoroacetic acid (50 ml) to 90°C for 16 h under reflux. The reaction mixture was poured still hot into 2 M HCl (150 ml) and stirred for 8 h. An off-white precipitate was filtered, washed with water (50 ml) and vacuum dried over P_2O_5 to yield an off white powder (3.039 g, 90%). (Anal. Calc. for $C_{11}H_{13}BrO_2.0.5H_2O$: C, 49.6; H, 5.3. Found: C, 50.0 H, 5.6%); ^{1}H NMR (250 MHz, CDCl$_3$): δ_H (ppm) 1.15 (s, 9H, C(C*H*$_3$)$_3$), 7.33 (d, 1H, Ar*H*), 7.63 (s, 1H, Ar*H*), 9.68 (s, 1H, C*H*O), 11.2 (br, 1H, O*H*); ^{13}C NMR (63 MHz, CDCl$_3$): δ_C (ppm) 31.6 (3C, C(**C**H$_3$)$_3$), 34.7, (1C, **C**(CH$_3$)$_3$), 111.2 (1C, aromatic **C**), 121.0 (1C, aromatic **C**), 129.8 (1C, aromatic **CH**), 138.0 (1C, aromatic **CH**), 144.6 (1C, aromatic **C**), 156.2 (1C, aromatic **C**), 196.7 (1C, Ar**C**HO); FABMS *m/z* 258 (MH$^+$).

2-Hydroxy-3-nitro-5-*tert*-octylbenzaldehyde (9). **(4)** (5.22 g, 22.3 mmol) was dissolved in glacial acetic acid (50 ml) and cooled over an ice bath. Nitric acid (70%, 2.5 ml, 40 mmol) in acetic acid (5 ml) was added slowly with stirring to give a yellow solution, which was allowed to come to room temperature and stirred for a further 16 hr. Water (50 ml) was added and the product extracted with hexane (3 x 100 ml), washed with water and dried over MgSO$_4$. Removal of solvent gave a yellow oil which was purified by silica-60 wet flash column chromatography (5 % ethyl acetate in hexane eluent) to give a yellow oil (5.34 g, 86%). (Anal. Calc. for $C_{15}H_{21}NO_4$: C, 64.5; H, 7.6; N, 5.0. Found: C, 64.1; H, 7.8; N, 5.6%); ^{1}H NMR (250 MHz, CDCl$_3$): δ_H (ppm) 0.66 (s, 9H, C(C*H*$_3$)$_3$), 1.33 (s, 6H, C(C*H*$_3$)$_2$), 1.70 (s, 2H, C*H*$_2$), 8.06 (d, 1H, Ar*H*), 8.25 (d, 1H, Ar*H*), 10.33 (s, 1H, ArC*H*O), 11.18 (s, 1H, ArO*H*); ^{13}C NMR (63 MHz, CDCl$_3$): δ_C (ppm) 31.5 (2C, C(**C**H$_3$)$_2$), 32.3 (3C, C(**C**H$_3$)$_3$), 32.7 (1C, **C**(CH$_3$)$_3$), 38.8 (1C, **C**(CH$_3$)$_2$), 56.7 (1C, **C**H$_2$), 125.2 (1C, aromatic **C**), 128.9 (1C, aromatic **CH**), 135.1 (1C, aromatic **C**), 135.3 (1C, aromatic **CH**), 143.2 (1C, aromatic **C**), 154.8 (1C, aromatic **C**), 189.8 (1C, Ar**C**HO); FABMS *m/z* 280 (MH$^+$).

68

Oximation General Procedure. *c*1.2 equivalents of KOH and NH$_2$OH.HCl were dissolved separately in EtOH, mixed thoroughly and a white KCl precipitate removed by filtration. The filtrate was added to the precursor aldehyde, refluxed for 3 hr and the solvent removed *in vacuo*. The residue was redissolved in CHCl$_3$, washed with water 3 times, dried over MgSO$_4$ and the solvent removed *in vacuo* to yield the crude product.

5-*tert*-Butyl-2-hydroxybenzaldehyde oxime (L1). Hydroxylamine hydrochloride (3.89 g, 56 mmol), potassium hydroxide (3.19 g, 56 mmol) and (**3**) (10.20 g, 57 mmol) were reacted according to the general procedure to give an off-white solid, which was recrystallised from hexane to yield white needles (7.13 g, 65.0%). Crystals suitable for XRD analysis were grown by slow evaporation of a hexane/chloroform solution. (Anal. Calc. for C$_{11}$H$_{15}$NO$_2$: C, 68.4; H, 7.8; N, 7.3. Found: C, 68.7; H, 8.1; N, 7.3%); ν_{max}/cm^{-1} (CHCl$_3$) 3575 (free NOH), 3408br (H-bonded NOH), 3221br (PhOH), 2966 (C-H), 1623 (C=N); ^{1}H NMR (250 MHz, CDCl$_3$): δ_H (ppm) 1.35 (s, 9H, C(C*H*$_3$)$_3$), 7.00 (d, 1H, Ar*H*), 7.22 (s, 1H, Ar*H*), 7.38 (d, 1H, Ar*H*), 8.30 (s, 1H, ArC*H*N); ^{13}C NMR (63 MHz, CDCl$_3$): δ_C (ppm) 31.8 (3C, C(**C**H$_3$)$_3$), 34.4, (1C, **C**(CH$_3$)$_3$), 116.1 (1C, aromatic **C**), 116.6 (1C, aromatic **C**H), 127.7 (1C, aromatic **C**H), 129.0 (1C, aromatic **C**H), 143.0 (1C, aromatic **C**), 153.8 (1C, Ar**C**HN), 155.1 (1C, aromatic **C**); FABMS *m/z* 194 (MH$^+$).

5-*tert*-Butyl-2-hydroxy-3-methylbenzaldehyde oxime (L2). Hydroxylamine hydrochloride (1.73 g, 25.0 mmol), potassium hydroxide (1.40 g, 25.0 mmol) and (**5**) (4.00 g, 20.8 mmol) were reacted according to the general procedure to give an off white solid (2.76 g, 64%). Crystals suitable for XRD analysis were grown by slow evaporation of a hexane/chloroform solution. (Anal. Calc. for C$_{12}$H$_{17}$NO$_2$: C, 69.5; H, 8.3; N, 6.8. Found: C, 69.3; H, 8.0 ; N, 6.7 %); ν_{max}/cm^{-1} (CHCl$_3$) 3574 (free NOH), 3416br (H-bonded NOH), 3200br (PhOH), 2965 (C-H), 1623 (C=N); ^{1}H NMR (250 MHz, CDCl$_3$): δ_H (ppm) 1.17 (s, 9H, C(C*H*$_3$)$_3$), 2.20 (s, 3H, ArC*H*$_3$), 6.92 (m, 1H, Ar*H*), 7.10 (m, 1H, Ar*H*), 8.13 (s, 1H, ArC*H*N); ^{13}C NMR (63 MHz, CDCl$_3$): δ_C (ppm) 15.0 (1C, Ar**C**H$_3$), 30.4 (3C, C(**C**H$_3$)$_3$), 32.9 (1C, **C**(CH$_3$)$_3$), 114.1 (1C, aromatic **C**), 123.9 (1C, aromatic **C**), 124.0 (1C, aromatic **C**H), 128.9 (1C,

69

aromatic **CH**), 141.2 (1C, aromatic **C**), 151.8 (1C, aromatic **C**), 152.4 (1C, Ar**C**HN); FABMS *m/z* 208 (MH⁺).

3,5-Di-*tert*-butyl-2-hydroxybenzaldehyde oxime (L3). Hydroxylamine hydrochloride (1.42 g, 20.5 mmol), potassium hydroxide (1.15 g, 20.5 mmol) and 3,5-di-*tert*-butyl-2-hydroxybenzaldehyde (4 g, 17.1 mmol) were reacted according to the general procedure to yield a light yellow microcrystalline solid (3.51 g, 82%). Crystals suitable for XRD analysis were grown by slow evaporation of a hexane/chloroform solution. (Anal. Calc. for $C_{15}H_{23}NO_2$: C, 72.3; H, 9.3; N, 5.6. Found: C, 72.5; H, 9.1; N, 5.5%); v_{max}/cm^{-1} (CHCl$_3$) 3577 (free NOH), 3443br (H-bonded NOH), 3162br (PhOH), 2964 (C-H), 1624 (C=N); ^{1}H NMR (250 MHz, CDCl$_3$): δ_H (ppm) 1.24 (s, 9H, C(C*H$_3$*)$_3$), 1.36 (s, 9H, C(C*H$_3$*)$_3$), 6.94 (m, 1H, Ar*H*), 7.28 (m, 1H, Ar*H*), 8.17 (s, 1H, ArC*H*N); ^{13}C NMR (63 MHz, CDCl$_3$): δ_C (ppm) 29.9 (3C, C(**CH$_3$**)$_3$), 31.9 (3C, C(**CH$_3$**)$_3$), 34.6 (1C, **C**(CH$_3$)$_3$), 35.5 (1C, **C**(CH$_3$)$_3$), 116.1 (1C, aromatic **C**), 126.0 (1C, aromatic **CH**), 126.6 (1C, aromatic **CH**), 136.9 (1C, aromatic **C**), 141.8 (1C, aromatic **C**), 154.5 (1C, aromatic **C**), 154.7 (1C, Ar**C**HN); FABMS *m/z* 250 (MH⁺).

5-*tert*-Butyl-2-hydroxy-3-nitrobenzaldehyde oxime (L4). Hydroxylamine hydrochloride (0.709 g, 10.2 mmol), potassium hydroxide (0.674 g, 10.2 mmol) and **(6)** (2.00 g, 9.00 mmol) were reacted according to the general procedure to yield a bright yellow solid (1.94 g, 90%). Crystals suitable for XRD analysis were grown by slow evaporation of a DCM solution. (Anal. Calc. for $C_{11}H_{14}N_2O_4$: C, 55.5; H, 5.9; N, 11.8. Found: C, 55.4; H, 5.7; N, 11.8%); v_{max}/cm^{-1} (CHCl$_3$) 3575 (free NOH), 3402br (H-bonded NOH), 3230br (PhOH), 2968 (C-H), 1633 (C=N), 1537s (NO$_2$); ^{1}H NMR (250 MHz, CDCl$_3$): δ_H (ppm) 1.26 (s, 9H, C(C*H$_3$*)$_3$), 7.93 (d, 1H, Ar*H*), 8.05 (d, 1H, Ar*H*), 8.45 (s, 1H, ArC*H*N); ^{13}C NMR (63 MHz, CDCl$_3$): δ_C (ppm) 31.4 (3C, C(**CH$_3$**)$_3$), 35.0, (1C, C(**CH$_3$**)$_3$), 122.1 (1C, aromatic **C**), 123.6 (1C, aromatic **CH**), 132.7 (1C, aromatic **CH**), 134.7 (1C, aromatic **C**), 143.7 (1C, aromatic **C**), 146.5 (1C, Ar**C**HN), 151.3 (1C, aromatic **C**); FABMS *m/z* 239 (MH⁺).

5-*tert*-Butyl-3-chloro-2-hydroxybenzaldehyde oxime (L5). Hydroxylamine hydrochloride (0.709 g, 10.2 mmol), potassium hydroxide (0.674 g, 10.2 mmol) and **(7)** (2.00 g, 9.41 mmol) were reacted according to the general procedure to yield a white solid (1.95 g, 95%). Crystals suitable for XRD analysis were grown by slow evaporation of a hexane/chloroform solution. (Anal. Calc. for $C_{11}H_{14}ClNO_2$: C, 58.0; H, 6.2; N, 6.2. Found: C, 57.6; H, 5.7; N, 6.1%); v_{max}/cm^{-1} (CHCl$_3$) 3568 (free NOH), 3433br (H-bonded NOH), 3172br (PhOH), 2967 (C-H), 1624 (C=N); ^{1}H NMR (250 MHz, CDCl$_3$): δ_H (ppm) 1.21 (s, 9H, C(C*H*$_3$)$_3$), 7.02 (s, 1H, Ar*H*), 7.32 (s, 1H, Ar*H*), 8.16 (s, 1H, C*H*N); ^{13}C NMR (63 MHz, CDCl$_3$): δ_C (ppm) 31.6 (3C, C(**C**H$_3$)$_3$), 34.6, (1C, **C**(CH$_3$)$_3$), 117.3 (1C, aromatic **C**), 121.3 (1C, aromatic **C**), 126.3 (1C, aromatic **C**H), 129.3 (1C, aromatic **C**H), 143.8 (1C, aromatic **C**), 150.8 (1C, aromatic **C**), 152.9 (1C, Ar**C**HN); FABMS *m/z* 228 (MH$^+$).

3-Bromo-5-*tert*-butyl-2-hydroxybenzaldehyde oxime (L6). Hydroxylamine hydrochloride (0.709 g, 10.2 mmol), potassium hydroxide (0.674 g, 10.2 mmol) and **(8)** (2.00 g, 7.8 mmol) were reacted according to the general procedure to yield a white solid (2.00 g, 94%). Crystals suitable for XRD analysis were grown by slow evaporation of a hexane/chloroform solution. (Anal. Calc. for $C_{11}H_{14}BrNO_2$: C, 48.6; H, 5.2; N, 5.2. Found: C, 48.4; H, 5.0; N, 5.3%); v_{max}/cm^{-1} (CHCl$_3$) 3569 (free NOH), 3437br (H-bonded NOH), 3160br (PhOH), 2968 (C-H), 1625 (C=N); ^{1}H NMR (250 MHz, CDCl$_3$): δ_H (ppm) 1.20 (s, 9H, C(C*H*$_3$)$_3$), 7.06 (d, 1H, Ar*H*), 7.48 (d, 1H, Ar*H*), 8.13 (s, 1H, C*H*N); ^{13}C NMR (63 MHz, CDCl$_3$): δ_C (ppm) 31.7 (3C, C(**C**H$_3$)$_3$), 34.6, (1C, **C**(CH$_3$)$_3$), 110.6 (1C, aromatic **C**), 117.3 (1C, aromatic **C**), 127.2 (1C, aromatic **C**H), 132.2 (1C, aromatic **C**H), 144.3 (1C, aromatic **C**), 151.7 (1C, aromatic **C**), 152.6 (1C, Ar**C**HN); FABMS *m/z* 273 (MH$^+$).

5-*tert*-Butyl-2-hydroxy-3-methoxybenzaldehyde oxime (L7). Hydroxylamine hydrochloride (0.348 g, 5 mmol), potassium hydroxide (0.280 g, 5 mmol) and 5-*tert*-butyl-2-hydroxy-3-methoxybenzaldehyde (0.501 g, 2.4 mmol) were reacted according to the general procedure to yield a white solid (0.51 g, 95%). Crystals suitable for XRD analysis were grown by slow evaporation of an acetone solution. (Anal. Calc. for $C_{12}H_{17}NO_3$: C, 64.6; H, 7.7; N, 6.3. Found: C, 64.2; H, 7.6; N,

6.2%); ν_{max}/cm^{-1} (CHCl$_3$) 3573 (free NOH), 3413br (H-bonded NOH), 3177br (PhOH), 2967 (C-H), 1624 (C=N); ^{1}H NMR (250 MHz, CDCl$_3$): δ_H (ppm) 1.25 (s, 9H, C(CH_3)$_3$), 3.85 (s, 3H, OCH_3), 6.74 (d, 1H, ArH), 6.89 (d, 1H, ArH), 8.16 (s, 1H, CHN), 9.6 (br, 1H, OH); ^{13}C NMR (63 MHz, CDCl$_3$): δ_C (ppm) 31.8 (3C, C(**CH**$_3$)$_3$), 34.7, (1C, **C**(CH$_3$)$_3$), 56.7 (1C, O**CH**$_3$), 111.9 (1C, aromatic **CH**), 116.2 (1C, aromatic **C**), 119.1 (1C, aromatic **CH**), 143.0 (1C, aromatic **C**), 145.1 (1C, aromatic **C**), 148.5 (1C, aromatic **C**), 153.4 (1C, Ar**CH**N); FABMS *m/z* 224(MH$^+$).

2-Hydroxy-5-*tert*-octylbenzaldehyde oxime (L8). Hydroxylamine hydrochloride (0.709 g, 10.2 mmol), potassium hydroxide (0.674 g, 10.2 mmol) and **(4)** (2.120 g, 9.1 mmol) were reacted according to the general procedure to give a yellow oil, which solidified overnight. This was recrystallised from hexane, yielding a white crystalline solid (1.375 g, 60%). Crystals suitable for XRD analysis were grown by slow evaporation of a hexane/chloroform solution. (Anal. Calc. for C$_{15}$H$_{23}$NO$_2$: C, 72.3; H, 9.3; N, 5.6. Found: C, 72.6; H, 9.4; N, 5.7%); ν_{max}/cm^{-1} (CHCl$_3$) 3575 (free NOH), 3393br (H-bonded NOH), 3221br (PhOH), 2957 (C-H), 1622 (C=N); ^{1}H NMR (250 MHz, CDCl$_3$): δ_H (ppm) 0.64 (s, 9H, C(CH_3)$_3$), 1.23 (s, 6H, C(CH_3)$_2$), 1.58 (s, 2H, CH_2), 6.80 (d, 1H, ArH), 7.01 (s, 1H, ArH), 7.20 (dd, 1H, ArH), 8.12 (s, 1H, ArCHN); ^{13}C NMR (63 MHz, CDCl$_3$): δ_C (ppm) 31.2 (2C, C(**CH**$_3$)$_2$), 31.2 (2C, C(**CH**$_3$)$_3$), 32.7 (1C, **C**(CH$_3$)$_3$) 38.3, (1C, **C**(CH$_3$)$_2$), 57.3 (1C, **CH**$_2$), 115.9 (1C, aromatic **C**), 116.4 (1C, aromatic **CH**), 128.5 (1C, aromatic **CH**), 129.9 (1C, aromatic **CH**), 141.9 (1C, aromatic **C**), 153.9 (1C, Ar**CH**N), 155.1 (1C, aromatic **C**); FABMS *m/z* 250 (MH$^+$).

2-Hydroxy-3-nitro-5-*tert*-octyl-benzaldehyde oxime (L9). Hydroxylamine hydrochloride (0.709 g, 10.2 mmol), potassium hydroxide (0.674 g, 10.2 mmol) and **(9)** (1.380 g, 4.94 mmol) were reacted according to the general procedure to yield a bright yellow solid (1.14 g, 79%). Crystals suitable for XRD analysis were grown by slow evaporation of a hexane/chloroform solution. (Anal. Calc. for C$_{15}$H$_{22}$N$_2$O$_4$: C, 61.2; H, 7.5; N, 9.5. Found: C, 61.3; H, 7.7; N, 9.3%); ν_{max}/cm^{-1} (CHCl$_3$) 3547 (free NOH), 3428br (H-bonded NOH), 3232br (PhOH), 2964 (C-H), 1633 (C=N), 1538s (NO$_2$); ^{1}H NMR (250 MHz, CDCl$_3$): δ_H (ppm) 0.67 (s, 9H, C(CH_3)$_3$), 1.31 (s, 6H,

C(CH_3)$_2$), 1.67 (s, 2H, CH_2), 7.91 (d, 1H, ArH), 8.03 (d, 1H, ArH), 8.44 (s, 1H, ArCHN), 10.9 (br, 1H, ArOH); ^{13}C NMR (63 MHz, CDCl$_3$): δ_C (ppm) 31.6 (2C, C(CH$_3$)$_2$), 32.3 (3C, C(CH$_3$)$_3$), 32.8 (1C, **C**(CH$_3$)$_3$), 38.7 (1C, **C**(CH$_3$)$_2$), 56.8 (1C, **C**H$_2$), 122.1 (1C, aromatic **C**), 124.1 (1C, aromatic **C**H), 133.2 (1C, aromatic **C**H), 134.6 (1C, aromatic **C**), 143.0 (1C, aromatic **C**), 146.6 (1C, aromatic **C**), 151.1 (1C, Ar**C**HN); FABMS m/z 295 (MH$^+$).

2.7.3 Copper(II) Complex Synthesis

All copper(II) complexes of the ligands were synthesised using the following general procedure. Stoichiometric amounts of the ligand and metal acetate (0.5 equivalents) were mixed in methanol (50 ml) for 24 h. Colour changes due to complex formation occurred immediately, along with precipitation. Complexes were isolated by filtration and dried under vacuum.

[Cu(L1-H)$_2$]. Cu(OAc)$_2$.H$_2$O (0.301 g, 1.51 mmol) and **L1** (0.582 g, 3.00 mmol) yielded a dark brown solid from the method above (0.529 g, 79%). Crystals suitable for X-ray diffraction analysis were grown by slow evaporation of a CHCl$_3$ solution. (Anal. Calc. for C$_{22}$H$_{28}$O$_4$N$_2$Cu: C, 59.0; H, 6.3; N, 6.3. Found: C, 59.2; H, 5.9; N, 6.2%); ν_{max}/cm^{-1} (CHCl$_3$) 3167br (NOH), 2964 (C-H), 1609 (C=N); FABMS m/z 447 (MH$^+$).

[Cu(L2-H)$_2$]. Cu(OAc)$_2$.H$_2$O (0.522 g, 2.61 mmol) and **L2** (1.071 g, 5.17 mmol) yielded a light brown solid from the method above (1.040 g, 84%). Crystals suitable for X-ray diffraction analysis were grown by slow evaporation of a hexane/CHCl$_3$ solution. (Anal. Calc. for C$_{24}$H$_{32}$O$_4$N$_2$Cu: C, 60.6; H, 6.8; N, 5.9. Found: C, 60.3; H, 6.8; N, 5.7%); ν_{max}/cm^{-1} (CHCl$_3$) 3160br (NOH), 2965 (C-H), 1603 (C=N); FABMS m/z 475 (MH$^+$).

[Cu(L3-H)$_2$]. Cu(OAc)$_2$.H$_2$O (0.281 g, 1.41 mmol) and **L3** (0.701 g, 2.81 mmol) yielded a light brown solid from the method above (0.673 g, 81%). Crystals suitable

for X-ray diffraction analysis were grown by slow evaporation of a $CHCl_3$ solution. (Anal. Calc. for $C_{30}H_{44}O_4N_2Cu$: C, 64.3; H, 7.9; N, 5.0. Found: C, 64.3; H, 7.7; N, 5.0%); ν_{max}/cm^{-1} ($CHCl_3$) 3224br (NOH), 2963 (C-H), 1604 (C=N); FABMS m/z 559 (MH$^+$).

[Cu(L4-H)$_2$]. Cu(OAc)$_2$.H$_2$O (0.460 g, 2.30 mmol) and **L4** (1.011 g, 4.43 mmol) yielded a bright green solid from the method above (0.903 g, *73%*). Crystals of a bis-pyridine adduct suitable for X-ray diffraction analysis were grown by pressure diffusion of hexane into a pyridine solution. (Anal. Calc. for $C_{22}H_{26}O_8N_4Cu$: C, 49.1; H, 4.9; N, 10.4. Found: C, 48.2; H, 3.3; N, 9.8%); ν_{max}/cm^{-1} (THF) 3257br (NOH), 2969 (C-H), 1631 (C=N), 1519s (NO$_2$); FABMS m/z 539 (MH$^+$).

[Cu(L5-H)$_2$]. Cu(OAc)$_2$.H$_2$O (0.240 g, 1.20 mmol) and **L5** (0.501 g, 2.30 mmol) yielded a brown solid from the method above (0.541 g, *88%*). (Anal. Calc. for $C_{22}H_{26}Cl_2O_4N_2Cu$: C, 51.1; H, 5.1; N, 5.4. Found: C, 51.7; H, 5.4; N, 5.2%); ν_{max}/cm^{-1} ($CHCl_3$) 3204br (NOH), 2966 (C-H), 1604 (C=N); FABMS m/z 516 (MH$^+$).

[Cu(L6-H)$_2$]. Cu(OAc)$_2$.H$_2$O (0.100 g, 0.50 mmol) and **L6** (0.270 g, 1.01 mmol) yielded a brown solid from the method above (0.284 g, *88%*). Crystals suitable for X-ray diffraction analysis were grown by slow evaporation of a MeOH solution. (Anal. Calc. for $C_{22}H_{26}Br_2O_4N_2Cu$: C, 43.6; H, 4.3; N, 4.6. Found: C, 43.9; H, 4.1; N, 4.5%); ν_{max}/cm^{-1} ($CHCl_3$) 3216br (NOH), 2966 (C-H), 1602 (C=N); FABMS m/z 607 (MH$^+$).

[Cu(L7-H)$_2$]. Cu(OAc)$_2$.H$_2$O (22.4 mg, 0.11 mmol) and **L7** (50.0 mg, 0.22 mmol) yielded a brown solid from the method above (45.8 mg, *82%*). Crystals suitable for X-ray diffraction analysis were grown by slow evaporation of a hexane/DCM solution. (Anal. Calc. for $C_{24}H_{32}O_6N_2Cu$: C, 56.7; H, 6.4; N, 5.5. Found: C, 56.6; H, 6.1; N, 5.5%); ν_{max}/cm^{-1} ($CHCl_3$) 3160br (NOH), 2964 (C-H), 1605 (C=N); FABMS m/z 507 (MH$^+$).

[Cu(L8-H)$_2$]. Cu(OAc)$_2$.H$_2$O (40.0 mg, 0.20 mmol) and **L8** (99.5 mg, 0.40 mmol) yielded a brown powder from the method above (103.5 mg, 93%). (Anal. Calc. for C$_{30}$H$_{44}$O$_4$N$_2$Cu: C, 64.3; H, 7.9; N, 5.0. Found: C, 64.3; H, 8.0; N, 5.1%); ν_{max}/cm^{-1} (CHCl$_3$) 3175br (NOH), 2959 (C-H), 1606 (C=N); FABMS m/z 560 (MH$^+$).

[Cu(L9-H)$_2$]. Cu(OAc)$_2$.H$_2$O (38.0 mg, 0.19 mmol) and **L9** (108.7 mg, 0.37 mmol) yielded a bright green solid from the method above (119.0 mg, 96%). (Anal. Calc. for C$_{30}$H$_{42}$O$_8$N$_4$Cu: C, 55.4; H, 6.5; N, 8.6. Found: C, 55.2; H, 6.3; N, 8.0%); ν_{max}/cm^{-1} (CHCl$_3$) 3241br (NOH), 2960 (C-H), 1603 (C=N), 1519s (NO$_2$); FABMS m/z 649 (MH$^+$).

2.7.4 X-Ray Structure Determinations

All crystal structures were solved by Fraser White at the University of Edinburgh Crystallography Service. Details of each solution, along with appropriate cif files, are located in appendix 7.2.1.

2.7.5 pH Dependence of Copper(II) Loading from Sulfidic Media

Experiments were carried out by contacting chloroform solutions (5 ml) of the ligands at concentrations of 0.01 mol dm^{-3}, with aqueous solutions (5 ml) of copper(II) sulfate at concentrations of 0.01 mold m^{-3}. The aqueous solution was prepared from 4 ml of 0.0125 mol dm^{-3} copper(II) sulfate solution, to which was added 1 ml of 0.1 mol dm^{-3} sodium hydroxide/water or 1 ml of 2.5 mol dm^{-3} sulfuric acid/water solution to change pH. After vigorous stirring for 16 h at room temperature, the mixtures were separated and 0.5 ml aliquots of the organic phase removed for copper analysis by ICP-OES. The calculated percentage copper(II) uptake into the organic phase was plotted against the measured equilibrium pH of the aqueous phase to give s-curves. pH$_{0.5}$ values were calculated by plotting log([Cu]$_{org}$/[Cu]$_{aq}$) vs pH for intermediate values of copper loading, with the pH$_{0.5}$

taken as the point where the linear fitted expression crossed the x axis. All solvent extraction data are located in appendix 7.2.2.

2.8   References

[1]   P. J. Mackey, *CIM Magazine*, 2007, **2**, 35.

[2]   G. A. Kordosky, *International Solvent Extraction Conference, Cape Town, South Africa, Mar. 17-21*, 2002, 853.

[3]   J. Szymanowski, 'Hydroxyoximes and Copper Hydrometallurgy', CRC Press, 1993.

[4]   P. A. Tasker, P. G. Plieger, and L. C. West, *Comprehensive Coordination Chemistry II*, 2004, **9**, 759.

[5]   K. Cramer, J. Morrison, T. Moore, and S. Kentish, *EPD Congress 2002 and Fundamentals of Advanced Materials for Energy Conversion, Proceedings of Sessions and Symposia held during the TMS Annual Meeting, Seattle, WA, United States, Feb. 17-21*, 2002, 715.

[6]   A. G. Smith, P. A. Tasker, and D. J. White, *Coordination Chemistry Reviews*, 2003, **241**, 61.

[7]   M. J. Nicol, C. A. Fleming, and J. S. Preston, *Comprehensive Coordination Chemistry*, 1987, **6**, 779.

[8]   H. M. Irving and R. J. P. Williams, *Journal of the Chemical Society*, 1953, 3192.

[9]   P. M. Cole, K. C. Sole, and A. M. Feather, *Tsinghua Science and Technology*, 2006, **11**, 153.

[10]   M. A. Garcia, A. Mejias, D. Martin, and G. Diaz, *Lead-Zinc 2000, Proceedings of the Lead-Zinc 2000 Symposium, Pittsburgh, PA, United States, Oct. 22-25, 2000*, 2000, 751.

[11]   Anon, *Mining Magazine*, 2007, 11.

[12]   M. B. Bogacki, *Solvent Extraction and Ion Exchange*, 1997, **15**, 731.

[13]   J. Szymanowski, *Critical Reviews in Analytical Chemistry*, 1995, **25**, 143.

[14]   R. F. Dalton, *Canadian Institute of Mining and Metallurgy*, 1979, **21**, 40.

[15]   J. A. Tumilty, R. F. Dalton, and J. P. Massam, *Adv. Extr. Metall., Int. Symp., 3rd*, 1977, 123.

[16]   D. C. Cupertino and A. D. Sugarman, in 'Aldoximes and ketoximes in organic phase for solvent extraction of copper and other metals from leaching solutions', WO Patent, 2001.

[17]   M. J. Virnig, R. Grinstein, R. B. Sudderth, G. Wolfe, and S. Olafson, in 'Extraction of copper from aqueous feed solution by contact with organic oxime-containing phase', WO Patent, 2000.

[18]   M. D. Soderstrom, in 'Organic solvent with oximes and phase modifiers suitable for extraction of metals from ore-leaching solutions', USA Patent, 2004.

[19]   F. A. Settle, 'Handbook of Instrumental Techniques for Analytical Chemistry', Prentice Hall, 1997.

[20]   Sigma Aldrich, 2007.

[21]   Fluorochem, 2007.

[22]   R. Aldred, R. Johnston, D. Levin, and J. Neilan, *Journal of the Chemical Society, Perkin Transactions 1: Organic and Bio-Organic Chemistry (1972-1999)*, 1994, 1823.

[23]   L. F. Lindoy, G. V. Meehan, and N. Svenstrup, *Synthesis*, 1998, 1029.

[24]   D. Masilamani and M. M. Rogic, *Journal of Organic Chemistry*, 1981, **46**, 4486.

[25]   F. Michel, F. Thomas, S. Hamman, E. Saint-Aman, C. Bucher, and J.-L. Pierre, *Chemistry - A European Journal*, 2004, **10**, 4115.

[26]   D. Stepniak-Biniakiewicz, *Polish Journal of Chemistry*, 1980, **54**, 1567.

[27]   J. C. Cuevas, J. De Mendoza, and P. Prados, *Journal of Organic Chemistry*, 1988, **53**, 2055.

[28]   J. L. Wood, 'PhD Thesis', University of Edinburgh, 2005.

[29]   J. March and M. B. Smith, 'March's Advanced Organic Chemistry, Reactions, Mechanisms and Structures', John Wiley's and Sons, 2001.

[30]   http://www.basf.de/en/produkte/chemikalien/anorganika/hydroxyl/hydroxyl_fb/hafb_safety.htm?id=V00-8JiYh4gz4bsf2TJ.

[31]   D. H. Williams and I. Fleming, 'Spectroscopic Measurements in Organic Chemistry', McGraw and Hill, 1995.

32   P. A. Wood, R. S. Forgan, D. Henderson, S. Parsons, E. Pidcock, P. A. Tasker, and J. E. Warren, *Acta Crystallographica, Section B*, 2006, **62**, 1099.

33   P. W. Atkins and D. F. Shriver, 'Inorganic Chemistry', Oxford University Press, 1999.

34   D. Stepniak-Biniakiewicz and J. Szymanowski, *Hydrometallurgy*, 1981, **7**, 299.

CHAPTER 3

ANALYSIS OF 3-SUBSTITUTED SALICYLALDOXIMES

Contents

3.1 Introduction

3.1.1 Aims

This chapter provides a more detailed analysis of the results reported in Chapter 2 on 3-substituted salicylaldoximes and their copper complexes in order to understand the origins of the differences in the copper(II) binding strengths of the extractant series. The work involves:

- the study of an analogous series of 3-substitued salicylaldoximes without 5-alkyl groups by X-ray crystallography,

- the introduction of analytical techniques to investigate the effect of the 3-substituent on the buttressing of intradimer and intracomplex hydrogen bonding,

- attempts to rationalise substituent effects and their relative importance, and

- the formulation of a tentative model which describes and predicts the effect of substitution on extractive efficacy.

A short review of methods to study hydrogen bond strengths and potential substituent effects in complexing agents and their copper(II) complexes follows.

3.1.2 Solid Phase Techniques

The solution of X-ray crystal structures provides an ever expanding bank of knowledge for the study of intermolecular interactions, of which H-bonding is the most important.[1] The advent of the Cambridge Structural Database (CSD) has allowed detailed statistical analyses of these contacts in over 250,000 structures[2] and continues to advance the understanding of the wide ranging interactions which fall under the "hydrogen-bonding" definition. A recent review by Steiner highlights the varying nature of these contacts and their overlap with other interactions, but also draws attention to a major limitation in analysis of crystal structures: the inability to

extract values for the energy of bonds without computational calculations.[1] Despite this, X-ray diffraction studies have proven unequivocally the presence of weak hydrogen bonds such as the C-H···π and C-H···F-C interactions,[3] and will continue to enhance the understanding of H-bonding.

A novel technique for the analysis of interactions energies *within* X-ray crystal structures is the PIXEL method of Gavezzotti, which models coulombic, polarisation, dispersive and repulsion contributions in the solid state.[4, 5] The molecular charge density is calculated by standard quantum chemical methods using the program GAUSSIAN98[6] with the MP2/6-31G** basis set. Using the OPiX[4] program, the charge density pixels are condensed to n x n x n blocks, and from these data the coulombic, polarisation, dispersion and repulsion energies are calculated, with the total interaction energy the sum of the contributions.[5] PIXEL calculations are particularly suited to hydrogen bonded dimers, and have been tested over many different systems. Results show good correlation with *ab initio* methods at a fraction of the computational cost.[7]

3.1.3 Solution Phase Techniques

In the solution phase, ^{1}H NMR and IR spectroscopy are standard techniques for the study of hydrogen bonding.[8] In the former, correlations between chemical shifts (δ) of the hydrogen atom and the distance between donor and acceptor atoms have been established for many systems.[1] The proton is deshielded to a greater extent by stronger H-bonds and so moves downfield, for example in the O-H···O hydrogen bond.[9] Unfortunately, NMR spectroscopy cannot be applied to the study of copper(II) complexes due to the paramagnetism of the Cu^{II} ion, which broadens spectra and makes them unusable.[10, 11]

In IR spectroscopy the frequency of the donor X-H stretching vibration, $\nu_{(X-H)}$, is easily studied due to its simplicity of identification and sensitivity to H-bond formation, with red shifting, broadening and intensification of the band common.[1]

For example, Gilli and Gilli[12] have demonstrated the correlation between the O···O distance in O-H···O hydrogen bonds with $\nu_{(O-H)}$ (Figure 3.1).
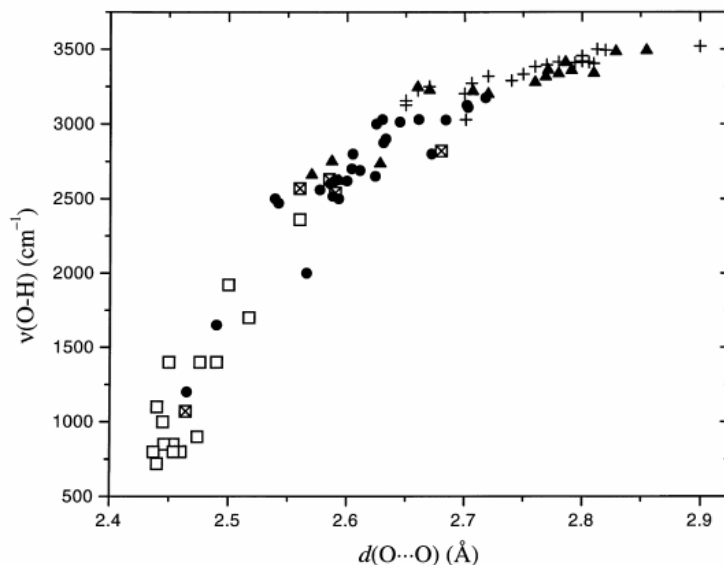
Figure 3.1: Scatter plot of O-H IR stretching frequencies of O-H···O hydrogen bonds against solid state O···O distance (squares are acid/base combinations, filled circles are resonance assisted H-bonds, triangles are σ-cooperative H-bonds and crosses are isolated H-bonds).[12]

This correlation is present in other H-bond types, and Rozenberg *et al*[13] have proposed the expression:

Equation 3.1 $$-\Delta H = 1.3\ (\Delta\nu)^{0.5}$$

for calculation of H-bond enthalpies from IR spectra (ΔH in kJ mol^{-1}, $\Delta\nu$ is the difference in $\nu_{(X-H)}$ for the H-bonded and uncomplexed species in cm^{-1}). If the H-bond acceptor is involved in an IR-active bond then it may also be investigated, for example in X-H···O=C interactions the O=C bond is weakened, subsequently lowering its stretching frequency.[1]

Although copper(II) complexes are unsuitable for NMR analysis, their paramagnetism makes them ideal candidates for study by electron paramagnetic resonance (EPR) spectroscopy. EPR spectroscopy is a technique which detects

chemical species containing an unpaired electron. The magnetic moment of an unpaired electron is very sensitive to local magnetic fields, for example those of surrounding nuclei, and so EPR can yield detailed structural information of its locus.[10]

By applying a strong magnetic field, B_0, to the paramagnetic species, the magnetic moment of the unpaired electron aligns itself either parallel ($M_s = -\frac{1}{2}$) or antiparallel ($M_s = +\frac{1}{2}$) to the external field, generating separate energy levels which allows the absorption of electromagnetic radiation to occur (Figure 3.2).
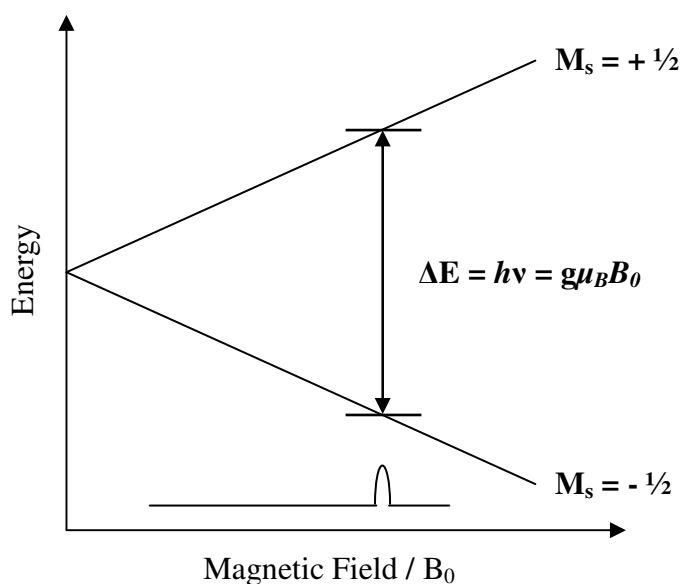
Figure 3.2: Variation of spin state energies as a function of the applied magnetic field.

The energy gap between the two states is defined by the equation:

Equation 3.2 $\qquad\qquad \Delta E = h\nu = g\mu_B B_0$

Where ΔE is the energy separation, h is Planck's constant, ν is the microwave frequency, g is the g-factor or spectroscopic splitting factor, μ_B is the Bohr magneton and B_0 the applied magnetic field. The EPR experiment is run by scanning the magnetic field whilst keeping the frequency constant, and a signal is observed when the magnetic field is resonant with the energy gap. To obtain structural information

from the spectrum, hyperfine coupling constants are measured, which arise from the local magnetic field induced by interaction of the unpaired electron and any nuclei in the species, and split the EPR spectrum. To predict the expected peak splitting, the following formula is used;

Equation 3.3 $\qquad$ No of peaks = 2nI+1

where n is the number of equivalent nuclei and I is their spin quantum number.[14] Therefore, in EPR spectra of bis-salicylaldoximato copper(II) complexes, we expect to see the signal split into four lines, resulting from interaction with the copper(II) ion ($I = 3/2$), and each line split into five further lines by interaction with two equivalent nitrogen nuclei ($I = 1$).[10]

The suitability of copper(II) for examination by EPR has resulted in the large volume of research in the area. In the field of copper extraction, a series of papers by Thornback and O'Brien[15-17] has shown that during extraction the reagents SME 529 (5-nonyl-2-hydroxyacetophenone oxime) and P50 (5-nonyl-2-hydroxybenzaldehyde oxime) form 2:1 complexes with copper(II) of the type discussed in Chapter 2 (Figure 3.3).
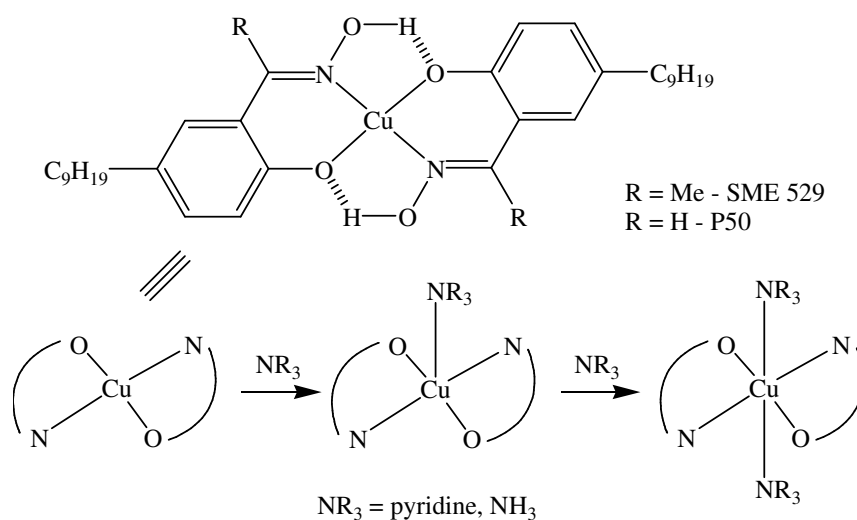
Figure 3.3: Solution structures of copper(II) complexes formed in extraction, alongside mono- and bis-amine adducts, all studied by EPR.[15-18]

The coordination of axial ligands can also be studied by EPR, with mono- and bis-pyridine adducts identified in solution by the technique (Figure 3.3).[15-18]

3.1.4   Gas Phase Techniques

Hydrogen bonding has long been a target area of molecular modelling calculations, in particular in the analysis of the water dimer. Calculations reveal[1] the varying extent of interaction in H-bonds, with enthalpies of bonding varying from approximately 1 kJ mol^{-1} to ~165 kJ mol^{-1}. Early calculations involved simple Hartree-Fock wavefunctions with small basis sets, and provided important information about the nature of H-bonds.[19] As computational power and thus the complexity of calculations increased, detailed description of H-bonding became dependent on the method employed, with a study by Del Bene *et al*[20] in 2001 illustrating these variations in the length and energy of the hydrogen bond in the water dimer. Of the *ab initio* methods studied, MP2/6-31+G(d,p) was recommended as the minimum level of theory for studying H-bonded systems.

Density Functional Theory (DFT) is also extensively applied in the computational study of H-bonds. A cursory check of the literature reveals the extent of its use: a search for "DFT hydrogen bonds" on SciFinder Scholar 2007[21] yielded 2568 hits.[22] There are many methods and basis sets available for use, with a comprehensive study by Riley *et al*[23] in 2007 covering 37 methods and 11 basis sets. The review found that hybrid-GGA and hybrid-meta-GGA methods with Pople split valence basis sets, particularly 6-31++G(d,p) gave the best combination of accuracy and computational efficiency.

Gas phase stabilities of complex ions can be measured by collision induced dissociation (CID) mass spectrometry. This is a tandem MS technique, which involves isolating the precursor ions of choice and subjecting them to breakdown by collision with an inert species, usually a buffer gas such as helium, and analysing the

ratio of the resulting fragment ions to the precursor ion intensity.[24] A simplified diagram of the process is shown in Figure 3.4.
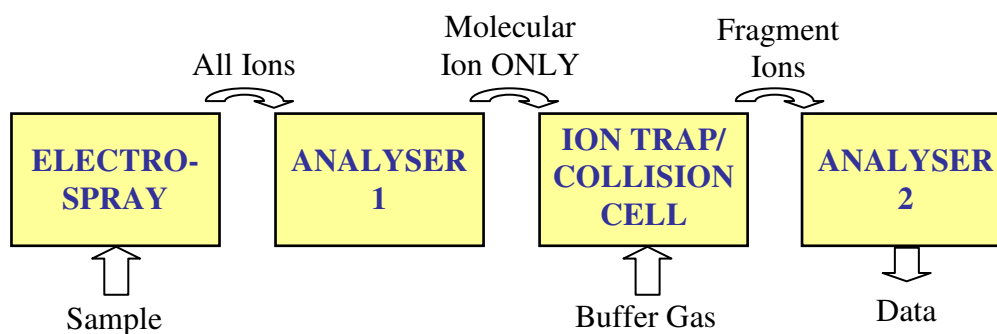
Figure 3.4: Simplified diagram of a CIDMS set up.

This versatile technique is used extensively in the sequencing of proteins, as the methods of ionisation developed for these species[25] inherently involve little dissociation and so the use of collision induced dissociation offers a method to dissociate a species under controlled (known) conditions and thus collect a great deal of structural information.[26] A particular advantage of this technique is the ability to vary the energy of the buffer gas in the ion trap whilst scanning the ratio of fragment ion peaks to the precursor ion peak, and in this manner produce a breakdown curve for a particular species. If other conditions are kept constant, then the breakdown curve for each complex ion can be measured and the required collision energies could give information about the relative stabilities of the complex ions in the gas phase.

3.1.5   Substituent Effects On Copper(II) Extraction

In formulating a model for predicting the extractive efficacy of 3-substituted phenolic oximes, variation of the 3-substituent can be considered in relation to:

- the acidity of the phenol,
- the basicity of the conjugate phenolate,
- the potential to form bifurcated hydrogen bonds in copper(II) complexes, and
- steric clashes with the hydrogen bonds.

Ligands with higher phenol acidity are expected to be stronger extractants but this effect may be countered by the lower basicity of the phenolate conjugate ion, which will be a poorer σ-donor.[27]

The electronic effects of the substituent will also affect the intracomplex hydrogen-bonding, which helps stabilise bis-salicylaldoximato copper(II) complexes.[28] Altering the donor properties of the phenolate oxygen will change the energies of the hydrogen bond, with previous work by Burger *et al*[29] indicating the H-bonding is weakened as the donor ability of the phenolate is weakened. The steric properties of the 3-substituent may also influences the hydrogen bonding arrangement with large, bulky groups disrupting the stabilising hydrogen bonding motif. It is also possible to introduce an additional hydrogen bond acceptor in the 3-position, to form a more stable, bifurcated hydrogen bond with the oximic proton[28] and thus possibly increase extractant strength.

3.2   Effect of Ligand pK_a on Copper(II) Extraction

As described in Chapter 2, the current consensus regarding substituent effects on salicylaldoxime extractive efficacy is that the more acidic the ligand, the stronger the extractant.[30, 31] To investigate the role of ligand acidity on extractant strength, pK_a values for the phenolic proton need to be determined. The pK_a values of the ligands could not be measured by pH titration, due to their tendency to hydrolyse in low pH solutions.[32] Values were calculated by Daniel Tackley at Intertek ASG on behalf of Cytec Industries UK Ltd, using ACD/Labs pK_a predictor v10.01. Calculated pK_a values for **L1**-**L9**, alongside their relative extractive efficacies, are shown overleaf in Table 3.1.

The calculated pK_a values vary in a similar fashion to the $pH_{0.5}$ values, suggesting that acidity of the phenol is more important than the basicity of the conjugate phenolate.

Ligand	Substituent	Calculated pK_a	$pH_{0.5}$
L1	H	9.32 ± 0.48	1.68
L2	Me	9.66 ± 0.50	1.67
L3	*t*-Bu	10.68 ± 0.50	2.64
L4	NO_2	6.58 ± 0.40	n/a[a]
L5	Cl	7.84 ± 0.50	0.91
L6	Br	7.77 ± 0.50	0.42
L7	OMe	9.31 ± 0.50	1.09
L8	H[b]	9.33 ± 0.50	1.73
L9	NO_2[b]	6.60 ± 0.40	0.70

[a]Could not be measured due to poor solubility of the Cu^{II} complex, as described in Chapter 2.

[b]These ligands have a *t*-octyl group in the 5-position, replacing the *t*-butyl groups of **L1** and **L4**.

Table 3.1: Calculated pK_a values for **L1-L9** alongside $pH_{0.5}$ values measured in Chapter 2.

If we consider the pH dependent equilibrium for formation of the neutral complex in a single phase, the equilibrium constant K_e is defined by:

Equation 3.4 $\qquad Cu^{2+} + 2LH \rightleftharpoons [CuL_2] + 2H^+ \qquad\qquad K_e = \dfrac{[CuL_2][H^+]^2}{[Cu^{2+}][LH]^2}$
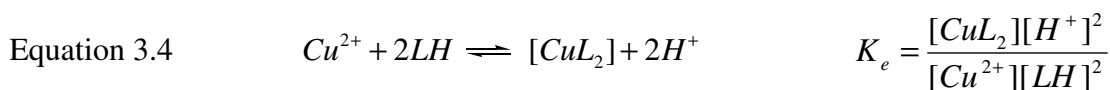
The two step replacement of water ligands and the overall equilibrium constant, ß$_2$, are represented by:

Equation 3.5 $\qquad Cu^{2+} + 2L^- \rightleftharpoons [CuL_2] \qquad\qquad \beta_2 = \dfrac{[CuL_2]}{[Cu^{2+}][L^-]^2}$
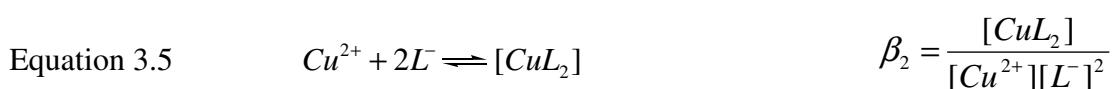
As the formation of the anionic form of the ligand LH is defined by the acid dissociation constant K_a,

Equation 3.6 $\qquad LH \rightleftharpoons L^- + H^+ \qquad\qquad K_a = \dfrac{[L^-][H^+]}{[LH]}$

by rearranging the expression for K_a and substituting the value for $[H^+]$ into the expression for K_e, we obtain:

Equation 3.7 $\qquad K_e = \beta_2 K_a^2$

The square dependence of K_e on K_a suggests that the phenol acidity has a greater effect on K_e than the phenolate basicity, but this may be an oversimplification in that *two* phenolates must coordinate to form the neutral complex.

Electron-withdrawing substituents (*e.g.* Cl, Br and NO_2 in **L5**, **L6** and **L9**) which increase K_a have a beneficial effect on "strength", but the most acidic ligand (**L9**) is not the strongest extractant (**L6**).   These substituents may also have a beneficial effect on intracomplex H-bonding by forming bifurcated H-bonds, "buttressing" the stabilising motif.   **L7**, which contains a substituent with slightly electron-donating properties, is a much stronger extractant than its unsubstituted analogue **L1**.   This suggests that the effect of the electronic properties of the substituent on the phenol group may not be as important as the ability to buttress the intracomplex H-bonding and provide a positive contribution to complex stability.   Consequently, a comprehensive study of the H-bonding in the ligands and their copper(II) complexes was undertaken in this chapter to determine which substituent effect is dominant.

3.3   Hole-Sizes

Both salicylaldoxime dimers and their copper(II) complexes form a *pseudo*macrocyclic, H-bonded cavity in the solid state, the size of which can be defined as the mean distance from the N and O donor atoms to the centroid of the cavity.   The "hole sizes" of dimers and complexes could give information to the strength of the H-bonding and thus extractive efficacy.

3.3.1 Copper(II) Complexes

It might be expected that the $N_2O_2{}^{2-}$ cavity, the "hole size" in solid state structures of copper(II) complexes of phenolic oximes similar to **L1**-**L9**, would relate to the "strength" of their ligands in extraction, with stronger extractants having smaller hole sizes. The determination of the structures of [Cu(**L1**-H)$_2$], [Cu(**L2**-H)$_2$], [Cu(**L3**-H)$_2$], [Cu(**L4**-H)$_2$(py)$_2$], [Cu(**L6**-H)$_2$] and [Cu(**L7**-H)$_2$] (Chapter 2) has shown that several different supramolecular architectures arise in the solid state from axial contacts to the copper atom and from other packing effects. Such architectures commonly result from face-to-face or edge-to-face association of [Cu(**L**-H)$_2$] units, with phenoxide or oxime oxygen atoms lying in the axial sites of the planar CuO_2N_2 units. Whatever the nature of intermolecular association in the solid state through these axial sites, it will perturb the bond lengths in the coordination sphere *via* Jahn-Teller distortions,[10] and consequently, we would not expect and do not find a correlation between the hole size in the solid state and the stability of the complex in solution. This is demonstrated by the data in Table 3.2 which show that the order of decreasing hole size does not correlate with increasing extraction strength.

Ligand	Substituent	Hole Size	pH$_{0.5}$
L6	Br	1.920(4)	0.42
L4[a]	NO$_2$	1.938(9)[b]	n/a[c]
L7	OMe	1.909(6)	1.09
L2	Me	1.909(5)[b]	1.67
L1	H	1.924(4)[d]	1.68
L3	*t*-Bu	1.922(11)[b]	2.64

[a]Crystallised as a bis-pyridine adduct. [b]Values are average of 2 crystallographically independent half-molecules. [c]Could not be measured due to poor solubility of the Cu^{II} complex as described in Chapter 2, but a value of 0.70 was measured for the 5-*t*-octyl substituted analogue **L8**. [d]Values are average of 3 crystallographically independent half-molecules.

Table 3.2: Comparison of solid state cavity sizes in copper(II) complexes of **L1**, **L2**, **L3**, **L4**, **L6** and **L7** with their respective pH$_{0.5}$ values measured in Chapter 2.

3.3.2 Ligands

As the solid state structures of the copper(II) complexes were deemed inappropriate for assessing ligand:ligand association, the X-ray crystal structures of the free ligands were investigated. Salicylaldoximes are known to dimerise in the solid state,[33] and it is expected that 3-substituents will "buttress" the hydrogen bonding in these dimers and so affect hole size (Figure 3.5). Groups which are capable of accepting a H-bond should stabilise the dimer by forming a bifurcated H-bond, the result of which is expected to be a smaller cavity size (defined as the mean distance from the donor atoms to the centroid of the dimer). Bulky groups will clash sterically with the H-bonds, and so weaken the dimer and increase cavity size.
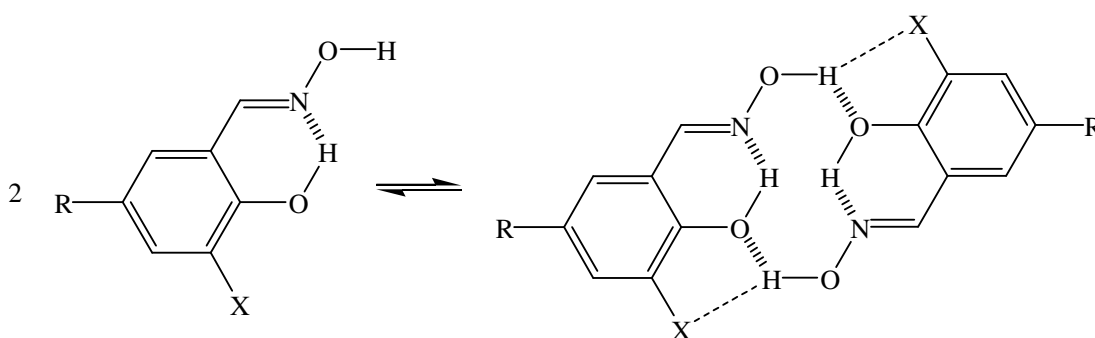
Figure 3.5: The interaction of the 3-substituent (X) with the *pseudo*macrocyclic hydrogen bonding motif of a salicylaldoxime dimer.

As described in Chapter 2, only ligands **L2**, **L3**, **L5** and **L6** formed *pseudo*macrocyclic dimers in the solid state, meaning a comprehensive hole-size study could not be undertaken. It is thought that bulky groups in the 5-position (R in Figure 3.5) inhibit dimerisation due to their steric influence on crystal packing.[33] For those ligands which did dimerise, the hole sizes are displayed in Table 3.3. The cavity size of the solid state dimers is smaller for **L5** and **L6**, which may be able to form bifurcated H-bonds, and larger for **L3**, which has a bulky *t*-butyl group. **L2** has an intermediate hole size value due to the methyl substituent's small size and inability to accept H-bonds. This provides tentative evidence of the effect of the 3-substituent on interligand hydrogen bonding, suggesting that the substituent can buttress the H-bonding and so possibly stabilise (or indeed weaken) salicylaldoxime dimers.

Ligand	Substituent	Hole Size / Å	pH$_{0.5}$
L6	Br	1.968(8)[a]	0.42
L5	Cl	1.973(8)[a]	0.91
L2	Me	2.003(2)	1.67
L3	*t*-Bu	2.025(1)	2.64

[a]Average of 4 crystallographically independent dimers.

Table 3.3: Solid state hole sizes of **L2**, **L3**, **L5** and **L6** and their pH$_{0.5}$ values measured in Chapter 2.

Cavity sizes also decrease as the extractive efficacy of the ligands increase, suggesting that this stabilisation may also occur in copper(II) complexes during solvent extraction. The hole sizes also roughly follow the pK$_a$ values, although **L6** is a stronger extractant than **L5** despite having substituents with similar electronic properties. To examine the hypothesis that H-bond buttressing may be mainly responsible for the strength of ligand:ligand association and hence copper(II) extraction strength, a more extensive range of free ligand dimers were prepared and studied. These have no 5-substituents as this appears to favour dimer formation in the solid state.[33]

3.3.3 Salicylaldoximes

Salicylaldoximes **L11**-**L16** (Figure 3.6) were synthesised from their salicylaldehyde precursors by the oximation process outlined in Chapter 2 (**L10**, salicylaldoxime itself, was available commercially). **L11**-**L15** were prepared in high yields and purity, and, along with **L10**, were successfully characterised by X-ray crystallography. The purification and crystallisation of 3-nitrosalicylaldoxime, **L16**, was hampered by the low solubility of the compound.
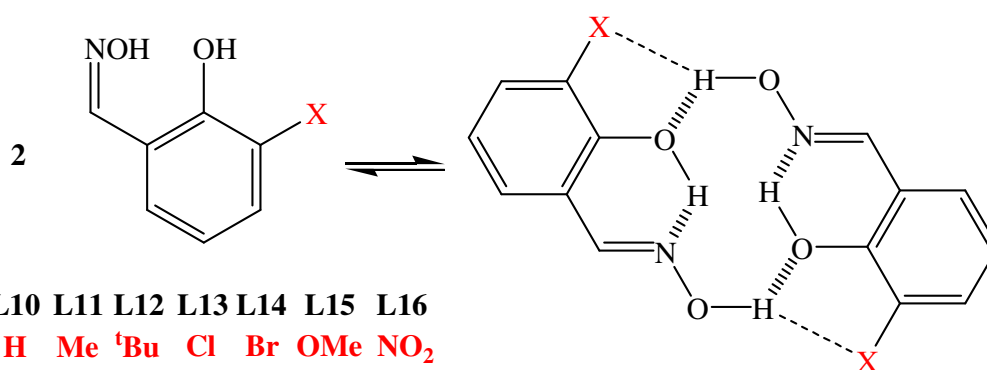
Figure 3.6: Potential interaction of the 3-X-substituent with the intradimer 14-membered *pseudo*macrocyclic H-bonding in the salicylaldoxime dimers **L10**-**L16**.

It may be expected that **L16** would not form 14-membered *pseudo*macrocyclic dimers in the solid state, as the previously characterised 3-nitrosalicylaldoximes **L4** and **L9** show an alternative arrangement with 6-membered oxime dimers, described in Chapter 2. For these reasons no further attempts were made to purify **L16**.

The crystal structures of **L10**-**L15** show the expected 14-membered *pseudo*macrocyclic dimeric arrangement, and the interaction of the 3-substituent with the H-bonding is evident in the structure of **L15** (Figure 3.7).
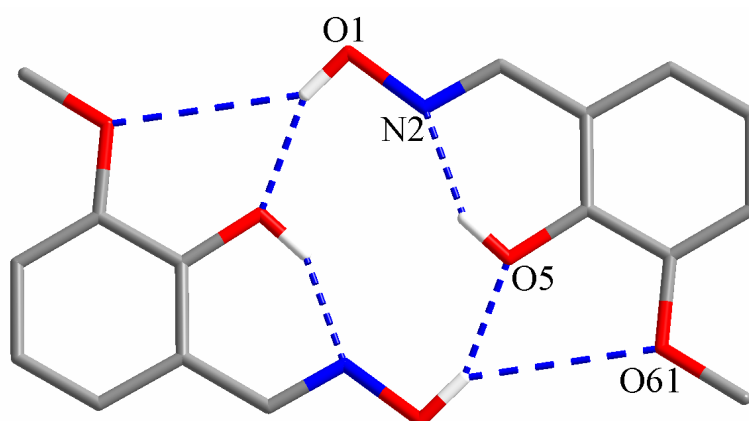
Figure 3.7: Interaction of the 3-OMe group with intermolecular hydrogen bonding in the solid state structure of **L15** (with selected atoms labels, hydrogen atoms not involved in H-bonding omitted for clarity).

The structures of **L10** and **L15** have been reported previously,[34,35] but were determined and refined again at Edinburgh under conditions identical to the rest of the series to ensure comparability of data with the other ligands. Interestingly, a novel polymorph of **L10** was also crystallised which does not show dimer formation. 1D H-bonded ribbons, similar to those seen in the structures of **L1**, **L7** and **L8**, are present.[36]

Cavity sizes were measured for the dimers of **L10**-**L15**, and are listed alongside the relative extractive efficacies of their 5-alkyl substituted analogues (**L1**, **L2**, **L3**, **L5**, **L6** and **L7**) in Table 3.4.

Substituent	Ligand	$pH_{0.5}$	Ligand	Hole Size / Å
H	L1	1.68	L10	2.0048(15)
Me	L2	1.67	L11	2.0237(18)
t-Bu	L3	2.64	L12	2.0367(19)
Cl	L5	0.91	L13	1.9837(12)
Br	L6	0.42	L14	1.9726 (53)
OMe	L7	1.09	L15	1.9492(19)

Table 3.4: Comparison of extractive efficacy of 3-X-5-alkyl-substituted ligands with the cavity sizes of the related 3-X-salicylaldoximes.

The cavity sizes follow the order **L15** (OMe) < **L14** (Br) < **L13** (Cl) < **L10** (H) < **L11** (Me) < **L12** (^{t}Bu). The radii of the cavities are significantly smaller in the dimers of **L13**, **L14** and **L15** which have hydrogen bond accepting 3-substituents and larger in **L12** which has a bulky 3-substituent, suggesting that buttressing of the hydrogen bonding by the 3-substituent is a dominant factor in stabilising the assembly.

The extractive efficacies of the 5-alkyl-substitued analogues **L1**-**L9** follow a similar trend. It is generally assumed (Section 3.2) that lowering the pK_a of the acidic groups in "pH-swing" extractants leads to an increase in strength.[30,31] If this were the

major influence in the series then the incorporation of an electron-releasing group such as OMe in **L7** would raise the pK_a of the phenol group relative to that in the unsubstituted ligand **L1** and weaken the extractant. This is clearly not the case, although the electron-releasing properties of the methoxy group may account for **L7** being a slightly weaker extractant than its chloro- and bromo- analogues, **L5** and **L6**. Overall, analysis of the data in Table 3.4 suggests that the effects of the 3-substituents on H-bond buttressing or on sterically hindering the formation of the 14-membered *pseudo*macrocycle are an important feature of ligand design to tune extractant strength.

3.3.4   Analysis of Intradimer Forces by PIXEL

Interaction energies within the dimers in the solid state (Table 3.5) were analyzed by the PIXEL method, which models coulombic, polarisation, dispersive and repulsion contributions.[4,5] Calculations were carried out by Dr Peter Wood and Professor Simon Parsons at the University of Edinburgh (Section 3.9.4). The calculations were based on the geometry of the ligand observed in the crystal structure; the differences listed in Table 3.5 were found by repeating the calculation with the same geometry, but with the substituent replaced by an H atom, and subtracting the initial values. This ensured the energies were not influenced by subtle crystal packing effects.

	L15 (OMe)	L14 (Br)	L13 (Cl)	L10 (H)	L11 (Me)	L12 (^tBu)
$E_{coulombic}$ / kJ mol^{-1}	-4.8	-2.2	-0.5	0.0	+0.2	+2.1
$E_{repulsion}$ / kJ mol^{-1}	-0.4	+0.7	0.0	0.0	+0.6	+6.2
$E_{polarisation}$ / kJ mol^{-1}	-1.0	-1.4	-1.0	0.0	-0.8	-2.7
$E_{dispersion}$ / kJ mol^{-1}	-0.8	-1.3	-1.5	0.0	-1.5	-5.8
E_{TOTAL} / kJ mol^{-1}	**-7.0**	**-4.2**	**-3.0**	**0.0**	**-1.5**	**-0.2**

Table 3.5: Interaction energies between the halves of each of the 3-substituted dimers relative to their unsubstituted analogues, as estimated by the PIXEL method.

Again the ligands with H-bond acceptor substituents, **L13, L14** and **L15**, show the most favourable ligand-ligand attraction. The coulombic term, E_{coul}, is favourable in all three cases, indicating formation of stabilising bifurcated H-bonds. The term is much larger for the OMe-substituted ligand **L15**, due possibly to its closer proximity to the hydrogen bonding or its properties as a good H-bond acceptor,[37] and the term is larger for the Br substituted ligand than the Cl substituted ligand. This suggests that the larger size of the Br atom either provides a better H-bond acceptor than the Cl atom, or is closer to the oxime proton and so a stronger interaction is possible.

A large repulsion term (E_{rep}) is seen for the ^{t}Bu substituted ligand **L12**, which may explain both its large hole size and poor extractive efficacy. This is further evidence of destabilising steric clashes between the bulky group and the H-bonding.

However, the method also suggests that there is a slightly stronger net attraction between the two halves of the Me and ^{t}Bu substituted dimers, [**L11**]$_2$ and [**L12**]$_2$, than in the unsubstituted system [**L10**]$_2$. Both have large, favourable dispersion terms, E_{disp}, due to the number of electrons in the substituents, and it is possible that this may be over estimated as it is the most parameterised.[38]

3.3.5   H-Bond Buttressing in Copper(II) Complexes

The results from Sections 3.3.3 and 3.3.4 suggest that the 3-substituent can interact in both a positive and negative manner with the intradimer hydrogen bonding in salicylaldoxime dimers. Despite the unsuitability of the copper(II) complexes for cavity size analysis (Section 3.3.1), the solid state structures can still be examined for evidence of interaction between the 3-substituent and the intracomplex hydrogen bonding motif.

A space filling diagram of one of the crystallographically independent molecules found in the crystal structure of [Cu(**L3**-H)$_2$] (Figure 3.8) shows the 3-t-butyl group and the oximic proton adopting a staggered conformation, to minimise disruption of

the hydrogen bonding without distorting the coordination sphere of the copper centre.
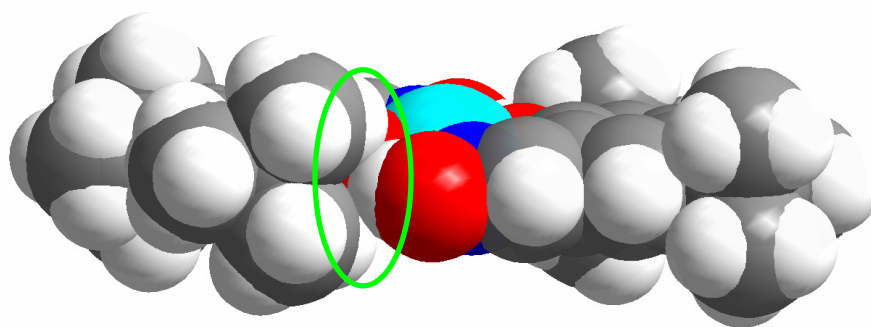
Figure 3.8: A space-filling diagram of the centrosymmetric molecule of [Cu(**L3**-H)$_2$] from its solid state structure, showing interaction of the 3-*t*-Bu substituent with the intracomplex hydrogen bonding motif.

In the solution phase, it is expected that free rotation of the ^{t}Bu group would disrupt the stabilising hydrogen bonding motif, and this may be the reason that **L3** is the weakest extractant.

The formation of bifurcated hydrogen bonds in the uncomplexed salicylaldoxime dimers of **L13**-**L15** (Section 3.3.3) have been shown to decrease cavity sizes and so stabilise the dimer. The solid state structure of [Cu(**L4**-H)$_2$(py)$_2$] (py = pyridine, Figure 3.9) clearly illustrates the formation of bifurcated hydrogen bonds in the copper(II) complex, which are expected to stabilise the molecule[29] and may explain the high extraction strength of **L4**.
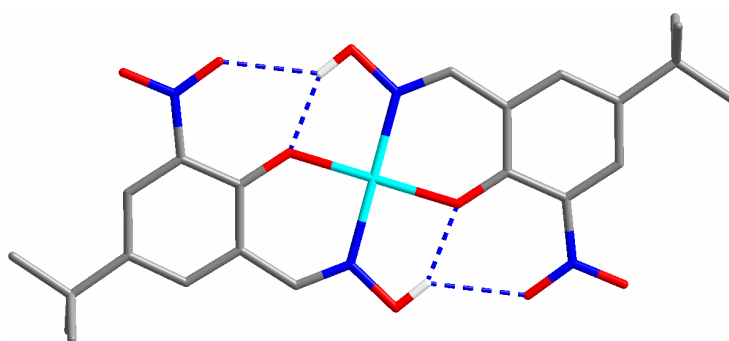
Figure 3.9: Bifurcated hydrogen bonds in the crystal structure of [Cu(**L4**-H)$_2$(py)$_2$]. Hydrogen atoms not involved in H-bonding and pyridine molecules removed for clarity.

3.4 Computational Chemistry

The experimental evidence to determine substituent effects has, to this point, been based on solid state structures and their comparison with binding strengths determined using solvent extraction, a solution technique. The gas phase may be seen as a similar medium to the non-polar solvents used in industrial processes, where complexes are likely to be poorly solvated. Consequently, *ab initio* and DFT calculations were carried out to determine if buttressing of interligand hydrogen bonding occurs in the gas phase.

All calculations were performed on the EaStCHEM Research Computing Facility using Gaussian 03[39] with the assistance and guidance of Dr Andrew Turner (Section 3.9.5). Various methods were assessed, including Hartree-Fock (HF), second order truncated Moller Plesset (MP2)[40-45] and the DFT exchange function of Tao, Perdew, Staroverov and Scuseria (TPSSTPSS).[46] The 6-31G basis set[47-53] was used and in some cases polarisation and diffuse functions were included.[54] To estimate basis set superposition errors in dimerisation calculations, the counterpoise correction was utilised.[55,56]

3.4.1 HF/6-31G

The first set of calculations was run at the HF/6-31G level, a simplified but fast method with a limited basis set which allows initial results to be determined and studied quite quickly, and is a good starting point on which to base higher level calculations.[20] Dimerisation enthalpies, alongside cavity sizes from the solid state structures and the optimised gas phase structures are listed in Table 3.6. Calculated enthalpies for dimerisation approximately follow the order predicted by the solid state hole sizes. The results show a good comparison between solid state and gas phase cavity sizes, however the calculated hole size for 3-Me-salox (**L11**) is smaller than the unsubstituted compound **L10**. This difference is not reflected in the

calculated dimerisation energies, with salicylaldoxime having a more favourable dimerisation enthalpy than 3-Me-salox.

	Hole Size / Å (XRD)	Hole Size / Å (calc)	Difference %	$\Delta E_{dimerisation}$ / kJ mol^{-1}	Corrected to H-Salox
L15 (OMe)	1.9492 (19)	1.9802	1.57%	-66.4	-17.8
L14 (Br)	1.9726 (53)	1.9799	0.38%	-54.0	-5.4
L13 (Cl)	1.9837 (12)	2.0073	1.18%	-54.7	-6.1
L10 (H)	2.0048 (15)	2.0242	0.96%	-48.6	0.0
L11 (Me)	2.0237 (18)	2.0219	0.09%	-47.0	1.6
L12 (^{t}Bu)	2.0367 (19)	2.0436	0.34%	-34.7	13.9

Table 3.6: Enthalpies of dimerisation and geometry minimised hole sizes calculated at the HF/6-31G level.

Also, the hole size calculated for 3-Br-salox (**L14**) is slightly smaller than that of 3-MeO-salox (**L15**) but has a significantly smaller dimerisation enthalpy, which is slightly less than that for 3-Cl-salox (**L13**). The PIXEL calculations reported earlier suggest that solid state dimerisation should be more favourable for **L14** than **L13**, and as these results are contradictory, it was assumed that a more accurate method was required.

Despite these problems, the initial results were encouraging, as, apart from **L14**, they show the expected trend between the enthalpy of dimerisation and the cavity size. It should also be noted that the solid state hole sizes may be influenced by subtle crystal packing effects, which are absent in the gas phase geometries calculated by Gaussian03.

3.4.2   HF/6-31++G(d,p)

The second set of calculations was run using the same Hartree-Fock method but with the larger basis set 6-31++G(d,p), which includes diffuse and polarisation functions for light and heavy atoms.   This added functionality is essential for accurate modelling of the H-bonding which is prevalent in the dimers.[23]   The results are listed in Table 3.7.

	Hole Size / Å (XRD)	Hole Size / Å (calc)	Difference %	$\Delta E_{dimerisation}$ / kJ mol^{-1}	Corrected to H-Salox
L15 (OMe)	1.9492 (19)	2.0375	4.34%	-40.2	-11.4
L14 (Br)	1.9726 (53)	2.0493	3.75%	-33.9	-5.1
L13 (Cl)	1.9837 (12)	2.0632	3.85%	-34.1	-5.3
L10 (H)	2.0048 (15)	2.0853	3.86%	-28.8	0.0
L11 (Me)	2.0237 (18)	2.0842	2.90%	-28.1	0.7
L12 (^{t}Bu)	2.0367 (19)	2.1301	4.38%	-18.7	10.0

Table 3.7: Enthalpies of dimerisation and geometry minimised hole sizes calculated at the HF/6-31++G(d,p) level.

Dimerisation enthalpies again follow the trend predicted by the solid state cavity sizes, with the magnitudes of the energy differences less than in the first set of calculations. However, geometry optimised hole sizes are considerably larger than the solid state structures, and again **L11** has a smaller hole size than **L10**. The calculated hole size for **L14** is now larger than that for **L15**, mirroring the trend seen in the crystal structures, but again the dimerisation enthalpy is not as favourable, being similar to that of **L13**.

The addition of extra functionality to the basis set with the intention of improving the results has had the opposite effect, taking the values further from experimental observations. However, the trends predicted by this method are more similar to those observed experimentally, suggesting that the larger basis set can aid accuracy. The

initial results using HF/6-31G appear to be the consequence of a combination of a simplified method and a small basis set giving seemingly good values which are not scientifically sound. For this reason, it was decided to investigate an alternative *ab initio* method.

3.4.3   MP2/6-31G

A third set of calculations was carried out using truncated second order Moller-Plesset (MP2) theory, which improves on the Hartree Fock method by taking into account electron correlation effects.[40-45] This method was expected to give a better description of the H-bonding in the systems. Calculations were run using the basis sets 6-31G and 6-31++G(d,p), but those involving the latter required very large computational power, and in most cases did not converge. This observation is consistent with other studies, and a debate exists regarding the reliability of the method for high order calculations.[57]

Due to this computational problem, results could only be attained for MP2/6-31G calculations, and are displayed in Table 3.8.

	Hole Size / Å (XRD)	Hole Size / Å (calc)	Difference %	$\Delta E_{dimerisation}$ / kJ mol^{-1}	Corrected to H-Salox
L15 (OMe)	1.9492 (19)	1.9581	0.46%	-75.1	-15.4
L14 (Br)	1.9726 (53)	1.9572	0.78%	-65.9	-6.2
L13 (Cl)	1.9837 (12)	1.9873	0.18%	-66.3	-6.6
L10 (H)	2.0048 (15)	2.0081	0.16%	-59.7	0.0
L11 (Me)	2.0237 (18)	2.0033	1.01%	-58.5	1.2
L12 (^{t}Bu)	2.0367 (19)	2.0144	1.10%	-49.5	10.2

Table 3.8: Enthalpies of dimerisation and geometry minimised hole sizes calculated at the MP2/6-31G level.

The dimerisation enthalpies show a similar trend to the HF calculated values, and have energy differences of similar magnitude. The similarity of solid state and gas phase cavity sizes is encouraging, but the MP2 method has also calculated the hole size of 3-Me-salox (**L11**) to be smaller than salicylaldoxime (**L10**). The calculated hole size for 3-Br-salox (**L14**) is again close to that of 3-MeO-salox (**L15**), but the dimerisation enthalpy is similar to 3-Cl-salox (**L13**). These issues are common to both *ab initio* methods. Del Bene *et al*[20] recommend MP2/6-31+G(d,p) as the minimum level of theory for studying hydrogen bonded complexes, and as MP2 calculations using the larger basis set failed, DFT methods were considered.

3.4.4 TPSSTPSS/6-31++G(d,p)

TPSSTPSS is a pure DFT functional, and was chosen as it was claimed to be a fast method to accurately model H-bonding without being computationally demanding.[46,58] Initial tests using this method with the 6-31++G(d,p) basis set confirmed these claims, running smoothly and converging appropriately, and so calculations with the smaller 6-31G basis set were not undertaken. The results are displayed in Table 3.9.

	Hole Size / Å (XRD)	Hole Size / Å (calc)	Difference %	$\Delta E_{dimerisation}$ / kJ mol^{-1}	Corrected to H-Salox
L15 (OMe)	1.9492 (19)	1.9715	1.13%	-50.2	-9.5
L14 (Br)	1.9726 (53)	1.9657	0.34%	-45.2	-4.5
L13 (Cl)	1.9837 (12)	1.9881	0.22 %	-45.7	-5.0
L10 (H)	2.0048 (15)	2.0049	<0.01%	-40.7	0.0
L11 (Me)	2.0237 (18)	2.0074	0.80%	-39.3	1.4
L12 (^{t}Bu)	2.0367 (19)	2.0452	0.42%	-29.1	11.6

Table 3.9: Enthalpies of dimerisation and geometry minimised hole sizes calculated at TPSSTPSS/6-31++G(d,p).

The correlation between solid state cavity size and gas phase dimerisation enthalpy is again present, with similar energy differences to the previous calculations. The predicted binding energies are similar to the H-bonding enthalpies measured experimentally by IR spectroscopy (to be discussed in Section 3.7), indicating the method gives good theoretical representation of experimental observations. The calculated cavity sizes give the best match with the solid state hole sizes of all the methods investigated, and the problem involving **L11** having smaller calculated hole sizes than **L10** in the *ab initio* methods has been resolved. However, the hole size of **L14** is again smaller than **L15**, which may indicate the ability of the 3-Br group to buttress the intermolecular H-bonding, but this is not reflected in the dimerisation enthalpy values. Despite this, the results show the best correlation with observed values, suggesting that the DFT method with the TPSSTPSS functional is the most appropriate for calculating the binding enthalpies for salicylaldoxime dimers.

3.4.5   Comparisons & Conclusions

Some interesting conclusions can be drawn when studying the results of the computational studies. It has been assumed so far that the differences in salicylaldoxime cavity size result from the variations in enthalpic favourability of the dimerisation process and, with the exclusion of the results obtained for 3-Br-salox (**L14**), this appears to be the case. Plotting the cavity sizes from the energy minimised geometries versus the calculated dimerisation energies gives an approximately monotonic relationship between calculated hole size and dimerisation energy, with the only deviation from this trend resulting from the 3-bromosalicylaldoxime hole size problem described previously.
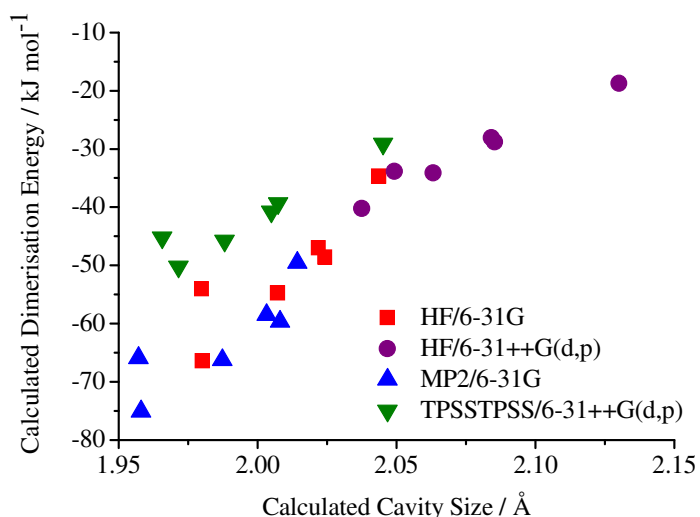
Figure 3.10: Comparison of calculated cavity sizes with calculated dimerisation energies for **L10**-**L15**.

The relationship becomes close to linearity when the basis set 6-31++G(d,p) is used, suggesting that the increased functionality models the system in a more accurate fashion. The issue may be resolved by further increasing the complexity of the calculations, but this is expected to be time-consuming and is outwith the remit of this project. Comparing the calculated dimerisation enthalpies with *observed* cavity sizes (Figure 3.11) further illustrates the good correlation obtained between theory and experiment, with the values again related in an approximately monotonic fashion.
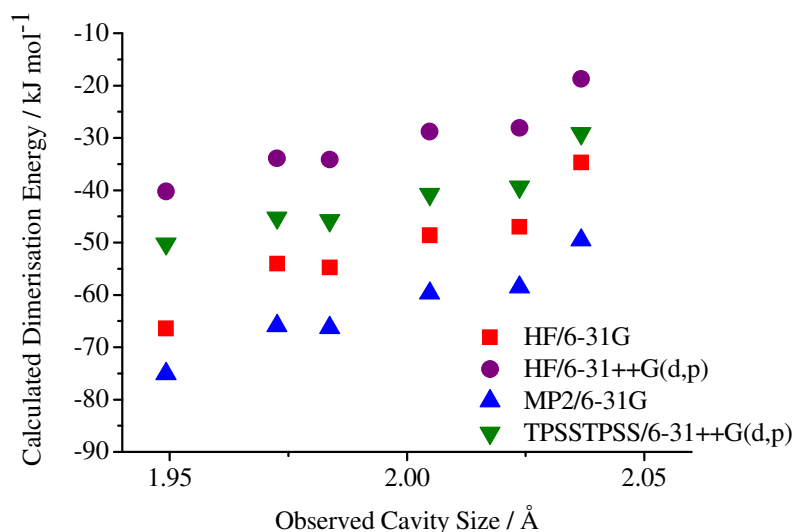
Figure 3.11: Comparison of observed solid state cavity sizes with calculated dimerisation energies for **L10**-**L15**.

107

The dimerisation enthalpy calculated for **L14** seems to better fit the trend of observed hole sizes rather than that of the theoretical hole sizes, suggesting that the smaller values obtained during calculations may be slightly inaccurate.

Overall, the gas phase calculations have proven very useful as a method of interpreting results depending on variations of ligand:ligand intermolecular interactions. A large basis set is essential for accurate modelling of the intradimer hydrogen bonding and the DFT functional TPSSTPSS was the most appropriate method of the four tested. The calculations have demonstrated that the order of dependence of observed cavity sizes on the nature of the 3-substituent correlates with the calculated enthalpy of association of the dimer, providing further evidence for buttressing of the intradimer hydrogen bonding motif by H-bond accepting substituents. **L13**, **L14** and **L15** have substituents capable of forming bifurcated H-bonds, and so dimerisation is more favourable and the cavity sizes are smaller than in the unsubstituted compound **L10**. **L11** has a substituent which can only slightly interact with the H-bonds and so has a very similar hole size and energy to **L10**. **L12** contains a bulky group which disrupts the H-bond motif *via* steric clashes, and so has the least favourable dimerisation energy and the largest hole size of the series.

3.5   Using FTIR to Probe Intradimer H-Bonding

Section 3.1.3 described the sensitivity of IR stretching frequencies of X-H bonds involved in H-bonding interactions. This phenomenon manifests itself in the IR spectra of salicylaldoximes, giving rise to characteristic bands in the O-H region of such spectra. IR spectra of salicylaldoximes in solution show three distinct O-H bands, at ~3600 cm^{-1}, ~3400 cm^{-1} and a broad signal at ~3200 cm^{-1} respectively, as seen in the spectrum of **L6** (Figure 3.12) which is typical.
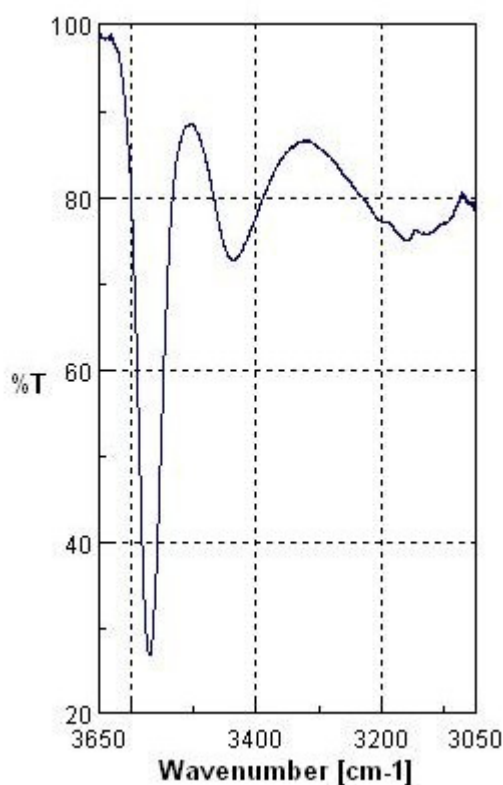
Figure 3.12: IR spectrum of a 0.05 M CHCl$_3$ solution of **L6**.

The three bands have previously been assigned to the free NOH stretch (~3600 cm^{-1}), the H-bonded NOH stretch (~3400 cm^{-1}) and the phenolic OH stretch (~3200 cm^{-1}).[59] As the peaks for both the free and H-bonded species are observed in the same spectrum, it is possible to estimate the enthalpy change associated with the solution H-bonding arrangement using the expression described by Rozenberg *et al*[13] (Section 3.1.3). Table 3.10 lists the peaks for the free and H-bonded oxime IR stretching vibrations alongside the estimated H-bond enthalpy and dimerisation enthalpy, which is twice the H-bond enthalpy as there are two H-bonds per dimer.

The dimerisation enthalpies do not follow any noticeable trend, and also show discrepancies between values for the 3-NO$_2$ substituted analogues **L4** and **L9**. They do not follow the pattern predicted by the calculations described in Section 3.4.4, but they are of similar magnitude, which, alongside previous literature reports, indicates that the IR technique is appropriate.

	Free NOH Stretch / cm^{-1}	H-Bonded NOH Stretch / cm^{-1}	$\Delta H_{\text{H-bond}}$ / kJmol^{-1}	$\Delta H_{\text{Dimerisation}}$ / kJmol^{-1}
L1	3574.9	3407.6	-16.8	-33.6
L2	3574.4	3416.3	-16.3	-32.7
L3	3576.8	3442.8	-15.0	-30.1
L4	3575.4	3401.8	-17.1	-34.3
L5	3568.2	3433.2	-15.1	-30.2
L6	3569.1	3436.5	-15.0	-29.9
L7	3573.5	3412.9	-16.5	-32.9
L8	3574.9	3392.7	-17.5	-35.1
L9	3547.4	3427.9	-14.2	-28.4

Table 3.10: Frequencies of NOH stretching vibrations and estimated H-bonding enthalpies for **L1**-**L9**.

It may be that the different types of solid state assemblies of **L1**-**L9**, detailed in Chapter 2, persist in solution and account for to the differences between theory and experiment, particularly in the 3-NO$_2$ substituted ligands **L4** and **L9**. This does not explain the differences seen in the values of these two analogous ligands, and it may be that the broad nature of the O-H stretching band makes accurate measurement difficult. For these reasons, IR spectroscopic techniques were not investigated further.

3.6 CIDMS Studies on Copper(II) Complexes

Collision Induced Dissociation Mass Spectrometry (CIDMS) was assessed as a technique to compare the relative gas-phase stabilities of the copper(II) complexes of **L1**-**L7**, with the assistance and guidance of Dr Bridgette Duncombe and Christopher Brooks. All data analysis was carried out by Dr Bridgette Duncombe (Section 3.9.7). Negative ion spectra were collected of the mass isolated precursor anion corresponding to the copper(II) complex exposed to varying intensities of collision-inducing buffer gas. Results are shown in the form of breakdown curves; normalised

plots of the ratio of precursor anion intensity to total ion current *vs.* the relative intensity of the buffer gas (Figure 3.13).
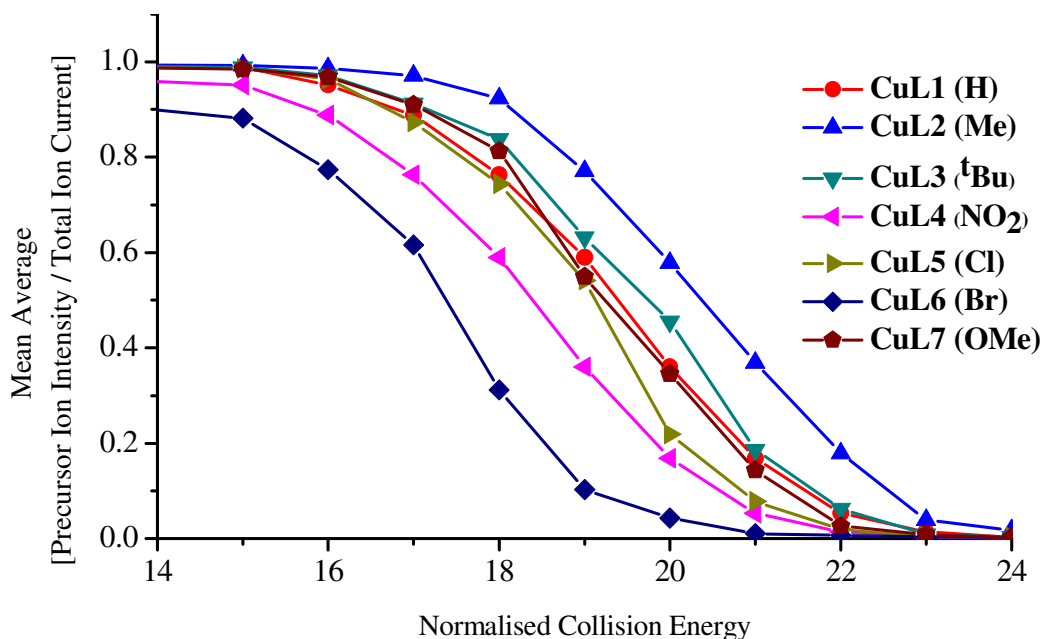
Figure 3.13: CIDMS breakdown curves for the gas phase anions [Cu(L-H)(L)]⁻ of the copper(II) complexes of **L1**-**L7**.

Figure 3.13 clearly shows the difference in the energy of the buffer gas required to induce breakdown of each complex, indicating the differing stabilities of the complexes in the gas phase. However, the relative stability order of the series is almost the opposite to that of the extractant strength order, with the Cu^{II} complex of the strongest extractant, **L6**, being the least stable in the gas phase. A comparison of the two illustrates their similarities:

Extractant strength (strongest first): $Br > NO_2 > Cl > OMe > Me \geq H > {}^tBu$

Gas-phase anion stability (lowest first): $Br < NO_2 < Cl < OMe \leq H < {}^tBu < Me$

Electron-withdrawing groups and good hydrogen bond accepting groups appear to lower the stability of the gas phase anions. Formation of the mono-anion is likely to involve loss of one of the oximic protons, giving an area of negative charge within the H-bonded *pseudo*macrocycle represented by the red circle in Figure 3.14.
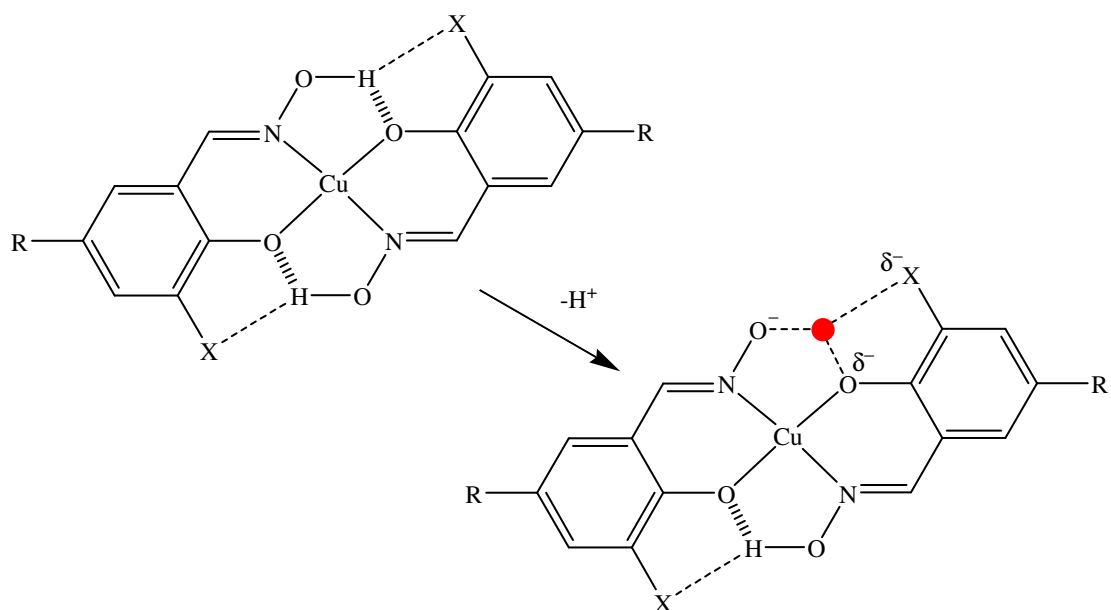
Figure 3.14: The potential effect of deprotonation on H-bonding and complex stability in the copper(II) complexes of **L1**-**L7**.

It is reasonable to expect that 3-substituents which buttress intracomplex H-bonding in the neutral complexes will have the opposite effect on negative ions. H-bond acceptors with well defined areas of partial negative charge lying in the plane of the complex will experience greater coloumbic repulsion and destabilise the complex. In the representation in Figure 3.14, the destabilisation caused by X in the upper region of the complex for which the proton has been lost is expected to exceed the stabilisation of the lower region with the bifurcated H-bond. Attempts to confirm this hypothesis will involve a more extensive range of experiments, including:

- extending the work to positive-ion mode,
- analysis of 5-substituted salicylaldoximes, which will only show the electronic effect of substitution on complex stability,
- analysis of salicylaldoxime dimers, allowing a simpler analysis of the effect of substitution on H-bonding, and
- DFT calculations to investigate the likely sites of protonation and deprotonation.

This work forms the basis of a new PhD studentship at the University of Edinburgh in collaboration with CYTEC Industries UK Ltd. Initial work has focussed on refining the experimental technique to ensure that comparability of data is not compromised by varying conditions inside the mass spectrometer. Optimisation of the method has shown that the same order as Figure 3.13, and thus the same substituent effects, persist and so further work will examine the gas phase substituent effects as described above.[60]

3.7 EPR Spectroscopy

The Cu^{II} ion in a square planar environment has a d^9 electron configuration, with its paramagnetic nature making it suitable for analysis by EPR spectroscopy.[10] Parameters measured in a copper(II) EPR spectrum can give information on the bonding and donor environment of the unpaired electron: the copper and nitrogen hyperfine splitting constants, A^{Cu} and A^N, can be used to predict the location of the unpaired electron in the system and the spectroscopic splitting factor, g, will vary from the value associated with a free electron, $g_e = 2.0023$, depending on the coupling environment.[10]

Spectra were recorded for the Cu^{II} complexes of **L1**-**L9** at concentrations of 0.01 M in $CHCl_3$, but the spectrum of $[Cu(\textbf{L4}-H)_2]$ could not be recorded due to its low solubility. The simulated[61] spectrum of $[Cu(\textbf{L3}-H)_2]$ is shown in Figure 3.15, and is typical of the spectra of each complex.

The signal is split into four lines, consistent with coupling to the Cu^{II} centre which has the nuclear spin quantum number $I_{Cu} = 1.5$. Each of these four lines is split into five further lines with relative intensities of 1:2:3:2:1, consistent with coupling to two equivalent nitrogen atoms (one from each salicylaldoxime ligand) as nitrogen has a nuclear spin quantum number $I_N = 1$.[62] These spectra are similar to many reported in the literature.[15-18]
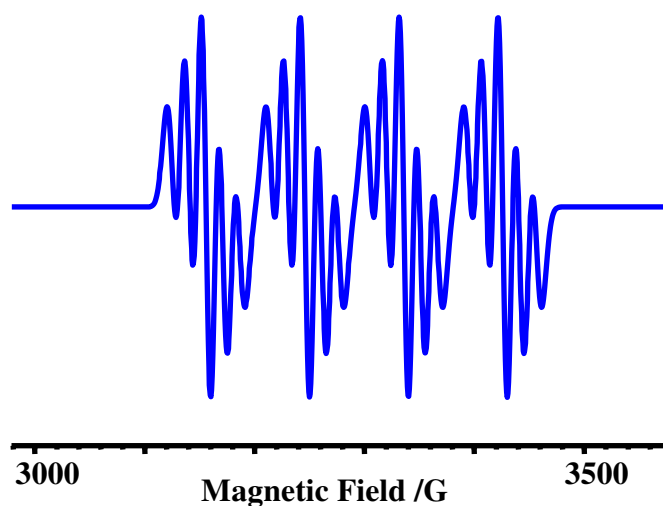
Figure 3.15: Simulated[61] EPR spectrum of [Cu(**L3**-H)$_2$], based on the experimentally determined hyperfine splitting constants and spectroscopic splitting factor.

Hyperfine coupling constants and spectroscopic splitting factors for all complexes studied, measured using WinEPR SimFonia,[61] are listed in Table 3.11.

Complex	A^{Cu} (G)	N^{Cu} (G)	g
[Cu(**L1**-H)$_2$]	90	18	2.0987
[Cu(**L2**-H)$_2$]	91	17	2.0977
[Cu(**L3**-H)$_2$]	90	18	2.0987
[Cu(**L5**-H)$_2$]	91	18	2.0987
[Cu(**L6**-H)$_2$]	91	18	2.0977
[Cu(**L7**-H)$_2$]	92	18	2.0957
[Cu(**L8**-H)$_2$]	91	17	2.0977
[Cu(**L9**-H)$_2$]	91	17	2.1007

Table 3.11: EPR parameters from experimental spectra.

The data in Table 3.10 shows that there are no significant differences in the EPR spectra of the Cu^{II} complexes. All show coupling of the unpaired electron to the copper centre and two identical nitrogen atoms, with similar hyperfine coupling

114

constants, and have $g > g_e$, indicating the electron is coupling to filled orbitals. The data confirm that the solid state structure persists in solution, but the technique is not sensitive enough to give information about any differences in the environment of the Cu^{II} centre in the complexes.

ENDOR (Electron Nuclear DOuble Resonance) spectroscopy is a more sensitive technique and may give further information on solution structure around the paramagnetic Cu^{II} ion.[63]

3.8   Conclusions and Future Work

Analysis of the solid state cavity sizes of **L2**, **L3**, **L6**, **L7** and **L10**-**L15** has shown the effect of 3-substitution on the stability of the *pseudo*macrocyclic H-bonded dimer assembly. Measurement of H-bond enthalpies by FTIR demonstrated the complexity of the substituent effects and of solution structures of the ligands. Pixel and DFT calculations on **L10**-**L15** have confirmed that the 3-substituent can buttress the H-bonding, with substituents capable of accepting H-bonds significantly stabilising the dimer. This stabilisation correlates well with the relative extraction strengths of **L1**-**L9** measured in Chapter 2, which indicates that H-bond buttressing is a major contributing factor to the differences in the extractive efficacies of salicylaldoxime ligands induced by 3-substitution. However, it is also evident that the electronic effect of the 3-substituent on the acidity of the ligand is an important factor in the design of new reagents.

Despite the unsuitability of the solid state structures of the copper(II) complexes for cavity size analysis, the interaction of the 3-substituent is apparent in the crystal structures of [Cu(**L3**-H)$_2$] and [Cu(**L4**-H)$_2$(py)$_2$]. Attempts to study the cavity sizes in solution by EPR spectroscopy showed the similarities in solution structure of the complexes, and the technique is not sensitive enough to detect the minor changes in the Cu^{II} coordination sphere.

Gas phase stabilities of the complexes were investigated by CID mass spectrometry, and initial tests showed a gas phase stability order which was approximately the reverse of the extraction strength order. This was thought to be due to the effects of ionisation on complex stability, alongside the prominence of electronic effects in the gas phase.

Having established the ability of 3-substituents to buttress the interligand hydrogen bonding in salicylaldoxime dimers and Cu^{II} complexes, the next logical areas of study are to investigate the effect with alternative ligands and transition metals. Salicylaldehyde hydrazones could potentially form complexes with divalent metal cations with a very similar *pseudo*macrocyclic H-bonding arrangement to phenolic oximes (Figure 3.16).
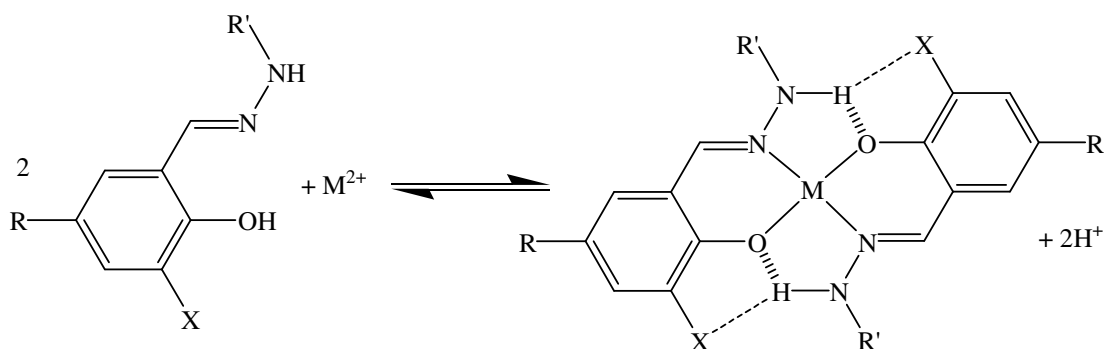
Figure 3.16: Potential buttressing of H-bonds in metal complexes of salicylaldehyde hydrazones.

These ligands are poor Cu^{II} extractants,[64] and so buttressing the H-bonding may sufficiently strengthen them to allow commercial application.

Pyrazolone oximes and 3-(2-hydroxyphenyl)-pyrazoles can both form complexes with divalent metal cations which show similar *pseudo*macrocyclic H-bonded arrays. Previous studies[59] within the group have shown that their copper(II) extraction strengths are unsuitable for industrial use (too high and too low respectively) and so H-bond buttressing (Figure 3.17) may be appropriate in tuning extraction strength and fulfilling the commercial potential of these ligands.
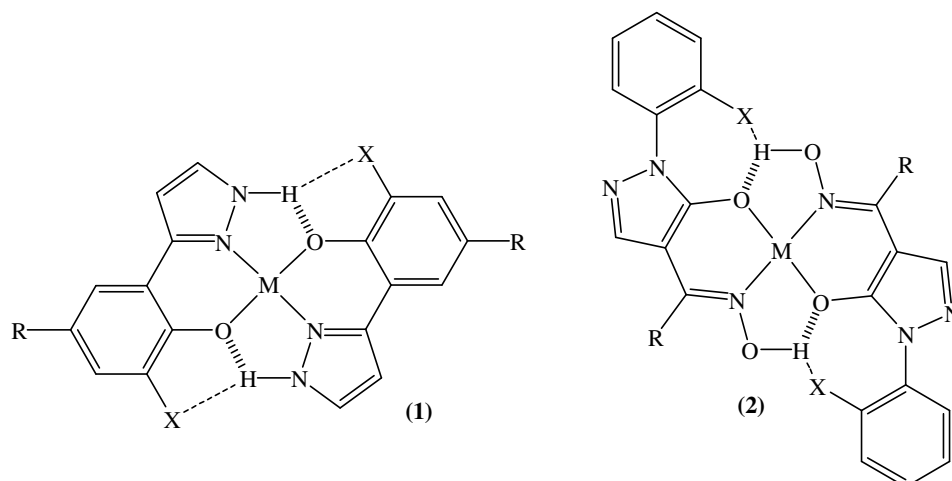
Figure 3.17: Potential buttressing of H-bonds in metal complexes of 3-(2-hydroxyphenyl)-pyrazoles (1) and pyrazolone oximes (2).

Phenolic oximes are unsuitable as Co^{II} extractants due to the spontaneous oxidation of the metal cation to Co^{III} to form octahedral complexes, which makes stripping at practicably low pH impossible.[30] However, it has been found that salicylaldoximes with a 3-NO$_2$ group stabilise the Co^{II} cation, and crystal structures of two DMSO-capped, octahedral Co^{II} complexes have been reported.[65] The origin of the effect is thought to lie in the weakening of the σ-bond donating property of the salicylaldoxime due to the inclusion of an electron-withdrawing substituent in the *ortho* position, giving a weaker-field ligand which favours Co^{II} stabilisation. However, it may be possible that the buttressing of the H-bonding and subsequent reduction in cavity size afforded by the 3-NO$_2$ group is a significant contributing factor, and a comprehensive study is required.

3.9   Experimental

3.9.1   Chemicals and Instrumentation

All solvents and reagents were used as received from Aldrich, Acros, Apollo and Fisher. ^{1}H and ^{13}C NMR were obtained using a Bruker AC250 spectrometer at ambient temperature. Chemical shifts (δ) are reported in parts per million (ppm)

relative to internal standards. Fast atom bombardment mass spectrometry (FABMS) was carried out using a Kratos MS50TC spectrometer with a thioglycerol or 3-NOBA matrix. Elemental analysis was carried out on a Carlo Erba CHNS analyser at the University of St Andrews.

3.9.2 Ligand Synthesis
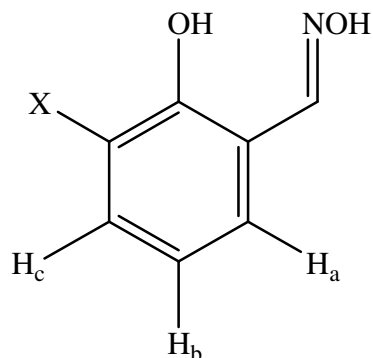
Figure 3.18: Numbering scheme for ^{1}H NMR interpretation

Oximation General Procedure. c1.2 equivalents of KOH and NH$_2$OH.HCl were dissolved separately in EtOH, mixed thoroughly and a white KCl precipitate removed by filtration. The filtrate was added to the precursor aldehyde, refluxed for 3 hr and the solvent removed *in vacuo*. The residue was redissolved in CHCl$_3$, washed with water 3 times, dried over MgSO$_4$ and the solvent removed *in vacuo* to yield the crude product.

Salicylaldoxime (L10). Purchased from Acros and recrystallised from petroleum ether (b.p. 60-80) to give fine white needles. A colourless block suitable for x-ray diffraction was grown by slow evaporation of a hexane/chloroform solvent.

3-Methylsalicylaldoxime (L11). Using the general procedure, 3-methylsalicylaldehyde (1.000 g, 7.4 mmol) was reacted with KOH (0.425 g, 7.6 mmol) and NH$_2$OH.HCl (0.530 g, 7.6 mmol) to yield a white powder, which was recrystallised from hexane to give an off white solid. (0.889 g, 80%). A colourless rod suitable for x-ray diffraction was grown by slow evaporation of a

hexane/chloroform solvent. (Anal. Calc. for $C_8H_9NO_2$: C, 63.6; H, 6.0; N, 9.3. Found: C, 63.2; H, 6.0; N, 9.4%); ^{1}H NMR (250 MHz, CDCl$_3$): δ_H (ppm) 2.20 (s, 3H, ArCH_3), 6.75 (t, 1H, ArH_b), 6.95 (dd, 1H, ArH_c), 7.08 (dd, 1H, ArH_a); ^{13}C NMR (63 MHz, CDCl$_3$): δ_C (ppm) 14.5 (1C, Ar-**CH$_3$**), 115.0 (1C, aromatic **C**), 118.5 (1C, aromatic **CH**), 125.0 (1C, aromatic **C**), 127.5 (1C, aromatic **CH**), 132.0 (1C, aromatic **CH**), 152.5 (1C, Ar-**CH**N), 154.5 (1C, aromatic **C**); FABMS m/z 152 (MH)$^+$, 83%.

3-*tert*-Butylsalicylaldoxime (L12). Using the general procedure, 3-*tert*-butylsalicylaldehyde (2.500 g, 14.0 mmol) was reacted with KOH (1.347 g, 24.0 mmol) and NH$_2$OH.HCl (1.418 g, 20.4 mmol) to yield a white powder, which was recrystallised from hexane to give white needles (2.341 g, 87%). A colourless block suitable for X-ray diffraction was grown by slow evaporation of a hexane/chloroform solvent. (Anal. Calc. for $C_{11}H_{15}NO_2$: C, 68.4; H, 7.8; N, 7.3. Found: C, 68.4; H, 8.3; N, 7.4%); ^{1}H NMR (250 MHz, CDCl$_3$): δ_H (ppm) 1.34 (s, 9H, C(CH_3)$_3$), 6.78 (t, 1H, ArH_b), 6.95 (dd, 1H, ArH_c), 7.22 (dd, 1H, ArH_a); ^{13}C NMR (63 MHz, CDCl$_3$): δ_C (ppm) 29.5 (3C, C(**CH$_3$**)$_3$), 35.5 (1C, **C**(CH$_3$)$_3$), 117.0 (1C, aromatic **C**), 119.5 (1C, aromatic **CH**), 129.5 (1C, aromatic **CH**), 130.0 (1C, aromatic **CH**), 138.0 (1C, aromatic **C**), 154.5 (1C, Ar-**CH**N), 157.0 (1C, aromatic **C**); FABMS m/z 194 (MH)$^+$, 100%.

3-Chlorosalicylaldoxime (L13). Using the general procedure, 3-chlorosalicylaldehyde (0.431 g, 2.8 mmol) was reacted with KOH (0.169 g, 3.0 mmol) and NH$_2$OH.HCl (0.209 g, 3.0 mmol) to yield a white powder (0.376 g, 80%). A colourless plate suitable for X-ray diffraction was grown by slow evaporation of DCM. (Anal. Calc. for $C_7H_6ClNO_2$: C, 49.0; H, 3.5; N, 8.2. Found: C, 49.4; H, 3.1; N, 8.0%); ^{1}H NMR (250 MHz, CDCl$_3$): δ_H (ppm) 6.78 (t, 1H, ArH_b), 7.05 (dd, 1H, ArH_a), 7.30 (dd, 1H, ArH_c), 8.15 (s, 1H, ArCHN); ^{13}C NMR (63 MHz, CDCl$_3$): δ_C (ppm) 117.0 (1C, aromatic **C**), 121.0 (1C, aromatic **CH**), 122.0 (1C, aromatic **C**), 129.5 (1C, aromatic **CH**), 132.0 (1C, aromatic **CH**), 153.0 (1C, Ar-**CH**N), 154.0 (1C, aromatic **C**); FABMS m/z 172 (MH)$^+$, 100%.

3-Bromosalicylaldoxime (L14). Using the general procedure, 3-bromosalicylaldehyde (0.499 g, 2.5 mmol) was reacted with KOH (0.280 g, 5.0 mmol) and NH$_2$OH.HCl (0.348 g, 5.0 mmol) to yield a white powder which was recrystallised from chloroform to give colourless needles (0.420 g, 78%). A colourless rod suitable for X-ray diffraction was grown by slow evaporation of toluene. (Anal. Calc. for C$_7$H$_6$BrNO$_2$: C, 38.9; H, 2.8; N, 6.5. Found: C, 39.1; H, 2.4; N, 6.2%); ^{1}H NMR (250 MHz, MeOD): δ_H (ppm) 5.24 (t, 1H, Ar*H$_b$*), 5.65 (dd, 1H, Ar*H$_a$*), 6.87 (dd, 1H, Ar*H$_c$*), 6.64 (s, 1H, ArC*H*N); ^{13}C NMR (63 MHz, MeOD): δ_C (ppm) 110.0 (1C, aromatic **C**), 118.8 (1C, aromatic **C**), 120.4 (1C, aromatic **CH**), 129.6 (1C, aromatic **CH**), 133.8 (1C, aromatic **CH**), 150.6 (1C, Ar-**C**HN), 154.0 (1C, aromatic **C**); FABMS *m/z* 217 (MH)$^+$, 35%.

3-Methoxysalicylaldoxime (L15). Using the general procedure, 3-methoxysalicylaldehyde (3.000 g, 19.7 mmol) was reacted with KOH (1.347 g, 24.0 mmol) and NH$_2$OH.HCl (1.418 g, 20.4 mmol) to yield an off-white powder, which was recrystallised from H$_2$O to give white needles (2.612 g, 79%). A colourless block suitable for X-ray diffraction was grown by slow evaporation of chloroform. (Anal. Calc. for C$_8$H$_9$NO$_3$: C, 57.5; H, 5.4; N, 8.4. Found: C, 57.4; H, 5.6; N, 8.6%); ^{1}H NMR (250 MHz, CDCl$_3$): δ_H (ppm) 4.12 (s, 3H, OC*H$_3$*), 7.08 (m, 3H, 3 x Ar*H*), 8.42 (s, 1H, ArC*H*N); ^{13}C NMR (63 MHz, CDCl$_3$): δ_C (ppm) 56.5 (1C, OCH$_3$), 113.0 (1C, aromatic **CH**), 117.0 (1C, aromatic **C**), 120.0 (1C, aromatic **CH**), 125.0 (1C, aromatic **CH**), 146.5 (1C, aromatic **C**), 147.5 (1C, aromatic **C**), 153.0 (1C, Ar-**C**HN); FABMS *m/z* 168 (MH)$^+$, 91%.

3-Nitrosalicylaldoxime (L16). Using the general procedure, 3-nitrosalicylaldehyde (1.000 g, 6.0 mmol) was reacted with KOH (0.341 g, 6.0 mmol) and NH$_2$OH.HCl (0.422 g, 6.0 mmol) to yield a yellow powder (0.827 g, 76%). (Anal. Calc. for C$_7$H$_6$N$_2$O$_4$: C, 46.2; H, 3.3; N, 15.4. Found: C, 38.9; H, 2.5; N, 13.3%); ^{1}H NMR (250 MHz, MeOD): δ_H (ppm) 7.12 (t, 1H, Ar*H$_b$*), 7.92 (dd, 1H, Ar*H$_a$*), 8.08 (dd, 1H, Ar*H$_c$*), 8.48 (s, 1H, ArC*H*N); ^{13}C NMR (63 MHz, MeOD): δ_C (ppm) 121.5 (1C, aromatic **CH**), 124.0 (1C, aromatic **C**), 128.0 (1C, aromatic **CH**), 135.5 (1C,

aromatic **CH**), 138.5 (1C, aromatic **C**), 148.0 (1C, Ar-**CH**N) 153.5 (1C, aromatic **C**); FABMS *m/z* 183 (MH)[+], 52%.

3.9.3 X-Ray Structure Determinations

The crystal structures of **L10**-**L13** and **L15** were solved by Dr Peter Wood and **L14** by Fraser White at the University of Edinburgh Crystallography Service. Diffraction data were collected for each compound at ambient pressure and temperature on a Bruker APEX diffractometer with graphite-monochromated Mo-K$_\alpha$ radiation (λ = 0.71073 Å). The data were integrated using SAINT[66] and corrected for absorption with SADABS[67]. The structures were solved using the program SIR-92[68] and refined using the program CRYSTALS[69]. Information on the solutions, and appropriate cif files can be found in appendix 7.3.1.

3.9.4 PIXEL Calculations

PIXEL calculations were carried out by Dr Peter Wood and Professor Simon Parsons at the University of Edinburgh. The geometry of the final crystal structure of each ligand was used to calculate the molecular electron density by standard quantum chemical methods using the program GAUSSIAN98[6] with the MP2/6-31G** basis set. H-atom distances were set to standard neutron values (CH = 1.083 Å, OH = 0.983 Å). The electron density model of the molecule was then analysed using the program package OPiX[4] which allow the calculation of dimer and lattice energies. The process was repeated in each case using the same geometry with the 3-substituent replaced by a proton, allowing calculation of the difference in energy between substituted and unsubstituted compounds. Dimer calculations were carried out for the pairs of molecules relating to the hydrogen bonded ring motif in each structure. The output from these calculations yields a total energy and a breakdown into its electrostatic, polarisation, dispersion and repulsion components.[5]

3.9.5 *Ab Initio* and DFT Calculations

All calculations were performed on the EaStCHEM RCF using Gaussian 03[39] with the assistance and guidance of Dr Andrew Turner. Using the crystal structure geometries or previously optimised geometries of the dimer and the free ligand, structural optimisations of both the dimer and the monomer were carried out and the dimerisation enthalpy was calculated as,

Equation 3.8 $\qquad\qquad \Delta H_{dimer} = E_D - 2E_M$

where E_D is the minimised energy of the dimer and E_M the minimised energy of the monomer. This is a valid calculation as the dimer has the same number of electrons as two monomers. To estimate the BSSE, a final counterpoise corrected calculation was run and the final enthalpy calculated as,

Equation 3.9 $\qquad\qquad \Delta H_{dimer} = E_{D(C)} - 2E_M$

where $E_{D(C)}$ is the minimised dimer energy corrected for BSSE using the counterpoise command. Calculated cavity sizes were measured from the geometry optimised structures of the dimers using ArgusLab 4.0.1.[70] Calculation spreadsheets and results can be found in appendix 7.3.3.

3.9.6 IR Conditions

0.05 M solutions of **L1**-**L9** in $CHCl_3$ were prepared and their IR spectra collected on a JASCO FT/IR 410 spectrometer in a glass cell, using a $CHCl_3$ background. Analysis of spectra was carried out using JASCO Spectra Manager version 1.53.00 (Build 1).[71] A spreadsheet of IR peaks for the OH groups of **L1**-**L7** and bond enthalpy calculations is located in appendix 7.3.4.

3.9.7 CIDMS Conditions

CIDMS experiments were performed in negative ion mode using a Finnigan liquid chromatograph quadrupole (LCQ) ion trap mass spectrometer. 40 μM solutions of the copper(II) complexes of **L1**-**L7** in methanol were injected into the spray emitter with a Hamilton syringe at a rate of 35 μl min^{-1}. Ionisation was achieved with a 5.03 kV potential difference between the spray emitter (5 kV) and heated capillary (-26 V) and a N$_2$ backing gas pressure of 50 arbitrary units. Droplet desolvation occurred in a stainless steel capillary that was heated to 443.15 K. Molecular ions of the complexes were mass selected and breakdown was achieved by variation of the normalised collision energy (NCE).

For each complex, spectra (average of 30 scans) were recorded over a range of normalised collision energies, and data analysed in Origin 7.5 SR6.[72] Breakdown was calculated for each NCE by taking the precursor ion (PI) intensity and dividing by total ion current (TIC). These values were normalised by dividing by the maximum observed PI / NTC value, and plotted against NCE to give an S-curve for molecular ion breakdown. The curves for each complex are plotted in Figure 3.12 and the data file located in appendix 7.3.5.

3.9.8 EPR Conditions

X-band EPR data were recorded on an X-band Bruker ER 200-D SRC spectrometer connected to a datalink 486DX desktop PC running EPR acquisition system version 2.42. 0.01 M solutions in CHCl$_3$ were run in a quartz flat cell. The copper and nitrogen hyperfine coupling constants (A^{Cu} and A^N) and the spectroscopic splitting factor (g) were measured using the program WinEPR SimFonia Version 1.25,[61] which was also used to simulate spectra. Spectra are located in appendix 7.3.6.

3.10   References

[1]   T. Steiner, *Angewandte Chemie International Edition*, 2002, **41**, 48.

[2]   F. H. Allen, *Acta Crystallographica Section B*, 2002, **58**, 380.

[3]   G. R. Desiraju, *Accounts of Chemical Research*, 2002, **35**, 565.

[4]   A. Gavezzotti, *Structural Chemistry*, 2005, **220**, 499.

[5]   J. D. Dunitz and A. Gavezzotti, *Angewandte Chemie International Edition*, 2005, **44**, 1766.

[6]   M. J. Frisch, G. W. Trucks, H. B. Schlegel, G. E. Scuseria, M. A. Robb, J. R. Cheeseman, V. G. Zakrzewski, J. A. J. Montgomery, R. E. Stratmann, J. C. Burant, S. Dapprich, J. M. Millam, A. D. Daniels, K. N. Kudin, M. C. Strain, O. Farkas, J. Tomasi, V. Barone, M. Cossi, R. Cammi, B. Mennucci, C. Pomelli, C. Adamo, S. Clifford, J. Ochterski, G. A. Petersson, P. Y. Ayala, Q. Cui, K. Morokuma, D. K. Malick, A. D. Rabuck, K. Raghavachari, J. B. Foresman, J. Cioslowski, J. V. Ortiz, B. B. Stefanov, G. Liu, A. Liashenko, P. Piskorz, I. Komaromi, R. Gomperts, R. L. Martin, D. J. Fox, T. Keith, M. A. Al-Laham, C. Y. Peng, A. Nanayakkara, C. Gonzalez, M. Challacombe, P. M. W. Gill, B. G. Johnson, W. Chen, M. W. Wong, J. L. Andres, M. Head-Gordon, E. S. Replogle, and J. A. Pople, in 'Gaussian 98 revision A.7', Pittsburgh, PA, USA, 1998.

[7]   A. Gavezzotti, *Journal of Chemical Theory and Computation*, 2005, **1**, 834.

[8]   G. A. Jeffrey, 'An Introduction to Hydrogen Bonding', Oxford University Press, 1997.

[9]   V. Bertolasi, P. Gilli, V. Ferretti, and G. Gilli, *Journal of the Chemical Society, Perkin Transactions 2: Physical Organic Chemistry*, 1997, 945.

[10]   P. W. Atkins and D. F. Shriver, 'Inorganic Chemistry', Oxford University Press, 1999.

[11]   D. H. Williams and I. Fleming, 'Spectroscopic Measurements in Organic Chemistry', McGraw and Hill, 1995.

[12]   G. Gilli and P. Gilli, *Journal of Molecular Structure*, 2000, **552**, 1.

[13]   M. Rozenberg, A. Loewenschuss, and Y. Marcus, *Physical Chemistry Chemical Physics*, 2000, **2**, 2699.

14   B. A. Goodman and J. B. Raynor, *Advances in Inorganic Chemistry and Radiochemistry*, 1970, **13**, 135.

15   B. McCudden, P. O'Brien, and J. R. Thornback, *Dalton Transactions*, 1983, 2043.

16   P. O'Brien and J. R. Thornback, *Hydrometallurgy*, 1982, **8**, 331.

17   P. O'Brien and J. R. Thornback, *Inorganica Chimica Acta*, 1982, **64**, 35.

18   I. Rani, K. B. Pandeya, and R. P. Singh, *Journal of Inorganic and Nuclear Chemistry*, 1981, **43**, 2743.

19   P. A. Kollman and L. C. Allen, *Chemical Reviews*, 1972, **72**, 283.

20   J. E. Del Bene and M. J. T. Jordan, *Theochem*, 2001, **573**, 11.

21   Scifinder Scholar, 2007.

22   Simple search for DFT hydrogen bonds on 31 March 2008.

23   K. E. Riley, B. T. Op't Holt, and K. M. Merz, Jr., *Journal of Chemical Theory and Computation*, 2007, **3**, 407.

24   E. de Hoffman and V. Stroobant, 'Mass Spectrometry - Principles and Applications', John Wiley & Sons, Ltd, 2001.

25   J. B. Fenn, M. Mann, C. K. Meng, S. F. Wong, and C. M. Whitehouse, *Science*, 1989, **246**, 64.

26   K. R. Jennings, *International Journal of Mass Spectrometry*, 2000, **200**, 479.

27   K. Burger and I. Egyed, *Journal of Inorganic and Nuclear Chemistry*, 1965, **27**, 2361.

28   K. Burger and I. Egyed, *Magyar Kemiai Folyoirat*, 1965, **71**, 143.

29   K. Burger, F. Ruff, I. Ruff, and I. Egyed, *Magyar Kemiai Folyoirat*, 1965, **71**, 282.

30   J. Szymanowski, 'Hydroxyoximes and Copper Hydrometallurgy', CRC Press, 1993.

31   J. Szymanowski and A. Borowiak-Resterna, *Critical Reviews in Analytical Chemistry*, 1991, **22**, 519.

32   J. March and M. B. Smith, 'March's Advanced Organic Chemistry, Reactions, Mechanisms and Structures', John Wiley's and Sons, 2001.

33   A. G. Smith, P. A. Tasker, and D. J. White, *Coordination Chemistry Reviews*, 2003, **241**, 61.

34 C. E. Pfluger and R. L. Harlow, *Acta Crystallographica, Section B*, 1973, **29**, 2608.

35 T. Xu, L.-z. Li, and H.-w. Ji, *Hecheng Huaxue*, 2004, **12**, 22.

36 P. A. Wood, R. S. Forgan, S. Parsons, E. Pidcock, and P. A. Tasker, *Acta Crystallographica*, 2006, **E62**, o3944.

37 M. Palusiak and S. J. Grabowski, *Journal of Molecular Structure*, 2002, **642**, 97.

38 A. Gavezzotti, Personal Communication, 2007.

39 M. J. T. Frisch, G. W.; Schlegel, H. B.; Scuseria, G. E.; Robb, M. A.; Cheeseman, J. R.; Montgomery, Jr., J. A.; Vreven, T.; Kudin, K. N.; Burant, J. C.; Millam, J. M.; Iyengar, S. S.; Tomasi, J.; Barone, V.; Mennucci, B.; Cossi, M.; Scalmani, G.; Rega, N.; Petersson, G. A.; Nakatsuji, H.; Hada, M.; Ehara, M.; Toyota, K.; Fukuda, R.; Hasegawa, J.; Ishida, M.; Nakajima, T.; Honda, Y.; Kitao, O.; Nakai, H.; Klene, M.; Li, X.; Knox, J. E.; Hratchian, H. P.; Cross, J. B.; Bakken, V.; Adamo, C.; Jaramillo, J.; Gomperts, R.; Stratmann, R. E.; Yazyev, O.; Austin, A. J.; Cammi, R.; Pomelli, C.; Ochterski, J. W.; Ayala, P. Y.; Morokuma, K.; Voth, G. A.; Salvador, P.; Dannenberg, J. J.; Zakrzewski, V. G.; Dapprich, S.; Daniels, A. D.; Strain, M. C.; Farkas, O.; Malick, D. K.; Rabuck, A. D.; Raghavachari, K.; Foresman, J. B.; Ortiz, J. V.; Cui, Q.; Baboul, A. G.; Clifford, S.; Cioslowski, J.; Stefanov, B. B.; Liu, G.; Liashenko, A.; Piskorz, P.; Komaromi, I.; Martin, R. L.; Fox, D. J.; Keith, T.; Al-Laham, M. A.; Peng, C. Y.; Nanayakkara, A.; Challacombe, M.; Gill, P. M. W.; Johnson, B.; Chen, W.; Wong, M. W.; Gonzalez, C.; and Pople, J. A, in 'Gaussian 03, Revision D.01', Wallingford, CT, 2004.

40 M. J. Frisch, M. Head-Gordon, and J. A. Pople, *Chemical Physics Letters*, 1990, **166**, 281.

41 M. J. Frisch, M. Head-Gordon, and J. A. Pople, *Chemical Physics Letters*, 1990, **166**, 275.

42 M. Head-Gordon and T. Head-Gordon, *Chemical Physics Letters*, 1994, **220**, 122.

43   M. Head-Gordon, J. A. Pople, and M. J. Frisch, *Chemical Physics Letters*, 1988, **153**, 503.

44   C. Moller and M. S. Plesset, *Physical Review*, 1934, **46**, 618.

45   S. Saebo and J. Almlof, *Chemical Physics Letters*, 1989, **154**, 83.

46   J. Tao, J. P. Perdew, V. N. Staroverov, and G. E. Scuseria, *Physical Review Letters*, 2003, **91**, 146401.

47   R. Ditchfield, W. J. Hehre, and J. A. Pople, *Journal of Chemical Physics*, 1971, **54**, 724.

48   W. J. Hehre, R. Ditchfield, and J. A. Pople, *Journal of Chemical Physics*, 1972, **56**, 2257.

49   P. C. Hariharan and J. A. Pople, *Molecular Physics*, 1974, **27**, 209.

50   P. C. Hariharan and J. A. Pople, *Theoretica Chimica Acta*, 1973, **28**, 213.

51   M. M. Francl, W. J. Pietro, W. J. Hehre, J. S. Binkley, M. S. Gordon, D. J. DeFrees, and J. A. Pople, *Journal of Chemical Physics*, 1982, **77**, 3654.

52   M. S. Gordon, *Chemical Physics Letters*, 1980, **76**, 163.

53   J.-P. Blaudeau, M. P. McGrath, L. A. Curtiss, and L. Radom, *Journal of Chemical Physics*, 1997, **107**, 5016.

54   T. Clark, J. Chandrasekhar, G. W. Spitznagel, and P. v. R. Schleyer, *Journal of Computational Chemistry*, 1983, **4**, 294.

55   S. F. Boys, Bernardi, F., *Journal of Molecular Physics*, 1970, **19**, 553.

56   S. Simon, M. Duran, and J. J. Dannenberg, *Journal of Chemical Physics*, 1996, **105**, 11024.

57   M. L. Leininger, W. D. Allen, H. F. Schaefer III, and C. D. Sherrill, *Journal of Chemical Physics*, 2000, **112**, 9213.

58   V. N. Staroverov, G. E. Scuseria, J. Tao, and J. P. Perdew, *Journal of Chemical Physics*, 2003, **119**, 12129.

59   L. C. Emeleus, 'PhD Thesis', University of Edinburgh, 1999.

60   B. Roach, P. A. Tasker, and B. Duncombe, Unpublished work, 2008.

61   Bruker, WINEPR SimFonia, 1996.

62   A. K. Wiersema and J. J. Windle, *Journal of Physical Chemistry*, 1964, 2316.

63   D. M. Murphy, Farley, R.D., *Chemical Society Reviews*, 2006, **35**, 249.

64   H. Bauer, T. Lin, and P. A. Tasker, Unpublished work, 2007.

65   D. Cupertino, M. McPartlin, and A. M. Zissimos, *Polyhedron*, 2001, **20**, 3239.

66   Bruker-Nonius, in 'SAINT version 7', Madison, Wisconsin, USA, 2006.

67   G. M. Sheldrick, in 'SADABS Version 2004-1', Madison, Wisconsin, USA, 2004.

68   A. Altomare, G. Cascarano, C. Giacovazzo, A. Guagliardi, B. M. C, G. Polidori, and M. Camalli, *Journal of Applied Crystallography*, 1994, **27**, 435.

69   P. W. Betteridge, J. R. Carruthers, R. I. Cooper, K. Prout, and D. J. Watkin, *Journal of Applied Crystallography*, 2003, **36**, 1487.

70   M. Thompson, ArgusLab 4.0.1, 2004.

71   JASCO Spectra Manager, 1996.

72   Origin 7.5 SR6, 2006.

CHAPTER 4

SYNTHESIS OF METAL SALT EXTRACTANTS

Contents

4.1   Introduction

4.1.1   Aims

This chapter deals with the synthesis of a new class of metal *salt* extractants based on a salicylaldoxime scaffold, and an initial investigation into their ability to extract both a metal cation and its attendant anion(s) into a water-immiscible solvent. The work involves:

- the synthesis of six novel metal salt extractants,
- the study of the loading of base metal sulfates and chlorides by the new extractants,
- an investigation of the mode of action of extractants which show unexpectedly high loading of $CuCl_2$ and $ZnCl_2$, and
- initial experiments to define the potential of these extractants for commercialisation.

Like many other reagents, ligands capable of binding both a metal cation and its attendant anion(s) have the potential to perform the unit operations of *concentration* and *separation* in extractive hydrometallurgical circuits by transporting metal *salts* from the aqueous pregnant leach solution.[1, 2]   Until recently, there have been few attempts to distinguish mechanisms by which cations and their attendant anions can be transferred into a water-immiscible solvent.[3]   Several issues are considered in the sections below.

A similar project ran in parallel with the research presented in Chapters 4 and 5. Dr David K. Henderson was engaged in contract research at the University of Edinburgh, on behalf of Noranda Falconbridge, to identify reagents for the extraction of $NiCl_2$ and $CoCl_2$, and therefore considered variants of the ligands described in Section 4.1.4.

4.1.2   Solvating Metal Salt Extractants

As in extraction using cation or anion exchange reagents (Chapter 1) the key to obtaining solubility of the metal-containing assembly in the water-immiscible solvent is that it should be charge neutral. This can be achieved if the assembly contains the ions of the salt associated with a neutral extractant, and accounts for such reagents being termed "solvating extractants".[1] A major application is the extraction of uranyl nitrate by tri-*n*-butylphosphate[4] described in Chapter 1.

The CUPREX process[5-8] for extracting $CuCl_2$ utilises a pyridine dicarboxylic acid diester, CLX50, shown in Figure 4.1.
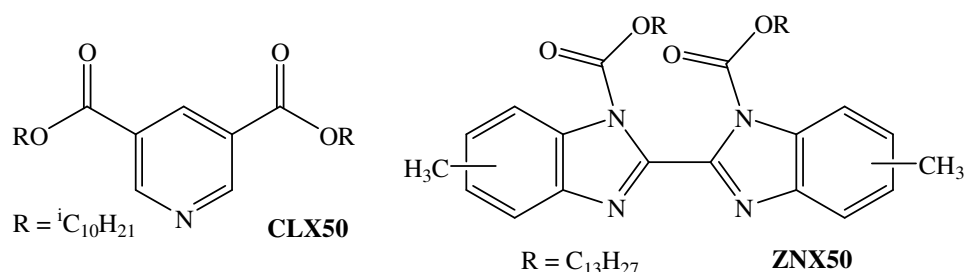
Figure 4.1:   The solvating extractants CLX50 and ZNX50, which extract $CuCl_2$ and $ZnCl_2$ respectively.

CLX50 is a "chloride swing" extractant – it extracts at high chloride activity and can be stripped by aqueous solutions with low chloride activity. Chloride activity, and hence the extraction equilibria, depend on the stability of the chlorometallate complexes in the feed solution. A simplified flowsheet (overleaf in Figure 4.2) describes the CUPREX process.

One of the main advantages of the CUPREX process follows from the oxidative ferric leach step which liberates sulfur.[9] Removal of the sulfur content of ores in its elemental form rather than as sulfuric acid can avoid acid build up in the front end of the hydrometallurgical circuit, which is costly to neutralise and remove.[10]

- Leach: $4FeCl_3 + 2Cu_2S_{(s)} \longrightarrow 2CuCl_2 + 4FeCl_2 + S_{(s)}$
- Extract: $2CuCl_2 + 4L_{(org)} \longrightarrow 2CuL_2Cl_{2\ (org)}$
- Strip: $2CuL_2Cl_{2\ (org)} \longrightarrow 2CuCl_2 + 4L_{(org)}$
- Electrowin: $2CuCl_2 \longrightarrow 2Cu_{(s)} + 2Cl_{2\ (g)}$
- Leach regen: $4FeCl_2 + 2Cl_{2\ (g)} \longrightarrow 4FeCl_3$

- Overall: $\mathbf{Cu_2S_{(s)}} \longrightarrow \mathbf{2Cu_{(s)} + S_{(s)}}$
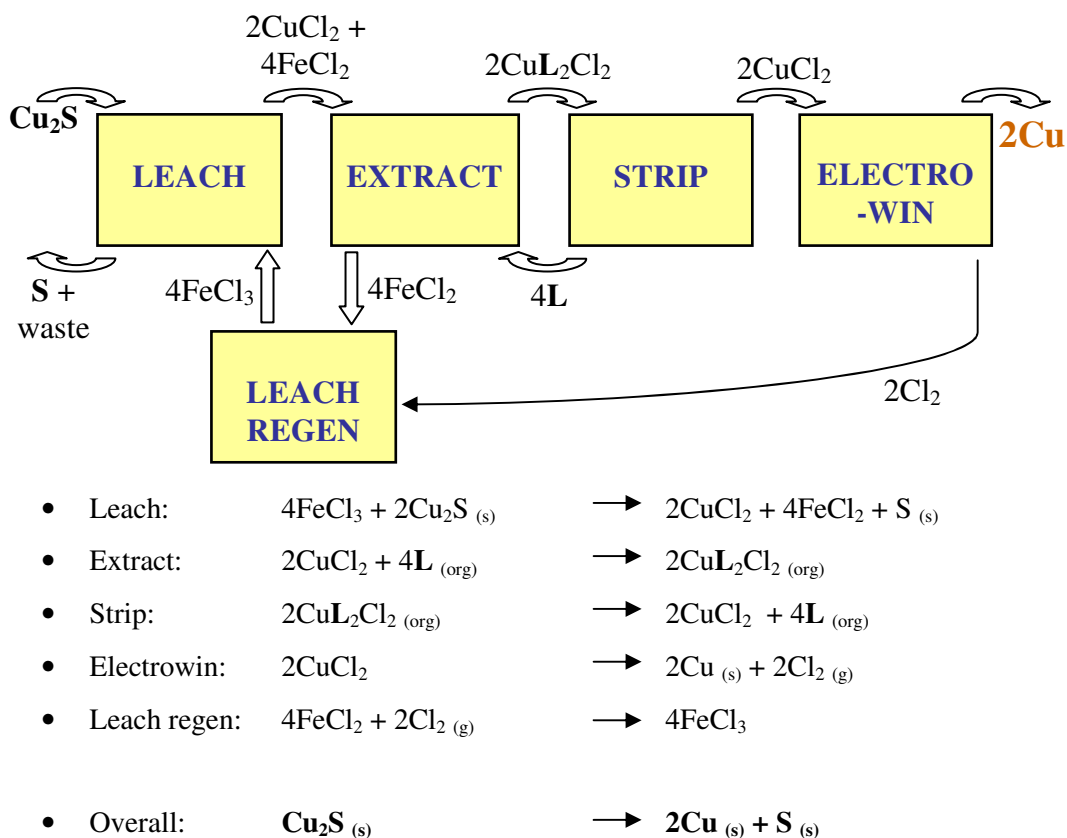
Figure 4.2: Flowsheet for $CuCl_2$ extraction by the CUPREX process.

However, chloride-based circuits can prove to be an engineering challenge. The high chloride activity means corrosion is an issue and more expensive materials are needed to construct plants. Electrowinning from chloride produces reactive copper granules rather than the copper sheets produced by traditional sulfate electrowinning.[11] Despite these technical issues, the emergence of a number of new chloride leaching processes and recent advances in plant engineering technology suggest that any reagent with the capacity to extract a metal chloride selectively could find commercial application.[1]

To overcome the problems associated with electrowinning copper from chloride, a reagent blend containing a solvating extractant (solvate) and a traditional phenolic oxime (chelate) has been proposed.[12-15] During the extract stage the copper is bound

---

[1] 16 papers discussing chloride hydrometallurgy were presented at the recent International Copper/Cobre conference, Toronto, August 2007.

as a neutral $CuCl_2$ complex [L^SCuCl_2] by the solvate ligand (L^S in Scheme 4.1) *e.g.* CLX50. Water stripping removes the chloride and transfers the copper to the chelate (L^C in Scheme 4.1) *e.g.* P50, allowing conventional sulfuric acid stripping of the copper to generate a sulfate electrolyte.

Extract: $CuCl_2 + 2L^C_{(org)} + L^S_{(org)}$ $\longrightarrow$ $[L^SCuCl_2]_{(org)} + 2L^C_{(org)}$

Cl strip: $[L^SCuCl_2]_{(org)} + 2L^C_{(org)} + H_2O \longrightarrow [Cu(L^C\text{-}H)_2]_{(org)} + L^S_{(org)} + H_2O + 2HCl$

Cu strip: $[Cu(L^C\text{-}H)_2]_{(org)} + L^S_{(org)} + H_2SO_4 \longrightarrow CuSO_4 + 2L^C_{(org)} + L^S_{(org)}$

E'win: $CuSO_4 + H_2O$ $\longrightarrow Cu_{(s)} + H_2SO_4 + \frac{1}{2}O_{2(g)}$

Overall: $\mathbf{CuCl_2 + H_2O}$ $\longrightarrow$ $\mathbf{Cu_{(s)} + 2HCl + \frac{1}{2}O_{2(g)}}$
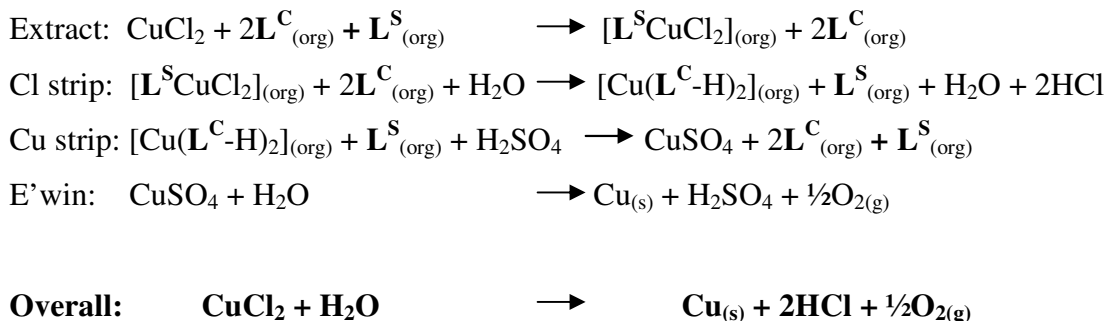
Scheme 4.1: Proposed flowsheet for $CuCl_2$ extraction, with transfer of copper into a conventional sulfate electrolyte, by a reagent blend containing a solvating (L^S) and a chelating (L^C) extractant.

The HCl generated could subsequently be recycled by using it in the leach stage. Important criteria for the design of the solvating reagents L^S, such as CLX50, are that they should not readily protonate and form stable ion pair complexes with tetrachloroferrate,

Equation 4.1 $L^S_{(org)} + H^+ + FeCl_4^- \rightleftharpoons [(L^SH)^+(FeCl_4)^-]_{(org)}$
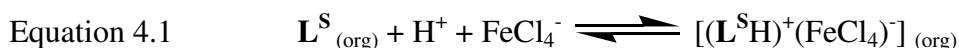
as this will lead to poor selectivity of Cu^{II}/Fe^{III} transport from mixed feeds.[16] A similar process has been proposed for $ZnCl_2$ extraction. The reagent ZNX50[17, 18] (Figure 4.1) shows high Zn^{II}/Fe^{III} selectivity due to the low basicity of the nitrogen donors, ensuring no transfer of Fe by such an ion pair mechanism:

Equation 4.2 $L_{(org)} + FeCl_3 + HCl \rightleftharpoons [LH]^+[FeCl_4]^-_{(org)}$
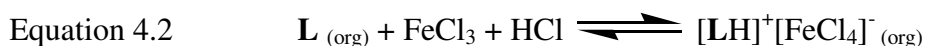
Extraction of $ZnCl_2$ with blends of ZNX50 and a chelating reagent have also been studied, and offer the same advantage of conventional sulfate electrowinning to the previously described processes for copper.[12, 13, 19, 20]

4.1.3 Zwitterionic Metal Salt Extractants

As described in Chapter 1, polytopic ligands containing separate cation and anion binding sites can extract a metal salt into a water-immiscible solvent. Substituted salicylaldimines, or "salens" have proven to be effective metal salt extractants, with the *cis* arrangement of the cation binding site forming a preorganised, doubly protonated anion binding site particularly suited to sulfate.[3] A striking example is shown in Figure 4.3, the crystal structure of a morpholinomethyl-substituted "salen" ligand binding copper sulfate.[21]
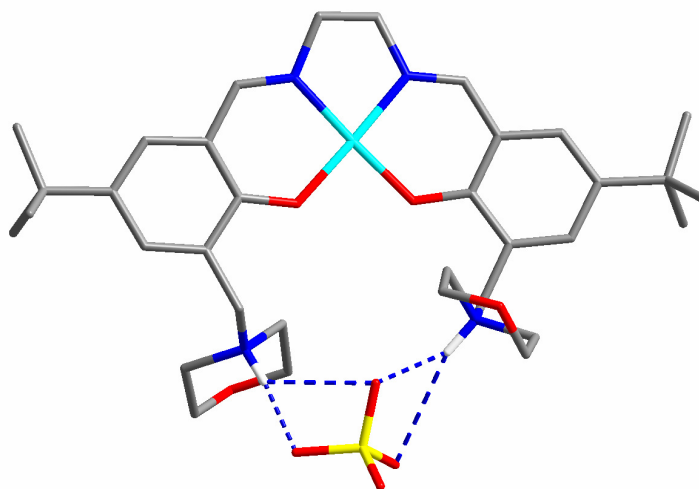
Figure 4.3: The copper(II) sulfate complex of the ditopic ligand 2,2'-[1,2-ethanediylbis(nitrilomethylidyne)]bis[4-(*t*-butyl)-6-(4-morpholinylmethyl)-phenol, hydrogen atoms not involved in H-bonding omitted for clarity.[21]

Tasker *et al*[21] describe the release of protons on binding of copper(II) and these protons can be accepted by the pendant amine arms to form the anion binding site. It has been shown by X-ray diffraction analysis that binding of the metal preorganises the anion binding site by templation, and UV/Vis spectroscopy shows the separation of the sites. With this ligand and related derivatives,[22, 23] both copper and sulfate can be sequentially loaded and stripped, showing potential for industrial use. However, the ease of acid hydrolysis of the imine functionality[24] renders them incompatible with most commercial solvent extraction applications which commonly use sulfuric acid concentrations of up to 150 gl^{-1} to strip the metal from the ligand.[25]

4.1.4   Ligand Design

Conventional phenolic oxime cation exchange extractants account for between 20%[26] and 30%[27] of the world's annual production of copper, and have half lives of over 2.5 yrs in kerosenes in contact with acid solutions.[25]   Incorporation of a pendant amine arm to this scaffold gives an anion binding site which, on protonation, offers the possibility of binding the conjugate anion *via* a combination of electrostatic, hydrogen and coordinate bonds, thus allowing the extraction of a metal salt (Figure 4.4).
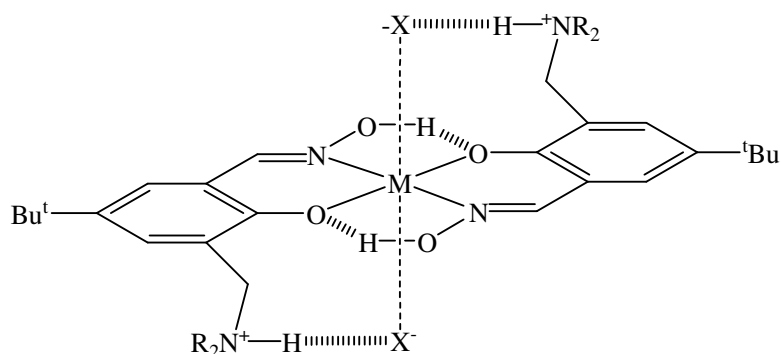
Figure 4.4: Potential metal salt binding motif of a salicylaldoxime substituted in the 3-position with a pendant amine arm, showing H-bonding and electrostatic interactions.

As salicylaldoximes bind base metal cations in a *trans* arrangement,[28] the anion binding sites are expected to be separated, forming a tritopic binding motif which may favour the binding of two monoanions *e.g.* two chloride anions.   This is in contrast to the previously described "salen" ligands which bind base metals in a *cis* arrangement, preorganising the anion binding site into a doubly protonated pocket well suited to the sulfate anion.[21-23]

Two different locations were chosen for incorporation of the anion binding site, based on the ease of synthesis and the potential effect of the location on the anion selectivity of the ligand.   Sites *ortho* and *para* to the phenol were chosen, which would yield ligands with pendant amine arms in the 3-position and 5-position respectively.   Figure 4.4 shows potential interactions of the anion with the metal

centre in the 3-substituted case, but in the 5-substituted ligands these interactions may be limited (Figure 4.5).
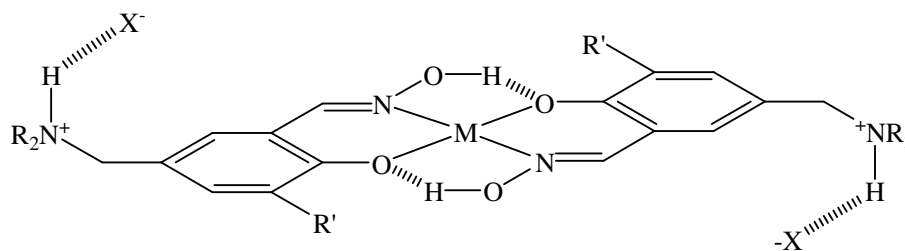
Figure 4.5: Potential metal salt binding motif of a salicylaldoxime substituted in the 5-position with a pendant amine arm.

Two separate amines were selected for incorporation into the molecule as anion binding sites. Piperidine was chosen, as "salen" type ligands with pendant piperidinomethyl groups are known to give crystalline complexes of both transition metal dications[21] and metal salts.[29] Dihexylamine was also used as its hydrophobicity should increase solubility in non-polar solvents suitable for solvent extraction studies. The target ligands are displayed in Figure 4.6.

"3-substituted" ligands   "5-substituted" ligands
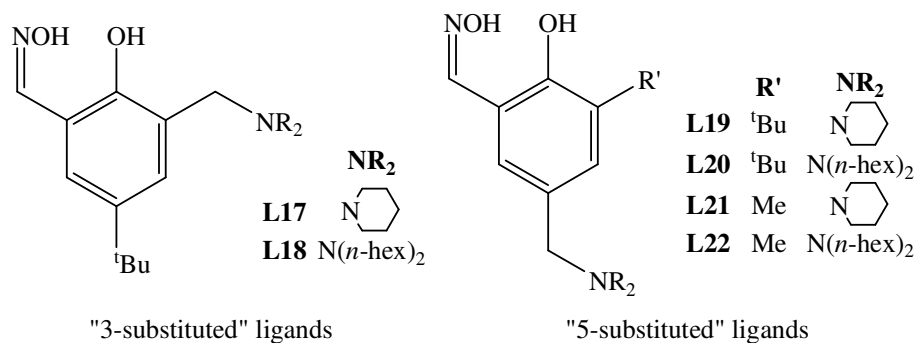
Figure 4.6: Salicylaldoxime based metal salt extractants with pendant dialkylaminomethyl arms in the 3- or 5-position.

In the text below, the 3-aminomethylated oximes are referred to as the "3-substituted" ligands and the 5-aminomethylated oximes are referred to as the "5-substituted".

4.2   Synthesis

Synthesis of the target metal salt ligands involved a four-step procedure from the appropriate alkyl phenol: formylation to yield a salicylaldehyde, a two step addition of the pendant amine arm *via* a modified Mannich reaction and oximation to generate the final ligand. The Mannich reaction involved firstly synthesising an N-ethoxymethyldialkylamine precursor, which was then coupled to the salicylaldehyde scaffold. The synthetic scheme listing all the compounds prepared in this thesis is shown in Scheme 4.2.
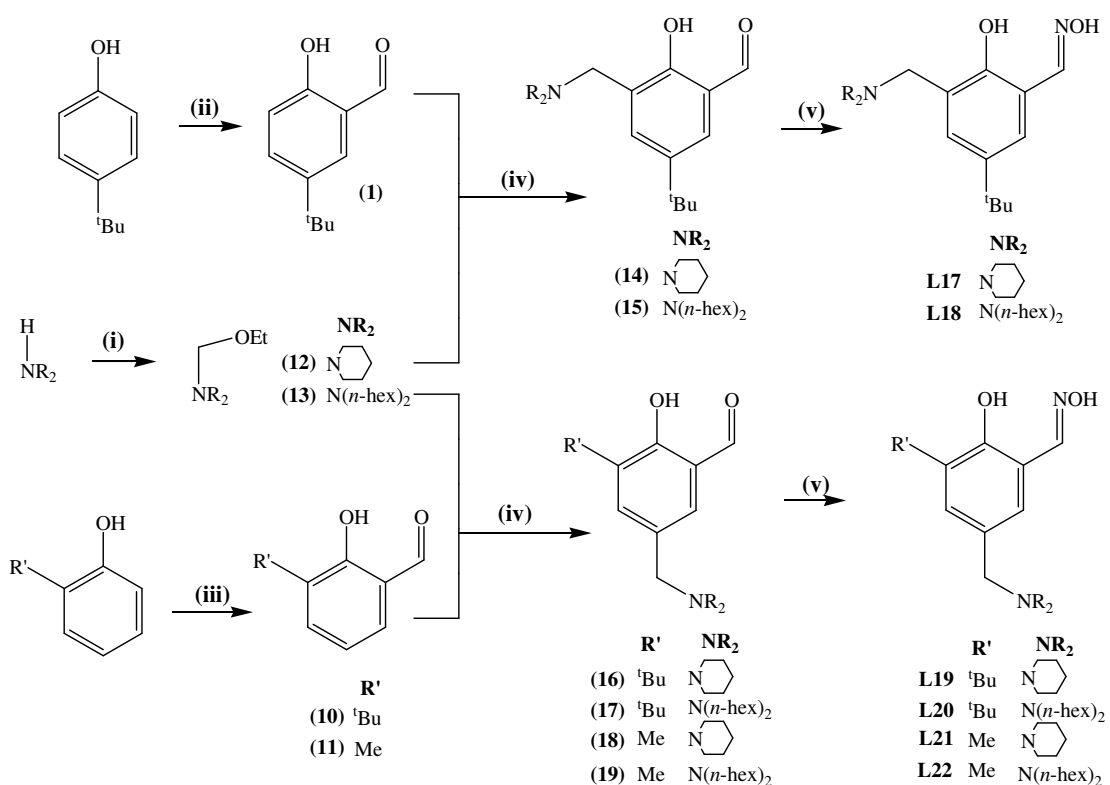
Scheme 4.2: Synthetic routes to 3- and 5-substituted ligands. (i) $(CH_2O)_n$, EtOH, K_2CO_3, 72 hr. (ii) $Mg(OMe)_2$, MeOH, $(CH_2O)_n$, toluene, H_2SO_4, Δ, 2 hr. (iii) various unsuccesful conditions. (iv) MeCN, N_2, Δ, 72 hr. (v) $NH_2OH \cdot HCl$, KOH, EtOH, Δ, 16 hr.

4.2.1 Formylation of 2- or 4-Alkylphenols

If ligands are to be used commercially as extractants, their syntheses must be cheap, robust and capable of being carried out on large scales.[1, 25] The preparation of (1) by the Levin[30] method has been described previously in Chapter 2, and the magnesium-mediated reaction with magnesium methoxide and paraformaldehyde generates approximately 100 g quantities of the pure material.

It was hoped that (10) and (11) could be prepared using an analogous route, starting from 2-alkylphenols. It was found, however, that the Levin synthesis was unsuccessful in attempts to produce large quantities of 3-alkyl-2-hydroxybenzaldehydes, giving mixed products in poor yields. A modified Duff reaction[31] was found to be a successful method in some cases in Chapter 2, but it too showed poor regioselectivity, and separation of the desired product was difficult. This is to be expected for the reasons outlined previously.

Other preparative routes have been tried, including formylation over a clay catalyst[32] and an anhydrous synthesis involving $MgCl_2$ and triethylamine,[33] but all are unsuitable for the production of large quantities of the required salicylaldehydes. (10) and (11) are available commercially[34] at a high cost, and so were purchased for the preparation of the 5-substituted ligands **L19-L22**, allowing proof-of-concept studies but precluding extensive analysis.

4.2.2 Mannich Reaction

Incorporation of the pendant amine arm to the salicylaldehyde scaffold was achieved by a modified Mannich reaction. The Mannich reaction proceeds by reaction of a carbonyl functionality (usually formaldehyde) and an amine to generate a reactive iminium ion, which subsequently reacts with the substrate by Michael addition to generate the product.[35-37] As the scaffold contains a carbonyl group, the possibility of unwanted side reactions between the amine and the salicylaldehyde occurs if a

conventional, one step Mannich reaction is carried out. For this reason a reactive precursor was synthesised to ensure no side reactions could occur.

The desired amine is firstly substituted in the N-position by an ethoxymethyl group, following the procedure of Fenton *et al*.[38] Stirring the appropriate dialkylamine with paraformaldehyde in ethanol, with potassium carbonate desiccant, gave both **(12)** and **(13)** in good yields after purification by vacuum distillation. Use of the N-ethoxymethyldialkylamines ensures ease of formation of the reactive iminium ion intermediate thought to be involved in the Mannich reaction.[36, 37] A proposed mechanism for the formation of **(12)** and **(13)** is outlined in Figure 4.7.
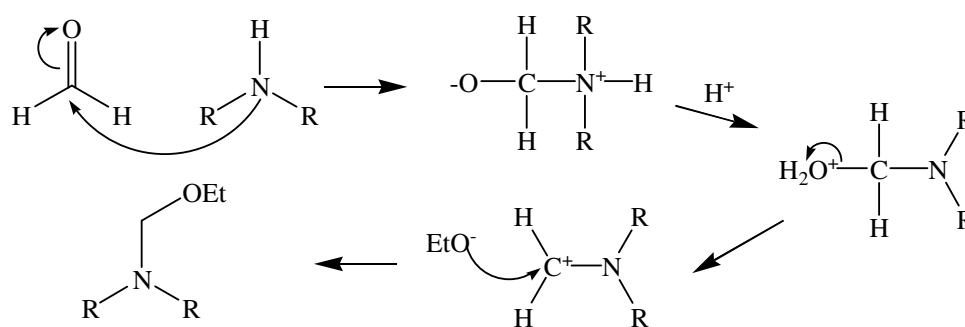
Figure 4.7: Proposed reaction mechanism for the formation of the N-ethoxymethyldialkylamines **(12)** and **(13)**.

Coupling of the pendant amine to the salicylaldehyde is achieved by simply refluxing the reactants in acetonitrile under a N_2 atmosphere. *In situ* generation of the active iminium ion is followed by a conjugate Michael addition, which ensures regioselective reaction in the *ortho* or *para* position to the phenol (Figure 4.8). In the preparations of the 3-substituted aldehydes **(14)** and **(15)** the reaction occurred exclusively in the *ortho* position, due to the *tert*-butyl group blocking the *para* position. For the 5-substituted aldehydes **(16-19)** the reaction was limited to the *para* position. All products were obtained in excellent yields (~80-90%) after appropriate purification, however it was noted that **(19)** appeared susceptible to degradation on the timescale of a few days, and so was used immediately upon isolation.
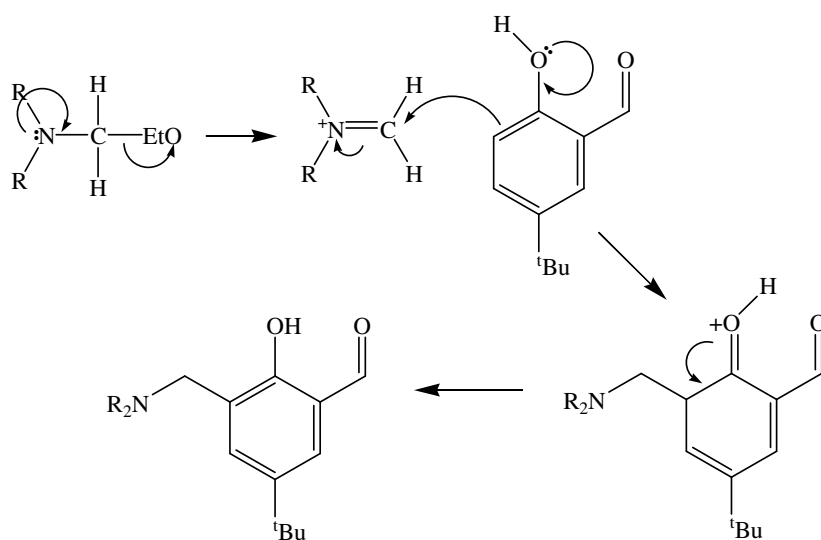
Figure 4.8: Proposed reaction mechanism for the Mannich addition to form the 3-substituted compounds **(14)** (NR$_2$ = N(C$_5$H$_{10}$)) and **(15)** (NR$_2$ = N(n-hexyl)$_2$).

4.2.3   Oximation

Oximation was carried out by the same procedure[39] described in Chapter 2 and found to be facile and high yielding, with yields of ~90% achieved. It was noticed that the solubilities of the 3-substituted ligands **L17** and **L18** in non polar solvents were generally better than that of their 5-substituted analogues **L19**-**L22**.   The piperidinomethyl substituted ligands **L17**, **L19** and **L21** were isolated as fine white powders, whereas the dihexylaminomethyl analogues **L18**, **L20** and **L22** were sticky, viscous oils. The 3-substituted ligands **L17** and **L18** were isolated in good purity, but isolation of the 5-substited ligands proved problematic. All were pure by ^{1}H and ^{13}C NMR, however acceptable CHN analysis was only obtained for **L20** and **L21**. The low solubility of **L19** hampered attempts at purification, while **L22** appeared to be prone to decomposition over the course of a few days, and so was prepared immediately prior to use in solvent extraction experiments.

4.3 Characterisation

4.3.1 NMR Spectroscopy

All ligands and precursors were fully characterised by both ^{1}H and ^{13}C NMR spectroscopy. ^{1}H NMR spectroscopy was used to monitor conversion of the aldehyde to the oxime as described in Chapter 2.

4.3.2 Mass Spectrometry

FAB mass spectra of each of the ligands show a peak assignable to the free ligand, although no evidence of salicylaldoxime dimers[28] analogous to those discussed in Chapter 3 was present. Molecular ion peaks and intensities for all ligands, alongside common breakdown peaks are shown in Table 4.1.

	[MH]$^+$	[M-17]$^+$	[M-diamine]$^+$
L17	291 (100%)	273 (49%)	206 (77%)
L18	391 (100%)	373 (24%)	206 (100%)
L19	291 (91%)	273 (24%)	206 (100%)
L20	391 (93%)	373 (40%)	206 (100%)
L21	249 (94%)	231 (20%)	164 (95%)
L22	349 (77%)	331 (49%)	164 (100%)

Table 4.1: Peaks and intensities seen in the FABMS spectra of **L17**-**L22**.

The peak at [M-17]$^+$ seen for each ligand is likely to involve the loss of a hydroxyl group, although the mechanism is unclear. All ligands show peaks corresponding to loss of the pendant amine arm, to leave a resonance-stabilised benzylic carbocation (A, B and C overleaf in Figure 4.9).
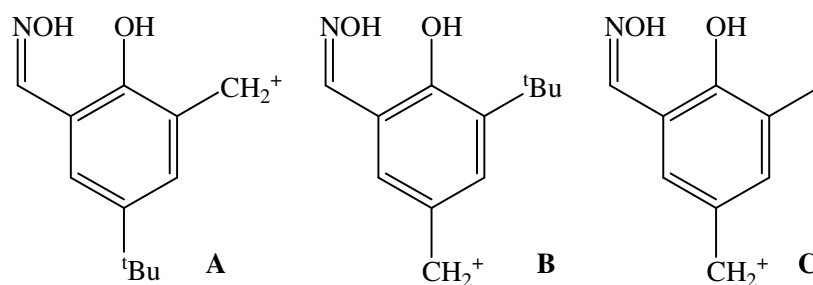
Figure 4.9: Benzylic carbocation breakdown products seen in the FAB mass spectra of **L17**-**L22**.

All precursors were also studied by FABMS, with parent ion peaks present for all compounds other than the N-ethoxymethylamine compounds **(12)** and **(13)**. In each case strong peaks for the iminium ions $(M - OEt)^+$ were noted, giving evidence for the ease of formation of these reactive species.

4.3.3 X-Ray Crystallography

The piperidinomethyl substituted ligands **L17**, **L19** and **L21** were analysed by X-ray crystallography and showed similar solid state structures. Crystallographic analysis of **L1**-**L9** in Chapter 2 detailed three types of solid state assemblies which phenolic oximes can adopt, two of which had been described previously.[28] Incorporation of a pendant amine arm gives an extra H-bond acceptor site in the neutral ligands, allowing a novel, fourth type of assembly in the solid state (Figure 4.10). An intermolecular hydrogen bond between the oxime proton of one molecule and the piperidino nitrogen of an adjacent molecule is present in each case, and the distances are listed overleaf in Table 4.2. The H-bonds form infinite 1D chains which pack together to give the overall solid state structures.
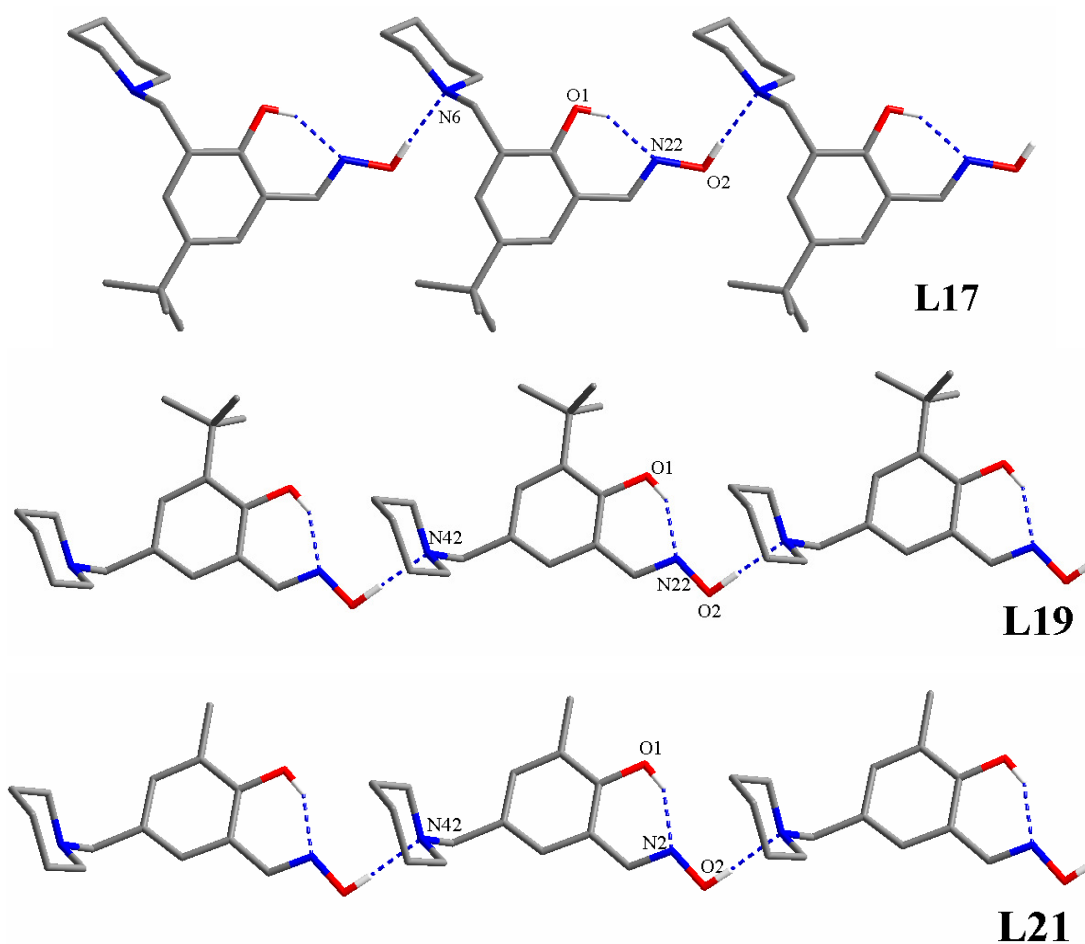
Figure 4.10: Formation of 1D chains by intermolecular H-bonding in solid state structures of **L17**, **L19** and **L21**. Hydrogen atoms not involved in H-bonding are removed for clarity.

An intramolecular hydrogen bond between the phenol proton and the oxime nitrogen is present for all three ligands, as in nearly all the other X-ray structures of free ligands in this thesis (**L4** and **L9** are the only exceptions).

	L17	L19	L21
Intermolecular H-bond (Å)	2.723(2)	2.669(3)	2.662(2)
Intramolecular H-bond (Å)	2.638(1)	2.578(3)	2.635(2)

Table 4.2: Comparison of H-bond distances in the solid state structures of **L17**, **L19** and **L21**.

The intermolecular H-bond is longer in the 3-substituted ligand **L17**, but is very similar for the 5-substituted ligands, suggesting that there is less steric hindrance

around the tertiary amine binding site and that anions may show closer approach to the binding site in these cases. The intramolecular H-bond in **L17** and **L21** is similar to those reported for the ligand series **L1**-**L9** in Chapter 2, but is shorter for the 3-*t*-Bu substituted ligand **L19**, indicating that a large bulky 3-substituent induces pressure on the adjacent phenolic oxygen, pushing it slightly closer to the imino nitrogen atom. This effect is also present in the crystal structure of the 3-*t*-Bu substituted ligand **L3** (Chapter 2) which, within experimental error, has an intramolecular H-bond of the same length as **L19**.

Differences in the crystal packing arrangements of the 1-D hydrogen bonded chains represent the most significant variations in the structures of **L17**, **L19** and **L21**. The chains of **L17** molecules pack without any further intermolecular interactions, but π-stacking interactions are present in the structure of **L19**. Molecules form π-stacked dimers (Figure 4.11) with a distance of 3.335 Å between the planes of the benzene rings. The piperidino groups of the dimers face away from each other and form the aforementioned intermolecular hydrogen bonds to an adjacent dimer, giving ribbons in the long range packing structure. Each dimer has two hydrogen bonds to adjacent dimers.
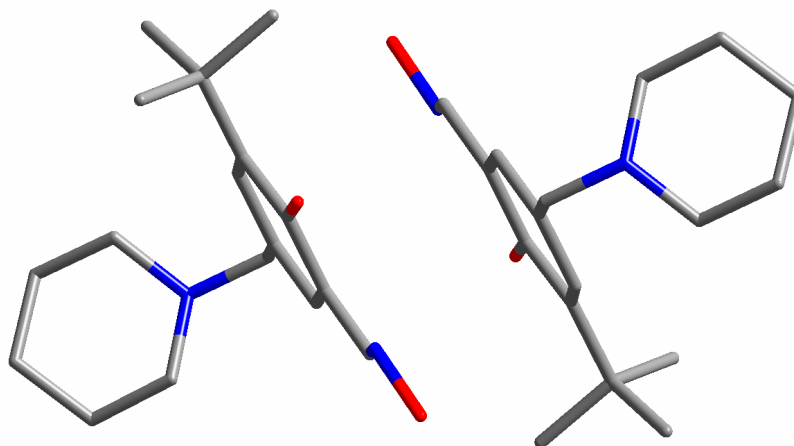
Figure 4.11: π-stacking in **L19**, with hydrogen atoms removed for clarity.

These ribbons pack together to form the overall 3D structure, with chloroform solvate molecules filling voids.

Dimers are also seen in the structure of **L21**, formed by C-H…π interactions between the methyl group of one molecule and the benzene ring of an adjacent (Figure 4.12) with the distance between the centroid of the benzene ring and the methyl carbon atom (C61) 3.488(2) Å. This interaction is reciprocal, giving two interactions per dimer, wherein the piperidino rings of each molecule face in opposite directions. This allows formation of intermolecular hydrogen bonds between dimers to give ribbons, which pack together to form the 3D structure.
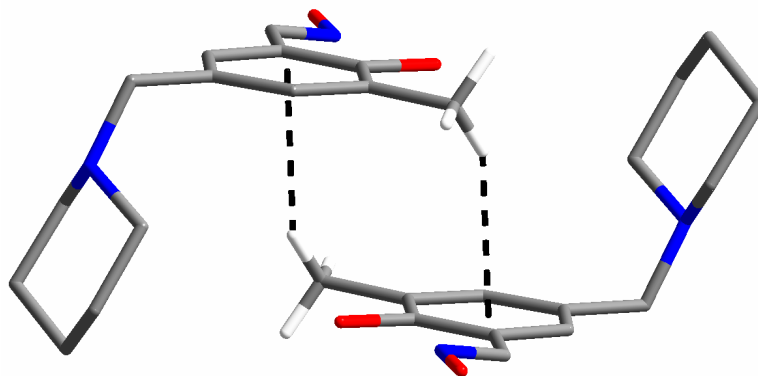
Figure 4.12: C-H… π interactions in **L21**, with hydrogen atoms not involved in intermolecular interactions removed for clarity.

4.4   Solvent Extraction

The uptake of metal salts, *via* the equilibrium shown in Equation 4.3, was studied by solvent extraction.

Equation 4.3: $2\mathbf{L}_{(org)} + MX_2 \rightleftharpoons [M(\mathbf{L})_2X_2]_{(org)}$

Solvent extraction proved to be a simple and effective method to establish proof-of-concept of metal salt binding, and was achieved by contacting a 0.01 M chloroform solution of each ligand with an aqueous (1 M) solution of the metal salt (Figure 4.13).
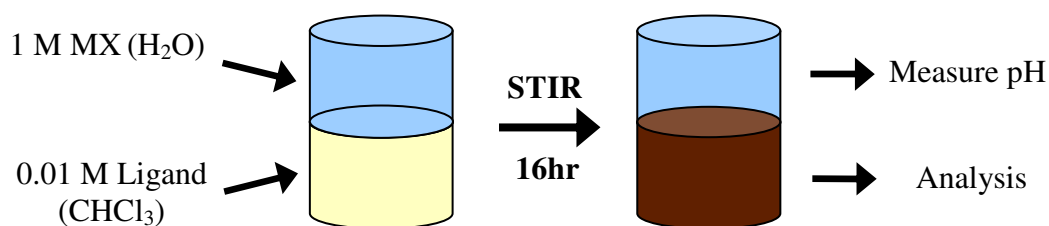
Figure 4.13: Solvent extraction experimental protocol to assess uptake of metal salts by **L17**-**L22**.

The metal salts chosen were the chlorides and sulfates of nickel(II), copper(II) and zinc(II). Metal and sulfate uptake were measured by ICP-OES spectroscopy and chloride uptake by back stripping the chloride ions into an aqueous phase, precipitating the chloride with a standard silver solution and measuring the remaining silver concentration by ICP-OES (Section 4.8.3.1).

4.4.1 Metal Salt Loading by 3-Substituted Ligands

The 3-substituted ligands **L17** and **L18** were tested initially, and it was thought that the potential for metal-anion interactions in their metal salt complexes (Figure 4.5) may make them more potent anion binders. The extraction of metal salts by **L17** is shown in Table 4.3, with percentage loading values calculated from Equation 4.3. Some precipitation of a white solid occurred when **L17** was contacted with $ZnCl_2$ solutions. Assuming this was the zinc chloride complex, the recorded concentrations of zinc and chloride in the chloroform solution do not represent the full uptake by the ligand.

An obvious difference is seen in the loading values for metals from chloride versus sulfate media. Metal extraction is much enhanced when chloride is the counter ion, and in the case of $CuCl_2$ greatly exceeds the expected maximum loading values.

	Metal	Chloride	Metal	Sulfate
Nickel	87	89	42	29
Copper	189	200	60	34
Zinc	70[a]	72[a]	3	4

Table 4.3: Extraction of base metal salts by 0.01 M chloroform solutions of **L17** from equal volumes of 1 M aqueous solutions of metal salts. 100% metal salt loading calculated from Equation 4.3. [a]Precipitation of metal salt complex occurs

This suggests that an alternative extractive mechanism is occurring which would allow a 1:1 ratio of metal salt:ligand, as shown in Equation 4.4.

Equation 4.4: $\qquad$ $\mathbf{L}_{(org)} + MX_2 \rightleftharpoons [MLX_2]_{(org)}$
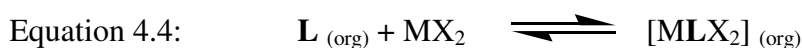
L17 extracted $NiCl_2$ to an efficiency of approximately 90%, and, as noted above, reached 70% $ZnCl_2$-loading before precipitation of the metal salt complex occurs. Metal sulfate loading values are much lower, and in the case of $ZnSO_4$ none was extracted. The Hofmeister bias, described in Chapter 1, predicts that the more heavily hydrated sulfate anion will be harder to extract from an aqueous phase than chloride,[40] and this may be one of the reasons for sulfate extraction being poorer than chloride. Another is that chloride is a much better ligand for base metal cations than sulfate and consequently transport of chloride into the organic phase *via* an inner sphere assembly will be more favourable.

It was expected that the solubility problems experienced with $ZnCl_2$ complexes of **L17** would be overcome using **L18**, which has a "greasy" pendant dihexylaminomethyl arm rather than a piperidinomethyl arm. The extraction of metal salts by **L18** is displayed in Table 4.4. Again, metal salt extraction is more efficient from chloride media. $NiCl_2$ loading is slightly lower in comparison to **L17** while $NiSO_4$ loading is slightly higher, but overall extraction from chloride media is still preferred.

	Metal	**Chloride**	**Metal**	**Sulfate**
Nickel	61	71	53	52
Copper	175	160	100	91
Zinc	138	143	10	18

Table 4.4: Extraction of base metal salts by 0.01 M chloroform solutions of **L18** from equal volumes of 1 M aqueous solutions of metal salts. 100% metal salt loading calculated from Equation 4.3.

$CuCl_2$ was loaded to 160%, and although the loading values are again slightly lower than for **L17**, it is clear that the 3-substituted ligands can extract $CuCl_2$ by an unexpected, highly efficient mechanism. $ZnCl_2$ loading reached approximately 140% with no precipitation, indicating that **L18** can also extract $ZnCl_2$ by an unknown mechanism and that **L17** may also be able to do so in more dilute solutions to prevent precipitation of the complex. The highly efficient extraction of $CuCl_2$ and $ZnCl_2$ by the 3-substituted ligands **L17** and **L18** is discussed in more detail in Section 4.5.

Metal sulfate loading values for **L18** are all higher than for **L17**. This may be attributable to the greasier ligand solubilising the sulfate anion more effectively than **L17**, leading to better phase transfer. $CuSO_4$ is loaded to approximately 95% efficiency, meaning **L18**, as well as being a highly efficient $CuCl_2$ and $ZnCl_2$ extractant, is also an effective $CuSO_4$ extractant, apparently operating in the expected mode to give a 1:2:1 assembly, $[Cu(\mathbf{L18})_2SO_4]$.

4.4.2 Metal Salt Loading by 5-Substituted Ligands

Extraction experiments involving the 5-substituted ligands **L19**-**L22** were carried out under identical conditions to those involving the 3-substituted ligands **L17** and **L18** to ensure comparability of data. Accurate loading values for **L19**, **L21** and **L22** could not be determined under these conditions due to the precipitation of complexes formed during extraction. The very low solubility of the complexes of these ligands

prevented further study by solvent extraction. **L20**, however, had the requisite solubility to perform a full series of extraction tests, with results shown in Table 4.5.

By locating the anion binding site in the 5-position, a potential site for attaching "greasy" branched alkyl groups to solubilise the extractant is lost. The location of such a group is restricted to the 3-position, and the findings of Chapters 2 and 3 indicate that a 3-substituent can have a great effect on the copper binding strength of the salicylaldoxime extractant. The 3-*tert*-butyl group of **L20** affords the appropriate solubility to carry out solvent extraction tests but may have a negative effect on metal extraction on steric grounds, disrupting the stabilising intracomplex H-bond array. It was hoped that the 3-methyl group of **L21** and **L22** would combine solubility with a minimal effect on metal binding but, as recorded above, the systems have insufficient solubility to allow extraction studies to be carried out.

	Metal	**Chloride**	**Metal**	**Sulfate**
Nickel	63	57	8	3
Copper	80	84	72	40
Zinc	20	93	0	0

Table 4.5: Extraction of base metal salts by 0.01 M chloroform solutions of **L20** from equal volumes of 1 M aqueous solutions of metal salts. 100% metal salt loading calculated from Equation 4.3.

It is clear that the 5-substituted ligand **L20** does not extract metal salts as well as its 3-substituted isomer **L18**, and metal sulfates are again poorly extracted when compared to metal chlorides. This may be due to the effect of the bulky 3-*tert*-butyl substituent, as explained previously, but more information on the modes of binding is required. Loading of $CuCl_2$ and $ZnCl_2$ does not reach values higher than 100%, suggesting that the mechanism of extraction available to the 3-substituted ligands is not possible for the 5-substituted ligands. $CuCl_2$ is only loaded to ~80% of the ligand's capacity, a value much lower than the ~160% figure seen for **L18**, and $ZnCl_2$ loading is greatly reduced, with very little zinc but nearly 100% chloride extracted. This disparity indicates that zinc and chloride are bound to separate parts of the molecule, and that the reagent is binding the metal salt in a tritopic fashion.

4.4.3 Summary of the Proof-of-Concept Studies

The extraction experiments detailed above allowed an initial assessment of the suitability of the ligands for commercial application. Problems with the solubilities of the metal salt complexes of **L19**, **L21** and **L22** meant that extraction data were only available for **L17**, **L18** and **L20**. Both **L17** and **L18** are suitable for solvent extraction experiments, but as they are differentiated only by the nature of the alkyl groups on their respective tertiary amine anion binding sites **L18** was chosen as the 3-substituted ligand to be tested further, due to the higher solubility of its metal salt complexes.

The 3-substituted ligands **L17** and **L18** are better extractants than the 5-substituted ligand **L20**, particularly for $CuCl_2$ and $ZnCl_2$, where a 1:1 binding motif is possible. Extraction of $CuCl_2$ seems to be the more favourable of the two, reaching higher loading values, and so this process is considered in more detail. The remainder of Chapter 4 focuses on elucidating this mechanism and analysing the potential commercial application of the 3-substituted extractants, while Chapter 5 investigates the reasons for the differences seen in the loading profiles of **L18** and **L20**.

4.5 Efficient $CuCl_2$/$ZnCl_2$ Extraction by 3-Substituted Ligands

Investigations into the mechanisms of $CuCl_2$ and $ZnCl_2$ binding by the 3-substituted ligands were focussed on two areas; characterisation by crystallographic analysis of isolated metal salt complexes of **L17**, and solvent extraction experiments using **L18**. It was hoped that solid state structural data could be used alongside solvent extraction results to suggest possible binding motifs in solution. The solvent extraction experiments were carried out with $CuCl_2$ only, as extraction appeared to be stronger than $ZnCl_2$ and showed considerable commercial promise.

The unexpectedly high loading of $CuCl_2$ and $ZnCl_2$ by the 3-substituted ligands **L17** and **L18** can be explained by crystal structures obtained by Dr D. K. Henderson and

Dr J. E. Davidson as exemplification in a patent (confidential) relating to the analogous nonyl-substituted ligand for the recovery of metal(II) chlorides from chloride leach solutions.[41] The structures of [Cu(**L17**)Cl$_2$] and [Zn$_2$(**L17**)$_2$Cl$_4$] both show a metal salt:ligand ratio of 1:1, but have notable differences.

4.5.1   Crystal Structure of [Cu(L17)Cl$_2$]

Crystals of [Cu(**L17**)Cl$_2$] were isolated from the residues of the extraction experiments described in Section 4.8.3.1. The structure is shown in Figure 4.14.
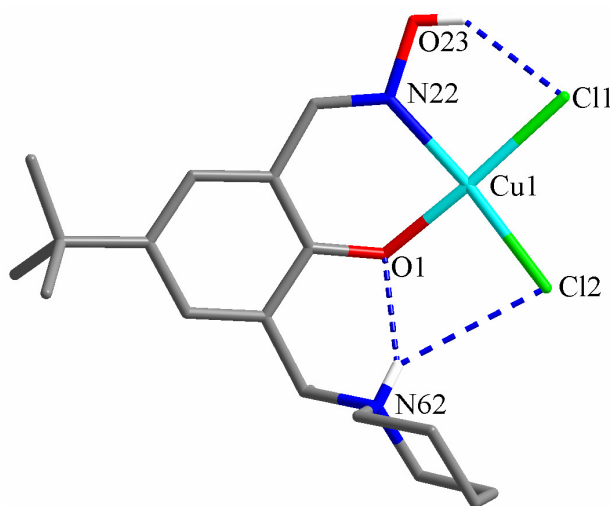
Figure 4.14:   Crystal structure of [Cu(**L17**)Cl$_2$]. Hydrogen atoms not involved in H-bonding are removed for clarity.

The mode of metal salt binding is different from that expected (Figure 4.5) with the anions bound in the inner coordination sphere of the copper(II) ion. With the phenol oxygen deprotonated and the piperidine nitrogen protonated, the ligand is in a zwitterionic, neutral form which allows the 1:1 binding of ligand:CuCl$_2$ to occur, generating a neutral assembly [Cu(**L17**)Cl$_2$] which is soluble in chloroform.

Intracomplex hydrogen bonding appears to stabilise the assembly, and may be the driving force behind its formation. The piperidinium proton H-bonds to the

phenolate oxygen (N62···O1 = 2.754(3) Å) and may also form a long range contact with one of the chlorides (N62···Cl2 = 3.560(3) Å), giving a bifurcated hydrogen bond. The oximic proton is involved in a contact with the other chloride anion, but at a much shorter distance (O23···Cl1 = 2.925(3) Å). As the 5-substituted ligands **L19**-**L22** did not form complexes with 1:1 ligand:CuCl$_2$ ratios, it appears that this binding motif is only favourable when the protonated piperidinium arm is able to form a hydrogen bond with the phenolate oxygen and also interact with one of the chloride ligands.

Complex molecules also associate *via* an axial copper contact with a phenolate oxygen atom of an adjacent molecule (Cu1···O1' = 2.507(2) Å) and the copper tends towards an overall distorted trigonal bipyramidal coordination sphere (Figure 4.15).
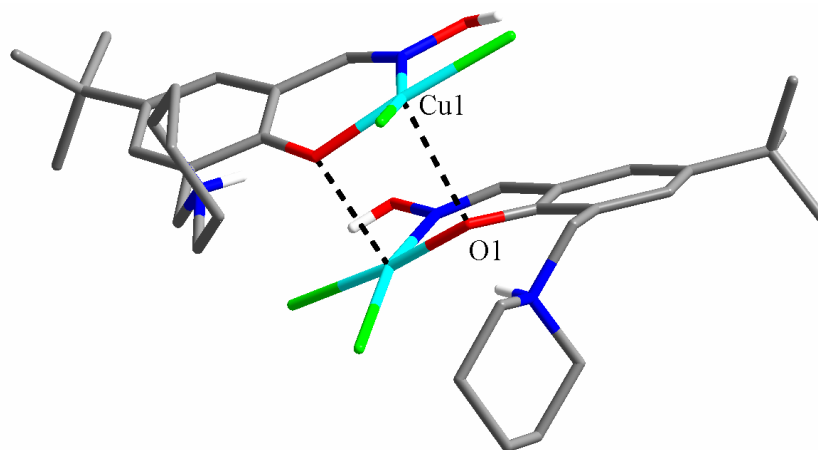
Figure 4.15: Dimerisation in the solid state structure of [Cu(**L17**)Cl$_2$]. Hydrogen atoms not involved in H-bonding are removed for clarity.

Dimerisation has the effect of gathering some of the polar regions of two molecules together and leaving the non-polar sections exposed. If this dimerisation were to persist in solution, the configuration could "shield" the polar regions from a non-polar solvent, and may tentatively explain the high solubilities of the complexes in water-immiscible media.

4.5.2 Crystal Structure of [Zn₂(L17)₂Cl₄]

Colourless crystals were isolated from the chloroform phases of the $ZnCl_2$ extractions detailed in Section 4.8.3.1, and subsequently $[Zn_2(L17)_2Cl_4]$ was identified as a tetrakis-chloroform solvate. As with $[Cu(L17)Cl_2]$, the compound also has chloride ligands in the inner coordination sphere of the metal centre (Figure 4.16).
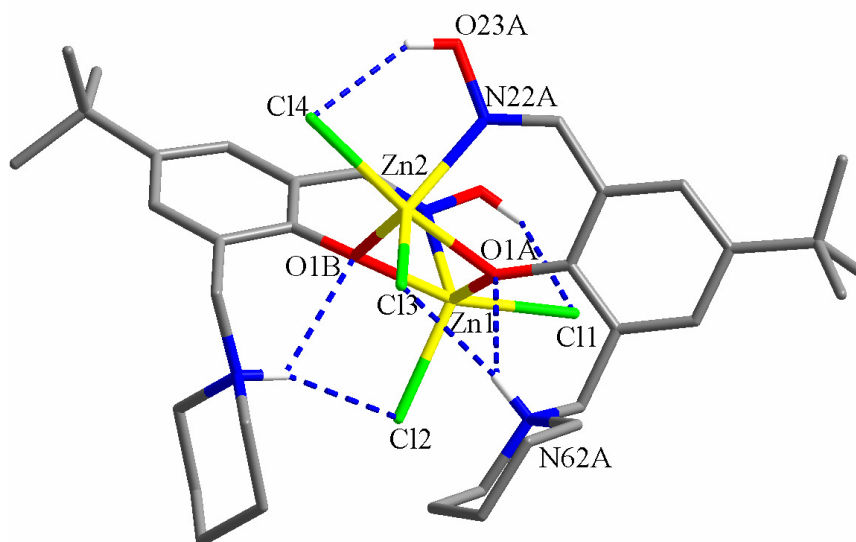
Figure 4.16: Solid state structure of $[Zn_2(L17)_2Cl_4]$ with chloroform solvent molecules and hydrogen atoms not involved in H-bonding are removed for clarity.

A 1:1 ligand:MCl_2 ratio is again present, but the structure is different from that of $[Cu(L17)Cl_2]$, with the phenolate groups forming similarly strong bonds to both zinc atoms (Zn1-O1A = 2.031(2) Å, Zn1-O1B = 2.109(2) Å, Zn2-O1A = 2.078(2) Å, Zn2-O1B = 2.021(3) Å). The oximic N and two chloride ligands complete the distorted trigonal bipyramidal $NO_2Cl_2{}^{3-}$ coordination sphere. The piperidino arms are again protonated, giving a neutral complex with zwitterionic ligands. Intramolecular hydrogen bonds are formed between each oximic proton and a chloride ligand (O23A···Cl4 = 3.003(2) Å, O23B···Cl1 = 2.987(3) Å) and between the protonated piperidine group and the remaining chloride ligands (N62A···Cl3 = 3.379(3) Å, N62B···Cl2 = 3.446(2) Å). The intracomplex hydrogen bonds again appear to be integral to the stability of the complex, with no analogous 1:1 ligand:$ZnCl_2$ complexes seen for the 5-substituted ligands.

Comparison of certain bond lengths, angles and contact distances between the two structures reveals interesting similarities and also emphasises the main differences. A third structure of a related compound, isolated by the author whilst on secondment to Massey University, New Zealand and outwith the remit of this thesis, is also included for comparison. Linking two salicylaldoxime moieties with $CH_2NR(CH_2)_nNRCH_2$ straps gives ligands capable of forming a 2:2 Cu:L assembly with a well defined cavity which can encapsulate anions (Figure 4.17).
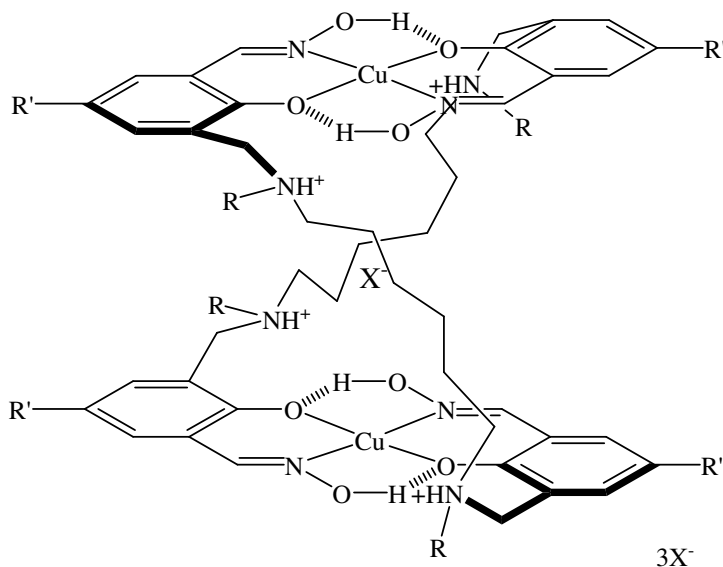
Figure 4.17: Formation of anion-binding cavities by copper(II) complexes of phenolic oximes linked with $CH_2NR(CH_2)_nNRCH_2$ straps.[42]

When such reagents are combined with $CuCl_2$ in a 2:1 $CuCl_2$:ligand ratio, structures similar to the $[Cu(\mathbf{L17})Cl_2]_2$ dimer are observed, and relevant distances and angles from the structure of a complex of a ligand with a C_5 strap and N-benzyl groups, designated $[Cu_2(\mathbf{L'})Cl_4]$, are included in Table 4.6.[42]

The stability of the $CuCl_2$ binding motif is implicit in the fact that both $[Cu(\mathbf{L17})Cl_2]$ and $[Cu_2(\mathbf{L'})Cl_4]$ are observed in the solid state, rather than their conventional 2:1 salox:Cu^{II} complexes. The main differences in the two structures are the longer $Cu\cdots O1'$ and $Cu\cdots Cu$ distances in $[Cu_2(\mathbf{L'})Cl_4]$, which suggests that the C_5 strap imposes a restriction to the approach of the two copper centres. In both copper

structures, the large differences in the Cu-O1 and Cu⋯O1' distances show that the geometry around the Cu^{II} atoms is essentially 4-coordinate, with a long range apical interaction facilitating dimerisation.

Contact (Å) or Angle (°)[a]	[Cu(L17) Cl$_2$]$^{[b]}$	[Cu$_2$(L') Cl$_4$]$^{[b]}$	[Zn$_2$(L17)$_2$ Cl$_4$] Zn1	[Zn$_2$(L17)$_2$ Cl$_4$]Zn2
M-O1 (Å)	1.933(2)	1.931(2)	2.109(2)	2.078(2)
M-N22 (Å)	2.021(3)	2.002(2)	2.116(3)	2.121(2)
M-Cl1 (Å)	2.269(1)	2.268(1)	2.372(1)	2.362(1)[c]
M-Cl2 (Å)	2.268(1)	2.253(1)	2.268(1)	2.285(1)[d]
M-O1' (Å)	2.570(2)	2.680(3)	2.031(2)	2.021(3)
M⋯M (Å)	3.370(1)	3.610(1)	3.162(1)	3.162(1)
O1-M-O1' (°)	81.69(8)	73.47(8)	77.90(7)	78.83(7)
N22-M-O1' (°)	99.34(10)	98.38(8)	121.19(9)	116.21(10)
Cl1-M-O1' (°)	93.49(5)	95.47(5)	94.79(5)	97.61(8)[c]
Cl2-M-O1' (°)	94.47(6)	105.44(5)	112.05(6)	114.54(6)[d]

[a]Atoms labelled with a prime refer to the atom on the opposite side of the dimer. [b]Each half of the dimer is related by a 2-fold axis in the *b* direction. [c]Distance or angle refers to atom Cl4. [d]Distance or angle refers to atom Cl3.

Table 4.6: Comparison of bond lengths, angles and contact distances in the coordination spheres of [Cu(**L17**)Cl$_2$]$_2$, [Zn$_2$(**L17**)$_2$Cl$_4$] and [Cu$_2$(**L'**)Cl$_4$].

In contrast, the Zn⋯Zn distance in [Zn$_2$(**L17**)$_2$Cl$_4$] is much shorter and the Zn-O and Zn-O' distances in the two crystallographically independent halves are very similar, with all the Zn-O' interactions short enough to be described as bonds The phenolate groups of each ligand bridge to both Zn^{II} cations and the coordination geometry can be described as 5-coordinate, with a distorted trigonal bipyramidal coordination sphere.

4.5.3 Dependence of Cu-Loading of L18 on Chloride Concentration

If the $CuCl_2$ binding motif seen in the solid state persists in solution, then the concentration of chloride ions in an aqueous copper feed solution could affect the uptake of copper by the extractant. Varying the concentration of anions in a solvent extraction experiment can affect the uptake of a metal by a conventional pH swing reagent, for example Lakshmanan *et al* found that increased sulfate concentration in an aqueous feed depressed extraction of copper by phenolic oxime reagents.[43] This variation could be very pronounced in the extraction of $CuCl_2$ by **L18**, shown in Equation 4.5, as the anion is bound in the inner coordination sphere of the copper centre.

Equation 4.5: $\qquad$ **L18** $_{(org)}$ + MCl_2 $\rightleftharpoons$ [M(**L18**)Cl$_2$] $_{(org)}$

To study this effect, extraction experiments were carried out with an equimolar ratio of **L18**:Cu (copper was added as $CuCl_2$) and varying concentrations of chloride (added as NaCl, see Section 4.8.3.2) and the results are displayed in Figure 4.18.
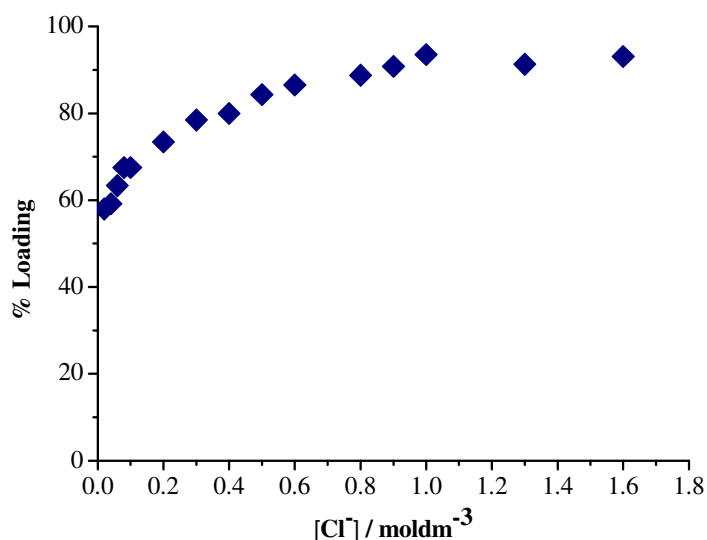

Figure 4.18: Dependence of Cu^{II} loading by **L18** on chloride concentration when a 0.01 M chloroform solution of **L18** was contacted with a 0.01 M solution of $CuCl_2$, with [Cl$^-$] adjusted by addition of NaCl. Loading values are based on Equation 4.5, equilibrium pH values were measured and all fell in the range 2.6-2.9.

The dependence of copper extraction on chloride concentration is clear. When the concentration of chloride is twice that of copper, *i.e.* equivalent to an aqueous feed containing an equimolar ratio of **L18**:CuCl$_2$, then only 55% uptake of copper occurs. An increase in copper loading follows a gradual increase in the chloride concentration of the aqueous phase, with a maximum copper loading of approximately 90% reached at a chloride concentration of 0.8 M, which is an 80-fold excess of chloride. This result is concomitant with the initial experiments of Section 4.4, where copper loading reaches a similar maximum when the chloride concentration is 2.0 M.

4.5.4 pH-Loading Profile of L18 *vs.* CuCl$_2$

The success of an extractant depends on its ability to load and strip the extracted species over a series of conditions, in our case over a pH range. To determine the CuCl$_2$ pH-loading profile of **L18**, an extraction experiment (Section 4.8.3.3) was devised which would allow maximum loading to occur whilst being comparable with previous work[10, 44] by having equimolar amounts of **L18** and copper, but a constant excess of chloride (0.8 M). The results are shown in Figure 4.19.
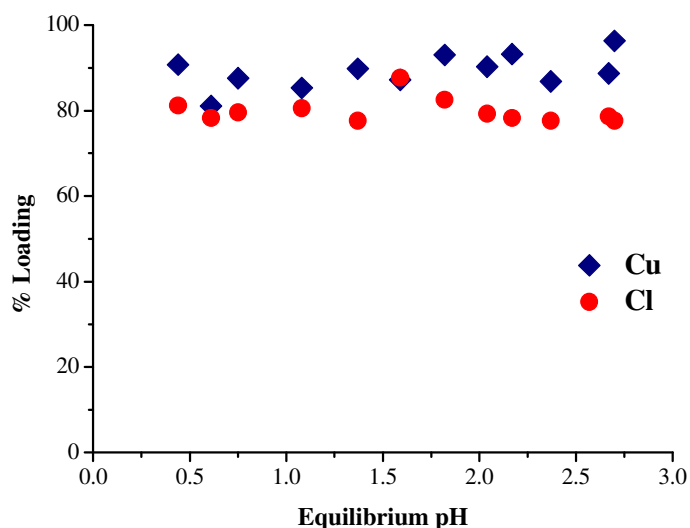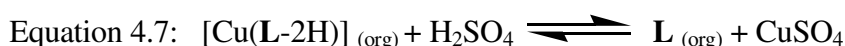

Figure 4.19: pH-profiles for loading of copper (blue) and chloride (red) by 0.01 M chloroform solutions of **L18** from equal volumes of aqueous solutions with metal concentrations of 0.01 M and chloride concentrations of 0.8 M. 100% CuCl$_2$ loading based on a 1CuCl$_2$:1**L18** ratio.

Copper loading reaches approximately 90% over a pH range of ~0.5-3.0 (100% loading assumed to be a 1:1 **L18**:CuCl$_2$ complex) with chloride loading generally slightly lower, at approximately 80%. This is consistent with 80% of the ligand extracting copper as the [Cu(**L18**)Cl$_2$] species and the remaining 20% extracting the species [Cu(**L18**-H)$_2$], demonstrating the preference of **L18** to extract copper as the 1:1 species rather than the 1:2 species.

4.5.5   Copper Stripping of [Cu(L18)Cl$_2$]

For an extractant to operate in an industrial process, it must be possible to reverse the extraction equilibrium and strip the metal cation back into an aqueous phase for electrowinning.[45]   As described in Chapter 1, CuCl$_2$ complexes of polytopic, zwitterionic metal salt extractants, *e.g.* the "salen" types described in Section 4.1.3, could undergo a sequential stripping protocol to remove the chloride anions as a salt and generate a copper sulfate electrolyte, which is preferable to a chloride electrolyte due to its better suitability to electrowinning:[16]

Equation 4.6:   [CuLCl$_2$] $_{(org)}$ + 2NaOH $\rightleftharpoons$ [Cu(L-2H)] $_{(org)}$ + 2NaCl + 2H$_2$O

Equation 4.7:   [Cu(L-2H)] $_{(org)}$ + H$_2$SO$_4$ $\rightleftharpoons$ L $_{(org)}$ + CuSO$_4$

This option was not considered for the new oxime ligands because the 1:1 stoichiometry of the loaded ligand with copper chloride in the inner coordination sphere will not allow a neutral copper-only complex to form, because this has a 2:1 ligand:Cu stoichiometry, [Cu(**L18**-H)$_2$].

In conventional "pH swing" processes, stripping is achieved by contacting the loaded organic phase with a low pH aqueous phase, usually consisting of ~150 g L^{-1} H$_2$SO$_4$ in copper recovery.[25]   It is also possible to recover copper by the electrolytic reduction of CuCl$_2$. Consequently, tests were undertaken (Section 4.8.3.4) to establish whether [Cu(**L18**)Cl$_2$] could be effectively stripped with HCl:

Equation 4.8: $[Cu(\textbf{L18})Cl_2]_{(org)} + HCl \rightleftharpoons CuCl_2 + [\textbf{L18}+H]Cl_{(org)}$

A chloroform solution of **L18** was contacted with aqueous 1 M CuCl$_2$, as in Section 4.4, to fully load the ligand and generate $[Cu(\textbf{L18})Cl_2]$. The loaded organic phase was separated, an aliquot taken for copper analysis, and the remainder contacted with aqueous HCl solutions of varying concentrations. After overnight stirring and separation, an aliquot of the organic phase was removed for copper analysis by ICP-OES, and the results are displayed in Table 4.7.

[HCl] (g L^{-1}) for strip	% Cu loaded	% Cu after strip	% Cu transport
55	92	8	84
110	92	8	84
165	92	7	85
220	92	4	88

Table 4.7: Percentage copper transported by **L18** when a 0.01 M chloroform solution is contacted with 1 M CuCl$_2$, allowed to equilibrate, and then stripped with varying concentrations of HCl. Loadings based on 1CuCl$_2$:1**L18** ratio.

Copper is readily stripped from **L18** by HCl and net copper transport reaches values over 80% for each case, showing that **L18** could operate as an effective copper extractant in a pH swing process. Increasing the concentration of HCl used in the stripping step to 220 g L^{-1} does increase net copper transfer but only by a small amount, indicating that highly concentrated strip solutions would not be required.

The efficiency of metal transport is measured by calculating the "mass transport efficiency", which corresponds to the mass of copper (in grams) transported by 1 kg of ligand.[25] Under these conditions, **L18** has an *observed* mass transport efficiency of 143 g kg^{-1} when stripped with 220 g L^{-1} HCl, which is a significant increase on the *theoretical* maximum copper transport efficiency of 121 g kg^{-1} calculated for the commercially available reagent P50 (5-nonyl-2-hydroxybenzaldehyde oxime). This

increased efficiency of copper transport is another attractive property of **L18** which indicates its suitability for use in a hydrometallurgical circuit, and potential flowsheets involving **L18** are discussed in the section below.

4.6   Potential Commercial Application of L18

The extraction studies detailed in Section 4.5 indicate that **L18** is capable of transporting $CuCl_2$ from an aqueous feed solution to a purified electrolyte with excellent efficiency, and therefore could function as a metal salt extractant in commercial processes. Further testing is required, but an evaluation of potential flowsheets may identify conditions in which the reagent will be expected to operate, and so guide the in depth assessment and development of the ligand.

The CUPREX process, described in Section 4.1, uses an oxidative ferric chloride leach process to generate a $CuCl_2$ pregnant leach solution.[5-8] **L18** or an analogous ligand could operate as a metal salt extractant, with separate cation and anion stripping stages generating a $CuCl_2$ electrolyte and a NaCl salt by-product. In the flowsheet (Scheme 4.3) a copper chloride pls is generated by the oxidative ferric leach process, eliminating elemental sulfur.

Leach: $\quad\quad\quad 4FeCl_3 + 2Cu_2S_{(s)} \quad\longrightarrow\quad 2CuCl_2 + 4FeCl_2 + S_{(s)}$

Extract: $\quad\quad\;\; 2CuCl_2 + 2L_{(org)} \quad\longrightarrow\quad 2CuLCl_{2\,(org)}$

Copper Strip: $2CuLCl_{2\,(org)} + 2HCl \quad\longrightarrow\quad 2CuCl_2 + 2[LHCl]_{(org)}$

Chloride Strip: $2[LHCl]_{(org)} + 2NaOH \quad\longrightarrow\quad 2L_{(org)} + 2NaCl + 2H_2O$

Electrowin: $\quad 2CuCl_2 \quad\longrightarrow\quad 2Cu_{(s)} + 2Cl_{2\,(g)}$

Leach regen: $\;\; 4FeCl_2 + 2Cl_{2\,(g)} \quad\longrightarrow\quad 4FeCl_3$

Overall: **$Cu_2S_{(s)} + 2NaOH + 2HCl \quad\longrightarrow\quad 2Cu_{(s)} + S_{(s)} + 2NaCl + 2H_2O$**
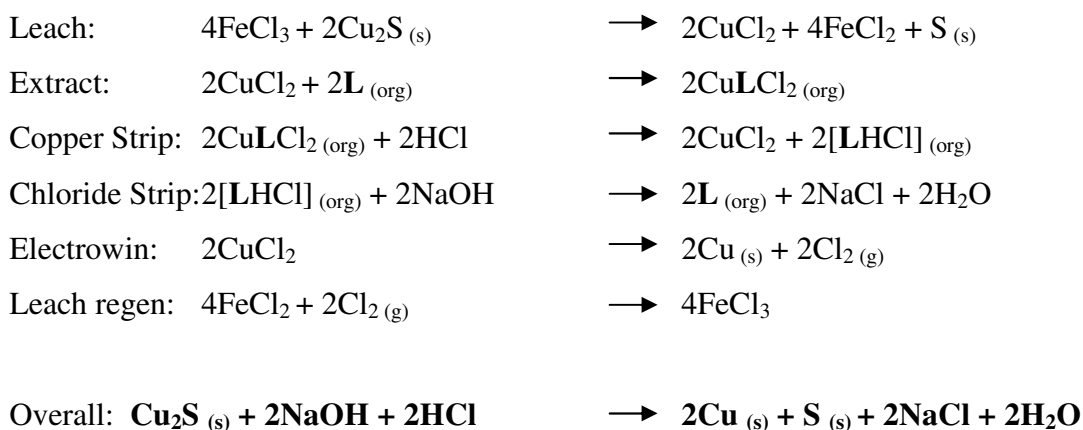
Scheme 4.3: Flowsheet for the processing of sulfidic copper ores, combining CUPREX[TM] technology with the metal salt extractant **L18**.

L18 or an analogue is used to extract $CuCl_2$, and the subsequent copper and chloride stripping stages consume one mole of HCl and NaOH and produce one mole of NaCl for every mole of copper produced. Copper is electrowon and the chlorine gas released is used to regenerate the ferric chloride leachant.

The materials balance is poor and the consumption of HCl and NaOH undesirable, but these problems could be overcome by using the chloralkali process. NaCl is electrolytically processed to give NaOH which can be reused in chloride stripping, and H_2 and Cl_2 which can be combined to give HCl for copper stripping. Integrating these steps into the flowsheet (Scheme 4.4) gives an ideal materials balance, effectively splitting copper(I) sulfide ores into their component elements with the consumption of electrical power.

Leach:	$4FeCl_3 + 2Cu_2S_{(s)}$	$\longrightarrow$ $2CuCl_2 + 4FeCl_2 + S_{(s)}$
Extract:	$2CuCl_2 + 2L_{(org)}$	$\longrightarrow$ $2CuLCl_{2\,(org)}$
Copper Strip:	$2CuLCl_{2\,(org)} + 2HCl$	$\longrightarrow$ $2CuCl_2 + 2[LHCl]_{(org)}$
Chloride Strip:	$2[LHCl]_{(org)} + 2NaOH$	$\longrightarrow$ $2L_{(org)} + 2NaCl + 2H_2O$
Chloralkali:	$2NaCl + 2H_2O$	$\longrightarrow$ $2NaOH + 2H_{2\,(g)} + Cl_{2\,(g)}$
Strip regen:	$2H_{2\,(g)} + Cl_{2\,(g)}$	$\longrightarrow$ $2HCl$
Electrowin:	$2CuCl_2$	$\longrightarrow$ $2Cu_{(s)} + 2Cl_{2\,(g)}$
Leach regen:	$4FeCl_2 + 2Cl_{2\,(g)}$	$\longrightarrow$ $4FeCl_3$
Overall:	$\mathbf{Cu_2S_{(s)}}$	$\longrightarrow$ $\mathbf{2Cu_{(s)} + S_{(s)}}$
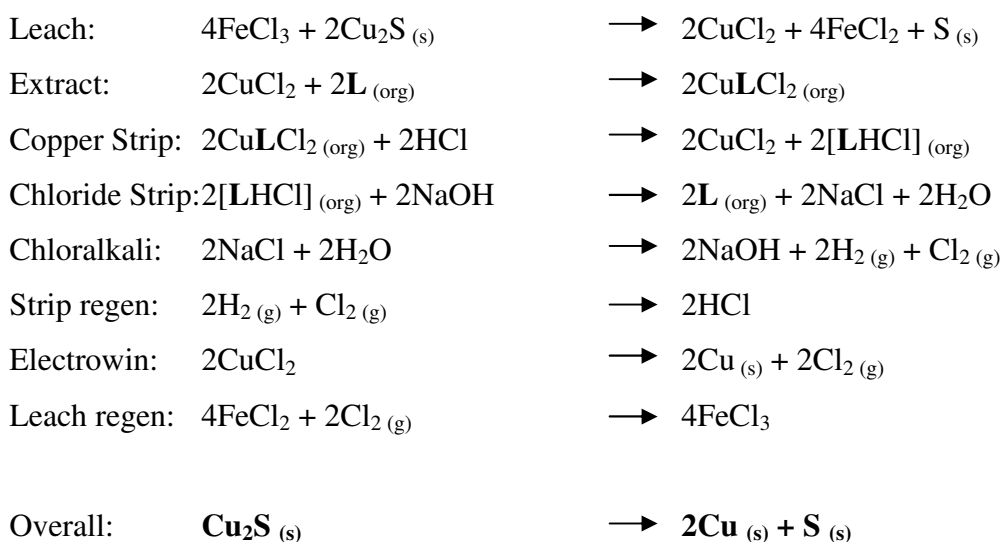
Scheme 4.4: Flowsheet for the processing of sulfidic copper ores, combining CUPREX[TM] technology and the Chloralkali process with the metal salt extractant **L18**.

Conceptually, this is similar to the leach/solvent extraction/electrowinning process for the recovery of copper from oxidic ores (Chapter 1), generating copper and gaseous oxygen, which currently accounts for between 20%[26] and 30%[27] of the world's copper production. The use of a chloralkali cell to generate NaOH, Cl_2 and H_2 from a NaCl by-product has gained acceptance in extractive metallurgy, being an essential part of the HydroCopper® process. Cu_2O is precipitated from a purified

solution of $Cu^I Cl$ with NaOH. The resulting NaCl is routed to a chloralkali cell for conversion to NaOH to be reused in the precipitation stage, Cl_2 gas which is used during leaching and H_2 gas for the reduction of the purified Cu^I oxide to copper metal.[46, 47]

To operate in a system such as this, the ligand must extract $CuCl_2$ strongly and selectively from a feed with high Fe^{II}/Fe^{III} content, high chloride concentrations and the subsequent high proton activity. Selectivity of cation and anion extraction is imperative and is studied in detail in Chapter 5.

4.7   Conclusions and Further Work

Six novel ligands for use as metal *salt* extractants were easily prepared in high yielding syntheses on the gram scale. Two basic architectures have been employed, based on 3- and 5-substituted aminomethyl ligands, of which the 3-substituted ligands were found to have higher solubility in non-polar solvents, a key property for any practicable solvent extractant. The poor solubility of the metal salt complexes of **L19**, **L21** and **L22** precluded these ligands from study as extractants.

The 3-substituted ligands **L17** and **L18** show similar extractive properties; extracting $CuCl_2$ and $ZnCl_2$ with unexpectedly high efficiency corresponding to a metal salt:ligand ratio of 1:1, and also showing useful levels of metal sulfate extraction, particularly the extraction of $CuSO_4$ by **L18**. $CuCl_2$ and $ZnCl_2$ uptake levels are explained by crystal structure determination of [Cu(**L17**)Cl$_2$] and [Zn$_2$(**L17**)$_2$Cl$_4$], which provide a plausible binding motif in solution. Such a H-bond stabilised motif is available only to the 3-substituted ligands.

A chloroform solution of the 5-substituted ligand **L20** showed reasonable $CuCl_2$ loading but did not extract any metal salt to the same extent as its 3-substituted isomer **L18**. This is consistent with the 3-*tert*-butyl group of **L20** hindering metal

extraction, as described in Chapters 2 and 3, but this can only be confirmed by more detailed analysis, which will be discussed in Chapter 5.

Further testing on the extraction of $CuCl_2$ by **L18** showed an expected dependence of loading on high chloride concentration, and also that **L18** is a very strong extractant, loading to 90% capacity over a pH range from 1.0 - 3.0. Copper can also be stripped by 55 gL^{-1} HCl, leading to high copper transport efficiency and suggesting that the ligand could act as a pH-swing reagent in hydrometallurgical circuits.

Having established proof-of-concept metal salt extraction by **L17**, **L18** and **L20**, further testing was required to evaluate their commercial applicability. Understanding the selectivity of metal salt uptake is key to developing new reagents, and so Chapter 5 details solvent extraction experiments to determine both anion and cation selectivities, alongside the preparation of copper salt complexes with a number of anions to examine the binding motif in the solid state.

4.8   Experimental

4.8.1   Chemicals & Instrumentation

All solvents and reagents were used as received from Aldrich, Fisher and Acros. ^{1}H and ^{13}C NMR were obtained using a Bruker AC250 spectrometer at ambient temperature. Chemical shifts (δ) are reported in parts per million (ppm) relative to internal standards. Fast atom bombardment mass spectrometry was carried out using a Kratos MS50TC spectrometer with a 3-nitrobenzyl alcohol (NOBA) or thioglycerol matrix. IR spectra were collected on a JASCO FT/IR 410. Analytical data was obtained on a CE-440 Elemental Analyser by the University of Edinburgh Microanalytical Service. ICP-OES analysis was carried out using a Perkin Elmer Optima 5300DV spectrometer. The measurement of pH was carried out using a Fisher Scientific AR50 pH meter. X-ray crystal structures were obtained by the University of Edinburgh Crystallography service.

4.8.2 Ligand Synthesis

Attempts were made[30-33] to synthesise **(10)** and **(11)**, but these did not achieve satisfactory yields, and so the compounds were purchased from Sigma Aldrich.[34]

1-Ethoxymethylpiperidine (12). Piperidine (27.42 g, 320 mmol) was added to a suspension of potassium carbonate (59.51 g, 430 mmol) and paraformaldehyde (12.10 g, 400 mmol) in ethanol (1.5 l) dropwise over 30 minutes and the mixture left to stir for 72 h in an ice/water/NaCl bath. After filtration the solvent was removed *in vacuo* to give a colourless liquid, which was purified by vacuum distillation (19.8 g, 43%). (Anal. Calc. for $C_8H_{17}NO$: C, 67.1; H, 12.0; N, 9.8. Found: C, 66.4; H, 12.5; N, 10.2%); ^{1}H NMR (250 MHz, $CDCl_3$): δ_H (ppm) 1.15 (t, 3H, CH_3), 1.31 (m, 2H, $NCH_2CH_2CH_2$), 1.50 (m, 4H, 2 x $NCH_2CH_2CH_2$), 2.50 (m, 4H, 2 x $NCH_2CH_2CH_2$), 3.72 (q, 2H, OCH_2CH_3), 4.00 (s, 2H, NCH_2O); ^{13}C NMR (63 MHz, $CDCl_3$): δ_C (ppm) 17.5 (1C, OCH_2CH_3), 23.0 (1C, $NCH_2CH_2CH_2$), 25.0 (2C, 2 x $NCH_2CH_2CH_2$), 50.0 (2C, 2 x $NCH_2CH_2CH_2$), 63.5 (1C, OCH_2CH_3), 88.5 (1C, NCH_2O); FABMS *m/z* 99 (**12**-OEt)$^+$.

1-Ethoxymethyldihexylamine (13). Dihexylamine (59.60 g, 320 mmol) was added to a suspension of potassium carbonate (85.53 g, 620 mmol) and paraformaldehyde (12.10 g, 400 mmol) in ethanol (1.5 l) dropwise over 30 minutes and the mixture left to stir for 72 h in an ice/water/NaCl bath. After filtration the solvent was removed *in vacuo* to give a colourless liquid, which was purified by vacuum distillation (60.4 g, 77 %). (Anal. Calc. for $C_{15}H_{33}NO$: C, 74.0; H, 13.7; N, 5.8. Found: C, 74.8; H, 13.6; N, 6.7%); ^{1}H NMR (250 MHz, $CDCl_3$): δ_H (ppm) 1.15 (t, 6H, 2 x $N(CH_2)_5CH_3$), 1.45 (t, 3H, OCH_2CH_3), 1.55 (m, 12H, 2 x $N(CH_2)_2C_3H_6CH_3$), 1.72 (m, 4H, 2 x $NCH_2CH_2C_4H_9$), 2.88 (t, 4H, 2x $NCH_2C_5H_{11}$), 3.74 (q, 2H, OCH_2CH_3), 4.41 (s, 2H, NCH_2O); ^{13}C NMR (63 MHz, $CDCl_3$): δ_C (ppm) 13.5 (2C, 2 x $N(CH_2)_5$ CH_3), 15.0 (1C, OCH_2CH_3), 22.5 (2C, 2 x $N(CH_2)_4CH_2CH_3$), 27.0 (2C, 2 x $N(CH_2)_3CH_2C_2H_5$), 28.0 (2C, 2 x $N(CH_2)_2CH_2C_3H_7$), 32.0 (2C, 2 x $NCH_2CH_2C_4H_{11}$), 52.0 (2C, 2 x $NCH_2C_5H_{11}$), 63.0 (1C, OCH_2CH_3), 85.5 (1C, NCH_2O); FABMS *m/z* 199 (**13**-OEt)$^+$.

5-*tert*-Butyl-2-hydroxy-3-piperidin-1-ylmethylbenzaldehyde (14). **(1)** (10.01 g, 57 mmol) and **(12)** (8.78 g, 61 mmol) were refluxed in acetonitrile (500 ml) for 72 h under an atmosphere of nitrogen. The solvent was removed *in vacuo* and the resulting sticky yellow solid was recrystallised from hexane to give a light yellow solid (14.23 g, 92%). (Anal. Calc. for $C_{17}H_{24}NO_2$: C, 74.2; H, 9.1; N, 5.1. Found: C, 74.4; H, 9.3; N, 5.2%); ^{1}H NMR (250 MHz, CDCl$_3$): δ_H (ppm) 1.20 (s, 9H, C(CH_3)$_3$), 1.45 (m, 2H, NCH$_2$CH$_2$CH_2), 1.60 (m, 4H, 2 x NCH$_2$CH_2CH$_2$), 2.48 (m, 4H, 2 x NCH_2CH$_2$CH$_2$), 3.63 (s, 2H, ArCH_2N), 7.19 (s, 1H, ArH), 7.58 (s, 1H, ArH), 10.35 (s, 1H, CHO); ^{13}C NMR (63 MHz, CDCl$_3$): δ_C (ppm) 24.0 (1C, NCH$_2$CH$_2$CH$_2$), 26.0 (2C, 2 x NCH$_2$CH$_2$CH$_2$), 31.5 (3C, C(CH$_3$)$_3$), 35.0, (1C, **C**(CH$_3$)$_3$), 53.5 (2C, 2 x NCH$_2$CH$_2$CH$_2$), 58.5 (1C, ArCH$_2$N), 122.7 (1C, aromatic **C**), 123.1 (1C, aromatic **CH**), 124.3 (1C, aromatic **CH**), 132.8 (1C, aromatic **C**), 141.9 (1C, aromatic **C**), 160.3 (1C, aromatic **C**), 190.5 (1C, Ar**C**HO); FABMS *m/z* 276 (MH)$^+$.

5-*tert*-Butyl-3-dihexylaminomethyl-2-hydroxybenzaldehyde (15). **(1)** (15.01 g, 84 mmol) and **(13)** (20.48 g, 84 mmol) were refluxed in acetonitrile (250 ml) for 5 days under an atmosphere of nitrogen. The solvent was removed *in vacuo* and 10 g of the resulting dark red oil was purified by silica-60 flash chromatography (10% ethyl acetate in hexane eluent) yielding a bright yellow oil (8.56 g, 86%). (Anal. Calc. for $C_{24}H_{41}NO_2$: C, 76.8; H, 11.0; N, 3.7. Found: C, 76.9; H, 11.4; N, 5.0%); ^{1}H NMR (250 MHz, CDCl$_3$): δ_H (ppm) 0.80 (t, 6H, 2 x N(CH$_2$)$_5$CH_3), 1.23 (s, 21H, C(CH_3)$_3$ + 2 x N(CH$_2$)$_2$C$_3$$H_6CH_3$), 1.48 (m, 4H, 2 x NCH$_2CH_2C_4H_9$), 2.48 (m, 4H, 2 x NC$H_2C_5H_{11}$), 3.72 (s, 2H, ArC$H_2$N), 7.20 (s, 1H, Ar$H$), 7.60 (s, 1H, Ar$H$), 10.35 (s, 1H, C$H$O); ^{13}C NMR (63 MHz, CDCl$_3$): δ_C (ppm) 13.5 (2C, 2 x N(CH$_2$)$_5$CH$_3$), 22.5 (2C, 2 x N(CH$_2$)$_4$CH$_2$CH$_3$), 26.0 (2C, 2 x N(CH$_2$)$_3$CH$_2$C$_2$H$_5$), 27.0 (2C, 2 x N(CH$_2$)$_2$CH$_2$C$_3$H$_7$), 31.5 (3C, C(CH$_3$)$_3$), 32.0 (2C, 2 x NCH$_2$CH$_2$C$_4$H$_{11}$), 34.0, (1C, **C**(CH$_3$)$_3$), 53.5 (2C, 2 x NCH$_2$C$_5$H$_{11}$), 57.0 (1C, Ar**C**H$_2$N), 121.1 (1C, aromatic **C**) 122.0 (1C, aromatic **CH**), 123.5 (1C, aromatic **CH**), 132.0 (1C, aromatic **C**), 141.0 (1C, aromatic **C**), 159.5 (1C, aromatic **C**), 190.5 (1C, Ar**C**HO); FABMS *m/z* 376 (MH)$^+$.

3-*tert*-Butyl-2-hydroxy-5-piperidin-1-ylmethylbenzaldehyde (16). 3-*tert*-Butyl-2-hydroxybenzaldehyde (3.31 g, 18.6 mmol) and **(12)** (2.93 g, 20.5 mmol) were refluxed in acetonitrile (25 ml) under nitrogen for 4 days. The solvent was removed *in vacuo* to yield an orange-brown oil which was used without further purification (4.96 g, 97%). (Anal. Calc. for $C_{17}H_{25}NO_2$: C, 74.1; H, 9.2; N, 5.1. Found: C, 70.1; H, 8.6; N, 4.1%); ^{1}H NMR (CDCl$_3$, 250 MHz): δ_H (ppm) 1.61 (9H, s, C(CH_3)$_3$), 1.57 (2H, d, NCH$_2$CH$_2$CH_2), 1.78 (4H, m, 2 x NCH$_2$CH_2CH$_2$), 2.57 (4H, m, 2 x NCH_2CH$_2$CH$_2$), 3.62 (2H, s, NCH_2Ar), 7.60 (2H, s, 2 x ArH), 10.06 (1H, s, CHO), 11.89 (1H, s, OH); ^{13}C NMR (CDCl$_3$, 63 MHz): δ_C (ppm) 24.3 (1C, NCH$_2$CH$_2$**C**H$_2$), 25.8 (2C, 2 x NCH$_2$**C**H$_2$CH$_2$), 29.1 (3C, C(**C**H$_3$)$_3$), 34.7 (1C, **C**(CH$_3$)$_3$), 54.3 (2C, 2 x N**C**H$_2$CH$_2$CH$_2$), 62.9 (1C, N**C**H$_2$Ar), 120.2 (1C, aromatic **C**), 129.2 (1C, aromatic **C**), 131.9 (1C, aromatic **C**H), 135.2 (1C, aromatic **C**H), 137.7 (1C, aromatic **C**), 160.0 (1C, aromatic **C**), 197.1 (1C, **C**HO); FABMS *m/z* 84 (100 %), 276 (MH)$^+$ not observed.

3-*tert*-Butyl-5-dihexylaminomethyl-2-hydroxybenzaldehyde (17). 3-*tert*-Butyl-2-hydroxybenzaldehyde (4.84 g, 27.2 mmol) and **(13)** (7.18 g, 29.9 mmol) were refluxed in acetonitrile (25 ml) under nitrogen for 4 days. The solvent was removed *in vacuo* to yield an orange oil which was purified by silica-60 wet flash column chromatography (2% ethyl acetate in PET40-60 eluent) to yield a bright yellow oil (9.39 g, 92%). (Anal. Calc. for $C_{24}H_{41}NO_2$: C, 76.8; H, 11.0; N, 3.7. Found: C, 77.6; H, 11.1; N, 4.2%.); ^{1}H NMR (CDCl$_3$, 250 MHz): δ_H (ppm) 0.92 (6H, t, 2 x N(CH$_2$)$_5$CH_3), 1.29 (16H, m, 2 x NCH$_2$(CH_2)$_4$CH$_3$), 1.45 (9H, s, C(CH_3)$_3$), 2.43 (4H, t, 2 x NCH_2C$_5$H$_{11}$), 3.53 (2H, s, NCH_2Ar), 7.36 (1H, d, ArH), 7.56 (1H, dd, ArH), 9.89 (1H, s, CHO), 11.64 (1H, br, OH); ^{13}C NMR (CDCl$_3$, 63 MHz): δ_C (ppm) 14.0 (2C, 2 x N(CH$_2$)$_5$**C**H$_3$), 22.6 (2C, 2 x N(CH$_2$)$_4$**C**H$_2$CH$_3$), 26.9 (2C, 2 x N(CH$_2$)$_3$**C**H$_2$C$_2$H$_5$), 27.1 (2C, 2 x N(CH$_2$)$_2$**C**H$_2$C$_3$H$_8$), 29.1 (3C, C(**C**H$_3$)$_3$), 31.6 (2C, 2 x NCH$_2$**C**H$_2$C$_4$H$_9$), 34.7 (1C, **C**(CH$_3$)$_3$), 53.6 (2C, 2 x N**C**H$_2$C$_5$H$_{11}$), 57.7 (1C, N**C**H$_2$Ar), 120.1 (1C, aromatic **C**), 130.9 (1C, aromatic **C**), 131.3 (1C, aromatic **C**H), 134.9 (1C, aromatic **C**H), 137.6 (1C, aromatic **C**), 160.0 (1C, aromatic **C**), 197.1 (1C, **C**HO); FABMS *m/z* 376 (MH)$^+$.

2-Hydroxy-3-methyl-5-piperidin-1-ylmethylbenzaldehyde (18). A mixture of 2-hydroxy-3-methylbenzaldehyde (3.46 g, 25.5 mmol) and **(12)** (4.00 g, 28.0 mmol) in acetonitrile (*ca*. 15 mL) was heated under reflux under nitrogen for 5 days. After cooling to room temperature the solvent was removed *in vacuo* to yield an orange-brown oil which was used without further purification (5.93 g, 93%). (Anal. Calc for $C_{14}H_{19}NO_2$: C, 72.1; H, 8.2; N, 6.0. Found: C, 71.2; H, 8.2; N, 5.4%); ^{1}H NMR (CDCl$_3$, 250 MHz): δ_H (ppm) 1.56 (2H, d, N(CH$_2$)$_2$C*H*$_2$), 1.75 (4H, q, 2 x NCH$_2$C*H*$_2$), 2.36 (3H, s, C*H*$_3$), 2.47 (4H, br, 2 x NC*H*$_2$CH$_2$), 3.49 (2H, s, 2 x ArC*H*$_2$N), 7.44 (2H, d, 2 x Ar*H*), 9.96 (1H, s, C*H*O), 11.20 (1H, br, ArO*H*); ^{13}C NMR (CDCl$_3$, 63 MHz): δ_C (ppm) 14.8 (1C, **C**H$_3$), 24.1 (1, N(CH$_2$)$_2$**C**H$_2$), 25.7 (2C, 2 x NCH$_2$**C**H$_2$), 54.2 (2C, 2 x N**C**H$_2$CH$_2$), 62.6 (1C, Ar**C**H$_2$N), 119.3 (1C, aromatic **C**), 126.2 (1C, aromatic **C**), 129.4 (1C, aromatic **C**), 131.3 (1C, aromatic **C**H), 138.7 (1C, aromatic **C**H), 158.7 (1C, aromatic **C**), 196.5 (1C, **C**HO); FABMS *m/z* 234 (MH)$^+$.

5-Dihexylaminomethyl-2-hydroxy-3-methylbenzaldehyde (19). 2-Hydroxy-3-methylbenzaldehyde (4.98 g, 37 mmol) and **(13)** (9.00 g, 37 mmol) were refluxed in acetonitrile (250 ml) under nitrogen for 5 days. The solvent was removed *in vacuo* to yield an orange oil which was purified by silica-60 wet flash column chromatography (5% ethyl acetate in hexane eluent) to yield a yellow oil (10.32 g, 84%). The product was found to decompose to a solid if left to stand and so no CHN data is available. ^{1}H NMR (CDCl$_3$, 250 MHz): δ_H (ppm) 1.03 (6H, t, 2 x N(CH$_2$)$_5$C*H*$_3$), 1.44 (12H, m, 2 x N(CH$_2$)$_2$(C*H*$_2$)$_3$CH$_3$), 1.62 (4H, m, 2 x NCH$_2$C*H*$_2$), 2.45 (3H, s, ArC*H*$_3$), 2.55 (4H, t, 2 x NC*H*$_2$C$_5$H$_{11}$), 3.66 (2H, s, NC*H*$_2$Ar), 7.52 (1H, s, Ar*H*), 7.56 (1H, s, Ar*H*), 10.05 (1H, s, C*H*O), 11.37 (1H, s, O*H*); ^{13}C NMR (CDCl$_3$, 63 MHz): δ_C (ppm) 13.4 (2C, 2 x N(CH$_2$)$_5$**C**H$_3$), 14.4 (1C, Ar**C**H$_3$), 22.1 (2C, 2 x N(CH$_2$)$_4$**C**H$_2$CH$_3$), 26.2 (2C, 2 x N(CH$_2$)$_3$**C**H$_2$C$_2$H$_5$), 26.5 (2C, 2 x N(CH$_2$)$_2$**C**H$_2$C$_3$H$_8$), 31.1 (2C, 2 x NCH$_2$**C**H$_2$C$_4$H$_9$), 53.1 (2C, 2 x N**C**H$_2$C$_5$H$_{11}$), 57.0 (1C, N**C**H$_2$Ar), 119.0 (1C, aromatic **C**), 125.8 (1C, aromatic **C**), 130.4 (1C, aromatic **C**H), 130.5 (1C, aromatic **C**), 138.1 (1C, aromatic **C**H), 158.3 (1C, aromatic **C**), 196.2 (1C, **C**HO); FABMS *m/z* 334 (MH)$^+$.

5-*tert*-Butyl-2-hydroxy-3-piperidin-1-ylmethylbenzaldehyde   oxime   (L17).

Potassium hydroxide (2.24 g, 40 mmol) and hydroxylamine hydrochloride (2.85 g, 41 mmol) were mixed in ethanol (300 ml) and a white KCl precipitate was removed by filtration. The filtrate was added to **(14)** (10.01 g, 36.4 mmol) in ethanol (1 l), stirred for 3 h and the solvent removed *in vacuo* to give a pale cream solid. The solid was dissolved in DCM (200 ml), washed three times with water (50 ml) and the solvent removed *in vacuo* to give a white powder (7.81 g, 74%). Crystals suitable for analysis by X-ray diffraction were grown by slow evaporation of a methanol/chloroform solution. (Anal. Calc. for $C_{17}H_{25}N_2O_2$: C, 70.3; H, 9.0; N, 9.7. Found: C, 70.0; H, 9.1; N, 9.4%); $\tilde{v}_{max}$/cm^{-1} (nujol) 3416br (NOH), 3145br (PhOH), 1613 (C=N), 1016 (C-N); ^{1}H NMR (250 MHz, CDCl$_3$): δ_H (ppm) 1.20 (s, 9H, C(C*H*$_3$)$_3$), 1.45 (m, 2H, NCH$_2$CH$_2$C*H*$_2$), 1.60 (m, 4H, 2 x NCH$_2$C*H*$_2$CH$_2$), 2.50 (m, 4H, 2 x NC*H*$_2$CH$_2$CH$_2$), 3.65 (s, 2H, ArC*H*$_2$N), 7.20 (s, 1H, Ar*H*), 7.57 (s, 1H, Ar*H*), 8.38 (s, 1H, ArC*H*N); ^{13}C NMR (63 MHz, CDCl$_3$): δ_C (ppm) 24.3 (1C, NCH$_2$CH$_2$**C**H$_2$), 26.1 (2C, 2 x NCH$_2$**C**H$_2$CH$_2$), 31.8 (3C, C(**C**H$_3$)$_3$), 34.4, (1C, **C**(CH$_3$)$_3$), 54.3 (2C, 2 x N**C**H$_2$CH$_2$CH$_2$), 62.2 (1C, Ar**C**H$_2$N), 118.2 (1C, aromatic **C**), 122.2 (1C, aromatic **C**), 123.1 (1C, aromatic **C**H), 128.0 (1C, aromatic **C**H), 141.8 (1C, aromatic **C**), 148.4 (1C, Ar**C**HN), 154.8 (1C, aromatic **C**); FABMS *m/z* 291 (MH)$^+$.

5-*tert*-Butyl-3-dihexylaminomethyl-2-hydroxybenzaldehyde   oxime   (L18).

Potassium hydroxide (1.42 g, 25 mmol) and hydroxylamine hydrochloride (1.80 g, 26 mmol) were mixed in ethanol (300 ml) and a white KCl precipitate was removed by filtration. The filtrate was added to **(15)** (8.56 g, 23 mmol) in ethanol (1 l), stirred for 3 h and the solvent removed *in vacuo* to give a tarry yellow solid (7.57 g, 85%) which was used without further purification. (Anal. Calc. for $C_{24}H_{42}N_2O_2$: C, 73.8; H, 10.8; N, 7.2. Found: C, 73.9; H, 10.5; N, 7.0%); $\tilde{v}_{max}$/cm^{-1} (CHCl$_3$) 3581br (NOH), 3172br (PhOH), 1607 (C=N), 1028 (C-N); ^{1}H NMR (250 MHz, CDCl$_3$): δ_H (ppm) 0.80 (t, 6H, 2 x N(CH$_2$)$_2$C*H*$_3$), 1.21 (m, 21H, C(C*H*$_3$)$_3$ + 2 x N(CH$_2$)$_2$C$_3$*H*$_6$CH$_3$), 1.55 (m, 4H, 2 x NCH$_2$C*H*$_2$C$_4$H$_9$), 2.56 (m, 4H, 2 x NC*H*$_2$C$_5$H$_{11}$), 3.83 (s, 2H, ArC*H*$_2$N), 7.20 (s, 1H, Ar*H*), 7.40 (s, 1H, Ar*H*), 8.33 (s, 1H, ArC*H*N); ^{13}C NMR (63 MHz, CDCl$_3$): δ_C (ppm) 14.5 (2C, 2 x N(CH$_2$)$_5$**C**H$_3$), 22.5 (2C, 2 x

N(CH$_2$)$_4$**CH$_2$CH$_3$**), 26.0 (2C, 2 x N(CH$_2$)$_3$**CH$_2$**C$_2$H$_5$), 27.5 (2C, 2 x N(CH$_2$)$_2$**CH$_2$**C$_3$H$_7$), 31.5 (3C, C(**CH$_3$**)$_3$), 32.0 (2C, 2 x N**CH$_2$CH$_2$**C$_4$H$_{11}$), 34.0, (1C, **C**(CH$_3$)$_3$), 53.0 (2C, 2 x N**CH$_2$**C$_5$H$_{11}$), 58.0 (1C, Ar**CH$_2$**N), 117.6 (1C, aromatic **C**), 122.0 (1C, aromatic **C**), 122.5 (1C, aromatic **CH**) 127.5 (1C, aromatic **CH**), 142.0 (1C, aromatic **C**), 147.9 (1C, Ar**CH**N), 154.6 (1C, aromatic **C**); FABMS *m/z* 391 (MH)$^+$.

3-*tert*-Butyl-2-hydroxy-5-piperidin-1-ylmethylbenzaldehyde oxime (L19).
Hydroxylamine hydrochloride (1.10 g, 15.9 mmol) and potassium hydroxide (0.89 g, 15.9 mmol) were dissolved in ethanol (100 ml) and a white precipitate removed by filtration. The filtrate was added to **(16)** (4.37 g, 15.9 mmol) and heated under reflux for 2 hours to give an orange solution. The solvent was removed *in vacuo* to give a pale orange solid. Dichloromethane (3 x 30 ml) was added to the flask and the resulting orange suspension filtered. The solvent was removed from the filtrate *in vacuo* to yield a white solid (3.69 g, 80%). Crystals suitable for study by X-Ray diffraction were grown by slow evaporation of a methanol/chloroform solution. (Anal. Calc. for C$_{17}$H$_{26}$N$_2$O$_2$.(CHCl$_3$)$_{0.5}$; C, 60.0; H, 7.6; N, 8.0. Found: C, 61.6; H, 7.9; N, 8.3%); $\tilde{v}_{max}$/cm^{-1} (KBr) 3420br (NOH), 3236br (PhOH), 2940 (C-H), 1614 (C=N), 1024 (C-N); ^{1}H NMR (CDCl$_3$, 250 MHz): δ_H (ppm) 1.31 (9H, s, C(C*H$_3$*)$_3$), 1.43 (2H, s, NCH$_2$CH$_2$C*H$_2$*), 1.59 (4H, m, 2 x NCH$_2$C*H$_2$*CH$_2$), 2.41 (4H, m, 2 x NC*H$_2$*CH$_2$CH$_2$), 3.40 (2H, s, NC*H$_2$*Ar), 6.97 (1H, d, Ar*H*), 7.07 (1H, d, Ar*H*), 8.10 (1H, s, C*H*NOH), 10.32 (1H, s, O*H*); ^{13}C NMR (63 MHz, CDCl$_3$): δ_C (ppm) 24.0 (1C, NCH$_2$CH$_2$**CH$_2$**), 25.5 (2C, 2 x NCH$_2$**CH$_2$**CH$_2$), 29.5 (3C, C(**CH$_3$**)$_3$), 35.0, (1C, **C**(CH$_3$)$_3$), 54.5 (2C, 2 x N**CH$_2$**CH$_2$CH$_2$), 63.5 (1C, Ar**CH$_2$**N), 118.5 (1C, aromatic **C**), 130.0 (1C, aromatic **C**), 130.5 (1C, aromatic **CH**), 137.0 (1C, aromatic **CH**), 140.5 (1C, aromatic **C**), 153.5 (1C, aromatic **C**), 158.0 (1C, Ar**CH**N); FABMS *m/z* 291 (MH)$^+$.

3-*tert*-Butyl-5-dihexylaminomethyl-2-hydroxybenzaldehyde oxime (L20).
Hydroxylamine hydrochloride (1.64 g, 23.5 mmol) and potassium hydroxide (1.32 g, 23.5 mmol) were mixed in ethanol (200 ml) and a white precipitate removed by filtration. The filtrate was added to **(17)** (8.82 g, 23.5 mmol) and refluxed for 3

hours to give a yellow solution. The solvent was removed *in vacuo* to give a highly viscous pale orange oil, which was used without further purification (9.17 g, 100%). (Anal. Calc. for $C_{24}H_{42}N_2O_2$: C, 73.8; H, 10.8; N, 7.2. Found: C, 72.8; H, 10.8; N, 7.7%); $\tilde{v}_{max}$/cm^{-1} (CHCl$_3$) 3576br (NOH), 3156br (PhOH), 1611 (C=N), 1017 (C-N); ^{1}H NMR (CDCl$_3$, 250 MHz): δ_H (ppm) 1.16 (6H, m, 2 x N(CH$_2$)$_5$C*H*$_3$), 1.59 (16H, m, 2 x NCH$_2$(C*H*$_2$)$_4$CH$_3$), 1.69 (9H, d, C(C*H*$_3$)$_3$), 2.76 (4H, 2 x NC*H*$_2$C$_5$H$_{11}$), 3.86 (2H, s, NC*H*$_2$Ar), 7.31 (1H, d, Ar*H*), 7.53 (1H, d, Ar*H*), 8.49 (1 H, d, C*H*NOH), 10.80 (1 H, s, O*H*); ^{13}C NMR (CDCl$_3$, 63 MHz): δ_C (ppm) 13.9 (2C, 2 x N(CH$_2$)$_5$**C**H$_3$), 22.4 (2C, 2 x N(CH$_2$)$_4$**C**H$_2$CH$_3$), 25.6 (2C, 2 x N(CH$_2$)$_3$**C**H$_2$C$_2$H$_5$), 27.1 (2C, 2 x N(CH$_2$)$_2$**C**H$_2$C$_3$H$_7$), 29.2 (3C, C(**C**H$_3$)$_3$), 31.3 (2C, 2 x NCH$_2$**C**H$_2$C$_4$H$_9$), 34.7 (1C, **C**(CH$_3$)$_3$), 53.1, (2C, 2 x N**C**H$_2$C$_5$H$_{11}$), 57.5 (1C, N**C**H$_2$Ar), 116.8 (1C, aromatic **C**), 127.0 (1C, aromatic **C**), 129.5 (1C, aromatic **C**H), 129.7 (1C, aromatic **C**H), 136.5 (1C, aromatic **C**), 152.4 (1C, Ar**C**HN), 155.7 (1C, aromatic **C**); FABMS *m/z* 391 (MH)$^+$.

2-Hydroxy-3-methyl-5-piperidin-1-ylmethylbenzaldehyde oxime (L21). Hydroxylamine hydrochloride (1.56 g, 22.4 mmol) and potassium hydroxide (1.26 g, 22.4 mmol) were mixed in ethanol (200 ml) and a white precipitate removed by filtration. The filtrate was added to **(18)** (5.23 g, 22.4 mmol). The solution was heated under reflux for 2 hours and a white precipitate formed immediately on boiling. The suspension was cooled to room temperature and the solvent removed *in vacuo*. Water (100 mL) and chloroform (150 mL) were added to the flask and a white solid was obtained on filtration (3.46 g, 62%). (Anal. Calc. for $C_{14}H_{20}N_2O_2$: C, 67.7; H, 8.1; N, 11.3. Found: C, 67.0; H, 8.1; N, 10.5%); $\tilde{v}_{max}$/cm^{-1} (KBr) 3440br (NOH), 3238br (PhOH), 2933 (C-H), 1616 (C=N), 1010 (C-N); ^{1}H NMR (*d8*-THF, 250 MHz): δ_H (ppm) 1.43 (2H, d, N(CH$_2$)$_2$C*H*$_2$), 1.57 (4H, 2 x NCH$_2$C*H*$_2$), 2.19 (3H, s, C*H*$_3$), 2.31 (4H, 2 x NC*H*$_2$CH$_2$), 3.30 (2H, s, ArC*H*$_2$N), 7.00 (1H, s, Ar*H*), 7.05 (1H, s, Ar*H*), 8.18 (1H, s, CHNOH), 10.21 (1H, s, ArO*H*); ^{13}C NMR (*d8*-THF, 63 MHz): δ_C (ppm), 15.9 (1C, **C**H$_3$), 25.5 (1C, N(CH$_2$)$_2$**C**H$_2$), 27.0 (2C, 2 x NCH$_2$**C**H$_2$), 55.2 (2C, 2 x N**C**H$_2$CH$_2$), 63.8 (1C, Ar**C**H$_2$N), 117.0 (1C, aromatic **C**), 125.5 (1C, aromatic **C**), 129.3 (1C, aromatic **C**H), 130.1 (1C, aromatic **C**), 133.2 (1C, aromatic **C**H), 152.8 (1C, aromatic **C**H), 155.6 (1C, **C**HN), FABMS *m/z* 249 (MH)$^+$.

5-Dihexylaminomethyl-2-hydroxy-3-methylbenzaldehyde   oxime   (L22).
Hydroxylamine hydrochloride (1.10 g, 15.9 mmol) and potassium hydroxide (0.89 g, 15.9 mmol) were dissolved in ethanol (100 ml) and a white precipitate removed by filtration. The filtrate was added to **(19)** (3.33 g, 10.0 mmol) and refluxed for 3 hours to give a yellow solution. The solvent was removed *in vacuo* to give a highly viscous pale orange oil, which was used without further purification (3.23 g, 93%). The product was found to decompose to a solid if left to stand and so no CHN data is available. $\tilde{v}_{max}$/cm^{-1} (CHCl$_3$) 3576br (NOH), 3164br (PhOH), 1617 (C=N), 1015 (C-N); ^{1}H NMR (CDCl$_3$, 250 MHz): δ_H (ppm) 1.06 (6H, t, 2 x N(CH$_2$)$_5$CH_3), 1.51 (12H, m, 2 x N(CH$_2$)$_2$(CH_2)$_3$CH$_3$), 1.62 (4H, m, 2 x NCH$_2$CH_2), 2.45 (3H, s, ArCH_3), 2.75 (4H, t, 2 x NCH_2C$_5$H$_{11}$), 3.80 (2H, s, NCH_2Ar), 7.16 (1H, s, ArH), 7.26 (1H, s, ArH), 8.35 (1H, s, ArCHN), 9.8 (1H, br, OH); ^{13}C NMR (CDCl$_3$, 63 MHz): δ_C (ppm) 14.4 (2C, 2 x N(CH$_2$)$_5$**C**H$_3$), 16.1 (1C, Ar**C**H$_3$), 23.0 (2C, 2 x N(CH$_2$)$_4$**C**H$_2$CH$_3$), 26.0 (2C, 2 x N(CH$_2$)$_3$**C**H$_2$C$_2$H$_5$), 27.2 (2C, 2 x N(CH$_2$)$_2$**C**H$_2$C$_3$H$_8$), 31.8 (2C, 2 x NCH$_2$**C**H$_2$C$_4$H$_9$), 53.6 (2C, 2 x N**C**H$_2$C$_5$H$_{11}$), 57.8 (1C, N**C**H$_2$Ar), 116.7 (1C, aromatic **C**), 125.7 (1C, aromatic **C**), 127.5 (1C, aromatic **C**), 129.7 (1C, aromatic **C**H), 133.6 (1C, aromatic **C**H), 152.2 (1C, Ar**C**HN), 155.3 (1C, aromatic **C**); FABMS *m/z* 349 (MH)$^+$.

4.8.3   Solvent Extraction

All solvent extraction data is available in appendix 7.4.1. In all cases for metal and sulfur analysis an aliquot (0.5 ml) of the organic phase was removed, the solvent was removed *in vacuo*, the residue was dissolved in butan-1-ol (10 ml) and the concentration measured by ICP-OES. Two methods of chloride analysis were utilised. In the initial extraction of metal salts by the **L17**-**L22** (Section 4.4), chloride concentration was measured by stirring a 2 ml aliquot of the organic phase with 10 ml of 0.1 M HNO$_3$ overnight, to strip all chloride ions into the aqueous phase. After separation, a 4 ml aliquot was contacted with 1 ml of a stock solution of AgNO$_3$ (0.02 M) to precipitate the chloride as AgCl. The mixture was centrifuged and filtered through a 0.2 µm single-use syringe filter, and a 2 ml aliquot of the filtrate

was made up to 10 ml in a volumetric flask to measure the remaining silver concentration by ICP-OES. Chloride loading values were calculated from the concentration of Ag^+ ions remaining in solution, with each loading value an average of two runs and corrected from values obtained by blank solutions.

This method proved to be time consuming and contained many potential sources of error. For these reasons, a protocol involving a chloride sensitive electrode was developed in subsequent testing. A 2 ml aliquot of the organic phase was again stirred overnight with 0.1 M aqueous HNO_3 (10 ml), the aqueous phase extracted and a 5 ml aliquot made up to 10 ml with 0.1 M NaOH. Chloride concentration of the solution was then measured with a chloride sensitive electrode.

4.8.3.1 Extraction of Metal Salts

All extractions were performed to the same general procedure. 0.01 M solution of **L** in chloroform (10 ml) was added to 1 M metal salt aqueous solution (10 ml) and stirred for 24 hrs. The organic phase was extracted, a 0.5 ml aliquot taken to be used for metal/sulfur analysis and a 2.0 ml aliquot taken for chloride analysis by the AgCl precipitation method described above. The residues of $[Cu(\mathbf{L17})Cl_2]$ were not sufficiently soluble in butan-1-ol for ICP-OES analysis, so were carefully dissolved in concentrated HNO_3, diluted to 10 ml with deionised water and run as aqueous ICP-OES samples.

4.8.3.2 Dependence of Cu-Loading of **L18** on [Cl⁻]

A 0.01 M solution of **L18** in chloroform (5 ml) was contacted with an aqueous phase consisting of 1 ml of 0.05M aqueous $CuCl_2$ and 4 ml of a mixture of aqueous 2M NaCl and water to vary the chloride concentration. This ensured a 1:1 ratio of **L18**:Cu throughout the experiment. The organic phase was extracted, a 0.5 ml aliquot taken for Cu analysis and the equilibrium pH of the aqueous phase measured.

4.8.3.3   CuCl$_2$ pH-Loading Profile of **L18**

A 0.01 M solution of **L18** in chloroform (5 ml) was contacted with an aqueous phase consisting of 63 µl of 0.8 M aqueous CuCl$_2$ solution and 4.937 ml of a pre-made mixture of 0.8 M NaCl and 0.8 M HCl of varying pH. This ensured a constant chloride concentration of 0.8 M and copper concentration of 0.01 M in the aqueous phase, and a 1:1 ratio of **L18**:Cu throughout the experiment. The organic phase was extracted, a 0.5 ml aliquot taken for copper analysis, a 2 ml aliquot taken for chloride analysis by a chloride selective electrode and the equilibrium pH of the aqueous phase measured.

4.8.3.4   Stripping of Cu from Loaded Solutions of **L18**

0.01 M solutions of **L18** (5 ml) were stirred vigourously with a 1 M aqueous solution of CuCl$_2$ (5 ml) overnight to fully load the ligand. The phases were separated, a 0.5 ml aliquot of the organic phase taken for copper analysis by ICP-OES, and the remainder contacted with aqueous solutions of HCl of varying concentrations. The mixtures were stirred overnight to ensure equilibrium, the organic phase separated and a 0.5 ml aliquot taken for copper analysis by ICP-OES.

4.8.4. X-Ray Structure Determinations

Crystal structures were determined at the University of Edinburgh crystallography service. The structures of **L19** and **L21** were solved by Fraser White, the structure of **L17** by Dr Stephen Moggach, the structure of [Cu(**L17**)Cl$_2$] by Dr James Davidson, the structures of [Zn$_2$(**L17**)$_2$Cl$_4$] by Professor Simon Parsons. Details on the solutions and cif files are available in appendix 7.4.2.

4.9 References

[1] P. A. Tasker, P. G. Plieger, and L. C. West, *Comprehensive Coordination Chemistry II*, 2004, **9**, 759.

[2] S. G. Galbraith and P. A. Tasker, *Supramolecular Chemistry*, 2005, **17**, 191.

[3] P. A. Tasker, C. C. Tong, and A. N. Westra, *Coordination Chemistry Reviews*, 2007, **251**, 1868.

[4] H. Singh and C. K. Gupta, *Mineral Processing and Extractive Metallurgy Review*, 2000, **21**, 307.

[5] R. F. Dalton, A. Burgess, R. Price, and E. Hermana, *Process Metallurgy*, 1992, **7B**, 1145.

[6] R. F. Dalton, G. Diaz, R. Price, and A. D. Zunkel, *Jom*, 1991, **43**, 51.

[7] R. F. Dalton, R. Price, P. M. Quan, and D. Stewart, in 'Extraction of metal values', EP, 1982.

[8] R. F. Dalton, R. Price, E. Hermana, and B. Hoffman, *Mining Engineering*, 1988, **40**, 24.

[9] R. W. Gibson and N. M. Rice, *Hydrometallurgy and Refining of Nickel and Cobalt, Annual Hydrometallurgy Meeting of CIM, 27th, Sudbury, Canada, Aug. 17-20, 1997*, 1997, 247.

[10] S. G. Galbraith, 'PhD Thesis', Edinburgh University, 2005.

[11] A. Borowiak-Resterna, G. Kyuchoukov, and J. Szymanowski, *International Solvent Extraction Conference, Cape Town, South Africa, Mar. 17-21, 2002*, 2002, 988.

[12] G. Kyuchoukov and I. Mishonov, *Solvent Extraction Research and Development, Japan*, 1999, **6**, 1.

[13] I. Mishonov and G. Kyuchoukov, *Hydrometallurgy*, 1996, **41**, 89.

[14] G. Kyuchoukov and I. Mishonov, *Solvent Extraction and Ion Exchange*, 1993, **11**, 555.

[15] G. Kyuchoukov and Y. Mihaylov, *Hydrometallurgy*, 1991, **27**, 361.

[16] G. Kyuchoukov and J. Szymanowski, *Journal of Radioanalytical and Nuclear Chemistry*, 2000, **246**, 675.

17   R. F. Dalton and P. M. Quan, *Publications of the Australasian Institute of Mining and Metallurgy*, 1993, **7/93**, 347.

18   R. F. Dalton, A. Burgess, and P. M. Quan, *Hydrometallurgy*, 1992, **30**, 385.

19   G. Kyuchoukov, A. Jakubiak, and J. Szymanowski, *Solvent Extraction Research and Development, Japan*, 1997, **4**, 1.

20   A. Jakubiak, G. Cote, and J. Szymanowski, *Solvent Extraction Research and Development, Japan*, 1999, **6**, 24.

21   R. A. Coxall, L. F. Lindoy, H. A. Miller, A. Parkin, S. Parsons, P. A. Tasker, and D. J. White, *Dalton Transactions*, 2003, 55.

22   S. G. Galbraith, Plieger, P.G., Tasker, P.A., *Chemical Communications*, 2002, 2662.

23   H. A. Miller, N. Laing, S. Parsons, A. Parkin, P. A. Tasker, and D. J. White, *Dalton Transactions*, 2000, 3773.

24   J. March and M. B. Smith, 'March's Advanced Organic Chemistry, Reactions, Mechanisms and Structures', John Wiley's and Sons, 2001.

25   J. Szymanowski, 'Hydroxyoximes and Copper Hydrometallurgy', CRC Press, 1993.

26   P. J. Mackey, *CIM Magazine*, 2007, **2**, 35.

27   G. A. Kordosky, *International Solvent Extraction Conference, Cape Town, South Africa, Mar. 17-21*, 2002, 853.

28   A. G. Smith, P. A. Tasker, and D. J. White, *Coordination Chemistry Reviews*, 2003, **241**, 61.

29   J. Manonmani, R. Thirumurugan, M. Kandaswamy, M. Kuppayee, S. S. S. Raj, M. N. Ponnuswamy, G. Shanmugam, and H. K. Fun, *Polyhedron*, 2000, **19**, 2011.

30   R. Aldred, R. Johnston, D. Levin, and J. Neilan, *Journal of the Chemical Society, Perkin Transactions 1: Organic and Bio-Organic Chemistry (1972-1999)*, 1994, 1823.

31   L. F. Lindoy, G. V. Meehan, and N. Svenstrup, *Synthesis*, 1998, 1029.

32   F. Bigi, M. L. Conforti, R. Maggi, and G. Sartori, *Tetrahedron*, 2000, **56**, 2709.

33   N. U. Hofslokken and L. Skattebol, *Acta Chemica Scandinavica*, 1999, **53**, 258.

34   Sigma Aldrich, 2007.

35   J. Clayden, N. Greeves, S. Warren, and W. Peter, 'Organic Chemistry', Oxford University Press, 2001.

36   P. Castro, L. E. Overman, X. Zhang, and P. S. Mariano, *Tetrahedron Letters*, 1993, **34**, 5243.

37   M. Tramontini and L. Angiolini, *Tetrahedron*, 1990, **46**, 1791.

38   H. Adams, N. A. Bailey, D. E. Fenton, and G. Papageorgiou, *Dalton Transactions*, 1995, 1883.

39   D. Stepniak-Biniakiewicz, *Polish Journal of Chemistry*, 1980, **54**, 1567.

40   T. G. Levitskaia, M. Marquez, J. L. Sessler, J. A. Shriver, T. Vercouter, and B. A. Moyer, *Chemical Communications*, 2003, 2248.

41   P. A. Tasker, R. S. Forgan, and D. K. Henderson, 'Metal Salt Extraction', UK patent filing, 2006.

42   R. S. Forgan, P. G. Plieger, and P. A. Tasker, Unpublished work, 2008.

43   V. I. Lakshmanan, G. J. Lawson, and J. L. Tomliens, *Journal of Inorganic and Nuclear Chemistry*, 1975, **37**, 2181.

44   D. C. R. Henry, 'PhD Thesis', University of Edinburgh, 2007.

45   F. Habashi, 'A Textbook of Hydrometallurgy', 1994.

46   O. Hyvaerinen and M. Haemaelaeinen, *Hydrometallurgy*, 2005, **77**, 61.

47   O. Hyvaerinen, M. Haemaelaeinen, and R. Leimala, *Chloride Metallurgy 2002: Practice and Theory of Chloride/Metal Interaction, Annual Hydrometallurgy Meeting, 32nd, Montreal, QC, Canada, Oct. 19-23, 2002*, 2002, **2**, 609.

CHAPTER 5

SELECTIVITY OF METAL SALT EXTRACTANTS

Contents

5.1   Introduction

5.1.1   Aims

The aim of the work described in this chapter was to examine the selectivity of anion and cation binding of ligands **L17**-**L20**, with focus on potential commercialisation of kerosene-soluble analogues with multiply branched nonyl groups replacing the *tert*-butyl substituents. As described previously, the metal salt complexes of **L21** and **L22** were found to be poorly soluble in organic media and this precluded the ligands from study. The work involved:

- the synthesis and characterisation of "metal-only" complexes, where the cation binding site is filled and the anion binding site is vacant, to use in anion selectivity extraction experiments,

- determination of the anion selectivities of **L18** and **L20** in the presence of copper and nickel by solvent extraction,

- the isolation and characterisation of metal salt complexes of **L17** to analyse binding motifs in the solid state, and

- the assessment of the cation selectivity of **L18** in solvent extraction experiments.

A review of attempts to design selective anion extractants and of suitable anion detection techniques follows.

5.1.2   Reversing the Hofmeister Bias

The extractability of anions from an aqueous phase into a water-immiscible solvent is dominated by the level of solvation of the anion, with the Hofmeister bias, discussed in detail in Chapter 1, often able to predict the selectivity orders of anion binding.[1] Larger, more charge-diffuse anions are more easily extracted as they are less hydrophilic, and it is often possible to predict distribution coefficients from the

Gibbs free energies of solvation.[2, 3]   In the liquid/liquid extraction of anions, the following series is usually observed, with the most readily extracted anions on the left and the least readily on the right:[2]

$$ClO_4^- > I^- > SCN^- > NO_3^- > Br^- > Cl^- >> SO_4^{2-} > CO_3^{2-} > PO_4^{3-}$$
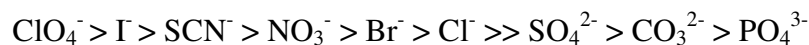
To achieve truly selective anion extraction, the Hofmeister bias must often be reversed, or at least attenuated in some way. An extractant must bind the anion with sufficient "strength" to overcome the required dehydration in the transfer of the target species to the organic phase.

Receptors containing electron deficient Lewis acid sites can form bonding interactions with anions by overlap of orbitals, and have found particular application in the field of ion selective electrodes.[2, 4]   Striking examples are the ion selective electrodes synthesised by Chandra et al[5], with ionophores based on organotin compounds. The electrodes show entirely non-Hofmeister selectivity orders, with an example ionophore and its anion selectivity order displayed in Figure 5.1.

$$F^- > OAc^- > Cl^- > I^- \sim Br^- > ClO_4^- > NO_2^- > NO_3^- > SCN^-$$
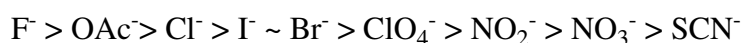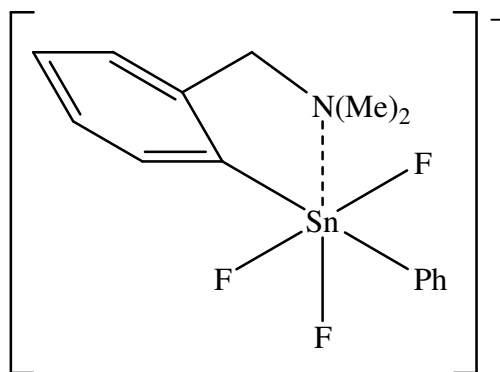
Figure 5.1: An organotin compound which shows a non-Hofmeister order for anion binding.[5]

Hydrogen bond donors can provide favourable interactions with the bound anion, for example Sessler et al have developed calixpyrroles,[6] some fluorinated,[7] which

extract the caesium salts of smaller anions such as chloride and nitrate into nitrobenzene as effectively as caesium iodide (Figure 5.2).
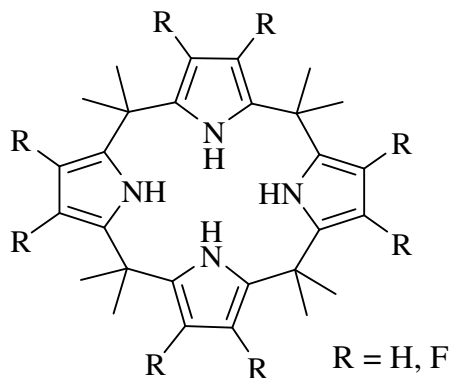

Figure 5.2: *meso*-Octamethylcalix[4]pyrolles for the binding of caesium salts.[6, 7]

Increasing the cavity size and hydrogen-bond donor functionality of macrocyclic receptors can favour the extraction of larger, more complex anions, such as the octamethyl-octaundecylcyclo[8]pyrolle (Figure 5.3) designed by Moyer *et al*[8], which is the first reagent to selectively extract sulfate in the presence of high nitrate concentrations.

R = $C_{11}H_{23}$, C_2H_5
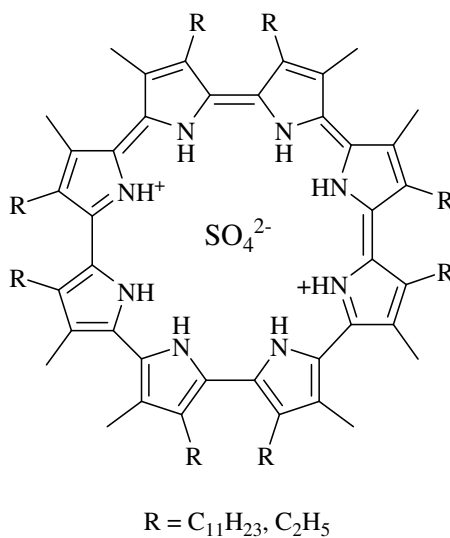
Figure 5.3: Octamethyl-octaalkylcyclo[8]pyrolle for the extraction of sulfate.[8]

A highly organised, singly charged, steroid-based receptor with urea H-bond donors developed by Davis *et al*[9] has been shown to extract bromide and iodide more

strongly than hexafluorophosphate and perchlorate. The complexity of the structure (Figure 5.4) illustrates the difficulties in synthesising receptors with appropriate geometries and H-bond donors to achieve selective anion transport against the Hofmeister bias.
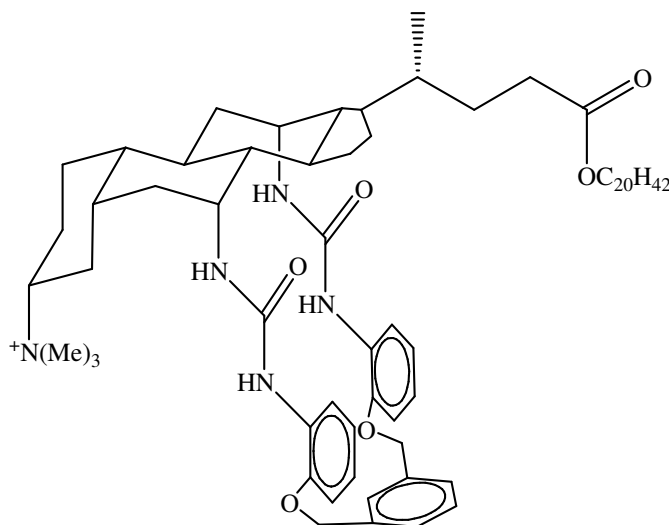
Figure 5.4: Steroid based anion receptor of Davis *et al.*[9]

Moyer *et al*[1] have also demonstrated that "dual host" systems, containing a cation binding species and an anion binding species, can extract anions against the Hofmeister bias. A calix-crown cation host alongside a disulfonamide anion host show synergistic, anti-Hofmeister behaviour in the extraction of caesium salts.

A novel tactic for overcoming the Hofmeister bias is to extract not only the anion, but also some of its hydration sphere into the organic phase. Plieger *et al*[10] have described the solid state structure of a $CuSO_4$ complex of a macrocyclic ligand based on a "salen" unit (described in Chapter 4) wherein the sulfate is bound as a water bridged dimer (Figure 5.5). This solid state phenomenon may also be mirrored in solvent extraction experiments, as the ligand shows a greater strength of sulfate extraction compared to other, similar ligands. This suggests that the extraction of partially hydrated anions may be key to achieving the selective transport of hydrophilic anions in a solvent extraction process.
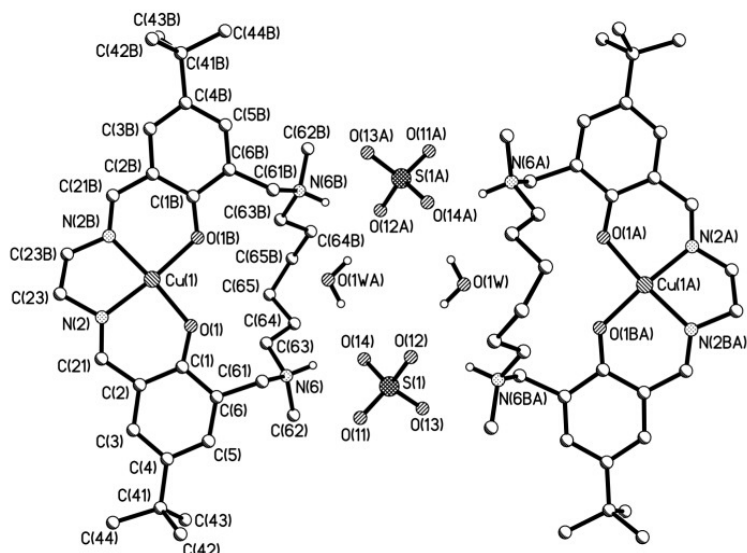
Figure 5.5: The solid state structure of a macrocyclic ligand binding Cu^{II} and partially hydrated sulfate anions.[11]

The examples illustrated suggest that attenuating the Hofmeister bias is achievable using a number of strategies. However, attaining a complete reversal of the series is very difficult and will probably require the use of highly complex, synthetically challenging receptors.[12]

5.1.3   Techniques to Determine Anion Selectivity

In order to measure accurately anion selectivity orders, a robust, reliable analytical technique must be employed. Most literature techniques involve single phase measurements of the stability of anion complexation, with the most common being NMR spectroscopy. Changes in the experimentally measured parameters, *i.e.* chemical shift and coupling constants, can give information not only on the strength of binding but solution structure. The NMR sensitive nuclei which show the greatest perturbation in chemical shift can be identified as those most heavily involved in the binding of the anion, and in most cases the location of binding in solution can be confirmed.[13]   However, NMR techniques can show low sensitivity due to the relatively high concentrations of both the anion and the receptor required to attain

signals with appropriate intensities for use.[14] The technique also suffers from its intolerance to some paramagnetic centres, rendering it unsuitable for experiments to determine the anion selectivities of metal salt extractants designed to bind the paramagnetic Cu^{II} ion alongside various anions.[15]

Potentiometry, most often pH-metry, is a well defined method for measuring stability constants, usually in aqueous solutions.[16, 17] The technique involves analysing the consumption or liberation of protons as the receptor binds the anion by measuring the pH of the solution. It requires the basicity constants of the ligand and the anion(s) involved in the experiment to be determined previously, and subsequent pH titrations are carried out using a solution of the receptor, anion and protons to determine the effect on pH. Stability constants can then be extracted from the data using computer programs.[2] The technique depends on the understanding of all equilibrium processes in solution, and so the added complexities incurred when analysing cation *and* anion extraction (there are estimated to be over 11 species present in $CuSO_4/H_2SO_4$ aqueous solutions)[18] preclude it from use in our case.

In the field of anion sensing, the inclusion of transition metals in receptors makes it possible to take advantage of the optical and electrochemical properties conferred by the metal cation. A recent review by Beer *et al*[19] describes the inclusion of ferrocene and cobaltocenium moieties to allow anion detection by cyclic voltammetry, and of ruthenium chromophores which facilitate anion detection by UV/Vis spectroscopy. Two examples are shown in Figure 5.6.
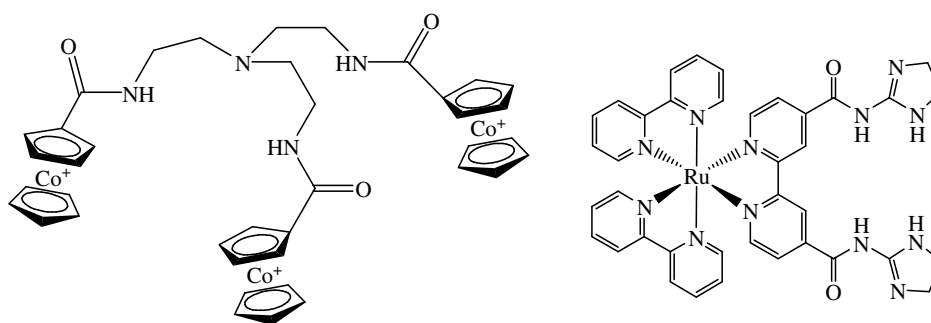

Figure 5.6: Examples of metal-based anion receptors which allow measurement of anion binding by electrochemical and optical techniques.[19]

Fluorimetric analytical techniques are also becoming prominent in anion sensing, and employ the similar strategy of incorporating a fluorophore into receptor design. Gunnlaugsson et al^{20} have recently reviewed the area, but these strategies require complexity of receptor design, which is not favourable in the development of ligands for use in extractive processes and so are not detailed further.

Anion selective electrodes are becoming an increasingly popular and applied method for measuring anion concentrations in aqueous solutions. Whilst the current range of detectable anions is low, halide-selective electrodes are commercially available and successful.[2] Care must be taken when using such electrodes that interfering anions and cations are not present in the analytical solution, for example the presence of certain transition metal cations leads to the formation of chlorometallate anions, altering the chloride ion concentration and adversely affecting results through the equilibrium:

Equation 5.1 $$M^{x+} + yCl^- \rightleftharpoons MCl_y^{(x-y)-}$$

as anion selective electrodes only measure the *free* anion concentration. The solvent extraction experiments described in this chapter focus on the selectivity of metal salt extractants for the commercially relevant anions Cl^- and SO_4^{2-} in the presence of Cu^{II} and Ni^{II}, which do not form chloro-complexes under extraction conditions. For this reason, a chloride sensitive electrode was used to measure chloride uptake.

As ICP-OES (Chapter 2) is used to measure metal ion concentration in extraction experiments, it would save time and effort if anion selectivity could be measured using this technique. Unfortunately, most non-metallic elements cannot be analysed as their atomic and ionic emission spectra lie in the wrong region or have too low intensity for reliable detection.[21] However, sulfur does have emission lines in the correct region, and so sulfate analysis was carried out alongside metal analysis using ICP-OES.

5.1.4 Anion Selectivity by Solvent Extraction

As described in Chapter 1, it is possible to determine the relative cation binding strengths of a series of ligands by carrying out solvent extraction experiments under identical conditions to obtain S-curves, and subsequently measuring the $pH_{0.5}$ value for cation binding. It has been shown recently within the group that it is also possible to use solvent extraction experiments to obtain *anion* loading S-curves, and $pH_{0.5}$ values for anion loading give information on anion selectivity.[10, 22] As the anion binding site must be protonated to operate, anions associated with higher $pH_{0.5}$ values will be bound more "strongly", and so in a comparative experiment the extractant will be selective for the anion which shows the highest $pH_{0.5}$ (Figure 5.7).[23]
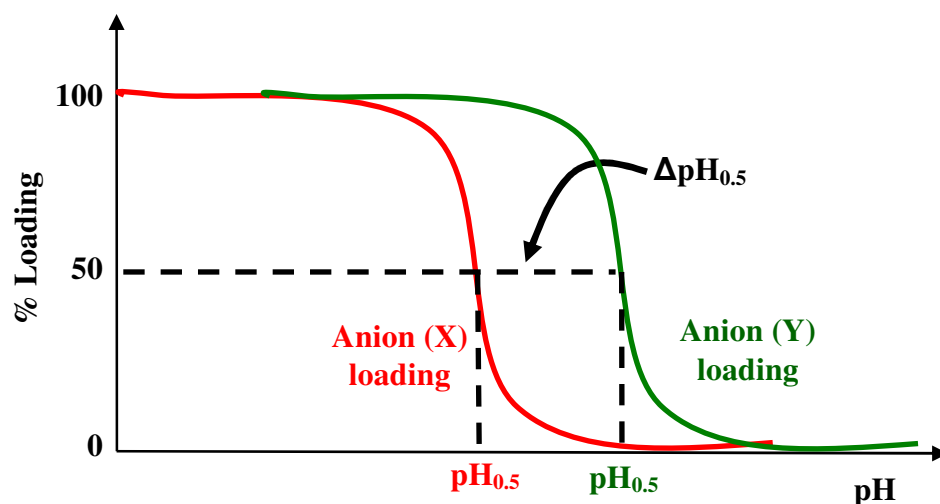
Figure 5.7: Loading S-curves for two different anions for pH-dependent uptake $L_{(org)} + H^+ + X^-$ $\rightleftharpoons$ $[LH.X]_{(org)}$.

The difference in $pH_{0.5}$ values for two anions provides a quantitative measure of selectivity. In the scheme shown in Figure 5.7, the receptor binds anion Y at a higher pH than anion X, and so the receptor is selective for Y over X.

5.2 Synthesis and Characterisation of Metal-Only Complexes

"Metal-only" complexes, [M(**L**-H)$_2$], formed by the deprotonated salicylaldoxime units, can be used to study anion-uptake properties: occupying all cation binding sites allows focus on anion binding. The preparation of metal-only complexes, by mixing ligands and metal acetates, proved simple and high yielding. On complexation of the metal, the protons lost from the phenol groups were expected to react with the acetate anions to form acetic acid, which could be removed *in vacuo*.

Equation 5.2: $[M(OAc)_2] + 2\mathbf{L} \rightleftharpoons [M(\mathbf{L}\text{-H})_2] + 2AcOH$
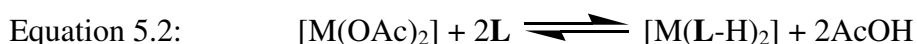
An aqueous ammonia wash was also employed to ensure no acetate anions remained associated with the complexes. Due to the solubility problems described in Chapter 4, only the complexes of **L17**-**L20** were studied.

The physical properties of these highly coloured solids varied with the nature of the ligand and the metal. Firstly, it was noticed that the brown Cu^{II} and green Ni^{II} complexes of the "5-substituted" ligands were less soluble in organic media than their "3-substituted" isomers. Secondly, the piperidinomethyl substituted ligands gave complexes which were polycrystalline solids, while dihexylaminomethyl substituted ligands gave amorphous or waxy solid complexes with higher solubility in organic media.

5.2.1 Mass Spectrometry

Synthesis of the metal-only complexes was confirmed by FAB mass spectroscopy, with molecular ion peaks observed for each complex (Table 5.1). Peaks corresponding to the ligands were common to all spectra, and no signals for complexes with associated acetate anions were present.

Complex	MH$^+$	Ligand
[Cu(**L17**-H)$_2$]	642 (100%)	291 (29%)
[Ni(**L17**-H)$_2$]	637 (28%)	291 (42%)
[Cu(**L18**-H)$_2$]	842 (6%)	391 (45%)
[Ni(**L18**-H)$_2$]	837 (6%)	391 (36%)
[Cu(**L19**-H)$_2$]	642 (24%)	291 (42%)
[Ni(**L19**-H)$_2$]	637 (59%)	291 (40%)
[Cu(**L20**-H)$_2$]	842 (21%)	391 (65%)
[Ni(**L20**-H)$_2$]	837 (18%)	391 (34%)

Table 5.1: Peaks and intensities seen in the FAB mass spectra of the metal-only complexes synthesised in this chapter.

5.2.2 X-Ray Crystallography

The X-ray crystal structures of [Ni(**L17**-H)$_2$] and [Cu(**L17**-H)$_2$] have been obtained by Dr D. K. Henderson and Dr J. E. Davidson to support exemplification in a patent (confidential) relating to the analogous nonyl-substituted ligand for the recovery of metal(II) chlorides from chloride leach solutions.[24]

[Ni(**L17**-H)$_2$] is a square-planar complex with the Ni^{II} atom lying on a crystallographic inversion centre. The complex has a bifurcated hydrogen bond similar to that seen in the structure of [Cu(**L4**-H)$_2$(py)$_2$] (Chapter 3), as the piperidino nitrogen atom can act as a hydrogen bond acceptor (O23A···N62A' = 2.831(2) Å). The hydrogen bond to the phenolate oxygen is the dominant bond with a smaller donor-acceptor distance (O23A···O1A' = 2.564(2) Å). The piperidine rings are located above and below the central NiN$_2$O$_2$ coordination plane, with the piperidino nitrogen atoms (N62 and N62A) of the rings displaced by 0.865 Å from the plane.
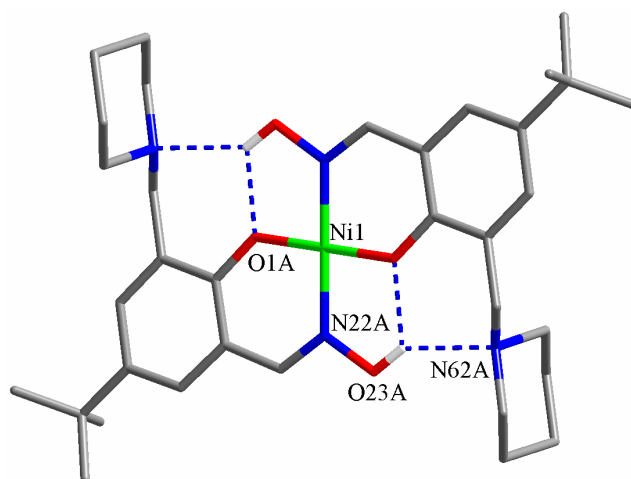
Figure 5.8: X-Ray crystal structure of the centrosymmetric [Ni(**L17**-H)$_2$] with selected atom labels. Hydrogen atoms not involved in H-bonding are omitted for clarity.

A similar structure is seen for [Cu(**L17**-H)$_2$] but there is no crystallographic inversion centre associated with the complex, so the two ligands are not symmetrically equivalent. Bifurcated H-bonds are again present, and the distances between donor and acceptor atoms are larger than in [Ni(**L17**-H)$_2$] for both the oxime oxygen to phenolate contact (O1A···O23B = 2.656(2) Å, O1B···O23A = 2.766(2) Å, average = 2.711(3) Å) and the oxime oxygen to piperidino nitrogen contact (O23B···N62A = 2.851(2) Å, O23A···N62B = 2.972(2) Å, average = 2.912(3) Å).
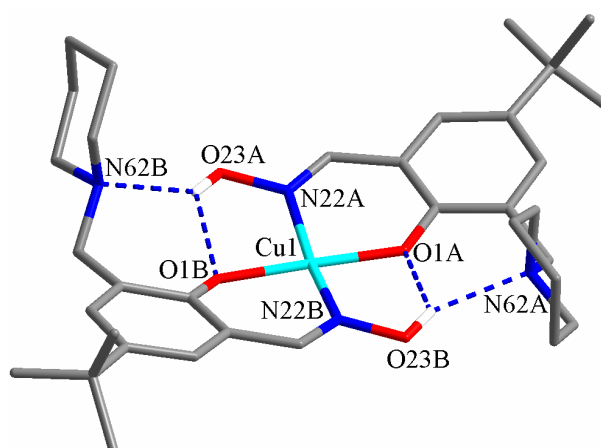
Figure 5.9: X-Ray crystal structure of [Cu(**L17**-H)$_2$] with selected atom labels. Hydrogen atoms not involved in H-bonding are omitted for clarity.

The molecule is distorted slightly with respect to the square-planar nickel structure and the piperidine rings are now both above the plane, with the nitrogen atoms at distances of 0.518 Å (N62A) and 1.270 Å (N62B) above the plane. This is due to the copper centre weakly interacting with phenolate oxygen atoms on a second complex molecule, forming an offset *pseudo*-dimer pairing (Cu1···O1A' = 2.516(1) Å) and forcing both pendant arms to point upwards, away from the other molecule. The dimer has an inversion centre at the centroid of the central Cu_2O_2 unit, shown in Figure 5.10, and the interaction is very similar to that seen in [Cu(**L17**)Cl$_2$] which has a Cu···O contact distance of 2.507(2) Å (Chapter 4).
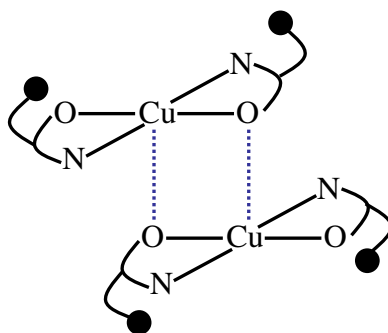

Figure 5.10: Schematic representation of the centrosymmetric dimer [Cu(**L17**-H)$_2$]$_2$ showing the orientation of the piperidine rings (black circles) relative to the Cu_2O_2 core.

These axial, long-range copper-oxygen interactions suggest that copper-*anion* interactions are possible, which could enhance anion binding. The structures also show the flexibility of the pendant amine arms, which are able to sit above or below the plane of the complex. As they are free to move as the environment changes, their position could respond to the need to accommodate anions with different sizes and shapes.

5.3 Synthesis of Metal Salt Complexes

Metal *salt* complexes of **L17** were synthesised and characterised crystallographically, to study the anion binding motif and to investigate the effects of

changing the anion on the complex and the mode of binding. Complexes were prepared in two ways: by mixing the metal salt and **L17** directly in methanol, or by contacting a chloroform solution of the metal-only complex with an acid containing the appropriate conjugate anion:

Equation 5.3 $\qquad [M(\textbf{L17}\text{-}H)_2]_{(org)} + 2HX \rightleftharpoons [M(\textbf{L17})_2X_2]_{(org)}$
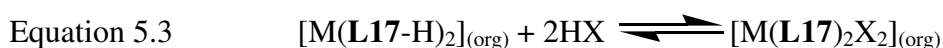
The isolation and characterisation of $[Cu(\textbf{L17})Cl_2]$ and $[Zn_2(\textbf{L17})_2Cl_4]$ has already been reported in Chapter 4.

5.3.1   [Cu(L17)Br$_2$]

By mixing copper(II) bromide with **L17** it was possible to isolate an analogue of $[Cu(\textbf{L17})Cl_2]$, with bromide ligands taking the place of the chlorides. The solid state structure of $[Cu(\textbf{L17})Br_2]$ is very similar to its chloride analogue (Figure 5.11).
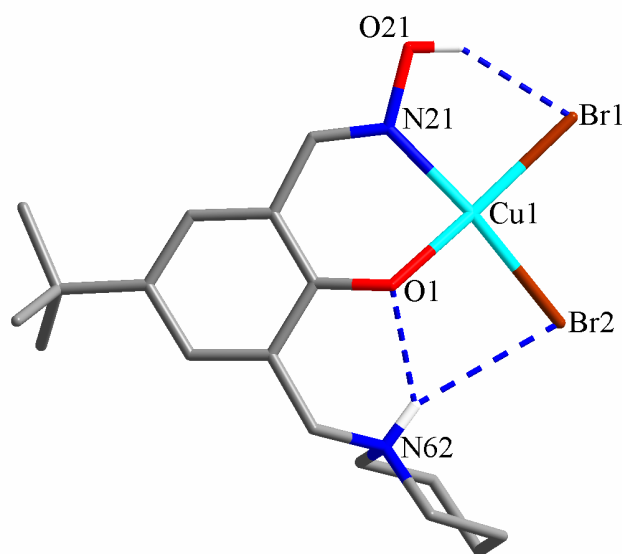

Figure 5.11: The solid state structure of $[Cu(\textbf{L17})Br_2]$, with selected atom labels. Hydrogen atoms not involved in H-bonding are omitted for clarity.

A comparison of the significant bonds and contacts in the two molecules (Table 5.2) reveals that the interactions in [Cu(**L17**)Br$_2$] are longer than those in [Cu(**L17**)Cl$_2$], which is to be expected as Br$^-$ is larger than Cl$^-$.[25]

Contact/Bond	[Cu(L17)Cl$_2$]	[Cu(L17)Br$_2$]
Oxime OH···X1	O23···Cl1 = 2.925(3)	O21···Br1 = 3.047(2)
Amine H···phenol	N62···O1 = 2.754(3)	N62···O1 = 2.803(3)
Amine H···X2	N62···Cl2 = 3.560(3)	N62···Br2 = 3.642(3)
Cu-X1	Cu-Cl1 = 2.269(1)	Cu-Br1 = 2.403(5)
Cu-X2	Cu-Cl2 = 2.268(1)	Cu-Br2 = 2.415(5)

Table 5.2: Selected contacts and bond distances (Å) in the solid state structures of the dichloro and dibromo complex of [Cu(**L17**)].

5.3.2   [Cu(L17)$_2$(NO$_3$)$_2$]

Direct combination of methanolic solutions of copper(II) nitrate and **L17** yielded the metal salt complex [Cu(**L17**)$_2$(NO$_3$)$_2$], which shows the expected tritopic metal salt binding motif (Chapter 4) with the metal cation and two nitrate anions in separated binding sites.
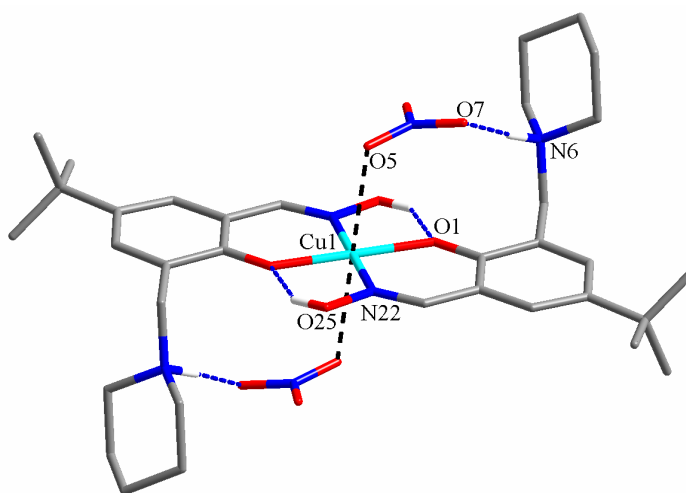

Figure 5.12: The solid state structure of [Cu(**L17**)$_2$(NO$_3$)$_2$], with selected atom labels. Hydrogen atoms not involved in H-bonding are omitted for clarity.

A crystallographic inversion centre is located on the Cu^{II} cation, which is complexed to two salicylaldoxime ligands in the 14-membered *pseudo*macrocyclic H-bond arrangement typical of bis-salicylaldoximato copper(II) species. Protonation of the piperidine moieties has generated two equivalent anion binding sites and the nitrate anions occupy these, bound by a combination of electrostatic and H-bond interactions (N6···O7 = 2.842(2) Å), with the metal salt again binding to a zwitterionic form of the ligand **L17**. One oxygen atom of each nitrate anion is located in a position axial to the copper(II) centre (Cu1···O5 = 2.722(2) Å) giving the copper an overall Jahn-Teller distorted octahedral coordination sphere. If this type of metal-anion interaction persists in solution, it should enhance metal salt binding.

5.3.3   [Cu(L17)$_2$(BF$_4$)$_2$]

[Cu(**L17**)$_2$(BF$_4$)$_2$] was synthesised and isolated in a similar fashion to [Cu(**L17**)$_2$(NO$_3$)$_2$] and has a comparable structure.
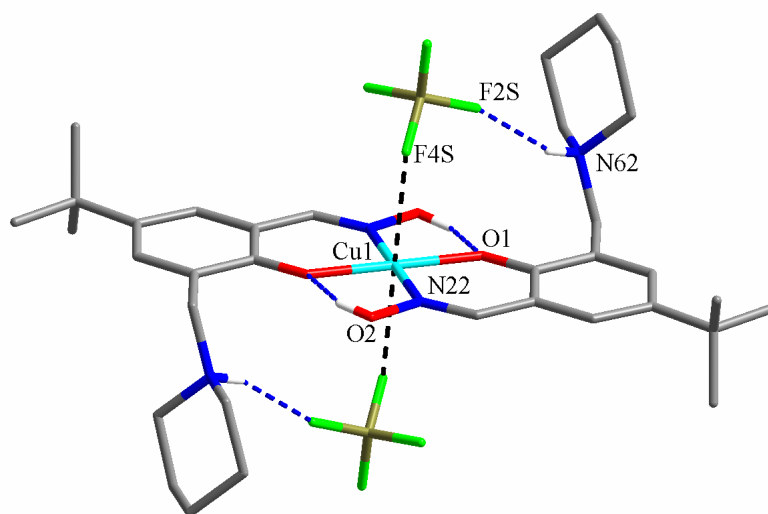

Figure 5.13: The solid state structure of [Cu(**L17**)$_2$(BF$_4$)$_2$], with selected atom labels. Hydrogen atoms not involved in H-bonding are omitted for clarity.

The copper(II) ion is again bound to two salicylaldoxime ligands and the anions are located adjacent to the protonated piperidine groups (N62···F2S = 2.780(4) Å). A

copper-anion interaction is again seen but at a shorter distance than in the nitrate structure (Cu1⋯F4S = 2.638(2) Å). This may be a consequence of the BF_4^- anion being larger than NO_3^-.[25]

5.3.4 [Cu(L17)₂(CF₃CO₂)₂]

As [Cu(CF₃CO₂)₂] is not commercially available, [Cu(**L17**)₂(CF₃CO₂)₂] was synthesised by mixing the metal-only complex [Cu(**L17**-H)₂] in chloroform with an aqueous solution of trifluoroacetic acid and its sodium salt. The structure of the resulting complex is shown in Figure 5.14.
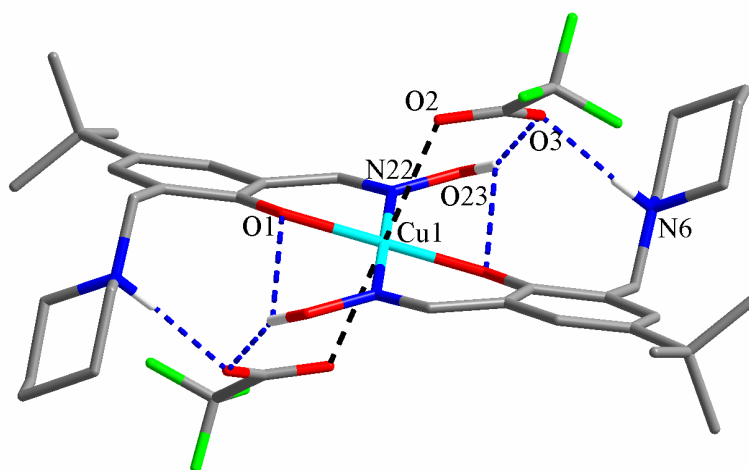

Figure 5.14: The solid state structure of [Cu(**L17**)₂(CF₃CO₂)₂], with selected atom labels. Hydrogen atoms not involved in H-bonding are omitted for clarity.

Anion binding has induced major changes in the copper(II) coordination sphere. The trifluoroacetate anion (TFA⁻) forms H-bonds with both the piperidinium proton (N6⋯O3 = 2.766(8) Å) *and* the oxime proton (O23⋯O3 = 2.700(6) Å) through one of the carboxylate oxygen atoms. The interaction with the oxime proton causes a distortion of the 14-membered *pseudo*macrocyclic H-bond array around the Cu^{II} centre, with the oxime proton forming a bifurcated H-bond with the anion and the phenolate of the adjacent ligand (O23⋯O1' = 2.878(6) Å). This might be expected to significantly destabilise copper binding. Weak copper-anion interactions are again

present, with the other carboxylate oxygen in the apical position relative to the copper ion (Cu1···O2 = 2.673(5) Å).

The effect of trifluoroacetate anion coordination can be seen clearly by comparing relevant contact and bond distances (Table 5.3). The three metal salt complexes of **L17** that show the expected motif are analysed alongside the metal-only complex [Cu(**L17**-H)$_2$].

Contact/Bond	Cu(NO$_3$)$_2$	Cu(BF$_4$)$_2$	Cu(TFA)$_2$	[Cu(L17-H)$_2$][a]
Cu-O	1.912(1) Å	1.919(2) Å	1.922(4) Å	1.896(1) Å
Cu-N	1.946(1) Å	1.943(2) Å	1.975(5) Å	1.958(2) Å
Hole Size (R$_H$)	1.929(1) Å	1.931(2) Å	1.949(6) Å	1.927(2) Å
Cu···X	2.722(2) Å	2.638(2) Å	2.673(5) Å	2.516(1) Å[b]
Oxime OH···OPh	2.626(2) Å	2.604(2) Å	2.878(6) Å	2.564(2) Å
Amine···X	2.842(2) Å	2.780(4) Å	2.766(2) Å	n/a

[a]Distances are the average of two crystallographically independent halves of the complex. [b]X is the phenoxide oxygen of the adjacent complex molecule, described in Section 5.2.2, and only one of the axial sites is occupied. All other examples have interactions at both axial sites.

Table 5.3: Selected bond and contact distances in the copper salt complexes and the copper only complex of **L17**.

Some interesting solid state trends can be extracted from the data in Table 5.3. If the species in the axial positions carried similar partial anionic charges, it might be expected that closer approach to the Cu^{II} would result in an increase in the Cu^{II} equatorial bond lengths due to Jahn-Teller effects.[15] This does not appear to be the case, as the hole size trend does not follow the Cu···anion contact distances. The hole sizes in all complexes are the same within experimental error, apart from the larger hole size of [Cu(**L17**)$_2$(TFA)$_2$], caused by the interaction of the trifluoroacetate anion with the H-bonding motif. This interaction is also presumably responsible for the significantly larger OH to phenolate oxygen interaction. It should be noted that the metal-only complex [Cu(**L17**-H)$_2$] has both the closest axial interaction, from an adjacent complex molecule, and the smallest hole size, but only one of the axial sites

is occupied, and the Cu^{II} ion is in an approximately square-based pyramidal geometry.

Another trend that can be seen is in the distance between the piperidinium N atom and the nearest atom in the anions, which follows the order $NO_3^- > BF_4^- > TFA^-$. This appears to be related to the size of the anion,[25] with the largest anion closest to the binding site.

5.3.5   Mass Spectrometry

FAB mass spectrometry could used to detect complex formation, with the loss of one of the bound anions providing a characteristic positive peak in each spectrum. Other peaks seen include the free ligand and the metal-only complex, and are displayed for all synthesised complexes in Table 5.4.

| Complex	MH$^+$	(M-anion)$^+$	Metal-only	Ligand
[Cu(**L17**)Cl$_2$]	514 (0%)	434 (51%)	642 (16%)	291 (75%)
[Cu(**L17**)Br$_2$]	426 (0%)	390 (90%)	642 (51%)	291 (100%)
[Cu(**L17**)$_2$(NO$_3$)$_2$]	769 (0%)	707 (16%)	642 (62%)	291 (44%)
[Cu(**L17**)$_2$(TFA)$_2$]	871 (0%)	758 (18%)	642 (65%)	291 (0%)
[Cu(**L17**)$_2$(BF$_4$)$_2$]	819 (0%)	731 (100%)	642 (96%)	291 (77%)

Table 5.4: Peaks and intensities seen in the FAB mass spectra of the metal salt complexes synthesised in this chapter.

5.4   Anion Selectivity by Solvent Extraction

The solvent extraction experiments described in this section were carried out under identical conditions, by contacting a 0.01 M chloroform solution of the metal-only complex [M(**L**-H)$_2$] with a 0.8 M aqueous solution of the appropriate anion, which

was made up using HX and NaX (where X$^-$ is the anion) with the anion concentration being kept constant. Varying the anion concentration in the aqueous phase of an extraction has been demonstrated to have a great effect on distribution coefficients (Chapter 4) and so keeping the concentration constant throughout the experiments is paramount if comparisons are to be made and anion selectivities inferred.

By measuring the metal and anion content of the organic phase and plotting the percentage loading values against the equilibrium pH of the aqueous phase, it is possible to determine both the anion loading S-curve and the cation stripping S-curve. The percentages are calculated by assuming the extraction equilibrium is as follows:

Equation 5.4 $\qquad$ $[M(\textbf{L}\text{-H})_2]_{(org)} + 2HX \rightleftharpoons [M\textbf{L}_2X_2]_{(org)}$
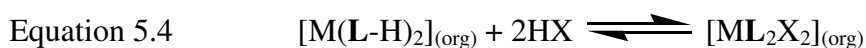
where 2HX is either 2HCl or H_2SO_4. To compare selectivities the $pH_{0.5}$ value is measured, which is the pH of the aqueous phase at which 50% of the theoretical maximum loading of the metal or anion is in the organic phase. For metals, the lower the $pH_{0.5}$ the stronger the binding, as explained in Chapter 1. As the anion binding site must be protonated to extract an anion, the *higher* the $pH_{0.5}$ for anion loading the stronger the binding.

5.4.1 Anion Selectivity of [Cu(L18-H)$_2$]

Investigating the anion selectivity of [Cu(**L18**-H)$_2$] is complicated by the formation of the unexpected metal salt complexes [Cu(**L**)X$_2$] described previously (Chapter 4). The anion is bound directly to the metal centre and so is in a different environment from that expected, and complex formation requires complete reorganisation of the metal-only complex being studied. The results of the experiment with chloride are displayed in Figure 5.15.
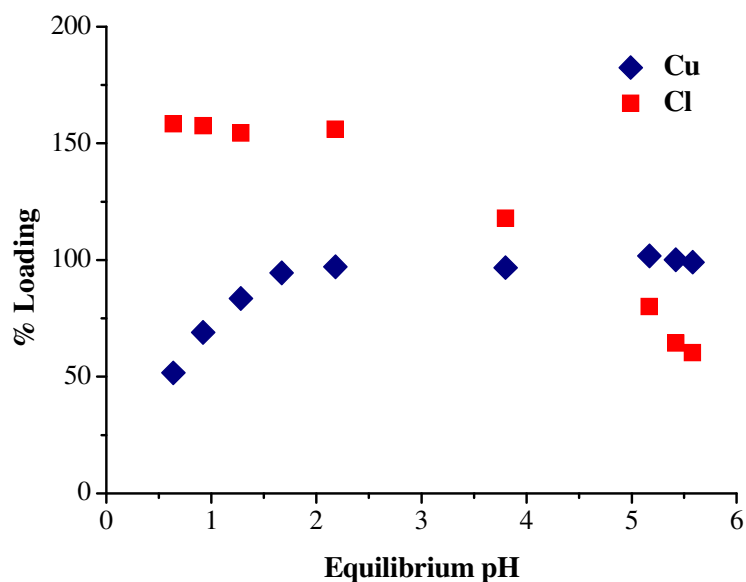
Figure 5.15: Copper (blue) and chloride (red) loading of the organic phase when a 0.01 M chloroform solution of [Cu(**L18**-H)$_2$] is contacted with 0.8 M aqueous chloride solutions of various pH values. 100% copper loading is based on a molar ratio of 1Cu : 2**L18**, and 100% chloride loading is based on a molar ratio of 2Cl : 2**L18**.

A typical curve for pH-dependent copper loading is seen. As the copper content of the organic phase is defined by the previously synthesised metal-only complex, it cannot reach a value greater than 100%. The copper is stripped into the aqueous phase at pH ≤ 1.5, with copper-loading having a pH$_{0.5}$ of 0.6.

Chloride loading reaches approximately 150%, indicating that the formation of [Cu(**L18**)Cl$_2$] is occurring in the organic phase. The flattening of the curve to give a plateau of 150% at lower pH values suggests both [Cu(**L18**)Cl$_2$] and [**L18**.HCl] are present in this pH region; at pH 2 these species are present in approximately equal concentrations and equation 5.5 applies:

Equation 5.5   [Cu(**L18**-H)$_2$]$_{(org)}$ + 3HCl $\rightleftharpoons$ [Cu(**L18**)Cl$_2$]$_{(org)}$ + [**L18**.HCl]$_{(org)}$

At pH values greater than 5.0 the chloride loadings are consistent with a mixture of [Cu(**L18**)Cl$_2$] and [Cu(**L18**-H)$_2$] being present in the organic phase. This observation has important industrial implications, as it suggests that by contacting a

loaded organic phase containing [Cu(**L18**)Cl$_2$] with a high pH aqueous phase, the chloride may be stripped and thus generate an organic phase containing only copper and the ligand. Conventional copper stripping by sulfuric acid may then be possible, generating a sulfate electrolyte which is preferable to generating a chloride electrolyte by conventional cation stripping with HCl.[26]

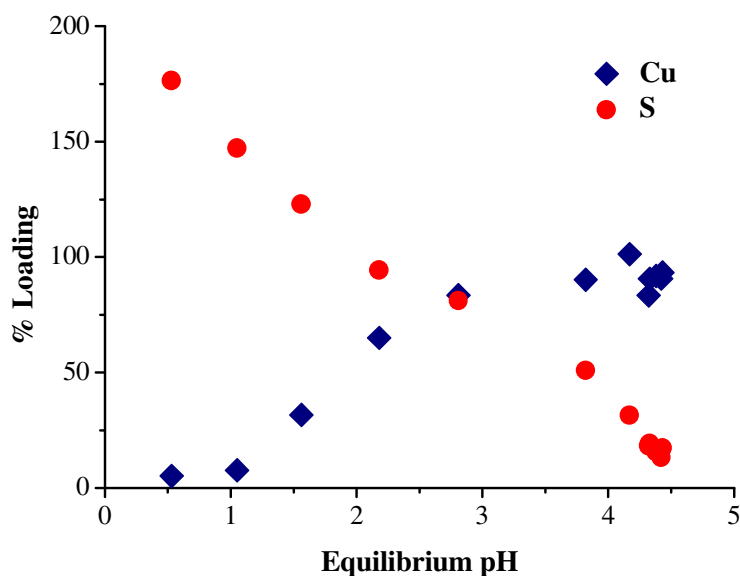The pH profile for [Cu(**L18**-H)$_2$] loading of sulfate is shown in Figure 5.16.

Figure 5.16: Copper (blue) and sulfate (red) loading of the organic phase when a 0.01 M chloroform solution of [Cu(**L18**-H)$_2$] is contacted with 0.8 M aqueous sulfate solutions of various pH values. 100% copper loading is based on a molar ratio of 1Cu : 2**L18**, and 100% sulfate loading is based on a molar ratio of SO$_4$: **L18**.

At a pH value of 2.8 there is approximately 80% loading of CuSO$_4$, confirming the observation in Chapter 4 that **L18** is capable of loading CuSO$_4$ to high levels. The pH-profile for copper loading is broader than that observed with chloride, which may be due to the different species formed in the two experiments. The pH$_{0.5}$ value for Cu-loading of approximately 2.0 is considerably higher than in the chloride case, and with the pH$_{0.5}$ for sulfur loading of ~3.8 being lower than that for chloride it is clear **L18** is selective for CuCl$_2$ rather than CuSO$_4$ and that this selectivity is due to the favourable formation of [Cu(**L18**)Cl$_2$]. At lower pH values sulfur loading exceeds

100%, and this is due to the extraction of the bisulfate anion, HSO_4^-, which is prevalent in copper sulfate solutions at pH<1.[18]

As attempts to examine the binding motif for $CuSO_4$ *via* X-ray crystallographic studies were unsuccessful, further solvent extraction experiments were carried out to determine the influence of copper on anion binding, by contacting **L18** with sulfate in the absence of copper under identical conditions.
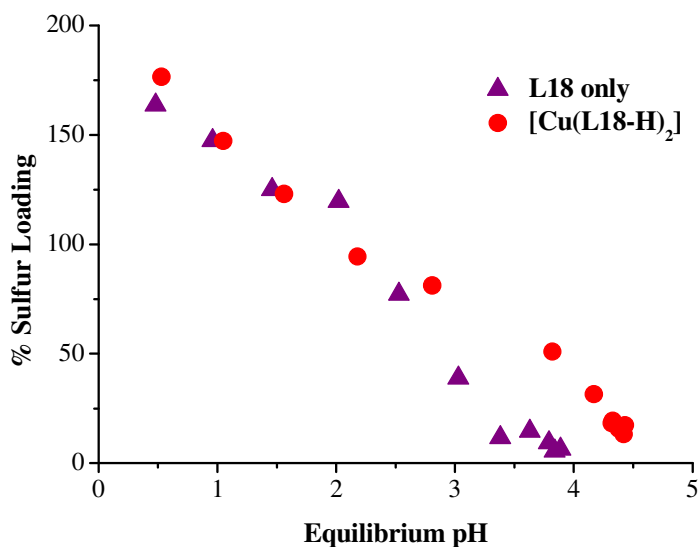

Figure 5.17: Loading of sulfate by in the organic phase when a 0.01 M chloroform solution of [Cu(**L18**-H)$_2$] (red circles) or **L18** (purple triangles) is contacted with 0.8 M aqueous sulfate solutions of various pH values. 100% sulfate loading is based on a molar ratio of SO_4: **L18**.

Figure 5.17 shows that sulfate loading by **L18** is enhanced when copper is present, *i.e.* the copper(II) complex of **L18** binds sulfate more strongly than the free ligand. The $pH_{0.5}$ for sulfate loading by **L18** only is ~2.8, compared to the value of 3.8 for [Cu(**L18**-H)$_2$], indicating possible synergistic $CuSO_4$ binding. This phenomenon has been observed previously in the uptake of $CuSO_4$ by the substituted salen ligands described in Chapter 4,[22, 23] and is attributed to the preorganisation of the anion binding site for sulfate when copper is bound. This is unlikely to be the case for **L18** as it binds copper in a *trans* configuration, and in the crystal structure of [Cu(**L17**-H)$_2$] the piperidino nitrogen atoms N62A and N62B are separated by 8.703(3) Å. A more likely explanation is that there is an interaction between the copper(II) centre

and the sulfate anion, expected to be similar to the apical Cu···O interactions seen in the crystal structures of $[Cu(\textbf{L17})_2(NO_3)_2]$, $[Cu(\textbf{L17})_2(BF_4)_2]$ and $[Cu(\textbf{L17})_2(CF_3CO_2)_2]$ (Section 5.3).

5.4.2   Anion Selectivity of [Ni(L18-H)₂]

Ligands capable of transporting $NiCl_2$ across a circuit could have major commercial applications in the hydrometallurgical recovery of nickel.[27]   Solvent extraction experiments were carried out using the nickel-only complex $[Ni(\textbf{L18}-H)_2]$ to determine if nickel salt transport was possible. The pH profile for $[Ni(\textbf{L18}-H)_2]$ *vs.* HCl is shown in Figure 5.18.
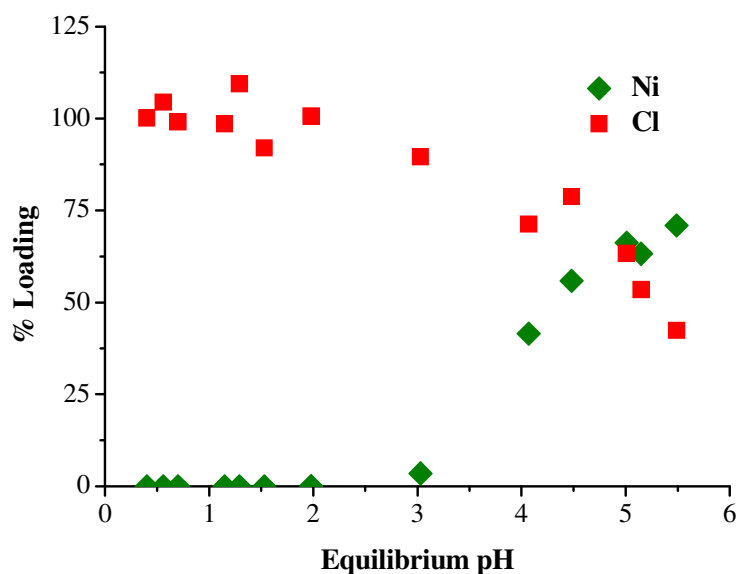

Figure 5.18:   Nickel (green) and chloride (red) loading of the organic phase when a 0.01 M chloroform solution of $[Ni(\textbf{L18}-H)_2]$ is contacted with 0.8 M aqueous chloride solutions of various pH values. 100% nickel loading is based on a molar ratio of 1Ni : 2**L18**, and 100% chloride loading is based on a molar ratio of 2Cl : 2**L18**.

L18 is a relatively weak extractant for nickel and at pH ~ 5.5 only 75% nickel loading is detected, demonstrating the selectivity of **L18** for copper over nickel. The $pH_{0.5}$ of approximately 4.3 for nickel is nearly 3 pH units higher than for copper, *i.e.*

the binding of copper is three orders of magnitude higher. Chloride loading reaches 100% at lower pH values, when no nickel is present in the organic phase, and has a $pH_{0.5}$ of ~5.3 which is similar to but slightly lower than the value when copper is present. 65% loading of $NiCl_2$ occurs at pH 5, which illustrates that $NiCl_2$ loading by these ligands is possible, but if they are to have any commercial application then loading efficiency will need to be improved significantly.

There are again marked differences in the extraction of sulfate by $[Ni(\mathbf{L18}\text{-}H)_2]$ (Figure 5.19) when compared to the extraction of chloride. The $pH_{0.5}$ value for nickel in the presence of sulfate (>5.5) is higher than that in the presence of chloride (4.3), suggesting that sulfuric acid will strip nickel from **L18** more efficiently than hydrochloric acid. As there is very little nickel in the organic phase the sulfate loading curve is very similar to that of the free ligand shown previously in Figure 5.17, with both curves having a $pH_{0.5}$ of approximately 2.8 for sulfate loading.
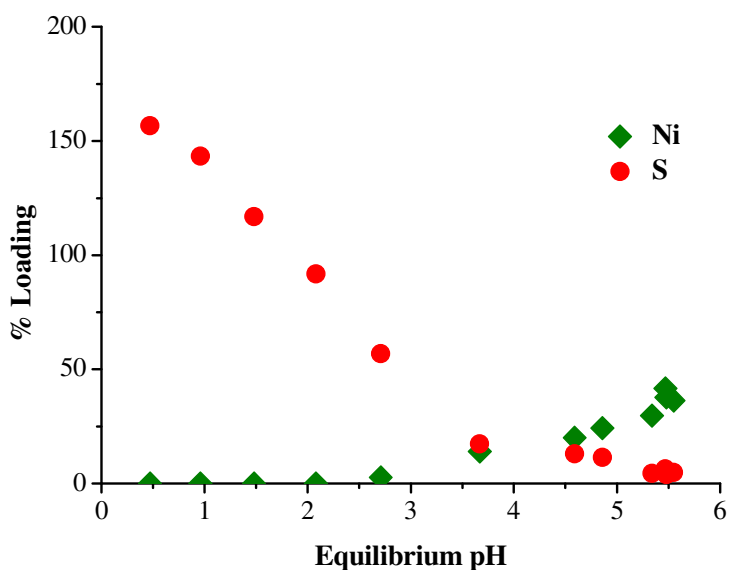

Figure 5.19: Nickel (green) and sulfate (red) loading of the organic phase when a 0.01 M chloroform solution of $[Ni(\mathbf{L18}\text{-}H)_2]$ is contacted with 0.8 M aqueous sulfate solutions of various pH values. 100% nickel loading is based on a molar ratio of 1Ni : 2**L18**, and 100% sulfate loading is based on a molar ratio of SO_4: **L18**.

Overall, the solvent extraction experiments using copper- and nickel-only complexes of **L18** show the selectivity of the ligand for CuCl$_2$, but also that chloride loading is more favourable than sulfate loading. This is to be expected, as the salen ligands discussed previously show chloride over sulfate selectivity, despite having a preorganised binding pocket.[22, 23] The Hofmeister bias[1] also dictates that chloride anions will be extracted much more easily than sulfate anions, and this effect is amplified by the formation of [Cu**L**Cl$_2$] complexes which favour chloride loading. The ligands are also selective for Cu^{II} against Ni^{II}, and this is predicted by the Irving Williams order.[28]

5.4.3 Anion Selectivity of [Cu(L20-H)$_2$]

Proof-of-concept experiments described in Chapter 4 showed that the 5-substituted ligand **L20** did not bind copper in the 1:1 **L**:CuCl$_2$ ratio observed for the 3-substituted ligands **L17** and **L18**. This observation was confirmed by the more detailed solvent extraction study involving **L20** carried out in this chapter.

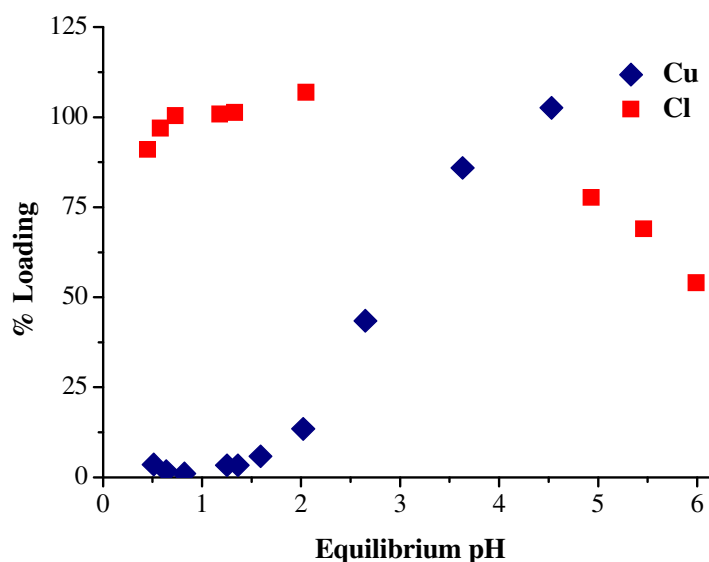**Figure 5.20:** Copper (blue) and chloride (red) loading of the organic phase when a 0.01 M chloroform solution of [Cu(**L20**-H)$_2$] is contacted with 0.8 M aqueous chloride solutions of various pH values. 100% copper loading is based on a molar ratio of 1Cu : 2**L20**, and 100% chloride loading is based on a molar ratio of 2Cl : 2**L20**.

The copper and chloride loadings for [Cu(**L20**-H)$_2$] in the presence of HCl are displayed in Figure 5.20. Chloride loading reaches 100% and stays at this maximum value, showing that CuCl$_2$ is likely bound in a 2:1 **L**:CuCl$_2$ ratio, with a maximum metal salt loading of ~85% at pH = 4. The pH$_{0.5}$ for chloride loading is slightly higher than for **L18**, in the region of pH 6-7 and the pH$_{0.5}$ value for copper uptake is higher (2.8) than for **L18**, which is expected due to the unfavourable steric effects of the 3-*t*-butyl group discussed previously in Chapters 2 and 3. Although measured under different conditions, the pH$_{0.5}$ for copper uptake of 2.8 is similar to that measured for copper loading by **L3** (pH$_{0.5}$ = 2.6), which also has a 3-*t*-butyl group.

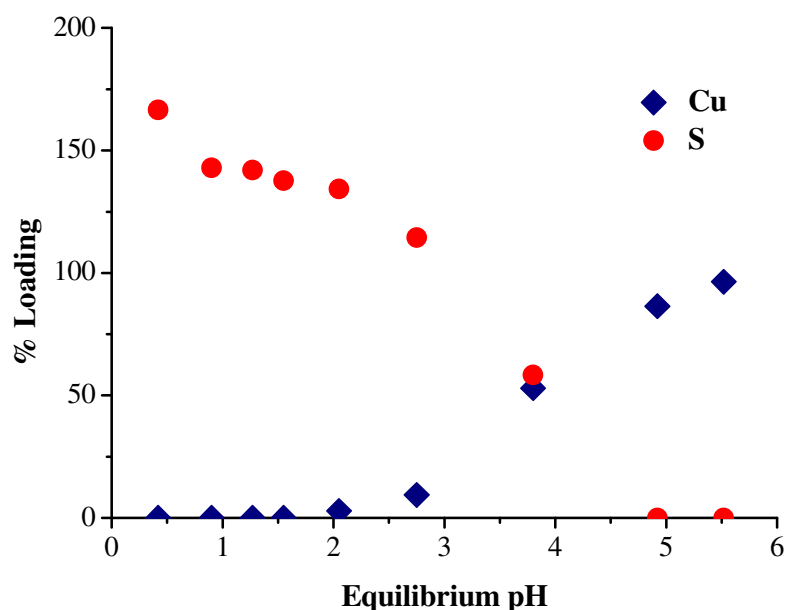**Figure 5.21:** Copper (blue) and sulfate (red) loading of the organic phase when a 0.01 M chloroform solution of [Cu(**L20**-H)$_2$] is contacted with 0.8 M aqueous sulfate solutions of various pH values. 100% copper loading is based on a molar ratio of 1Cu : 2**L20**, and 100% sulfate loading is based on a molar ratio of SO$_4$: **L20**.

Comparison with the analogous sulfate experiment (Figure 5.21) reveals similar trends to those seen with [Cu(**L18**-H)$_2$]. Again, copper stripping is more efficient when sulfuric acid is used compared to hydrochloric acid and the pH$_{0.5}$ for copper uptake in the presence of sulfate is 3.7, nearly a whole pH unit higher than the chloride value. The curve is also longer and flatter than the chloride curve. Sulfate uptake is again poorer than chloride, as expected, but the pH$_{0.5}$ for sulfate uptake

(4.0) is higher than the value for [Cu(**L18**-H)$_2$] (3.8). This is despite the probable lack of Cu···anion interactions in metal salt complexes of **L20**. Attempts to confirm this by measuring the sulfate loading of **L20** itself were hampered by the separation of a viscous third phase during solvent extraction experiments.

The results suggest that, like **L18**, **L20** is selective for CuCl$_2$ against CuSO$_4$. However, the binding of copper in these assemblies is less favourable for **L20,** which indicates that **L18** is a stronger cation binder due to the steric influence of the 3-*t*-butyl group in **L20**. **L20** appears to be a slightly better anion binder than **L18**, but this effect is negligible when compared to the destabilisation of cation binding.

5.4.4 Anion Selectivity of [Ni(L20-H)$_2$]

The extent of nickel stripping from [Ni(**L20**-H)$_2$] is again dependent on the anion involved. In the presence of high chloride concentration the pH$_{0.5}$ for nickel uptake in the organic phase is *ca.* 5.5 (Figure 5.22) whilst in the presence of sulfate it could not be recorded, as loading values did not reach above 20% up to pH ~ 5.5 (Figure 5.23). In all the studied examples in this section the cation is stripped more efficiently by sulfuric acid than hydrochloric acid, indicating that the mechanism of cation stripping involves the anion and possibly the anion binding site.

pH dependence of chloride loading by [Ni(**L20**-H)$_2$] is similar to that of the copper complex, and this is to be expected as the anion binding site is located in the 5-position, precluding any metal-anion interactions. Chloride loading has a pH$_{0.5}$ > 6 and does not exceed 100% in the pH range 0-6.
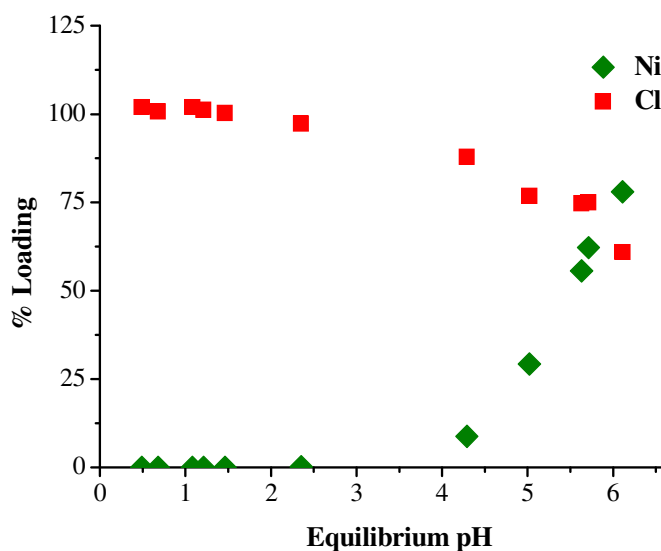
Figure 5.22: Nickel (green) and chloride (red) loading of the organic phase when a 0.01 M chloroform solution of [Ni(**L20**-H)$_2$] is contacted with 0.8 M aqueous chloride solutions of various pH values. 100% nickel loading is based on a molar ratio of 1Ni : 2**L20**, and 100% chloride loading is based on a molar ratio of 2Cl : 2**L20**.

As already discussed, nickel is stripped very easily from [Ni(**L20**-H)$_2$] by sulfuric acid. As might be expected, the sulfate loading curve has a similar profile to that for [Cu(**L20**-H)$_2$], because the sulfate uptake is essentially by the free ligand.

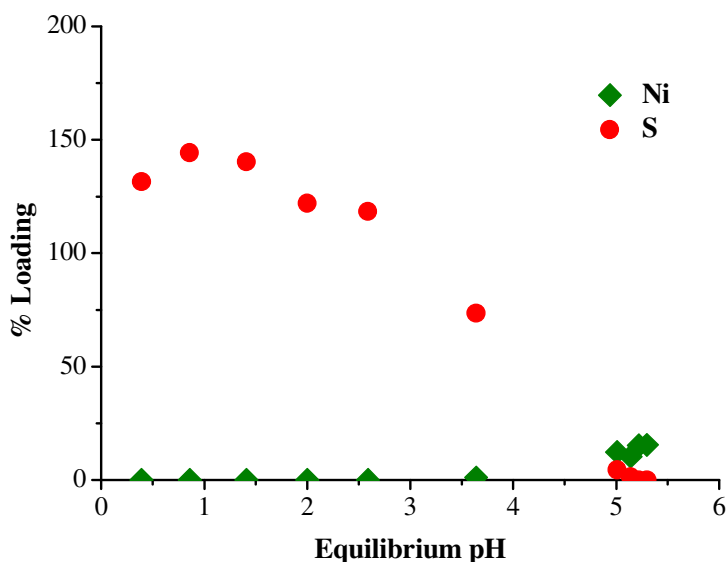**Figure 5.23:** Nickel (green) and sulfate (red) loading of the organic phase when a 0.01 M chloroform solution of [Ni(**L20**-H)$_2$] is contacted with 0.8 M aqueous sulfate solutions of various pH values. 100% nickel loading is based on a molar ratio of 1Ni : 2**L20**, and 100% sulfate loading is based on a molar ratio of SO$_4$: **L20**.

It appears that by locating the anion binding site in the 5-position (**L20**), rather than the 3-position (**L18**), that the cation and anion binding sites are truly separate, and the cation has no influence on anion binding. A comparison of the chloride loading curves for [Cu(**L20**-H)$_2$], [Ni(**L20**-H)$_2$] and **L20** illustrates this (Figure 5.23).
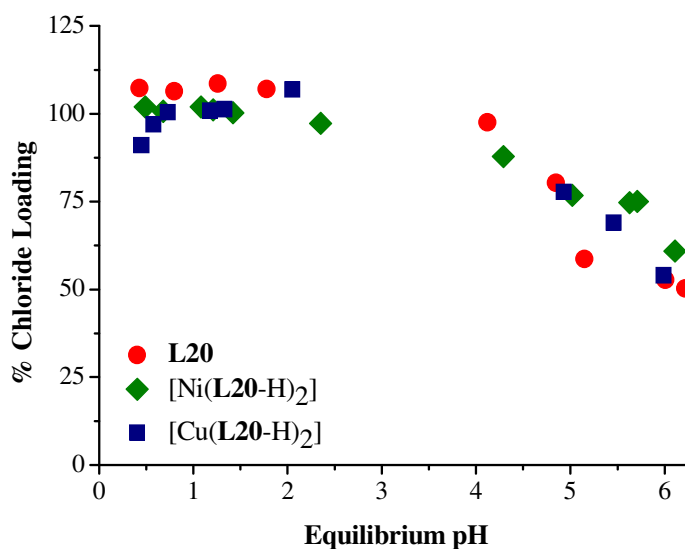
Figure 5.23: Chloride loading of the organic phase when a 0.01 M chloroform solution of **L20** (red) [Cu(**L20**-H)$_2$] (blue) or [Ni(**L20**-H)$_2$] (green) is contacted with 0.8 M aqueous chloride solutions of various pH values. 100% chloride loading is based on a molar ratio of 2Cl: 2**L20**.

The curves are, barring experimental error, superimposable, and in all cases have a pH$_{0.5}$ value greater than 6. A similar comparison of the sulfate loading curves of [Cu(**L20**-H)$_2$] and [Ni(**L20**-H)$_2$] shows the same feature, although this could not be wholly confirmed due to the problems encountered in measuring the sulfate loading of **L20**.

5.4.5   Summary

Solvent extraction has proved to be a very useful tool in the examination of the anion selectivity of ligands **L18** and **L20**. A summary of the pH$_{0.5}$ data gathered from these extractions is presented in Table 5.5.

Compound	Anion	$pH_{0.5}$ Metal	$pH_{0.5}$ Anion
[Cu(**L18**-H)$_2$]	Cl$^-$	0.6	5.8
[Cu(**L18**-H)$_2$]	SO$_4^{2-}$	2.0	3.8
[Ni(**L18**-H)$_2$]	Cl$^-$	4.3	5.3
[Ni(**L18**-H)$_2$]	SO$_4^{2-}$	>5.5[a]	2.8
L18	SO$_4^{2-}$	n/a	2.8
[Cu(**L20**-H)$_2$]	Cl$^-$	2.8	>6.0[a]
[Cu(**L20**-H)$_2$]	SO$_4^{2-}$	3.7	4.0
[Ni(**L20**-H)$_2$]	Cl$^-$	5.5	>6.0[a]
[Ni(**L20**-H)$_2$]	SO$_4^{2-}$	>>5.5[a]	4.0
L20	Cl$^-$	n/a	>6.0[a]
L20	SO$_4^{2-}$	n/a	n/a[b]

[a]Approximate values as higher pH values could not be reached.

[b]Could not be measured due to precipitation.

Table 5.5: $pH_{0.5}$ values for 50% loading of metal cation M^{II} and of anions when 0.01 M chloroform solutions of [M(**L**-H)$_2$] are contacted with 0.8 M aqueous solutions of NaCl or Na$_2$SO$_4$ at varying pH.

There are many conclusions that can be drawn from the work. It has been shown unequivocally that **L18** is a better extractant for copper and nickel than **L20**, with the 3-*t*-butyl group of **L20** destabilising its copper and nickel complexes by steric clashes within the *pseudo*macrocyclic H-bonding motif, as described in detail in Chapter 3. Both **L18** and **L20** extract copper at low pH values and are better extractants for copper(II) than nickel(II), a result which was expected and can be explained by the Irving Williams order.[28]

In the extraction of anions an overall selectivity trend has been established, with chloride being loaded at higher pH values than sulfate, indicating selectivity for chloride in all systems. This is again expected, being a consequence of the Hofmeister bias[1] (Chapter 1). **L20** is a slightly better anion extractant than **L18**, having higher $pH_{0.5}$ values for both sulfate and chloride loading. This is despite favourable metal-anion interactions in the extraction of CuCl$_2$ and CuSO$_4$ by **L18**, with solvent extraction showing its versatility by identifying both the presence and

the lack of these interactions. Incorporation of the anion binding site in the 5-position means it is too distant from the cation binding site for these interactions to occur. Despite the better anion extraction properties of **L20**, **L18** was thought to be the ligand most suited to commercial application as a metal salt extractant, due to:

- the solubility of loaded and unloaded reagents in organic media,
- its ability to extract metal cations at lower pH values, and
- the highly efficient extraction of $CuCl_2$.

For these reasons, **L18** was selected for further study.

5.5   Cation Selectivity by Solvent Extraction

The success of any extractant depends on its selectivity. Phenolic oximes are known to be selective for Cu^{II} against Fe^{III} and other base metals,[29, 30] which was one of the main reasons for basing the metal salt extractants synthesised in this thesis on a salicylaldoxime scaffold. To assess the impact on cation selectivity of the addition of the anion binding site, further solvent extraction experiments were carried out with **L18**, the extractant which had shown the most potential for commercial development.

5.5.1   Loading of Metals by L18 from Sulfate Media

To determine the cation selectivity of **L18** with minimal influence of the anion, extractions were carried out under the same conditions as those used to determine the copper binding strengths of **L1-L9** in Chapter 2, but using the sulfates and chlorides of manganese(II), iron(III), cobalt(II), nickel(II), copper(II) and zinc(II). This allowed the generation of S-curves for the loading of each metal, which provide information on the cation selectivity of the ligand (Section 5.7.6).
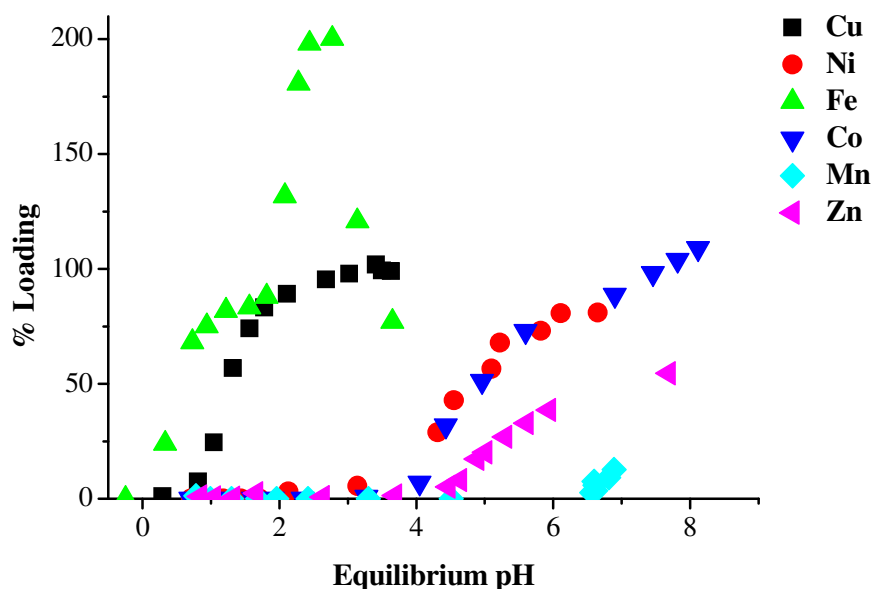
Figure 5.24: Extraction pH-profiles for loading of base metals by 0.01 M chloroform solutions of **L18** from equal volumes of 0.01 M aqueous solutions of metal sulfates. 100% metal loading based on a 1M:2**L18** ratio.

The cation selectivity of **L18** in the extraction of base metals from sulfate solutions, under the conditions shown in Figure 5.24, is (with $pH_{0.5}$ in brackets):

$$Fe^{III} (0.5) > Cu^{II} (1.3) > Ni^{II} (5.0) = Co^{II/III} (5.0) > Zn^{II} (7.6) > Mn^{II} (n/a)$$
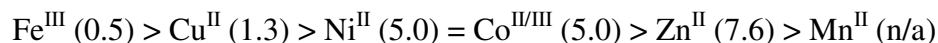
This potentially poses a problem should the ligand be developed for use as a copper extractant, as high Cu^{II}/Fe^{III} selectivity is one of the main requirements for industrial use.[29, 30] Iron loading occurs in two stages: a step in the loading profile at approximately 70% loading indicates the formation of a 3:1 $L:Fe^{III}$ complex at pH<2, and a second peak at 200% describes a 1:1 $L:Fe^{III}$ complex at a pH of approximately 2.5. At higher pH values, the loading values decrease due to precipitation of Fe^{III} from the aqueous phase as iron oxyhydroxides.[15] This result is very significant, potentially limiting commercial application of **L18** and its analogues.

Other interesting features of the loading profiles include the extraction of cobalt, which also occurs in two stages with a step at ~70% indicating formation of 3:1 $L:Co^{III}$ complexes in the organic phase. The oxidation of Co^{II} to Co^{III} during

extraction by phenolic oximes is well documented[29] and appears to be occurring in the experiments.   At higher pH values further loading occurs by an unknown mechanism and reaches approximately 120%. Nickel loading follows a very similar profile to that of cobalt but only reaches 75% loading, zinc loading only reaches approximately 50% at pH 8 and very little manganese extraction is observed.

5.5.2   Loading of Metals by L18 from Chloride Media

When chloride is used as counter ion rather than sulfate, there are some marked changes in the pH loading profiles for the base metals investigated (Figure 5.25).
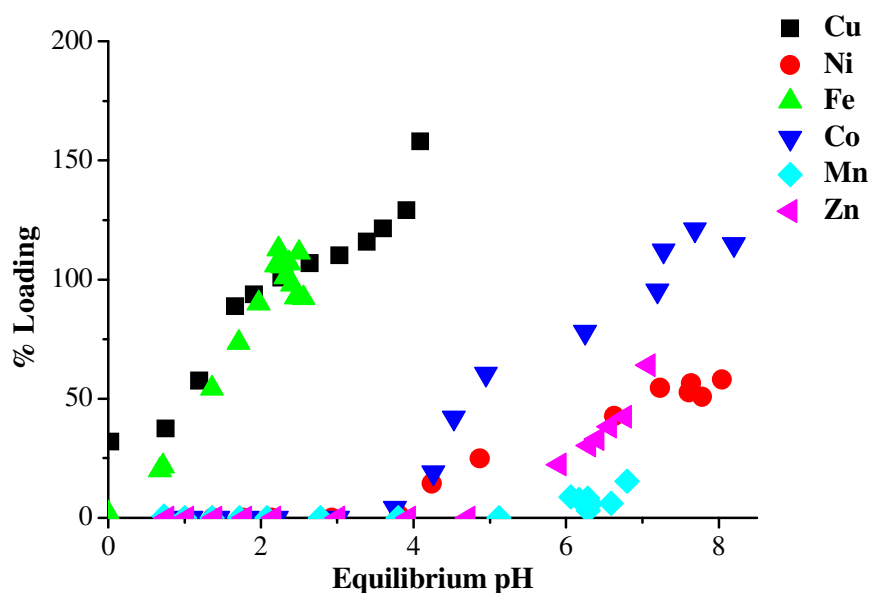
Figure 5.25: Extraction pH-profiles for loading of base metals by 0.01 M chloroform solutions of **L18** from equal volumes of 0.01 M aqueous solutions of metal chlorides. 100% metal loading based on a 1M:2**L18** ratio.

The Cu^{II}/Fe^{III} selectivity order has been reversed, although the $pH_{0.5}$ values are very similar, and the overall selectivity trend is:

$$Cu^{II} (1.1) > Fe^{III} (1.3) > Co^{II/III} (4.8) > Ni^{II} (7.5) \sim Zn^{II} (7.6) > Mn^{II} (n/a)$$
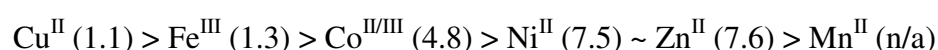
Fe^{III} loading does not reach higher than 100%, indicating formation of a 2:1 L:Fe^{III} complex which is assumed to have associated anions to balance the charge. Cobalt loading again shows formation of a 3:1 L:Co^{III} complex at lower pH and higher loading at higher pH values, and this is independent of the anion. An interesting feature is the apparent depression of nickel loading when compared to the sulfate case, with a difference in $pH_{0.5}$ of 2.5. This is the opposite to the trend seen in the anion selectivity extractions of Section 5.4, and illustrates the need to further assess the cation selectivity of the ligand. A summary of all the $pH_{0.5}$ values for metal loading is given in Table 5.6.

| Metal Salt	$pH_{0.5}$ for M Loading
$CuCl_2$	1.1
$CuSO_4$	1.3
$NiCl_2$	~7.5
$NiSO_4$	5.0
$CoCl_2$	4.8
$CoSO_4$	4.9
$ZnCl_2$	6.9
$ZnSO_4$	7.6
$FeCl_2$	1.3
$FeSO_4$	0.5, 2.2
$MnCl_2$	n/a
$MnSO_4$	n/a

Table 5.6: $pH_{0.5}$ values for loading of base metals by 0.01 M chloroform solutions of **L18** from equal volumes of 0.01 M aqueous solutions of metal sulfates or chlorides. 100% metal loading based on a 1M:2**L18** ratio.

5.5.3 Competitive Extractions

To confirm the selectivity orders described above, solvent extraction experiments were carried out with aqueous feeds containing a mixture of the metals Mn, Fe, Co,

Ni, Cu and Zn, with the concentration of each metal constant (Section 5.7.6.1). Extraction from metal sulfate solutions and metal chloride solutions was studied, and the results of extraction from the mixed metal sulfate feed are displayed in Figure 5.26.

Figure 5.26: Loading of base metals by 0.01 M chloroform solutions of **L18** from equal volumes of an aqueous solution containing each metal sulfate shown at a concentration of 0.01 M. 100% metal loading based on a 1M:2**L18** ratio.

Iron is the dominantly extracted metal, as expected from the S-curves and $pH_{0.5}$ values measured in Section 5.5.1. Small amounts of copper are also loaded, but copper uptake only starts to become significant in the pH range where iron is precipitated from aqueous solution (>2.5), meaning that all the iron remaining in the aqueous phase is being extracted by **L18**. This can be confirmed by comparing the iron loading S-curve taken from the mixed metal experiment with the analogous curve from the extraction experiment in Section 5.5.1, where the aqueous phase contained only iron (Figure 5.27).
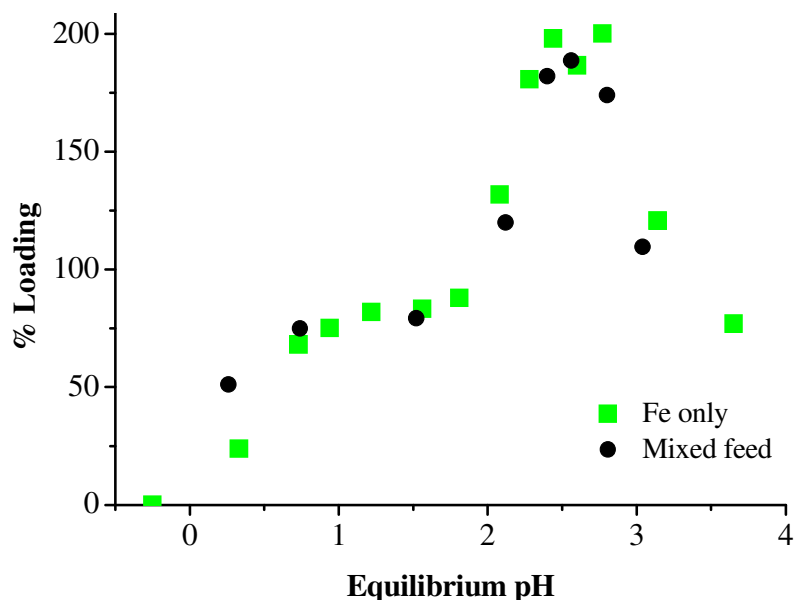
Figure 5.27: Comparison of iron loading by **L18** from a mixed feed solution and an iron-only feed solution, under the conditions used in extractions shown in Figures 5.24 and 5.26.

The curves are very similar, with iron loading from the mixed metal solution only slightly lower than the values obtained from the iron-only feed. As no other metals are extracted, this confirms that the ligand is selective for iron against the other base metals studied when extracting from sulfate solutions without an excess of anion.

When investigating the selectivity of metal binding from chloride solutions, the results are quite different. Section 5.5.2 described the similarity of the $pH_{0.5}$ values for iron and copper, and these similarities are reflected in the loading behaviour of **L18** (Figure 5.27, overleaf).

In the pH region (0.5-2.0) expected for commercial feeds, both iron and copper are loaded to approximately similar levels, but as the pH increases it is copper which is favoured, although iron loading does still occur. No other metals are loaded, showing that the ligand is selective for copper and iron over other base metals. Copper loading from chloride solutions is enhanced by increasing the anion concentration (Chapter 4), so similar experiments were carried out to investigate the effect of anion concentration of metal selectivity.
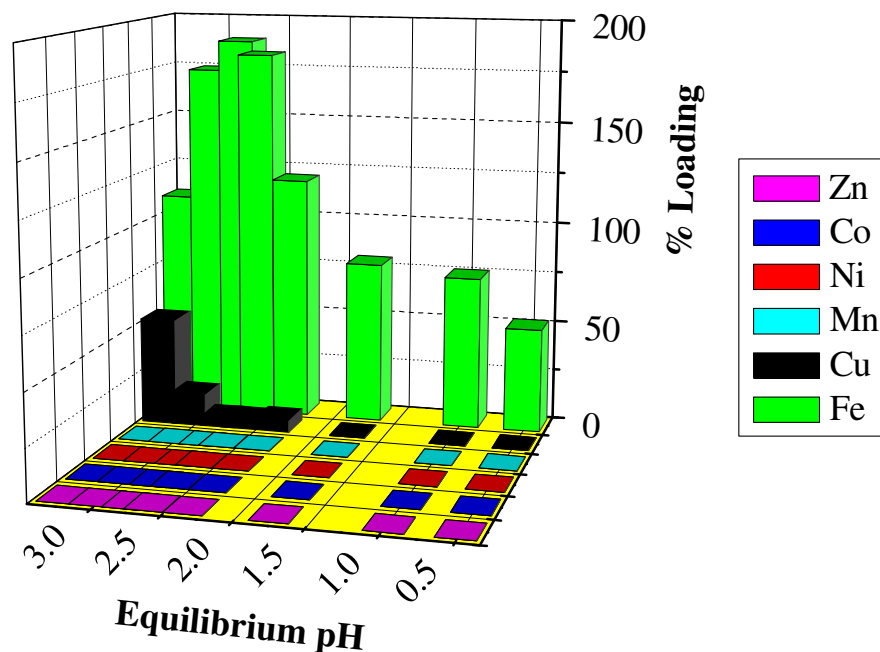
Figure 5.27: Loading of base metals by 0.01 M chloroform solutions of **L18** from equal volumes of an aqueous solution containing each metal chloride shown at a concentration of 0.01 M. 100% metal loading based on a 1M:2**L18** ratio.

5.5.4   Metal Loading by L18 from Excess Sulfate Media

As Cu^{II}/Fe^{III} selectivity is the most commercially significant and as these metal cations are the only two extracted by **L18** from a mixed metal feed, S-curves were determined for these two metal ions only. A 0.01 M solution of **L18** in chloroform was mixed with an aqueous feed with a concentration of 0.01 M of the appropriate metal cation, but with a sulfate concentration of 0.8 M. The pH was varied by using addition of Na_2SO_4/H_2SO_4 and careful control of the total sulfate concentration was ensured throughout. The S-curves can be seen in Figure 5.28.

Figure 5.28: pH-profiles for loading of Cu^{II} (black) and Fe^{III} (green) by 0.01 M chloroform solutions of **L18** from equal volumes of aqueous solutions with metal concentrations of 0.01 M and sulfate concentrations of 0.8 M. 100% metal loading based on a 1M:2**L18** ratio.

The effect of the increased sulfate concentration is to increase slightly the selectivity of **L18** for Fe^{III}: the $pH_{0.5}$ for Fe^{III} loading of 0.3 is slightly lower for feeds with no added sulfate, whilst the $pH_{0.5}$ for Cu^{II} loading of 1.5 is slightly increased. Previous examples have observed an increase in $pH_{0.5}$ for Cu^{II} loading by analogous phenolic oxime extractants when sulfate concentration in the aqueous phase is increased,[31] but the *decrease* in $pH_{0.5}$ for Fe^{III} loading indicates that the metal salt complex being formed involves some kind of cooperative interaction between the Fe^{III} cation and SO_4^{2-} anion. The other notable effect of increasing sulfate concentration is that plateaux at the loading stoichiometry of $3Fe^{III}$:1**L18** persists to a higher pH, again indicating that the complex formed involves a favourable interaction with the sulfate anion.

As the increase in sulfate concentration appears to favour Fe^{III} extraction and disfavour Cu^{II} extraction, it was expected that, when extracting from a mixed metal feed, **L18** would favour Fe^{III} uptake. This is confirmed by the data in Figure 5.29 which shows that Fe^{III} is extracted preferentially, with Cu^{II} extraction only occurring at pH values high enough for iron to be partially precipitated from the feed.

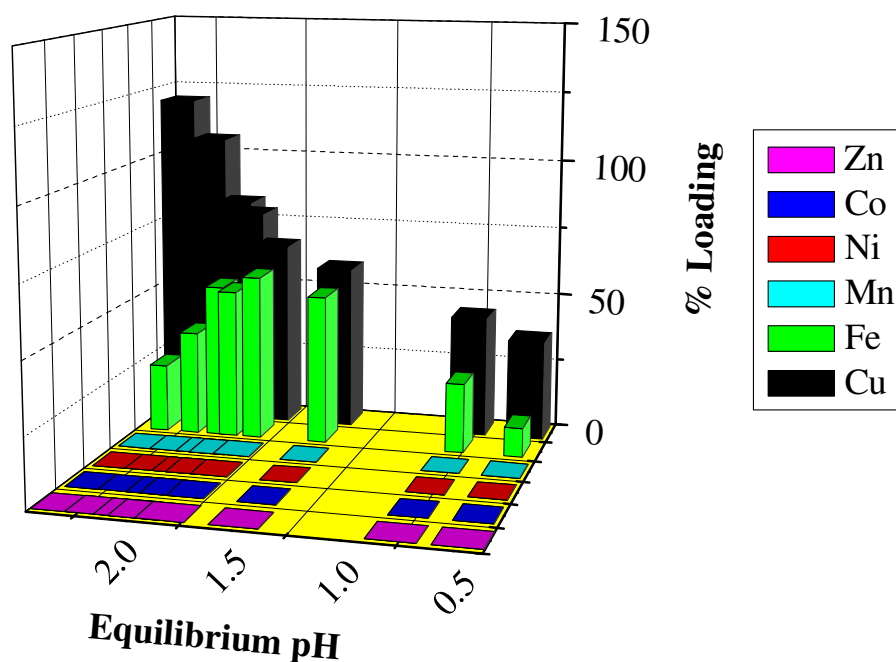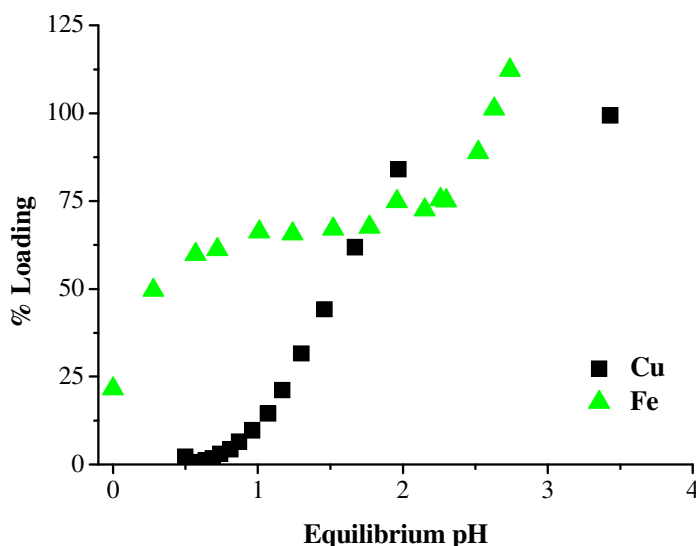**Figure 5.29:** Loading of base metals by 0.01 M chloroform solutions of **L18** from equal volumes of an aqueous solution containing each metal sulfate shown at a concentration of 0.01 M, with sulfate concentration adjusted to 0.8 M by addition of Na_2SO_4/H_2SO_4. 100% metal loading based on a 1M:2**L18** ratio.

5.5.5 Metal Loading by L18 from Excess Chloride Media

Similar extraction experiments were carried out to determine the effect of excess chloride concentration on the extractive efficacy of **L18**. This has been briefly investigated previously, in Chapter 4, and it was concluded that increasing chloride concentration increased the extractive efficacy of **L18** for copper. A 0.01 M solution of **L18** in chloroform was mixed with an aqueous feed with a concentration of 0.01 M of the appropriate metal cation, but with a chloride concentration of 0.8 M, and pH adjusted by HCl/NaCl (Figure 5.30).
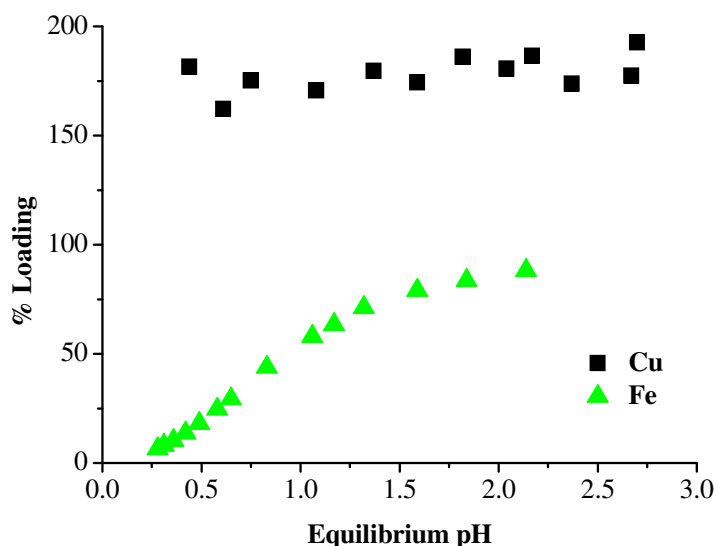
Figure 5.30: pH-profiles for loading of Cu^{II} (black) and Fe^{III} (green) by 0.01 M chloroform solutions of **L18** from equal volumes of aqueous solutions with metal concentrations of 0.01 M and chloride concentrations of 0.8 M. 100% metal loading based on a 1M:2**L18** ratio.

The S-curve for iron loading from chloride media also shows an improvement when the chloride anion is in excess. Loading reaches approximately 90% at pH ~ 2 and the $pH_{0.5}$ for Fe^{III} loading is 0.9, compared to the value of 1.3 measured previously with equimolar amounts of chloride present. This again indicates that a cooperative binding mechanism exists in the extraction of Fe^{III} and Cl^-. Comparing the S-curves suggests that **L18** may be selective for Cu^{II} over Fe^{III} when extracting from concentrated chloride media. This was investigated by contacting a 0.01 M chloroform solution of **L18** with a mixed metal feed (each metal has a concentration of 0.01 M) with 0.8 M chloride concentration. The results are displayed in Figure 5.31, and show that **L18** is not selective for $CuCl_2$.

Significant quantities of Fe^{III} are extracted alongside Cu^{II}, which means that **L18** will not be a suitable extractant for $CuCl_2$ from a high $[Cl^-]$ feed. A final extraction experiment was carried out to determine cation selectivity from an aqueous phase containing both chloride and sulfate in excess concentration.
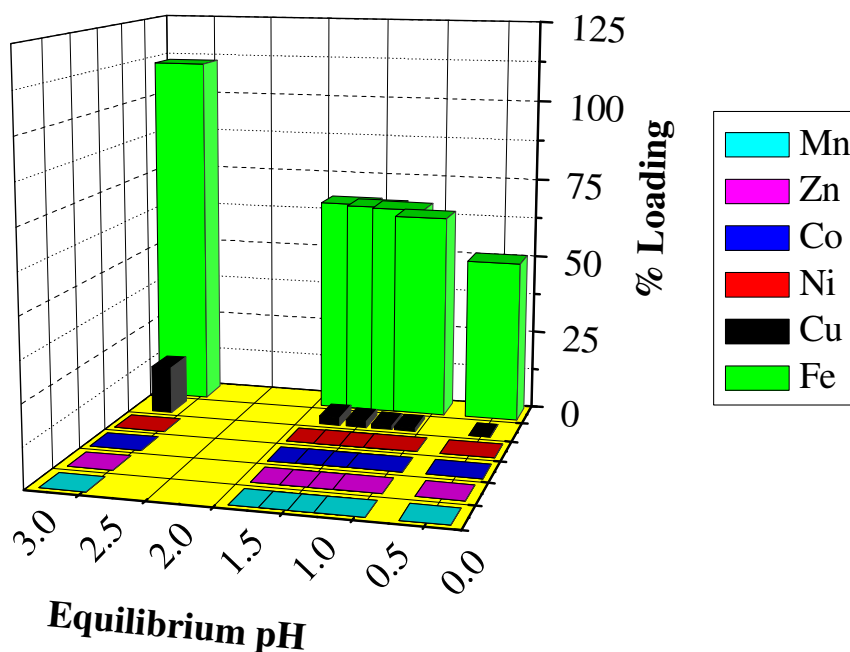
Figure 5.31: Loading of base metals by 0.01 M chloroform solutions of **L18** from equal volumes of an aqueous solution containing each metal chloride shown at a concentration of 0.01 M, with chloride concentration adjusted to 0.8 M with NaCl/HCl. 100% metal loading based on a 1M:2**L18** ratio.

5.5.6   Metal Loading by L18 from Excess Mixed-Anion Media

To ensure equal concentrations of chloride and sulfate anions in the feed solution, pH was adjusted by HCl/NaCl *and* H_2SO_4/Na_2SO_4 solutions, giving anion concentrations of 0.4 M each and a total ionic strength of 0.8 M. Metal loadings are displayed in Figure 5.32.

Again it is clear that **L18** is not selective for either Cu^{II} or Fe^{III}, but extracts a mixture of both metals. Cu^{II} is favoured slightly, with loadings of approximately double that of Fe^{III} over the pH range, but it seems the selectivity problem will persist while Fe^{III} is present in the aqueous phase.
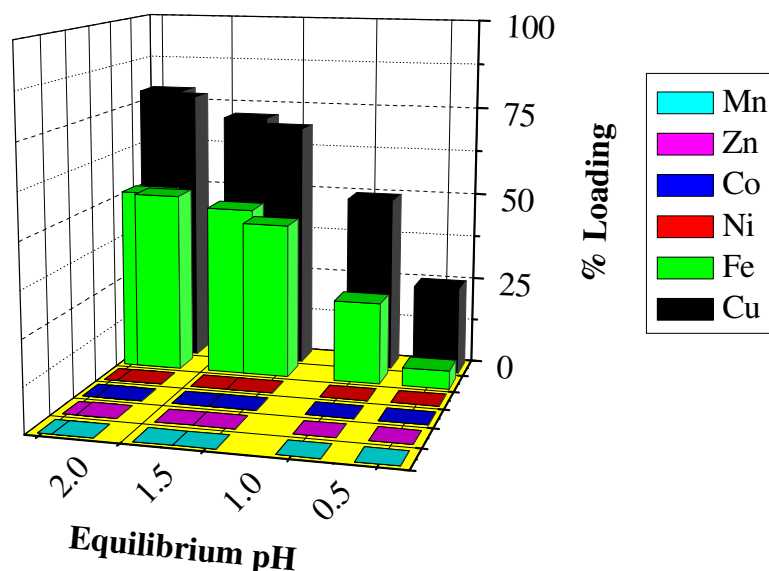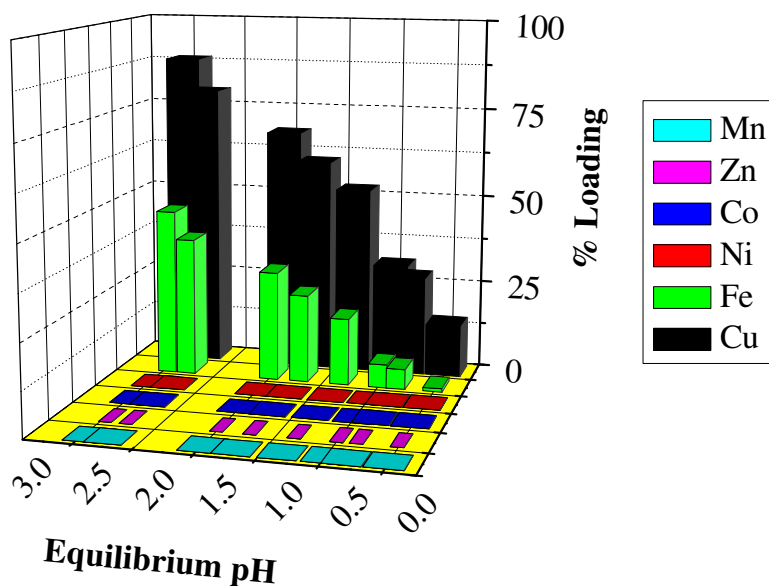
Figure 5.32: Loading of base metals by 0.01 M chloroform solutions of **L18** from equal volumes of an aqueous solution containing each metal shown at a concentration of 0.01 M, with chloride concentration adjusted to 0.4 M with NaCl/HCl and sulfate concentration adjusted to 0.4 M by addition of Na_2SO_4/H_2SO_4, giving a total ionic strength of 0.8 M. 100% metal loading based on a 1M:2**L18** ratio.

5.6   Conclusions and Further Work

Titration of metal-only complexes with anions has been used successfully in solvent extraction experiments to determine the pH loading profiles of both cations and anions by **L18** and **L20** for the sulfates and chlorides of copper and nickel. **L18** extracts both $CuCl_2$ and $CuSO_4$ effectively, but the cation binding of **L20** is adversely affected by its 3-*t*-butyl group for the reasons discussed in Chapters 2 and 3. Nickel-loading by both ligands is less favourable than copper, and occurs over higher pH ranges, showing the selectivity for copper predicted by the Irving-Williams order, with **L20** again less effective than **L18**. In all cases chloride is extracted to a higher pH-range than sulfate. This selectivity for chloride is to be expected as a consequence of the Hofmeister bias.

The solid state structures of copper salt complexes of **L17**, the piperidinomethyl substituted analogue of **L18**, illustrate the importance of cation-anion interactions in metal salt extraction. Such interactions are observed in all the structures obtained.

The potential for commercial application of **L18** as a highly efficient $CuCl_2$ extractant led to further experiments to ascertain its cation selectivity over a wider range of base metals. Selectivity was greatly affected by the anion in the aqueous feed, with Fe^{III} extracted preferentially in the presence of sulfate and a mixture of Fe^{III} and Cu^{II} extracted in the presence of chloride or a mixture of the two. This underlines the importance of cation-anion interactions during the extraction of metal salts. Co-extraction of iron poses a real problem which must be solved if analogues of **L18** are to find commercial application, particularly if an oxidative ferric chloride leach is employed.

Implications of the introduction of anion binding groups on the coordination chemistry of salicylaldoximes are considered further in the final chapter of this thesis.

5.7   Experimental

5.7.1   Chemicals and Instrumentation

All solvents and reagents were used as received from Aldrich, Fisher, Fluorochem and Acros. ^{1}H and ^{13}C NMR were obtained using a Bruker AC250 spectrometer at ambient temperature. Chemical shifts (δ) are reported in parts per million (ppm) relative to internal standards. Fast atom bombardment mass spectrometry was carried out using a Kratos MS50TC spectrometer with a 3-nitrobenzyl alcohol (NOBA) or thioglycerol matrix. Analytical data was obtained on a CE-440 Elemental Analyser by the University of Edinburgh Microanalytical Service. ICP-OES analysis was carried out using a Perkin Elmer Optima 5300DV spectrometer. The measurement of pH was carried out using a Fisher Scientific AR50 pH meter.

5.7.2   Metal-Only Complex Synthesis

"Metal-Only" Complex Synthesis, General Procedure.   Stoichiometric amounts of the ligand and appropriate metal acetate were mixed in methanol (150 ml) for 72 h.   The solvent was removed *in vacuo*, the complexes dissolved in DCM (150 ml), washed with aqueous NH_3 (3 x 150ml, pH 9) and the organic phase dried over magnesium sulfate.   The solvent was removed *in vacuo* to give the crude product [M(L-H)$_2$].   Only the complexes of **L17** could be purified by crystallisation, as the dihexylaminomethyl-substituted reagents **L18** and **L20** yielded amorphous complexes, and those of **L19** were poorly soluble.   For this reason CHN analyses were poor in some cases, and complexes of **L18** and **L20** were used as synthesised in extraction experiments.

[Ni(L17-H)$_2$].   Ni(OAc)$_2$.4H$_2$O (0.45 g, 1.8 mmol) and **L17** (1.03 g, 3.6 mmol) yielded a green crystalline crude product from the method above, which was recrystallised from hexane to give [Ni(**L17**-H)$_2$] (0.41 g, 37 %).   (Anal. Calc. for $C_{34}H_{50}N_4O_4Ni$: C, 64.1; H, 7.9; N, 8.8. Found: C, 64.1; H, 7.8; N, 8.5 %); $\tilde{v}_{max}$/cm^{-1} (CHCl$_3$) 3075br (NOH), 2940 (C-H), 1623 (C=N), 1031 (C-N); ^{1}H NMR (250 MHz, CDCl$_3$): δ_H (ppm) 1.15 (s, 9H, C(CH_3)$_3$), 1.45 (m, 2H, NCH$_2$CH$_2$CH_2), 1.50 (m, 4H, 2 x NCH$_2$CH_2CH$_2$), 2.15 (m, 4H, 2 x NCH_2CH$_2$CH$_2$), 3.22 (s, 2H, ArCH_2N), 6.90 (s, 1H, ArH), 6.95 (s, 1H, ArH), 7.78 (s, 1H, ArCHN); ^{13}C NMR (63 MHz, CDCl$_3$) δ_C (ppm) 24.0 (1C, NCH$_2$CH$_2$**C**H$_2$), 25.0 (2C, 2 x NCH$_2$**C**H$_2$CH$_2$), 31.5 (3C, C(**C**H$_3$)$_3$), 33.5, (1C, **C**(CH$_3$)$_3$), 54.0 (2C, 2 x N**C**H$_2$CH$_2$CH$_2$), 58.0 (1C, Ar**C**H$_2$N), 115.8 (1C, aromatic **C**), 126.5 (1C, aromatic **C**H), 127.3 (1C, aromatic **C**), 132.0 (1C, aromatic **C**H), 138.4 (1C, aromatic **C**), 147.3, (1C, Ar**C**HN), 155.7 (1C, aromatic **C**); FABMS *m/z* 637 (MH$^+$).

[Cu(L17-H)$_2$].   Cu(OAc)$_2$.H$_2$O (0.35 g, 1.8 mmol) and **L17** (1.01 g, 3.5 mmol) yielded a brown microcrystalline crude product from the method above, which was recrystallised from hexane to give [Cu(**L17**-H)$_2$] (0.41 g, 37 %).   (Anal. Calc. for $C_{34}H_{50}N_4O_4Cu$: C, 63.6; H, 7.9; N, 8.7. Found: C, 63.8; H, 8.3; N, 7.3 %); $\tilde{v}_{max}$/cm^{-1}

(CHCl$_3$) 3125br (NOH), 2949 (C-H), 1624 (C=N), 1016 (C-N); FABMS *m/z* 642 (MH$^+$).

[Ni(L18-H)$_2$]. Ni(OAc)$_2$.4H$_2$O (0.46 g, 1.8 mmol) and **L18** (1.42 g, 3.6 mmol) yielded a waxy green solid from the method above, crude [Ni(**L18**-H)$_2$] (1.04 g, 68 %). (Anal. Calc. for C$_{48}$H$_{82}$N$_4$O$_4$Ni: C, 68.8; H, 9.9; N, 6.7. Found: C, 67.3; H, 10.1; N, 6.5 %); $\tilde{v}_{max}$/cm^{-1} (CHCl$_3$) 3180br (NOH), 2961 (C-H), 2935 (C-H), 1606 (C=N), 1006 (C-N); ^{1}H NMR (250 MHz, CDCl$_3$): δ_H (ppm) 0.80 (t, 6H, 2 x N(CH$_2$)$_5$CH_3), 1.20 (m, 21H, C(CH_3)$_3$ + 2 x (CH$_2$)$_2$C$_3$$H_6CH_3$), 1.40 (m, 4H, 2 x NCH$_2CH_2C_4H_9$), 2.36 (m, 4H, 2 x NC$H_2C_5H_{11}$), 3.40 (s, 2H, ArC$H_2$N), 6.22 (s, 1H, Ar$H$), 6.55 (s, 1H, Ar$H$), 7.18 (s, 1H, ArC$H$N); ^{13}C NMR (63 MHz, CDCl$_3$): δ_C (ppm) 13.5 (2C, 2 x N(CH$_2$)$_5$**C**H$_3$), 23.0 (2C, 2 x N(CH$_2$)$_4$**C**H$_2$CH$_3$), 25.0 (2C, 2 x N(CH$_2$)$_3$**C**H$_2$C$_2$H$_5$), 26.5 (2C, 2 x N(CH$_2$)$_2$**C**H$_2$C$_3$H$_7$), 32.0 (3C, C(**C**H$_3$)$_3$), 32.2 (2C, 2 x NCH$_2$**C**H$_2$C$_4$H$_9$), 33.0, (1C, **C**(CH$_3$)$_3$), 54.5 (2C, 2 x N**C**H$_2$C$_5$H$_{11}$), 58.5 (1C, Ar**C**H$_2$N), 115.4 (1C aromatic **C**H), 119.4 (1C aromatic **C**H), 125.3 (1C aromatic **C**), 129.9 (1C aromatic **C**), 134.3 (1C, aromatic **C**), 139.9 (1C, aromatic **C**), 154.1 (1C, Ar**C**HN); FABMS *m/z* 837 (MH$^+$).

[Cu(L18-H)$_2$]. Cu(OAc)$_2$.H$_2$O (0.41 g, 2.1 mmol) and **L18** (1.58 g, 4.1 mmol) yielded a solid brown product from the method above, crude [Cu(**L18**-H)$_2$] (1.42 g, 82 %). (Anal. Calc. for C$_{48}$H$_{82}$N$_4$O$_4$Cu: C, 68.4; H, 9.8; N, 6.7. Found: C, 66.5; H, 10.0; N, 6.8); $\tilde{v}_{max}$/cm^{-1} (CHCl$_3$) 3131br (NOH), 2962 (C-H), 2930 (C-H), 1622 (C=N), 1017 (C-N); FABMS *m/z* 842 (MH$^+$).

[Ni(L19-H)$_2$]. Ni(OAc)$_2$.4H$_2$O (0.45 g, 1.8 mmol) and **L19** (1.02 g, 3.5 mmol) yielded a green crude product from the method above, which was used without further purification (0.71 g, 62 %). (Anal. Calc. for C$_{34}$H$_{50}$N$_4$O$_4$Ni: C, 64.1; H, 7.9; N, 8.8. Found: C, 60.2; H, 7.1; N, 9.5 %); $\tilde{v}_{max}$/cm^{-1} (KBr) 3423br (NOH), 2937 (C-H), 1613 (C=N), 1037 (C-N); ^{1}H NMR and ^{13}C NMR unavailable due to low solubility; FABMS *m/z* 637 (MH$^+$).

[Cu(L19-H)$_2$]. Cu(OAc)$_2$.H$_2$O (0.35 g, 1.8 mmol) and **L19** (1.03 g, 3.6 mmol) yielded a brown crude product from the method above, which was used without further purification (0.67 g, 58 %). (Anal. Calc. for C$_{34}$H$_{50}$N$_4$O$_4$Cu: C, 63.6; H, 7.9; N, 8.7. Found: C, 65.9; H, 8.6; N, 7.7 %); $\tilde{v}_{max}$/cm^{-1} (nujol) 3418br (NOH), 2958 (C-H), 2940 (C-H), 1610 (C=N), 1027 (C-N); FABMS *m/z* 642 (MH$^+$).

[Ni(L20-H)$_2$]. Ni(OAc)$_2$.4H$_2$O (0.46 g, 1.8 mmol) and **L20** (1.37 g, 3.5 mmol) yielded a waxy green solid from the method above, crude [Ni(**L20**-H)$_2$] (1.18 g, 78 %). (Anal. Calc. for C$_{48}$H$_{82}$N$_4$O$_4$Ni: C, 68.8; H, 9.9; N, 6.7. Found: C, 66.9; H, 8.4; N, 7.5 %); $\tilde{v}_{max}$/cm^{-1} (KBr) 3410br (NOH), 2956 (C-H), 2929 (C-H), 1607 (C=N), 1028 (C-N); ^{1}H NMR and ^{13}C NMR unavailable due to low solubility; FABMS *m/z* 837 (MH$^+$).

[Cu(L20-H)$_2$]. Cu(OAc)$_2$.H$_2$O (0.36 g, 1.8 mmol) and **L20** (1.38 g, 3.5 mmol) yielded a solid brown product from the method above, crude [Cu(**L20**-H)$_2$] (1.29 g, 85 %). (Anal. Calc. for C$_{48}$H$_{82}$N$_4$O$_4$Cu: C, 68.4; H, 9.8; N, 6.7. Found: C, 67.1; H, 9.0; N, 6.4); $\tilde{v}_{max}$/cm^{-1} (KBr) 3411br (NOH), 2957 (C-H), 2928 (C-H), 1607 (C=N), 1028 (C-N); FABMS *m/z* 842 (MH$^+$).

5.7.3   Metal Salt Complex Synthesis

[Cu(L17)Cl$_2$]. CuCl$_2$.2H$_2$O (32.0 mg, 0.187 mmol) and **L17** (51.5 mg, 0.177 mmol) were mixed in methanol (20 ml) for 16 hr and the solvent removed *in vacuo* to give crude [Cu(**L17**)Cl$_2$] as a fine purple solid (70.5 mg, 94 %). Crystals suitable for analysis by X-ray diffraction were grown by diffusion of diethyl ether into a methanol solution. (Anal. Calc. for. For C$_{17}$H$_{26}$Cl$_2$CuN$_2$O$_2$.CH$_3$OH: C, 47.3; H, 6.6; N, 6.1. Found: C, 47.4; H, 6.4; N, 5.8 %). FABMS *m/z* 390 (M-Cl)$^+$.

[Cu(L17)Br$_2$]. CuBr$_2$ (42.2 mg, 0.189 mmol) and **L17** (51.6 mg, 0.177 mmol) were mixed in methanol (20 ml) for 16 hr and the solvent removed *in vacuo* to give crude [Cu(**L17**)Br$_2$] as a fine purple solid (85.1 mg, 94 %). Crystals suitable for analysis

by X-ray diffraction were grown by diffusion of diethyl ether into a methanol solution and were noticed to decompose to an amorphous solid after ~1 week. (Anal. Calc. for $C_{17}H_{26}Br_2CuN_2O_2.(C_4H_{10}O)_{0.5}$: C, 41.4; H, 5.7; N, 5.1. Found: C, 41.1; H, 5.5; N, 5.1 %). FABMS *m/z* 434 (M-Br)$^+$.

[Cu(L17)$_2$(NO$_3$)$_2$]. Cu(NO$_3$)$_2$.3H$_2$O (23.3 mg, 0.096 mmol) and **L17** (52.0 mg, 0.179 mmol) were mixed in methanol (20 ml) for 16 hr and the solvent removed *in vacuo* to give brown needles of [Cu(**L17**)$_2$(NO$_3$)$_2$] (71.8 mg, 99 %). Crystals suitable for analysis by X-ray diffraction were grown by diffusion of diethyl ether into a methanol solution. (Anal. Calc. for $C_{34}H_{52}CuN_6O_{10}$: C, 53.2; H, 6.8; N, 10.9. Found: C, 53.6; H, 6.9; N, 10.3 %). FABMS *m/z* 707 (M-NO$_3$)$^+$.

[Cu(L17)$_2$(BF$_4$)$_2$]. Cu(BF$_4$)$_2$.6H$_2$O (43.0 mg, 12.4 mmol) and **L17** (52.5 mg, 0.181 mmol) were mixed in methanol (20 ml) for 16 hr and the solvent removed *in vacuo* to give crude [Cu(**L17**)$_2$(BF$_4$)$_2$] as a green solid (73.2 mg, 99 %). Crystals suitable for analysis by X-ray diffraction were grown by diffusion of diethyl ether into a methanol solution. (Anal. Calc. for $C_{34}H_{52}B_2CuF_8N_4O_4$: C, 49.9; H, 6.4; N, 6.9. Found: C, 44.1; H, 5.7; N, 5.8 %). FABMS *m/z* 758 (M-BF$_4$)$^+$.

[Cu(L17)$_2$(CF$_3$CO$_2$)$_2$]. A solution of [Cu(**L17**-H)$_2$] (64.1 mg, 0.1 mmol) in chloroform (10 ml) was mixed with an aqueous solution (10 ml) of NaCF$_3$CO$_2$ (136.1 mg, 1 mmol) and CF$_3$CO$_2$H (0.02 M, aqueous) was added dropwise with stirring while not allowing the pH to drop below 3. After approximately 10 ml addition [Cu(**L17**)$_2$(CF$_3$CO$_2$)$_2$] precipitated as a light green solid which was collected by filtration (61 mg, 70%). Crystals suitable for analysis by X-ray diffraction were grown by diffusion of diethyl ether into a methanol solution. (Anal. Calc. for $C_{38}H_{52}CuF_6N_4O_8.H_2O$: C, 51.4; H, 6.1; N, 6.3. Found: C, 51.1; H, 5.8; N, 6.1 %). FABMS *m/z* 731 (M-CF$_3$CO$_2$)$^+$.

[Zn$_2$(L17)$_2$Cl$_4$]. **L17** (29.0 mg, 0.1 mmol) in CHCl$_3$ (10 ml) and ZnCl$_2$ (1.36 g, 10 mmol) in water (10 ml) were stirred together for 16 hr, the phases separated and the organic phase slowly evaporated to give colourless crystals of

$[Zn_2(L17)_2Cl_4].4CHCl_3$. The crystals were sensitive to solvent loss, and after exposure to air gave an off white solid which analysed as $[Zn_2(L17)_2Cl_4].2CHCl_3$ (49.1 mg, 90 %). (Anal. Calc. for $[Zn_2(L17)_2Cl_4].2CHCl_3$: C, 39.6; H, 5.0; N, 5.1. Found: C, 39.9; H, 5.1; N, 5.3; FABMS m/z 818 $(M-Cl)^+$.

5.7.4 X-Ray Structure Determinations

Crystal structures were determined at the University of Edinburgh crystallography service. The structures of $[Cu(L17-H)_2]$ and $[Ni(L17-H)_2]$ were solved by Dr James Davidson, the structures of $[Cu(L17)_2(NO_3)_2]$, $[Cu(L17)_2(BF_4)_2]$ and $[Cu(L17)Br_2]$ by Fraser White and the structure of $[Cu(L17)_2(CF_3CO_2)_2]$ by Dr Francesca Fabbiani. Details on the solutions and cif files are available in appendix 7.5.1.

5.7.5 Solvent Extraction – Anion Selectivity

All extractions were performed to the same general procedure. 0.01 M $[M(L-H)_2]$ in chloroform (10 ml) was added to 0.8 M HX/NaX aqueous solution (10 ml) and stirred for 16 hrs. The organic phase was extracted, a 0.5 ml aliquot taken to be used for metal/sulfur analysis and a 2.0 ml aliquot taken for chloride analysis. For metal and sulfur analysis, the solvent was removed *in vacuo*, the residue was dissolved in butan-1-ol (10 ml) and the concentration measured by ICP-OES. For chloride analysis, the aliquot was stirred overnight with 0.1 M aqueous HNO_3 (10 ml), the aqueous phase extracted and a 5 ml aliquot made up to 10 ml with 0.1 M NaOH. Chloride concentration was determined *via* a chloride sensitive electrode. The equilibrium pH of the aqueous phase was measured and plots of metal and anion loading against equilibrium pH were used to determine the selectivities. All solvent extraction data from this chapter are available in appendix 7.5.2.

5.7.6   Solvent Extraction – Cation Selectivity

5.7.6.1   Equimolar Anion Concentration

Experiments were carried out by contacting chloroform solutions (5 ml) of **L18** at concentrations of 0.01 mol dm^{-3}, with aqueous solutions (5 ml) of the appropriate metal salt at concentrations of 0.01 mol dm^{-3}. The aqueous solution was prepared from 4 ml of 0.0125 mol dm^{-3} metal salt solution, to which was added 1 ml of 0.1 mol dm^{-3} sodium hydroxide/water or 1 ml of 2.5 mol dm^{-3} sulfuric acid/water solution to change pH. Where mixed metal solutions were used, the metal salt solution contained 0.0125 mol dm^{-3} of each appropriate metal salt. After vigorous stirring for 16 h at room temperature, the mixtures were separated and 0.5 ml aliquots of the organic phase removed for metal analysis by ICP-OES. The equilibrium pH of the aqueous phase was measured and plots of metal loading against equilibrium pH were used to determine the selectivity order.

5.7.6.2   Excess Anion Concentration

Experiments were carried out by contacting chloroform solutions (5 ml) of **L18** at concentrations of 0.01 mol dm^{-3}, with aqueous solutions (5 ml) of the appropriate metal salt at concentrations of 0.01 mol dm^{-3}. The aqueous solution was prepared from 1 ml of 0.05 mol dm^{-3} metal salt solution, to which was added 4 ml of a mixture of 0.99 mol dm^{-3} HX and 0.99 mol dm^{-3} NaX, altering pH and keeping anion concentration constant at 0.8 mol dm^{-3}. Where mixed metal solutions were used, the metal salt solution contained 0.05 mol dm^{-3} of each appropriate metal salt. In the extraction from a mixed metal, mixed anion feed, the aqueous phase was prepared as described, but using half the volume of both a chloride and sulfate feed to give 5 ml of an aqueous phase with metal concentrations of 0.01 mol dm^{-3}, and sulfate and chloride concentrations of 0.4 mol dm^{-3}. After vigorous stirring for 16 h at room temperature, the mixtures were separated and 0.5 ml aliquots of the organic phase removed for metal analysis by ICP-OES. The equilibrium pH of the aqueous phase

was measured and plots of metal loading against equilibrium pH were used to determine the selectivity order.

5.8 References

[1] K. Kavallieratos and B. A. Moyer, *Chemical Communications*, 2001, 1620.

[2] A. Bianchi, K. Bowman-James, E. Garcia-Espana, and Editors, 'Supramolecular Chemistry of Anions', 1997.

[3] B. A. Moyer, P. V. Bonnesen, L. H. Delmau, T. J. Haverlock, K. Kavallieratos, and T. G. Levitskaia, *International Solvent Extraction Conference, Cape Town, South Africa, Mar. 17-21, 2002*, 2002, 299.

[4] P. D. Beer and P. A. Gale, *Angewandte Chemie International Edition*, 2001, **40**, 486.

[5] R. Custelcean and B. A. Moyer, *European Journal of Inorganic Chemistry*, 2007, 1321.

[6] V. Kral, J. L. Sessler, T. V. Shishkanova, P. A. Gale, and R. Volf, *Journal of the American Chemical Society*, 1999, **121**, 8771.

[7] T. G. Levitskaia, M. Marquez, J. L. Sessler, J. A. Shriver, T. Vercouter, and B. A. Moyer, *Chemical Communications*, 2003, 2248.

[8] L. R. Eller, M. Stepien, C. J. Fowler, J. T. Lee, J. L. Sessler, and B. A. Moyer, *Journal of the American Chemical Society*, 2007, **129**, 11020.

[9] A. L. Sisson, J. P. Clare, and A. P. Davis, *Chemical Communications*, 2005, 5263.

[10] P. G. Plieger, P. A. Tasker, and S. G. Galbraith, *Dalton Transactions*, 2004, 313.

[11] S. G. Galbraith, 'PhD Thesis', Edinburgh University, 2005.

[12] B. A. Moyer, P. V. Bonnesen, R. Custelcean, L. H. Delmau, and B. P. Hay, *Kemija u Industriji*, 2005, **54**, 65.

[13] K. A. Connors, 'Binding Constants: The Measurements of Molecular Complex Stability', 1987.

[14] H. Xie, S. Yi, and S. Wu, *Journal of the Chemical Society, Perkin Transactions 2: Physical Organic Chemistry*, 1999, 2751.

[15] P. W. Atkins and D. F. Shriver, 'Inorganic Chemistry', Oxford University Press, 1999.

[16] A. Bianchi, M. Micheloni, and P. Paoletti, *Coordination Chemistry Reviews*, 1991, **110**, 17.

[17] R. M. Izatt, K. Pawlak, J. S. Bradshaw, and R. L. Bruening, *Chemical Reviews*, 1991, **91**, 1721.

[18] J. M. Casas, F. Alvarez, and L. Cifuentes, *Chemical Engineering Science*, 2000, **55**, 6223.

[19] P. D. Beer and E. J. Hayes, *Coordination Chemistry Reviews*, 2003, **240**, 167.

[20] T. Gunnlaugsson, M. Glynn, G. M. Tocci, P. E. Kruger, and F. M. Pfeffer, *Coordination Chemistry Reviews*, 2006, **250**, 3094.

[21] F. A. Settle, 'Handbook of Instrumental Techniques for Analytical Chemistry', Prentice Hall, 1997.

[22] S. G. Galbraith, Plieger, P.G., Tasker, P.A., *Chemical Communications*, 2002, 2662.

[23] P. A. Tasker, C. C. Tong, and A. N. Westra, *Coordination Chemistry Reviews*, 2007, **251**, 1868.

[24] P. A. Tasker, R. S. Forgan, and D. K. Henderson, 'Metal Salt Extraction', UK patent filing, 2006.

[25] H. D. B. Jenkins, H. K. Roobottom, J. Passmore, and L. Glasser, *Inorganic Chemistry*, 1999, **38**, 3609.

[26] G. Kyuchoukov and J. Szymanowski, *Journal of Radioanalytical and Nuclear Chemistry*, 2000, **246**, 675.

[27] B. Harris, Private Communication, 2007.

[28] H. M. Irving and R. J. P. Williams, *Journal of the Chemical Society*, 1953, 3192.

[29] J. Szymanowski, 'Hydroxyoximes and Copper Hydrometallurgy', CRC Press, 1993.

[30] P. A. Tasker, P. G. Plieger, and L. C. West, *Comprehensive Coordination Chemistry II*, 2004, **9**, 759.

[31] V. I. Lakshmanan, G. J. Lawson, and J. L. Tomliens, *Journal of Inorganic and Nuclear Chemistry*, 1975, **37**, 2181.

CHAPTER 6

CONCLUSIONS

6.1   Conclusions

This thesis has two main aims involving the development of phenolic oxime extractants of the type used commercially,

- to tune extractant "strength" by substitution on the benzene ring and in particular to improve our understanding of the major effects associated with changing the nature of the 3-substituent, and
- to establish whether their mode of action can be changed from transporting metal *cations* to transporting metal *salts* by incorporating anion binding functionality in the form of a protonatable aminomethyl group in the 3- or 5-position.

Both objectives have been achieved. Previous research into substituent effects on phenolic oxime extraction is limited and not systematic. **L1**-**L9**, with a range of substituents in the 3-position, were readily prepared and showed a remarkable range of copper binding strengths which varied by two orders of magnitude from the strongest reagent **L6** (3-Br) to the weakest **L3** (3-*t*-Bu).

The consensus in publications from industrial labs is that the electronic effect of a 3- or 5-substituent controls extractant strength; electron-withdrawing groups lower the pK_a of the phenol, allowing copper binding to occur at lower pH and thus increase the reagent strength.   Initially, this appeared to be the case for **L1**-**L9** but discrepancies in the $pH_{0.5}$ values emerged which challenged this conclusion. The 3-OMe substituted ligand **L7** would be expected to be a weaker extractant as a consequence of the 3-methoxy group's electron-donating properties, but, in fact, copper extraction is more favourable than for the unsubstituted ligand **L1**. Incorporation of an electron-donating 3-Me group into **L2** has no effect on extractive efficacy, while the bulkier 3-*t*-Bu group of **L3** dramatically weakens its copper binding.

The potential for the 3-substituent to interact with the stabilising H-bonding motif present in *pseudo*macrocyclic salicylaldoxime dimers and their copper(II) complexes was investigated. Proof-of-concept work using collision-induced dissociation mass spectrometry showed that this may prove to be a powerful tool for measuring the relative gas phase stabilities of copper(II) complexes. The proof-of-concept studies reported in this thesis have been incorporated into a new Industrial CASE PhD project at the University of Edinburgh with Cytec Industries, to further develop the technique. Analysis of the crystal structures of the dimers of **L10**-**L15** and comprehensive computational studies using DFT methods and PIXEL demonstrated that the ability of the 3-substituent to "buttress" the H-bonding motif is a major factor in controlling extractant strength (Figure 6.1). Electronic properties also have a significant effect on metal uptake, and both factors should be considered in tuning the strength of new reagents.
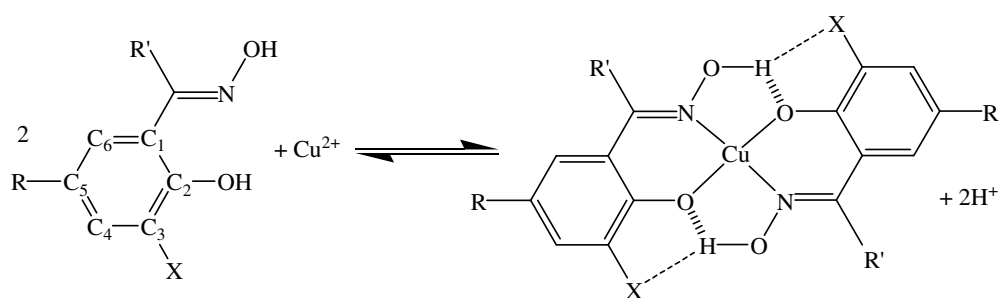

Figure 6.1: Buttressing of intracomplex H-bonding in bis-salicylaldoximato copper(II) complexes by a H-bond accepting 3-substituent (X).

Buttressing of H-bonding is not expected to be limited to phenolic oximes; ligands which form similar H-bonded arrays around complexed metal cations could be susceptible to tuning of extractant strength by appropriate substitution. Salicylaldehyde hydrazones form a *pseudo*macrocyclic cavity when binding divalent metal cations analogous to that of phenolic oximes, and initial work at the University of Edinburgh indicates that their strength can be altered by 3-substitution.[1] Subsequent studies may focus on pyrazolone oximes and 3-(2-hydroxyphenyl)-pyrazoles, whose extraction strengths are not suited to current circuits.

Overall, the first objective of the thesis has been met, and the implications will be considered in the design of phenolic oxime reagents for the extraction of metals for which the current reagents are too weak. Salicylaldoximes are also at the forefront of transition metal cluster chemistry and the ease of incorporation of substituents onto the scaffold could allow the tuning of the magnetic properties of such polynuclear clusters.[2-4] Research at the University of Edinburgh into single molecule magnets containing substituted phenolic oximes, including **L10**-**L16**, is ongoing in the Brechin research group.

As part of the second objective, six novel reagents with the potential to extract metal *salts* were prepared and characterised. These have a pendant dialkylaminomethyl arm in either the 3- or 5-position. The expected formation of tritopic metal salt complexes was confirmed for certain copper salts, for example [Cu(**L17**)$_2$(NO$_3$)$_2$]. In contrast, when contacted with chloride salts the 3-substituted ligand **L18** showed unexpectedly high loading efficiency, corresponding to a 1:1 L:MCl$_2$ ratio. This could have considerable impact on the development of new flowsheets for the recovery of base metals from chloride leaching. When **L18** operates in this way it appears that the function of the pendant amine is not to provide a separate binding site for chloride on protonation, but rather to assist in the binding of chloride in the inner coordination sphere of the metal and to ensure that the overall assembly is charge-neutral and organic-soluble. This assembly was confirmed in solid state structures of [Cu(**L17**)Cl$_2$] and [Zn$_2$(**L17**)$_2$Cl$_4$] in which the units dimerise through weak and strong O-M-O bridging respectively.
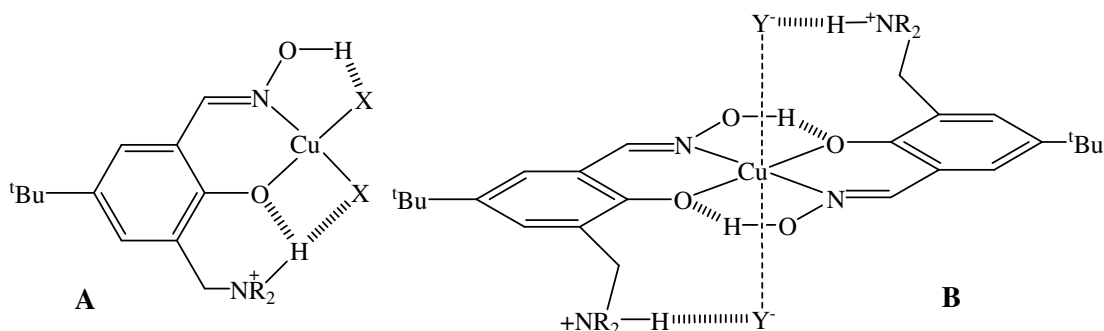

Figure 6.2: The two observed modes of anion binding in copper(II) salt complexes of the 3-substituted ligands: inner sphere anion coordination (**A**, X = Cl$^-$, Br$^-$) and outer sphere anion coordination (**B**, Y = NO$_3^-$, CF$_3$CO$_2^-$ and BF$_4^-$).

Crystal structures of copper complexes of **L17** with various anions have illustrated the importance of cation-anion interactions, as every structure contains such interactions and the formation of the simple tritopic assembly is mediated by $M \cdots X$ contacts. The consequences of this are very significant in terms of extractive metallurgy *e.g.* the cation selectivity of **L18**, which discriminates for Fe^{III} over Cu^{II} in the presence of sulfate, but extracts a mixture when chloride or both anions are present. Co-extraction of copper and iron is potentially a major problem if **L18** or its analogues are to be commercialised as metal *salt* extractants. Attempts to overcome this problem will benefit from a detailed understanding of the mode of binding of Fe^{III} in the presence of both sulfate and chloride. The Fe^{III} coordination chemistry of the 3-substituted reagents is expected to be varied and interesting, particularly given the propensity for salicylaldoximes to form Fe_n clusters[5] which have recently been shown to include sulfate anions.[4]

L18 could be an excellent $CuCl_2$ extractant from an iron-free feed, for example if the pH was raised above 3 to precipitate iron as its oxyhydroxides. If the aqueous feed was of high chloride concentration, then Fe^{III} may be extracted as its chlorometallate anion $FeCl_4^-$. If so, the $FeCl_4^-$ could potentially be removed in an anion stripping stage, allowing subsequent generation of a pure copper electrolyte. During the research programme for this thesis advances in the field of chloride hydrometallurgy have become apparent.[6] Novel leaching processes generate high tenor aqueous feeds with high chloride concentration, conditions which are ideal for extractants analogous to **L18** which do not release protons in the extract step.

An alternative to using reagents of the types **L17**-**L22** in extracting metal salts is to employ mixtures of cation and anion extractants - the "dual host" strategy.[7] This may be advantageous in that less elaborate receptors are required, lowering costs associated with synthesis, but this approach could remove the opportunity for the stabilising cation-anion interactions seen in metal salt complexes of polytopic ligands. Work within the group has shown that using a dual host approach, with mixtures of P50 and trioctylamine as cation and anion extractants, is not as effective

in the extraction of metal salts as the 3-dialkylaminomethyl-substituted phenolic oximes, *e.g.* **L18**.[8]

Metal salt extractants based on salicylaldoximes rather than the previously studied salicylaldimines ("salen" derivatives such as those described in Chapter 4) are much more stable to acid hydrolysis in two-phase systems, with 5-nonyl-substituted analogues of **L18** showing no degradation when contacted with acidic solutions (pH<1).[9] Hydrolytic stability is essential as acid-stripping is integral to flowsheets in extractive hydrometallurgy, and stripping of conventional phenolic oximes is achieved with 150 g L^{-1} sulfuric acid.

Phenolic oximes have many properties which are fundamental to their success as copper extractants, with hydrolytic stability an excellent example. The ease of incorporation of substituents is another, and the research presented in this thesis demonstrates the potential for further commercial application provided by substitution. Both main thesis objectives have been achieved and additional uses for substituted salicylaldoximes identified, including the potential for connecting phenolic oxime moeities with a functionalised strap. The properties of the strap could influence the nature of the complexes formed, with rigid spacers expected to allow control of the disposition of salicylaldoxime clusters which act as single molecule magnets. Ligands with straps of the type $CH_2NR(CH_2)_nNRCH_2$ are capable of forming 2:2 Cu:ligand assemblies with a well defined cavity capable of encapsulating anions, and these have been studied by the author while on secondment to Massey University, New Zealand.[10] Such examples further demonstrate the versatility of phenolic oximes and the wide-ranging applications made accessible by their amenability to substitution.

6.2 References

[1] H. Bauer, T. Lin, and P. A. Tasker, Unpublished work, 2007.

[2] C. J. Milios, S. Piligkos, and E. K. Brechin, *Dalton Transactions*, 2008, 1809.

[3] C. J. Milios, R. Inglis, A. Vinslava, R. Bagai, W. Wernsdorfer, S. Parsons, S. P. Perlepes, G. Christou, and E. K. Brechin, *Journal of the American Chemical Society*, 2007, **129**, 12505.

[4] I. A. Gass, C. J. Milios, A. Collins, F. J. White, L. Budd, S. Parsons, M. Murrie, S. P. Perlepes, and E. K. Brechin, *Dalton Transactions*, 2008, **15**, 2043.

[5] A. G. Smith, P. A. Tasker, and D. J. White, *Coordination Chemistry Reviews*, 2003, **241**, 61.

[6] J. Liddicoat and D. Dreisinger, *Hydrometallurgy*, 2007, **89**, 323.

[7] K. Wichmann, B. Antonioli, T. Soehnel, M. Wenzel, K. Gloe, K. Gloe, J. R. Price, L. F. Lindoy, A. J. Blake, and M. Schroeder, *Coordination Chemistry Reviews*, 2006, **250**, 2987.

[8] D. K. Henderson and P. A. Tasker, Unpublished work, 2008.

[9] P. A. Tasker, R. S. Forgan, and D. K. Henderson, 'Metal Salt Extraction', UK patent filing, 2006.

[10] R. S. Forgan, P. G. Plieger, and P. A. Tasker, Unpublished work, 2008.

CHAPTER 7

APPENDIX

Appendix

The following files and information are located on the appendix CD.

Chapter 1

7.1.1   Diagrams and figures used in Chapter 1.

Chapter 2

7.2.1   Crystal structure data and cif files for **L1**-**L9**, [Cu(**L1**-H)$_2$], [Cu(**L1**-H)$_2$], [Cu(**L3**-H)$_2$], [Cu(**L4**-H)$_2$(py)$_2$], [Cu(**L6**-H)$_2$] and [Cu(**L7**-H)$_2$].

7.2.2   Solvent extraction data for the extraction of copper(II) from sulfate solutions by **L1**-**L9**.

7.2.3   Diagrams and figures used in Chapter 2.

Chapter 3

7.3.1   Crystal structure data and cif files for **L10**-**L15**.

7.3.2   pK$_a$ calculations report.

7.3.3   DFT files and calculation spreadsheets.

7.3.4   Summary of IR spectra of **L1**-**L9**.

7.3.5   Analysis of CID mass spectra for the copper(II) complexes of **L1**-**L7**.

7.3.6   EPR spectra for copper(II) complexes of **L1**-**L3** and **L5**-**L9**.

7.3.7   Diagrams and figures used in Chapter 3.

Chapter 4

7.4.1   Solvent extraction data for the extraction of metal salts by **L17**, **L18** and **L20**, and detailed studied of the extraction of $CuCl_2$ by **L18**.

7.4.2   Crystal structure data and cif files for **L17**, **L19**, **L21**, $[Cu(L17)Cl_2]$ and $[Zn_2(L17)_2Cl_4]$.

7.4.3   Diagrams and figures used in Chapter 4.

Chapter 5

7.5.1   Crystal structure data and cif files for $[Cu(L17\text{-}H)_2]$, $[Ni(L17\text{-}H)_2]$, $[Cu(L17)Cl_2]$, $[Cu(L17)_2(NO_3)_2]$, $[Cu(L17)_2(CF_3CO_2)_2]$ and $[Cu(L17)_2(BF_4)_2]$.

7.5.2   Solvent extraction data for the anion selectivities of **L18** and **L20** and the cation selectivity of **L18**.

7.5.3   Diagrams and figures used in Chapter 5.

Chapter 6

7.6.1   Diagrams and figures used in Chapter 6.

Chapter 7

7.7.1   Published papers resulting from this thesis.